DEFECT ASSESSMENT USING RESONANT ULTRASOUND SPECTROSCOPY

A Thesis

by

KEVIN FLYNN

Submitted to the Office of Graduate Studies of
Texas A&M University
in partial fulfillment of the requirements for the degree of

MASTER OF SCIENCE

December 2008

Major Subject: Mechanical Engineering

DEFECT ASSESSMENT USING RESONANT ULTRASOUND SPECTROSCOPY

A Thesis

by

KEVIN FLYNN

Submitted to the Office of Graduate Studies of
Texas A&M University
in partial fulfillment of the requirements for the degree of

MASTER OF SCIENCE

Approved by:

Chair of Committee,	Miladin Radovic
Committee Members,	Vikram Kinra
	Raymundo Arroyave
Head of Department,	Dennis O'Neal

December 2008

Major Subject: Mechanical Engineering

ABSTRACT

Defect Assessment Using Resonant Ultrasound Spectroscopy. (December 2008)

Kevin Flynn, B.S., Pensacola Christian College

Chair of Advisory Committee: Dr. Miladin Radovic

This thesis demonstrates the practicability of using Resonant Ultrasound Spectroscopy (RUS) in combination with Finite Element Analysis (FEA) to determine the size and location of a defect in a material of known geometry and physical constants. Defects were analyzed by comparing the actual change in frequency spectrum measured by RUS to the change in frequency spectrum calculated using FEA.

FEA provides a means of determining acceptance/rejection criteria for Non-Destructive Testing (NDT). If FEA models of the object are analyzed with defects in probable locations; the resulting resonant frequency spectra will match the frequency spectra of actual objects with similar defects. By analyzing many FEA-generated frequency spectra, it is possible to identify patterns in behavior of the resonant frequencies of particular modes based on the nature of the defect (location, size, depth, etc.). Therefore, based on the analysis of sufficient FEA models, it should be possible to determine nature of defects in a particular object from the measured resonant frequency.

Experiments were conducted on various materials and geometries comparing resonant frequency spectra measured using RUS to frequency spectra calculated using FEA. Measured frequency spectra matched calculated frequency spectra for steel specimens both before and after introduction of a thin cut. Location and depth of the cut were successfully identified based on comparison of measured to calculated resonant frequencies. However, analysis of steel specimens with thin cracks, and of ceramic specimens with thin cracks, showed significant divergence between measured and

calculated frequency spectra. Therefore, it was not possible to predict crack depth or location for these specimens.

This thesis demonstrates that RUS in combination with FEA can be used as an NDT method for detection and analysis of cracks in various materials, and for various geometries, but with some limitations. Experimental results verify that cracks can be detected, and their depth and location determined with reasonable accuracy. However, experimental results also indicate that there are limits to the applicability of such a method, the primary one being a lower limit to the size of crack – especially thickness of the crack - for which this method can be applied.

ACKNOWLEDGEMENTS

I would like to thank my committee chair, Dr. Radovic, and my committee members, Dr. Arroyave and Dr. Kinra, and Prof. Benner, for their guidance and support throughout the course of this research.

I would also like to thank my fellow students, Patrick Mahaffey and Manisha, for their help and advice. Thanks also goes to Rodney Inmon and Jim Sajewski for their assistance in conducting experiments, and to Mike Walker and the rest of the personnel in the TAMU Mechanical Engineering Machine Shop for their help preparing test equipment.

Finally, thanks to my wife for her patience and love.

NOMENCLATURE

TAMU	Texas A&M University
RUS	Resonant Ultrasound Spectroscopy
FEA	Finite Element Analysis
NDT	Non-Destructive Testing

TABLE OF CONTENTS

Page

LIST OF FIGURES

Page

Page

Page

LIST OF TABLES

1. INTRODUCTION

1.1. NEED FOR NON-DESTRUCTIVE TESTING

In many industries, failure of single components can cause catastrophic results that include economic losses, limited availability of products, services and equipment, and in some cases, even loss of human life. The usual causes of the failure are defects in components such as cracks, voids, pores, surface scratches, etc. These defects can be introduced during improper manufacturing and processing; or during service as a result of overloading, creep, fatigue, environmental effects (corrosion), etc.

For example, the blades in gas turbines experience cyclic loading under severe service conditions such as high temperature and pressure. A failure of a single blade can cause catastrophic damage to other components of the gas turbine, as it is shown in Figure 1.1.[1] Another example of failure in a critical component is shown in Figures 1.2 and 1.3. In this case, poor design led to the growth of undetected fatigue cracks in the lower wing lug in a series of light agricultural aircraft. Propagation of these cracks over time and caused the aircraft to become unserviceable, and in two instances caused crashes.[2,3]

In the worst cases, failure of a single component can cause loss of human life, like in the case of the failure of a single bolt on a Bell 206 helicopter in Helmut, British Colombia, Canada on June 1, 2000. The bolt, located on the engine fuel control lines, failed due to stress corrosion cracking (hydrogen embrittlement cracking), probably as a result of poor manufacturing which left residual stresses in the manufactured bolt. The resulting fire and engine failure caused the aircraft to crash. The pilot did not survive.[4]

This thesis follows the style of *Nature*.

Figure 1.1 Failure of a first-stage blade damages all subsequent stages. [1]

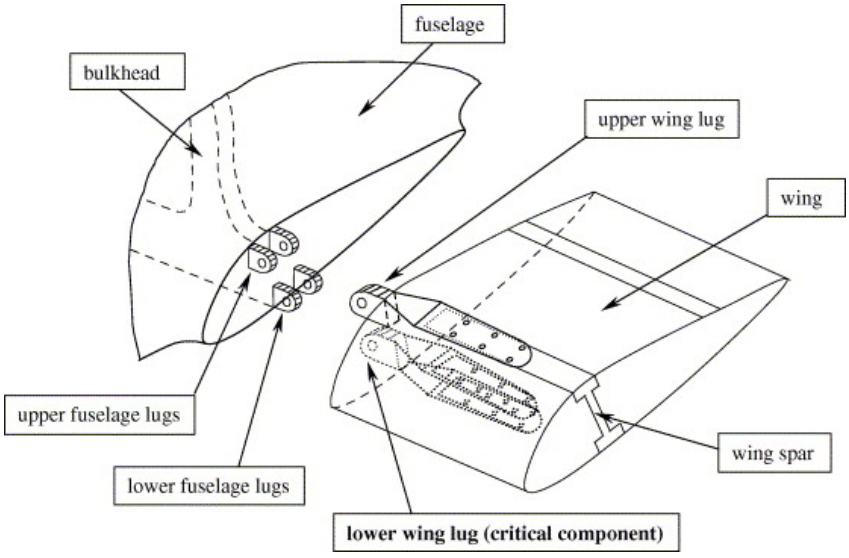

Figure 1.2 Schematic of wing root at fuselage attachment point. [3]

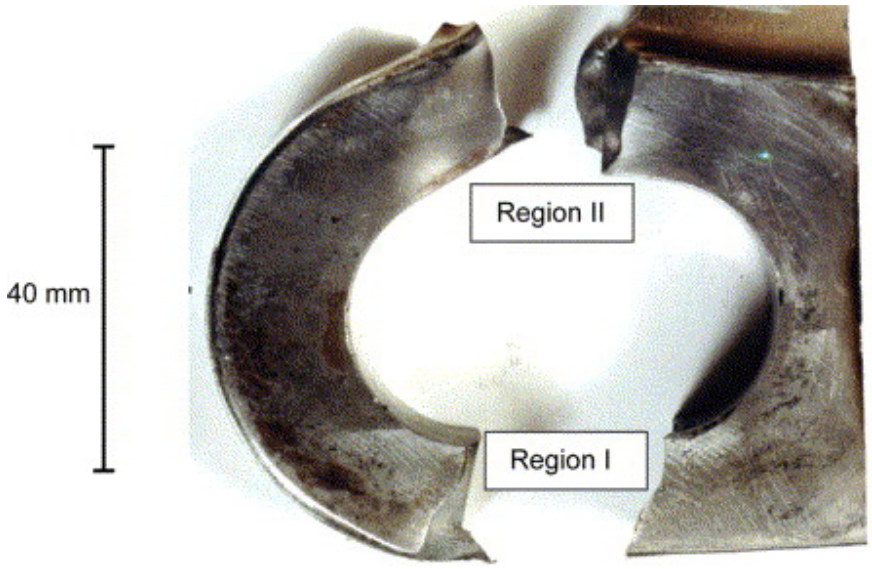

Figure 1.3 Failed lower wing lug. [3]

Since defects can cause catastrophic failures, it is desirable to identify them before they reach the critical threshold at which failure will occur. Defects can be detected either after manufacturing by regular product quality control, or in their service during the regular control/maintenance of equipment. It is the responsibility of engineers to anticipate and plan for possible failures of the components, and to develop reliable and economically feasible means for predicting failure in critical components. However, identifying a defect within a component that can cause its catastrophic failure is not always an easy task. In general, it is done by different testing methods, all of which fall into two categories: destructive and non-destructive testing.

Destructive testing includes any test that leaves the tested part unfit for further service.[5] Examples of such tests include stress tests, which determine if a defect is present by breaking the material; and metallographic tests, which require the material to be cut into small pieces and inspected under magnification. Destructive tests are typically simpler, more straightforward, and more informative than non-destructive tests.[5] However, it is often expensive, impractical, or inconvenient to destroy the test object.[5]

Non-destructive Testing (NDT) methods provide a means of identifying defects without damaging the tested item. Often, they can be performed on the object while it is in service. Thus, practical benefits of the non-destructive over destructive testing are obvious, as long as the method provides cost-effective and reliable results.[5]

NDT has been used for centuries to test the quality of different products. For example, blacksmiths listen to the ring of the object during manufacturing, while wheel-tappers tap the wheels of locomotives and listen to the sound they produce to detect the presence of cracks. Ordinary customers can usually be seen in shops around the globe, tapping glass objects to check for the presence of defects before purchase. All these examples are actually non-destructive testing using acoustic impact technique.[6]

However, over the last few decades, NDT has grown far beyond tapping glasses or locomotive wheels. Many different methods and techniques have been developed, some of which are reviewed in the following Sections (see Section 1.2). The importance of cost-effective and reliable early detection of defects in components in order to avoid premature failure is the most important driving force for the development of new NDT methods. In this thesis, we investigate the possibility of using Resonant Ultrasound Spectroscopy (RUS) in combination with Finite Element Modeling (FEM) as a non-destructive testing technique to detect and analyze defects, their size, and location in different components.

1.2. NON-DESTRUCTIVE TESTING METHODS

Non-destructive testing can be divided into various methods based on the particular physical principle that is employed to detect the presence of defects in the components.[5-7] Current testing methods include liquid dye penetrant tests, radiographic testing, impulse excitation technique, ultrasonic testing, electromagnetic testing, acoustic emission testing, thermography, and others. Advantages and limitations of some of the most popular NDT methods are briefly described in the following paragraphs, but detailed review of NDT can be found elsewhere.[5-7]

1.2.1. DYE PENETRANT TESTING

Liquid dye penetrant testing uses a liquid dye to increase the visibility of surface defects. Test kits typically require application of a dye and a developer chemical to the surface of the test object. Surface cracks become visible under visible or ultraviolet light, depending on the dye chemical compound used. Dye penetrant tests are used to detect surface flaws.[5-7]

Advantages of dye penetrant testing include ease of application, relatively high accuracy of results at low costs, and the simple and exact nature of the data provided about the length of a surface defect.[5-7] However, dye penetrant tests have many disadvantages, chief among which are the inability to identify the depth of a defect within the component or the width of a crack without difficulty and with a fairly large margin of error. In addition, dye penetrant tests can only be conducted on surfaces which are relatively smooth and easily accessible.[5-7]

1.2.2. ELECTROMAGNETIC TESTING

Magnetic particle testing is one of the most common electromagnetic testing methods. Other similar methods include alternating current field method (ACFM), alternating current potential drop method (ACPD), eddy-current testing (ECT), remote field testing (RFT), magnetic flux leakage (MFL), and others. All those methods work using a similar physical principle. A magnetic field is induced in the test material, and a sensor is used to detect distortions in the magnetic flux of the field.[5-7] In the case of magnetic particle testing, the "sensor" is created by sprinkling iron oxide particles on the surface of the test object. The particles are drawn to magnetic "leaks" on the surface of the test object, and outline the defect. Dyes or other additives are often added to the iron oxide particles to increase visibility.[5-7] Other testing methods use different means of detecting the distortions in the magnetic field.[5]

Electromagnetic methods can typically detect defects on or near the surface of the material.[6] Advantages of electromagnetic methods include the ability to use the method through thin coatings with some methods. As with dye penetrant testing, the results (in the case of magnetic particle testing) are fairly exact and easy to interpret as regards the orientation and length of the defect. Again, however, depth and width are more difficult or impossible to identify with these methods. Also, the material must again be relatively smooth and flat for these methods to yield useful information. It must also be ferromagnetic.[5-7]

1.2.3. RADIOGRAPHIC (X-RAY) TESTING

In radiographic testing, the test object is placed between a source of radiation and a radiographic film. Flaws in the material absorb less radiation than the rest of the material. The resultant film is analyzed, and the flaws located.[5-7]

Advantages include the ability to detect flaws at any depth within the material, and to identify at least two dimensions of the flaw with some accuracy. However, this analysis typically requires an expert to examine the film.[5-7] Also, the dimensions of the flaw are not exact, since the film provides only a 2-dimensional projection of the 3-dimensional flaw.[6] Other disadvantages include the difficulty and expense of the testing procedure, which requires special equipment, expensive film, and trained personnel, and protective equipment.[5] Radiographic testing may fail to detect closed cracks or cracks oriented in certain directions relative to the x-ray source.[5-7] Two opposite sides of the test object must be accessible.

1.2.4. ULTRASONIC TESTING

In ultrasonic testing, a transducer induces an ultrasonic wave into the material. The wave reflects off internal defects and discontinuities, and a receiver (typically collocated with the transducer) detects the reflected wave. This method can detect flaws

deep within an object, and can provide some information about the size, location, and orientation of the defect. Advantages of ultrasonic testing also include portability and ease of application.[5] However, the main disadvantage of ultrasonic testing is the requirement for trained personnel to conduct the test and evaluate the results.[5] Also, small, thin, inhomogeneous, or irregularly shaped parts often cannot be tested using this method.[5-7]

1.3. RESONANT NDT METHODS

Resonant NDT methods work by identifying the resonant frequency, or frequencies, of the test object.[6,8] The results are compared to theoretical or empirical resonant frequency data for a similar object where the extent of the defect is known (typically, an un-damaged object).[6] A simple example of this is acoustic emission testing of a bell. When struck, the tone from a cracked bell will be different than that of an undamaged bell.[6]

1.3.1. IMPACT EXCITATION TECHNIQUE

Impact excitation NDT identifies the natural frequency of the test object by applying a brief impact (typically, a blow from a hammer, or similar) and measuring the frequency of the resulting vibration of the object.[9-11] The object will tend to have maximum response vibration at its natural frequencies.[10,11] Since resonant frequency is determined (among other things) by the physical properties of the object, a defective object will vibrate at a different frequency than a non-defective object (for detailed explanation, see Section 2).[10,11] Comparison of the measured frequency to predicted or calculated resonant frequencies of a similar, but undamaged object will show if the test object is defective.[10,11]

Resonant frequencies for a non-defective object can be determined using measured data from a non-defective object. Theoretical calculations can also be used to

determine an exact solution for the resonant frequencies for a non-defective object. This can be done only in relatively few cases, since an exact solution can be determined for relatively few simple shapes. However, recent attempts to use finite element modeling to determine resonant frequencies of undamaged objects for impact tests have produced promising results.[9,10]

Advantages of impact testing include ease of application, particularly to objects in service; and its applicability to almost any geometry for which non-defective resonant frequency data can be acquired.[9,11] Impact testing shares many of the same disadvantages as resonant ultrasound spectroscopy (detailed below). The main disadvantages are the extensive analysis (either computational or experimental) that is required to determine an acceptability criteria for an object, and the sensitivity of the results to any change in dimensions or physical characteristics of the test object.[9-11] In other words, resonant frequencies of the test object are affected by too many factors, any one of which might produce results that appear unacceptable.[10]

The main disadvantage of impact testing, as compared to resonant ultrasound spectroscopy is that the excitation force is uncontrolled. Without the ability to excite the object at particular frequencies of interest, it may be difficult to gather data at those frequencies. Also, impact testing without constraining the test object presents difficulties, so most impact tests are done on constrained objects, which of course affects the resonant frequencies.

1.3.2. RESONANT ULTRASOUND SPECTROSCOPY

Relatively recently, Resonant Ultrasound Spectroscopy (RUS) was proposed as a non-destructive test for identifying and evaluating defects. A detailed description of RUS can be found in Section 2 of this thesis. Briefly, however, RUS operates by determining the free-body mode resonant frequencies - frequency spectrum - of an object. Every object has an infinite number of resonant mode frequencies, determined

by the object's physical properties (size, shape, material, etc.). Two identical objects would, in theory, have identical frequency spectra.[8,12]

Current RUS NDT methods rely on comparing the resonant frequencies of a suspect object to those of objects known to have defects within acceptable limits. An acceptable range of frequency spectra are determined by performing RUS tests on a large number of identical objects which are known to be acceptable. The frequency spectrum of a suspect object is determined using RUS. If one or more resonant frequencies of the suspect object are outside the acceptable range, the tested object is assumed to be flawed.[8,12] Migliori cites several examples of this technique in manufacturing applications, to detect flawed parts.[8] Schwarz et al recently reviewed additional examples.[12]

Although RUS is a relatively new NDT method, it is obvious that the major advantage of this technique over most other NDT techniques is the ability to test the entire object simultaneously to identify the presence of defects.[8] Any defect, no matter where located, will affect the frequency spectrum of the object. Smaller defects will be more difficult to detect, but given sufficiently restrictive rejection criteria, there is almost no limit to the precision of the test.[8] In addition, the testing and analysis process can be easily automated as a part of a production process.[8]

An obvious disadvantage of this method is the requirement that many parts of known quality must be available for testing to determine the acceptability criteria.[8,12] In addition, for reasons explained in Section 2, RUS is limited to small and light objects.[8] A third limitation is that RUS analysis does not work well on materials with high attenuation.[8,12]

Here, we explore the possibility of determining acceptable criteria for the frequency spectrum of an object without the requirement of testing a large number of undamaged and damaged objects. By using finite element analysis and/or theoretical calculations, it is possible to determine the free-body mode resonant frequencies of an object with and without various defects. In addition, this work will demonstrate that it is

possible to determine not only if on object has a defect, but to determine some of the physical characteristics of the defect by analyzing the frequency spectrum.

The idea of using RUS in combination with finite element modeling (FEM) to analyze defects in the components goes back to 1979, when first attempts were made to identify the location of defects by using resonant frequencies calculated from FEM models.[13] Migliori and a number of other sources successfully use FEM to identify resonant frequencies of undamaged objects.[8,13-19]

Lee et al [18], Kam et al [17], and Rizos et al [19] successfully identified location and depth of a defect in a one-dimensional beam model. However, some of these early efforts did not test the accuracy of FEM predictions by comparing them with actual defective parts. Also, all those models were developed for relatively large defects.[13,17-19] These studies had limited application to manufacturing, because they did not use RUS methods as a source of excitation and response measurement. Rather, they used a combination of strain gauges and electromechanical or acoustical vibrators. This limited applicability to relatively large specimens, since otherwise the mass of the test equipment would significantly affect the results.[13,17-19]

Belyaev et al attempted to use RUS to identify crack depth of actual cracks in silicon wafers. They found that FEM predictions of resonant frequency in undamaged specimens were within acceptable limits when compared to actual results. However, they found substantial variation between actual and predicted change in resonant frequency. They suggested that this might be caused by interaction between the crack faces.[14] They also found that FEM predicted mode shapes closely matched actual mode shapes.[16]

1.4. FUNDAMENTALS OF VIBRATIONS

Since the main topic of this thesis is application of resonant ultrasound spectroscopy as a non-destructive testing technique, the fundamentals of vibrations and resonance theory are given in this Section.

The resonant (or natural) frequency of a system is the frequency at which an unconstrinaed, undamped (amplitude of vibration is constant over time) object will tend to oscillate if no outside forces are applied.[20] The physical properties of an object determine its resonant frequency.[20] The following paragraphs describe how resonant frequencies of a system with one or more degrees of freedom depend on the physical properties of the system. Degrees of freedom are the number of dimensions necessary to fully define the position of a system.[20]

1.4.1 SYSTEMS WITH ONE DEGREE OF FREEDOM

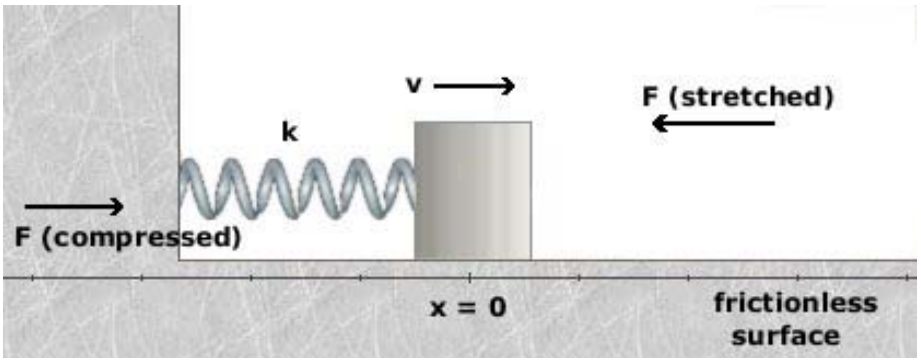

Figure 1.4 Spring-mass system.[21]

Natural frequencies and mode shapes of simple objects can be determined using the equations of motion. The system shown in Figure 1.4 has one degree of freedom.[20,22] The mass is assumed constrained from rotation in any dimension, and allowed to translate in only one dimension. If the mass is considered as a lumped-mass (i.e. no relative motion between two points on the mass), then only one dimension (displacement, x) is required to fully define the position of the system. If we consider the single degree of freedom system in Figure 1.4, we can apply Newton's second law of motion and, assuming no friction, the motion of mass m can be described by:[20,22]

$$m * a = -k * x \qquad \text{Eqn. 1.1}$$

Or

$$m * \frac{\partial^2 x}{\partial t^2} + k * x = 0 \qquad \text{Eqn. 1.2}$$

where m is mass, k is stiffness of the spring, t is time, and x is lateral displacement. This differential equation can be solved for x as a function of time. The solution $x = 0$ describes the static condition. The solution for the dynamic condition is given by the following equation:[20,22]

$$x = A\sin(\omega_n t) + B\cos(\omega_n t) \qquad \text{Eqn. 1.3}$$

Where A and B are constants determined by the initial conditions, and ω_n is the natural (resonant) frequency of the system (in radians/second), defined as:[20,22]

$$\omega_n = \sqrt{\frac{k}{m}} \qquad \text{Eqn. 1.4}$$

Substituting the initial conditions

$$\begin{aligned} x(0) &= x_0 \\ \frac{dx}{dt}(0) &= \dot{x}_0 \end{aligned} \qquad \text{Eqn. 1.5}$$

In Equation 1.3 yields:[22]

$$x = \frac{\dot{x}_0}{\omega_n}\sin(\omega_n t) + x_0\cos(\omega_n t) \qquad \text{Eqn. 1.6}$$

where x_o and $\dot{x}_o$ are the initial displacement and velocity of mass m. The resulting natural frequency of oscillation is:

$$f_n = \frac{1}{2\pi}\sqrt{\frac{k}{m}} \qquad \text{Eqn. 1.7}$$

Where f_n is the natural (resonant) frequency in cycles per second (hz).[20]

In other words, if the system is displaced (i.e. the mass is moved) and released, or if some initial velocity is imparted to the mass, it will oscillate back and forth indefinitely. Regardless of the magnitude of initial displacement or initial velocity, it will take the same amount of time to complete a single oscillation.[20] The frequency at

which the system will oscillate is a function of the physical properties of the system, i.e. mass *m* and stiffness of the spring *k*.

The simple example above assumes that the system has no outside forces acting on it. Oscillation is due to the initial displacement and/or initial velocity. However, if an outside, oscillatory force is applied to the system; the overall result will depend on both the resonant frequency and the frequency of the forcing function.[22] Consider the same spring-mass system with a cyclic driving force of magnitude $F_o\cos(\omega t)$ shown in Figure 1.5.

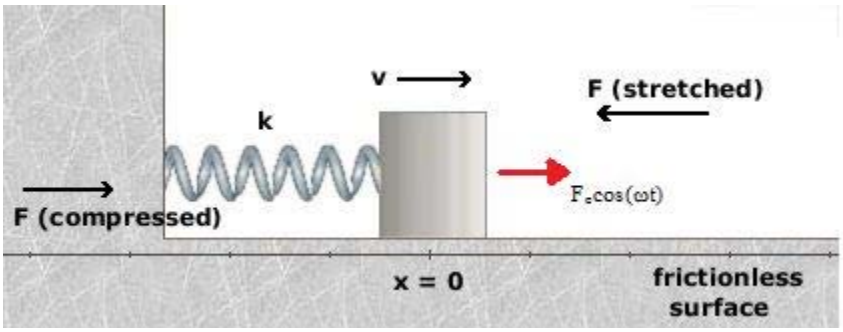

Figure 1.5 Spring-mass system with applied excitation force. [21]

Then the equation of motion for the mass in the system shown in Figure 1.5 is:[22]

$$m * \frac{\partial^2 x}{\partial t^2} + k * x = F_0 \cos(\omega t) \qquad \text{Eqn. 1.8}$$

where F_o is a constant and ω is the frequency (rad/s) of the driving force. Solving this differential equation for x yields:[22]

$$x = A\sin(\omega_n t) + B\cos(\omega_n t) + \frac{F_0 / m}{\omega_n^2 - \omega^2}\cos(\omega t) \qquad \text{Eqn. 1.9}$$

Where [22]

$$B = x_0 - \frac{F_0 / m}{\omega_n^2 - \omega^2} \qquad \text{Eqn. 1.10}$$

$$A = \frac{\dot{x}_0}{\omega_n}$$

Note that if $\omega = \omega_n$, the value of x goes to infinity. Real systems have damping (energy dissipation, such as friction, heat, plastic deformation, etc.), which prevents the system from reaching infinite displacement when forced to vibrate at resonant frequency.[22] Assuming a viscous damper (damping force = viscous damping coefficient (c) * velocity) in parallel with the spring in Figure 1.5 yields the following equation for displacement.[20]

$$x = \frac{F_o}{k} \frac{1}{\sqrt{\left(1 - \left(\frac{\omega}{\omega_n}\right)^2\right)^2 + \left(2\zeta \frac{\omega}{\omega_n}\right)^2}} \cos(\omega t - \phi) \qquad \text{Eqn. 1.11}$$

if $\zeta < 1$, where ζ is the damping ratio, defined as:[20]

$$2\zeta\omega_n = \frac{c}{m} \qquad \text{Eqn. 1.12}$$

where c is the viscous damping coefficient, and φ is the phase angle, defined as[20]

$$\phi = \arctan\left(\frac{2\zeta \frac{\omega}{\omega_n}}{1 - \left(\frac{\omega}{\omega_n}\right)^2}\right) \qquad \text{Eqn. 1.13}$$

While amplitude of the system in the case of damped vibrations no longer approaches infinity, it is still much greater at its natural frequency.[22] Therefore, if a system is subjected to an outside force of constant amplitude and varying frequency, the frequency where the largest response is observed will be the natural frequency of the system.[22] Figure 1.6 shows amplitude and phase angle response vs. frequency ratio.

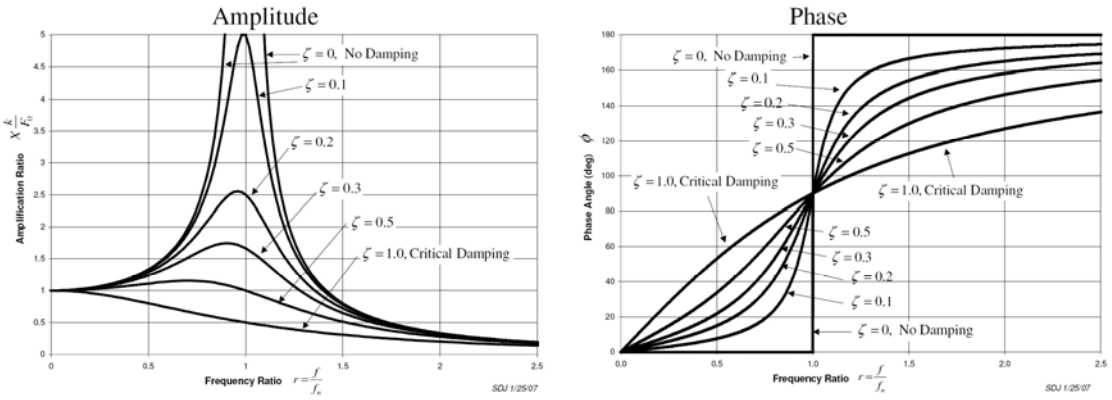

Figure 1.6 Amplitude and phase angle response varying damping and frequency ratio. [23]

Equation 1.7 shows that the resonant frequency depends on stiffness and mass, the physical parameters of this system. If either mass or stiffness changes, natural frequency will also change.[20,22] As the model grows more complex (see below), additional physical parameters will affect the natural frequency. Since defects may affect the stiffness and mass of an object, they may be expected to produce changes in natural frequency.[17-19]

1.4.2 SYSTEMS WITH MULTIPLE DEGREES OF FREEDOM AND MODE SHAPES

Objects have as many resonance modes and resonance frequencies as they have degrees of freedom.[20,22] A point mass has six dimensions required to fully define it's position: x, y, and z location, and x, y, and z rotation.[20,22] In the previous example, the mass was constrained so that it could only move in one of the six dimensions. Also, the mass was assumed to be "lumped," meaning that no one point on the mass could move relative to another. Real objects, of course, are not subject to these limitations. Real objects are made up of an infinite number of point masses, all of which can move relative to one another. Therefore, real objects have an infinite number of degrees of freedom.[20,22,24]

Since real systems have an infinite number of degrees of freedom; real systems have an infinite number of resonant frequencies. Real systems include any solid object or assembly. For example, equation of motion of a string under tension (assuming the string has mass, but no thickness, minimal deflection, pinned ends) is given by the equation:[24-27]

$$\sqrt{\frac{T}{\mu}}\frac{\partial^2 y}{\partial x^2} = \frac{\partial^2 y}{\partial t^2} \qquad \text{Eqn. 1.14}$$

where y is vertical deflection, x is location along the length (L) of the string, t is time, T is tension, and μ is mass per unit length. Solving the differential equation for the vertical deflection (y) at any point, and applying the boundary condition that $y = 0$ at $x = 0$, yields:[24-27]

$$y = \sin\left(\sqrt{\frac{\mu}{T}}\omega x\right)\left(A\sin(\omega t) + B\cos(\omega t)\right) \qquad \text{Eqn. 1.15}$$

where A and B are constants dependant on initial conditions, and ω is the resonant frequency. Applying the boundary condition that $y = 0$ at $x = L$ yields:[24]

$$\omega = \frac{n\pi}{L}\sqrt{\frac{T}{\mu}} \qquad \text{Eqn. 1.16}$$

where n is any integer number. This yields an infinite number of solutions, and the resonant frequencies are given by the equation:[24]

$$f = \frac{n}{2 * L}\sqrt{\frac{T}{\mu}} \qquad \text{Eqn. 1.17}$$

Each resonant frequency has a unique corresponding mode shape: the relative position of all points on a structure at that particular frequency. In the above single degree of freedom examples, the mode shape is the position of the mass, or the function $x = f(t)$. In this example, the mode shape is defined by the function $y = f(x,t)$. The actual position of the string at any time will depend on the initial conditions of displacement and velocity in the y axis, and will be a superposition of all mode shapes.[24] The first seven mode shapes, corresponding to $n = 1$ to 7, are shown in Figure 1.7.

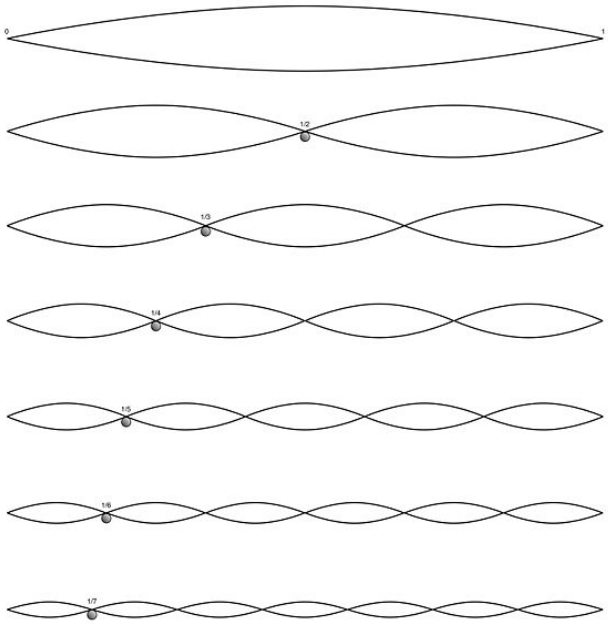

Figure 1.7 First seven mode shapes of pinned-pinned string. [27]

The spring-mass system had one dimension, and one degree of freedom. If the system could move in two dimensions, it would have two degrees of freedom, and thus two resonant frequencies. As with the single degree of freedom example above, the system has greater response to an outside oscillatory force if the frequency of the force corresponds to the frequency of one or more of its resonant frequencies.[8,20,22,24] For more information on determining resonant frequencies of a three-dimensional object, refer to Section 2.

1.4.3. USING RESONANT FREQUENCY TO DETERMINE PHYSICAL PROPERTIES OF AN OBJECT

As shown above, the resonant frequencies of a system can be determined if the dimensions, physical properties (density, elastic moduli, internal damping), and initial conditions are known. The reverse is also true: if the resonant frequencies are known,

the physical characteristics can be determined.[8,28,29] Using the tensioned-string example above, if the first three natural frequencies are known, it is possible to calculate the string's length, tension, and linear mass.

Since the natural frequency of an object is dependant on its physical constants, mass, and geometry; any defect in the object will change the resonant frequency spectrum. Within the frequency spectrum, all resonant frequencies will be affected by a defect. However, some frequencies will be more affected than others. For example, a longitudinal crack in a solid cylinder would probably have a greater affect on the bending and torsional modes than on the transverse bending mode.[8] Comparing the spectrum of an undamaged object to that of a suspect object can therefore be used to determine if the suspect object is damaged, and possibly also to identify location and severity of the defect.[8,9,17] Defects in an object may be identified from a resonant frequency spectrum in one of several ways: resonant frequency shifts, peak splitting, change in amplitude, increase in peak bandwidth, to name some of the most commonly used.[8]

Of course, the obvious example is frequency shifts. Damage changes the physical properties of an object, thus changing the resonant frequencies.[8] To take a simple example, an object with serious corrosion will have some change in density (and probably geometry). As a result, some of the resonant frequencies of the corroded object will have different values than the frequencies of the object prior to corrosion. Therefore, the frequency at which the damaged object has resonant vibration (i.e. the resonant frequencies) will be different than those of an undamaged, but otherwise identical object.[8] Cracks, for example, tend to reduce the magnitude of all the resonant frequencies for all modes (although some reduce more than others, and a few might even increase slightly).[8]

Peak splitting is a second method that can be used to identify defects within an object.[30] With multiple degrees of freedom, it is possible for two resonant frequencies to fall on the exact same value.[8,20,22,30] This phenomenon is most often seen when an object has 90 degree rotational symmetry about an axis.[8,19,20] Such cases are particularly useful

for determining the location of a defect.[8,30] Typically, defects eliminate the axial symmetry. As a result, the resonant frequencies of both modes change, but by different amounts.[8] On a frequency spectrum, this causes one peak to appear as two peaks.[8] In Figure 1.8, a single resonant frequency on the undamaged object became two resonant frequencies after a defect was introduced in the object.

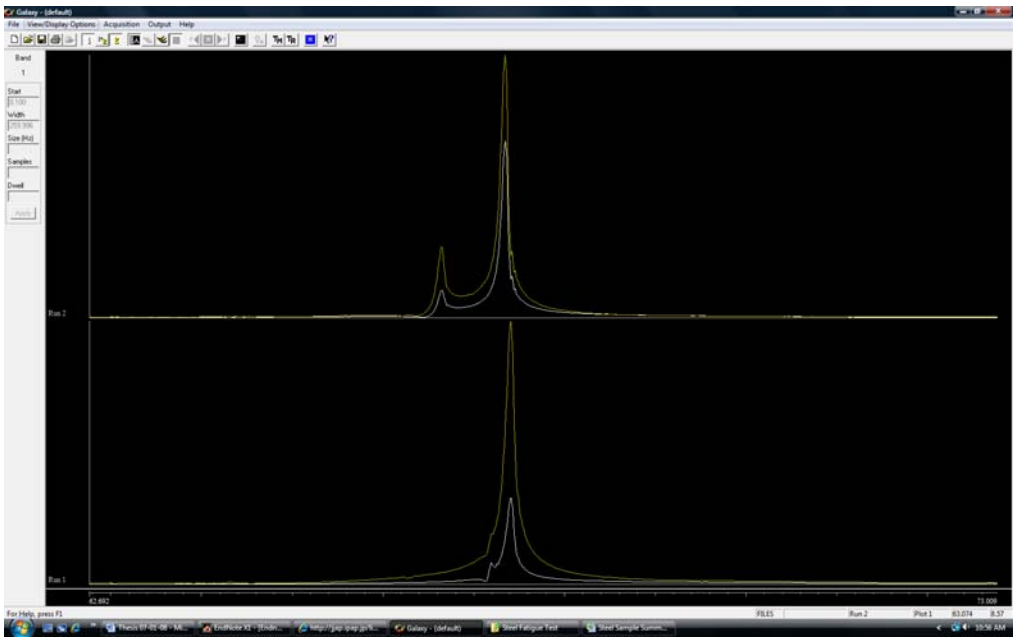

Figure 1.8 Example of peak splitting for Steel Cut Specimen #6 (see Section 3) before (bottom) and after (top) defect was introduced.

Increases in peak bandwidth may also indicate a defect.[14] Internal damping causes sharp peaks in the response/frequency graph become wider when a defect is introduced.[14] This is particularly useful when the crack is very small, or in the case of wet/dry testing.[8,14] A useful means of quantifying this change is measuring the width of the response peak at the half-peak value, expressed as a percentage of the modal natural frequency (Eqn. 3.1).

Other methods to identify the presence of a defect by noting changes in response amplitude at a particular frequency.[8] However, for this to work, the excitation force must be the same in all cases, and the response must be measured at the same point, which is not easy to achieve in practice.

2. EXPERIMENTAL AND COMPUTATIONAL METHODS

This Section contains description of the experimental and numerical methods that were used in this work. More details on the methods that were used to prepare the samples and introduce defects are given in Sections 3-5.

2.1. RESONANT ULTRASOUND SPECTROSCOPY

Resonant Ultrasound Spectroscopy (RUS) is a method of identifying the resonant frequencies of an object by measuring its response to ultrasonic excitation.[8,12,15,16,28-31] RUS has been used for identifying the elastic moduli of different solids since the 1960s.[8] In recent years, RUS has received increasing attention due to its potential quality control applications.[8,12,31]

2.1.1. SETUP AND METHOD

As shown in the previous Section, any real system will have an infinite number of resonant frequencies at which it will tend to oscillate.[20,24] If an outside oscillatory force is applied to the system, and that force oscillates at the same frequency as one or more of the system's resonant frequencies, the system will have a larger response than it would if the outside force oscillates at a non-resonant frequency.[20,24] Using this principle, it is possible to excite a system at various frequencies, record the amplitude response, and determine the resonant frequencies by identifying the peak responses. This is, in a nutshell, the description of resonant ultrasound spectroscopy (RUS).[8]

A small sample is rested lightly on two or more piezoelectric transducers. In this work, a three-transducer setup was used for all measurements, as shown in Figure 2.1. One transducer is used to excite the sample. The frequency of this driving transducer is swept through a range of frequencies of interest, which correspond to one or more of the resonant frequencies of the sample. The other two transducers measure the response of

the sample.[8,12,31] Figure 2.1 shows typical RUS equipment setup. The photos on the right show the three ultrasonic transducers (one to input the excitation signal, two to measure response). Figure 2.2 shows a typical diagram of a RUS spectrometer setup. Figure 2.3 shows typical results of a RUS frequency spectrum scan.

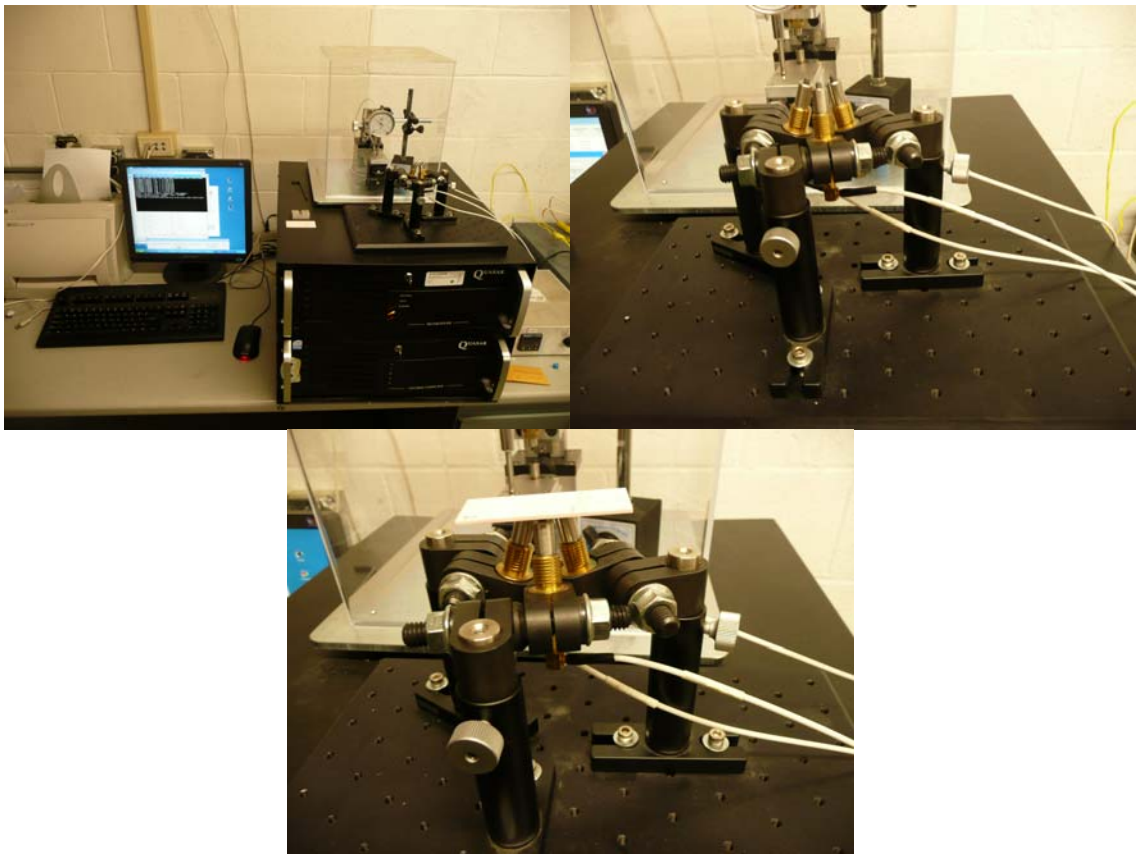

Figure 2.1 Photographs of the RUSpec Spectrometer setup.

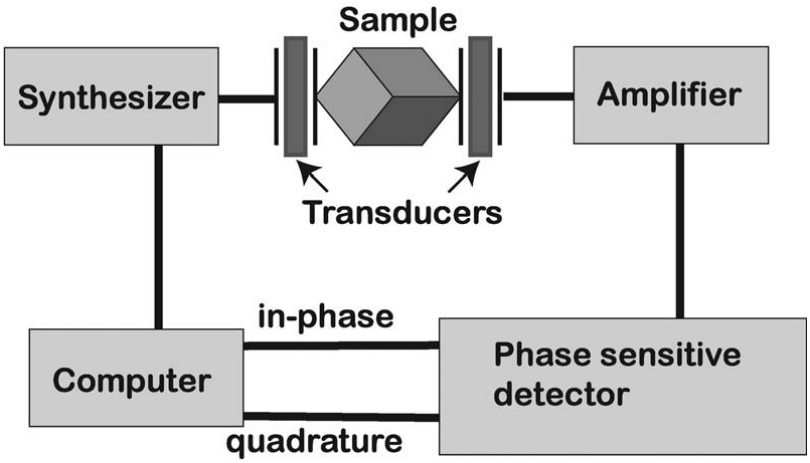

Figure 2.2 Schematic of a typical RUS spectrometer setup.[32]

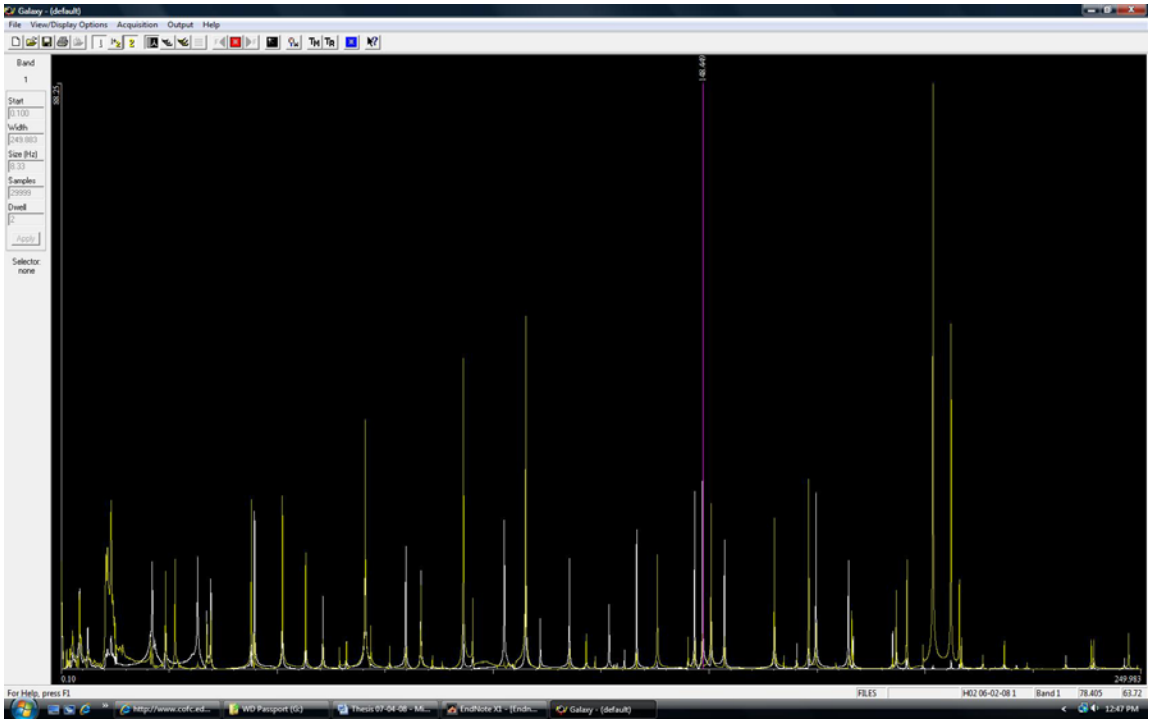

Figure 2.3 Resonant spectrum showing the peak amplitude at frequencies that correspond to the natural resonant frequencies of the object.

In this work, the RUSpec (Quasar International, NM) resonant spectrometer, together with Galaxy software (Quasar International, NM) were used to collect all resonant spectra of the examined samples.

2.1.2. DETERMINING RESONANT FREQUENCIES

As outlined above, RUS equipment is used to determine the resonant frequency spectrum of an object. In some cases, it is possible to calculate the resonant frequency spectrum of an object based on the object's physical properties. An outline of this process is presented in the following paragraphs

Resonant frequencies of a solid object are determined by the geometry of the object, and the elastic constants of the material. The elastic constants of a material define the relationship between applied stress, σ, and deformation (strain), ε. For the linear elastic solid, Hooke's Law states that three-dimensional stress and strain in any material are related by the following tensor equations:

$$\sigma_{ij} = C_{ijkl}\varepsilon_{kl} \qquad \text{Eqn. 2.1}$$

or

$$S_{ijkl}\sigma_{ij} = \varepsilon_{kl} \qquad \text{Eqn. 2.2}$$

where i, j, k, and l are values from 1 to 3, corresponding to the three primary axes in Cartesian coordinates.[22,33] Terms in the stiffness, (C), or compliance, (S), tensors are referred to as the "elastic constants." Since the two tensors are inversely related, it is only necessary to determine one.[33] In this work, the stiffness tensor will be considered.

The stiffness tensor is unique to a particular material; dependant not only on the composition, but also on the microscopic structure of the material. The tensor has eighty-one terms. However, by considering the nature of most common materials, and making some simplifying assumptions, it is possible to reduce the number of unique terms in the tensor. Without going into detail, if it is assumed that the material is symmetric, crystalline, and isotropic; most of the terms within the stiffness tensor

become inter-related. Only two independent values constants are needed to determine all of the elastic constants in polycrystalline, randomly-oriented materials.[8,34]

Applying those simplifying assumptions, and utilizing Voight Notation, the stress and strain tensors can be rewritten as vectors, and the compliance/stiffness tensors rewritten as matrices, yielding the following equation.[20,33]

$$\sigma = C\varepsilon \qquad \text{Eqn. 2.3}$$

where

$$\sigma = \begin{pmatrix} \sigma_1 \\ \sigma_2 \\ \sigma_3 \\ \sigma_4 \\ \sigma_5 \\ \sigma_6 \end{pmatrix} \qquad \text{Eqn. 2.4}$$

and σ_1, σ_2, and σ_3 are (respectively) principle stresses along the 1, 2, and 3 axes; and σ_4, σ_5, and σ_6 are (respectively) shear stresses in the 23, 13, and 12 directions. Then, strain can be related to displacement as follows:[20,33]

$$\varepsilon = \begin{pmatrix} u_{11} \\ u_{22} \\ u_{33} \\ \frac{1}{2}(u_{23} + u_{32}) \\ \frac{1}{2}(u_{13} + u_{31}) \\ \frac{1}{2}(u_{12} + u_{21}) \end{pmatrix} \qquad \text{Eqn. 2.5}$$

where u is displacement, and the compliance tensor reduces to:

$$C = \begin{pmatrix} c_{11} & c_{12} & c_{12} & . & . & . \\ c_{12} & c_{11} & c_{12} & . & . & . \\ c_{12} & c_{12} & c_{11} & . & . & . \\ . & . & . & c_{44} & . & . \\ . & . & . & . & c_{44} & . \\ . & . & . & . & . & c_{44} \end{pmatrix} \qquad \text{Eqn. 2.6}$$

where:

$$c_{12} = c_{11} - 2c_{44} \qquad \text{Eqn. 2.7}$$

When analyzing the spring-mass system, it was possible to determine the resonant frequency by solving the equations of motion. For the simple systems, determining and solving the equations of motion is a trivial exercise. However, determining the equations of motion for a complex solid is not always so easy.[22]

Instead, for complex systems (such as a 3-dimensional deformation of a solid body), the energy minimization technique is used. This technique identifies the relative deformation of the object (mode shapes) that correspond to the minimum energy configurations. Since, according to Newton's Second Law, any system will tend to stay at its minimum energy state, an ideal (undamped) system will tend to deform according to the relative displacements determined by minimizing the energy equation. These mode shapes correspond to the natural frequencies.[8] In other words, displacements that minimize the Lagrangian equation correspond to the free body vibrations of an elastic solid.[8,35]

The general form of the Lagrangian is:[8,35]

$$L = \int_V (KE - PE)dV \qquad \text{Eqn. 2.8A}$$

Assuming small motions, the kinetic, *KE*, and potential, *PE*, energy terms become:[8,35]

$$KE = \frac{1}{2}\sum_i p\frac{\partial u_i}{\partial t}\frac{\partial u_i}{\partial t} = \frac{1}{2}\sum_i p\omega^2 u_i^2 \qquad \text{Eqn. 2.8B}$$

$$PE = \frac{1}{2}\sum_{ijkl} c_{ijkl}\frac{\partial u_i}{\partial x_j}\frac{\partial u_k}{\partial x_l} = \frac{1}{2}\sum_{ijkl} c_{ijkl}\varepsilon_{ij}\varepsilon_{kl} \qquad \text{Eqn. 2.8C}$$

where i = 1, 2, or 3; corresponding to the three principle axes in Cartesian coordinate space (x_1, x_2, and x_3), ρ is density, and u_i is the i^{th} component of the displacement vector assuming harmonic time dependence with frequency ω in rad/sec.[8,35]

$$u(t) = u_0 e^{iwt} \qquad \text{Eqn. 2.8D}$$

A minimum of Lagrangian, Eq. 2.8A, for harmonic time dependence, Eq 2.8D, and kinetic and potential energies given by Eq. 2.8B and Eq. 2.8C respectively, yields the elastic wave equation:[8,35]

$$\rho\omega^2 u_i + \sum_{j,k,l} c_{ijkl} \frac{\partial^2 u_k}{\partial x_j \partial x_l} = 0 \qquad \text{Eqn. 2.9}$$

Note that the equations for potential and kinetic energy utilize the complete stress, strain, and compliance tensors. At this point, no simplifying assumptions have been made about the material.

Equation 2.9, if solved, would yield an exact solution. However, it is soluble only for a small number of cases. Instead, an approximate displacement vector as a series of polynomials (Φ) and constants (a) is assumed using the Rayleigh-Ritz method. This yields the following equation:[8,35]

$$u_i = \sum_{\lambda} a_{i\lambda} \Phi_\lambda = \sum_{\lambda} a_{i\lambda} x^l y^m z^n \qquad \text{Eqn. 2.10}$$

where $a_{i\lambda}$ are constants as yet unknown, and l, m, and n are a set of three non-negative integers such that $N \geq l+m+n$. For example, if N = 1, then the assumed function would have terms given by (l,m,n) = (0,0,0), (1,0,0), (0,1,0), and (0,0,1); a total of four terms. If N = ∞, this equation yields the exact solution. However, for computational purposes, up to 50 frequencies may be fit with reasonable accuracy using N = 10. Substituting the above equations into the Lagrangian yields:[8,35]

$$L = \int_V \left[\frac{1}{2} \sum_{i,i',\lambda,\lambda'} \delta_{ii'} \rho\omega^2 a_{i\lambda} a_{i'\lambda'} \Phi_\lambda \Phi_{\lambda'} - \frac{1}{2} \sum_{i,j,k,l,\lambda,\lambda'} c_{ijkl} a_{i\lambda} a_{i'\lambda'} \frac{\partial \Phi_\lambda}{\partial x_j} \frac{\partial \Phi_{\lambda'}}{\partial x_l} \right] dV \qquad \text{Eqn. 2.11}$$

where the summation on λ and λ' are from 1 to N. In matrix notation, this formula becomes:[8,35]

$$L = \frac{1}{2} \omega^2 \vec{a}^T \overleftrightarrow{E} \vec{a} - \frac{1}{2} \vec{a}^T \overleftrightarrow{\Gamma} \vec{a} \qquad \text{Eqn. 2.12}$$

Where matrices E and Γ have the following elements:

$$E_{\lambda i \lambda' i'} = \delta_{ii'} \int_V \Phi_\lambda \rho \Phi_{\lambda'} dV \qquad \text{Eqn. 2.13}$$

$$\Gamma_{\lambda i \lambda' i'} = \sum_{j,j'} c_{ijj'i'} \int_V \frac{\partial \Phi_\lambda}{\partial x_j} \frac{\partial \Phi_{\lambda'}}{\partial x_l} dV \qquad \text{Eqn. 2.14}$$

Equation 2.11 is a function of *a* only. Thus, varying the Eqn 2.11 arbitrarily on *V* yields equation:[8,35]

$$\delta L = \sum_{ij} \frac{\partial L}{\partial a_{ij}} \qquad \text{Eqn. 2.15}$$

Minimization of the Lagrangian, $\delta L = 0$, yields the following eigenvalue problem:[8,35]

$$\omega^2 \vec{\vec{E}} \vec{a} = \vec{\vec{\Gamma}} \vec{a} \qquad \text{Eqn. 2.16}$$

Solving this eigenvalue problem yields the eigenvalues, which correspond to the resonant frequencies of the object; and the eigenvectors, which correspond to its mode shapes.[8,35] Approximate solutions can be determined based approximated equations for displacement [u(t)] selected in Eqn. 2.10. Solutions exist for cylindrical, spherical, and parallelepiped objects.[8,35-37]

For example, the Specimen #1 (prior to the introduction of the defect) used in Section 3 of this thesis is a rectangular parallelepiped with dimensions 25.266 x 12.676 x 12.648 mm, and mass 31.963 grams. (Table 3.1) The frequencies for the first forty modes are identified from the RUS spectra (shown in Figure 2.4), and are listed in Appendix A, Tables A.2-A.13. Given the elastic constants for Specimen #1 (Table 3.1), calculation according to the method described above yields the first forty resonant frequencies, also listed in Appendix A, Tables A.2-A.7. The error between measured and calculated resonant frequencies for the first forty modes is an average of 0.16%, and the largest difference between any calculated and measured mode is less than 0.50%. For more details on the exact solution of a rectangular parallelepiped, consult Migliori.[8]

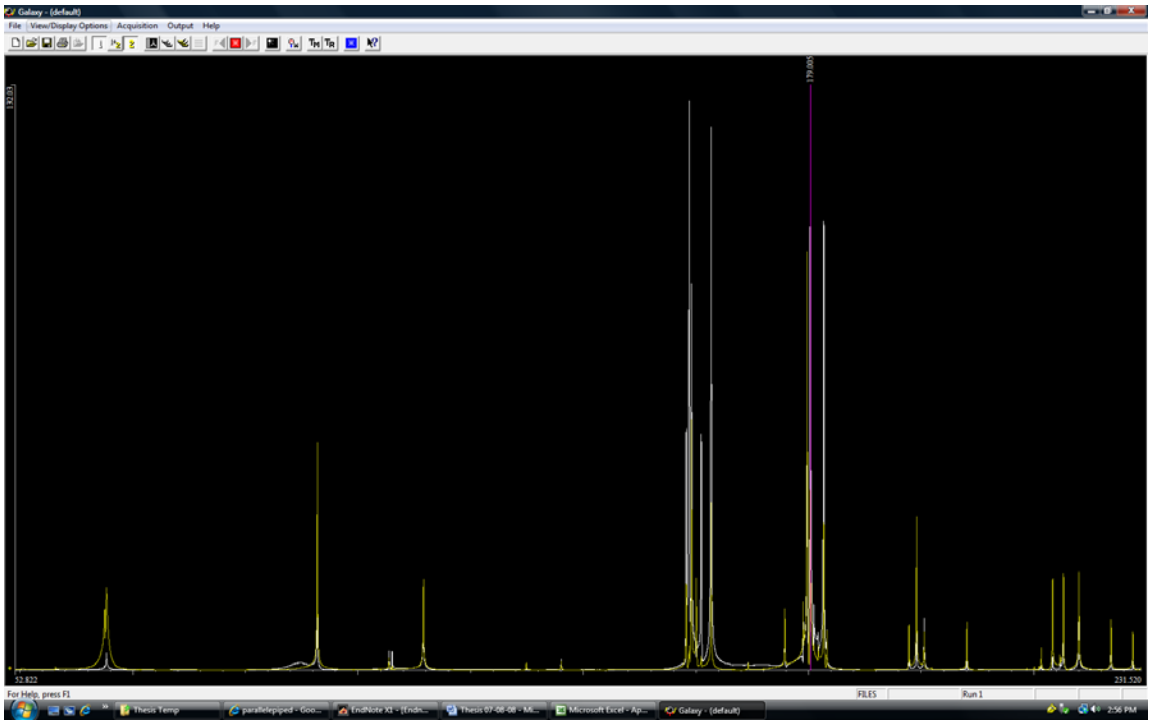

Figure 2.4 Resonant frequency spectra for Steel Cut Specimen #1.

At this point, simplifying assumptions may be applied based on the material properties. The previous section demonstrated how the stress, strain, and compliance tensors can be simplified if the material is assumed to be symmetric, crystalline, and isotropic. This is not always a requirement to solve the above equations, but it can simplify the problem.[8,35] Solutions exist for more general cases, including objects with less symmetry, and anisotropic objects.[35]

2.1.3. DETERMINING ELASTIC CONSTANTS

The eigenvalue problem in the equation above can be solved if the elastic properties of the material are known. Conversely, if the eigenvalues are known, the equation can be solved for the elastic constants. Since the eigenvalues correspond to the resonant frequencies, a resonant frequency spectrum such as that provided by RUS can

be used to identify the eigenvalues. Thus, a RUS spectrum can be used to determine the elastic constants of a material by calculating a frequency spectrum that best fits observed data. In fact, this is the most common use for the RUS method.[8,12,15,28,31,36]

This process has three steps: (1) assume some values for the elastic constants of the material, (2) use the assumed values to calculate the expected resonant frequencies, and (3) compare the calculated result to the RUS measurements. The above steps are repeated until sufficient agreement between calculated and measured values indicates the assumed elastic constants are correct.[8,35,36] Theoretical background for this process is presented below.

In order to solve for the elastic constants, it is only necessary to know as many resonant frequencies as there are independent terms in the compliance tensor. However, more accurate results are obtained by considering more resonant frequencies than strictly necessary. A "best-fit" solution for the elastic constants is then taken using some selected criteria. [8]

The Levenberg-Marquardt algorithm for minimization of the root mean squared (RMS) error between calculated and measured frequencies yields good results.[8] Starting with the equation:

$$\chi^2 = \sum_i^M (f_i^X - f_i^T)^2 \qquad \text{Eqn. 2.17}$$

where χ^2 is the root mean squared error between M calculated and measured frequencies. The process is as follows:

1. Assume an initial value for the elastic moduli. Assuming an isotropic, homogenous, cubic crystalline material, only two independent values are needed to determine all terms in the compliance tensor (see above).
2. Calculate the natural frequencies using the Lagrangian minimization process shown above.
3. Compare the calculated natural frequencies to the RUS frequency spectrum. Determine the RMS error using the equation above.

4. Assume new values for the elastic moduli, and repeat the process until a sufficiently small RMS error is achieved.[8]

Migliori recommends that the number of resonant frequencies used to determine the elastic constants be at least 5, and preferably 8-10, times the number of independent terms in the elastic tensor.[8] Using the above criteria, Migliori states that an RMS fit of 0.1-0.2% can be achieved.[8] In this work, RPModel v2.68b software developed by Quasar International was used to determine elastic constants of all examined material from their resonant spectra. The software is based on iterative calculations of the elastic constants until RMS minimized error is achieved as described above.

2.1.4 LIMITING ASSUMPTIONS

The RUS method for determining the natural frequency spectrum does have some limitations. Additional limitations come from the theoretical calculations used to determine resonant frequencies. Some of these limitations are discussed below.

The primary limiting assumption of the above calculations, and of the RUS method, is that the object is assumed to be in free-mode vibration. This means that the object is unconstrained, floating in space. The reason for this limitation is a constrained object will have a different resonance spectrum than an unconstrained object.[20,22]

Weight produces a constraint at the transducers, equivalent to a pinned connection. The heavier the object, the less the results match the theoretical results for free-mode vibration frequencies. In theory, the only unconstrained object is an object floating in space. In order to approximate free-mode vibration, the tested object should be very light. If the object is sufficiently light, it can be considered unconstrained for the purposes of the test.[8] Migliori recommends that the force between the transducer and the sample be no more than one gram weight equivalent.[8] He further states that experimental results indicate weights less than 0.1N result in less than 1% RMS error in frequencies.[8]

In addition, more massive (heavier) objects tend to have lower resonant frequencies. They also tend to respond less to a given input force. As a result, the resonant frequencies of more massive objects may get lost in signal noise, transducer sensitivity, and resonant frequencies of the testing equipment itself.[8] This points out a second limitation of RUS, which is that the lower limit of detectable resonant frequencies is a non-zero value.

The theoretical calculation method for determining resonant modes also has limitations. The first limitation is that only certain, simple geometries have theoretical solutions available for the Lagrangian method. At present, only solutions for spherical, cylindrical, and parallelepiped geometries are available, and all solutions assume homogeneous material properties throughout the object. Solutions to other simple shapes are possible, but the more complex the shape, the less useable the method.[8]

The second limitation of the Lagrangian method comes from the first: the sample is assumed to have very precise dimensions. Small changes in dimension can have a large affect on the resulting resonant frequencies. While this allows the use of RUS to identify the presence of tiny defects in the material, it requires a high degree of precision in preparing samples for use. Migliori suggests that all dimensional errors combined should not be greater than the level of accuracy of the results. He suggests that dimensions be precise within 0.1%, including parallelism and perpendicularity of faces.[8]

The RUS method can be used to determine elastic constants, even if no simplifying assumptions are made regarding the material. However, test materials are generally assumed to be isotropic. In the case where a material is not isotropic, the crystal structure and grain orientation must be known.[8]

However, regardless of all limitation, RUS is one of the most accurate techniques for determining elastic constants of materials.[34]

2.2 FINITE ELEMENT ANALYSIS

Previous sections of this thesis reviewed how to determine the resonant frequencies of a system (or object) by (a) solving the equations of motion, or (b) solving the energy equations using Lagrangian minimization. Both of these methods have limitations. Solution using equations of motion become too complex when applied to real systems, while Lagrange's equation is only applicable to geometries that can be approximated by continuous functions.[24] However, a third method exists for determining natural frequency, namely Finite Element Analysis (FEA). FEA solves the problems of complex geometries by reducing any object to a large number of simple building blocks. It is possible to approximate equations of motion for each block, and to solve them numerically and simultaneously using a computer code.[38-40]

2.2.1 FINITE ELEMENT ANALYSIS THEORY

All FEA problems begin with selection of a single element that will be propagated throughout the object. In three-dimensional FEA, this element is a typically either a four or six-sided polyhedron. The element is defined by nodes, points selected such that the behavior of the points will approximate the behavior of the element. Equations of motion are derived that describe the reaction of the element to loads and displacements at the nodes.[39,40] For a three-dimensional stress-strain problem (the problem that is used to determine, among other things, the natural frequencies), the equations of motion for a single element are:[39]

$$\begin{aligned}
\frac{\partial \sigma_{xx}}{\partial x} + \frac{\partial \sigma_{xy}}{\partial y} + \frac{\partial \sigma_{xz}}{\partial z} + f_x &= \rho \frac{\partial u_x}{\partial t^2} \\
\frac{\partial \sigma_{yx}}{\partial x} + \frac{\partial \sigma_{yy}}{\partial y} + \frac{\partial \sigma_{yz}}{\partial z} + f_y &= \rho \frac{\partial u_y}{\partial t^2} \\
\frac{\partial \sigma_{zx}}{\partial x} + \frac{\partial \sigma_{zy}}{\partial y} + \frac{\partial \sigma_{zz}}{\partial z} + f_z &= \rho \frac{\partial u_z}{\partial t^2}
\end{aligned} \qquad \text{Eqn. 2.18}$$

where x, y, and z are three orthogonal axes in Cartesian coordinate space, σ_{ij} is stress on the j^{th} face in the i^{th} direction, u_j is displacement in the j^{th} direction, f_j is force acting on the body in the j^{th} direction, ρ is density, and t is time.[39] Or, in matrix notation:[39]

$$D^T\sigma + f = \rho\ddot{u} \qquad \text{Eqn. 2.19}$$

where

$$\sigma = \begin{bmatrix} \sigma_{xx} \\ \sigma_{yy} \\ \sigma_{zz} \\ \sigma_{xy} \\ \sigma_{xz} \\ \sigma_{yz} \end{bmatrix}, \quad f = \begin{bmatrix} f_x \\ f_y \\ f_z \end{bmatrix}, \quad u = \begin{bmatrix} u_x \\ u_y \\ u_z \end{bmatrix} \qquad \text{Eqn. 2.20}$$

and D is defined as:

$$D = \begin{bmatrix} \frac{\partial}{\partial x} & & \\ & \frac{\partial}{\partial y} & \\ & & \frac{\partial}{\partial z} \\ \frac{\partial}{\partial z} & & \frac{\partial}{\partial x} \\ & \frac{\partial}{\partial z} & \frac{\partial}{\partial y} \\ \frac{\partial}{\partial y} & \frac{\partial}{\partial x} & \end{bmatrix} \qquad \text{Eqn. 2.21}$$

Further, if follows from the relationship between strain and displacement that:[39]

$$\varepsilon = Du \qquad \text{Eqn. 2.22}$$

where ε_{ij} is strain on the j^{th} face in the i^{th} direction, represented by the strain tensor ε:

$$\varepsilon = \begin{bmatrix} \varepsilon_{xx} \\ \varepsilon_{yy} \\ \varepsilon_{zz} \\ 2\varepsilon_{xz} \\ 2\varepsilon_{yz} \\ 2\varepsilon_{xy} \end{bmatrix} \qquad \text{Eqn. 2.23}$$

The form of the solution for relative displacement of each node, u_j, is assumed by selecting a function to approximate it. Typically, the function selected is an n^{th} order polynomial of x, y, and z; although other approximations may be used.[38-40] Taking Hooke's Law for a linear-elastic solid (Eqn. 2.1) and using functions for relative displacement determined by the shape of the element, this equation can be expressed in the standard form for elastic finite element problems:[39]

$$M^e \ddot{\Delta}^e + K^e \dot{\Delta}^e = F^e + Q^e \qquad \text{Eqn. 2.24}$$

where M^e (the element mass matrix), K^e (the element stiffness matrix), F^e (the element load vector), and Q^e (a vector of internal forces) are all integrals of polynomial functions of x, y, and z.[39] The variable Δ is a vector of displacements in nodal points.[38-40] Consult Reddy, Gupta et al, or Ross (references in appendix) for a full explanation regarding selection of polynomial functions of displacement. The matrices and vectors for individual elements are combined into global matrices and vectors, so that the final equation becomes:[38-40]

$$M\ddot{\Delta} + K\dot{\Delta} = F + Q \qquad \text{Eqn. 2.25}$$

where M, K, F, Q, and Δ are global aggregates of the individual element matrices listed above. For the purposes of free-body modal analysis, which approximates RUS results, the vector F is set equal to zero.[8,38-40] Assuming that displacement is a time-dependant function:[38-40]

$$\Delta(t) = \Delta_0 e^{iwt} \qquad \text{Eqn. 2.26}$$

where ω is frequency. This yields the resulting equation:[39]

$$(\omega^2 M + K)\Delta_0 = Q \qquad \text{Eqn. 2.27}$$

This is an eigenvalue/eigenvector problem, where the eigenvalues correspond to the natural frequencies, and the eigenvectors to the mode shapes.[38-40]

2.2.2 NUMERICAL SOLUTION

Since the size of the global stiffness and damping matrices depends on the number of nodes, which is a factor of the number of elements, these matrices are generally very large (in the analysis below, the stiffness (K) matrices were never smaller than 1,000 x 1,000, and usually much, much larger). Solution by hand is impractical.[40] Computerized numerical solution is possible, however. Various methods of numerical solution are available. The ABAQUS FEA program uses either the blocked Lanczos method or the subspace iteration method to determine the eigenvalues.[41]

The blocked Lanczos method converts the standard eigenvalue problem into a problem of a single matrix by using Cholesky decomposition on the stiffness matrix K.[38] It then uses the Householder and quarter-rotation (QR) methods to triangularize the matrix.[41] For a full explanation of the Lanczos and block Lanczos methods, see Gupta et al.[38] For a full explanation of the Hourseholder, QR, and subspace iteration method, see Gupta et al, or documentation for any commercial FEA program.[38,41]

In this thesis, Dassault Systems SolidWorks Education Edition SP4.0 2007 and CosmosWorks SP3.1 2004 were used for all finite element analyses.

2.2.3 ADVANTAGES AND LIMITATIONS OF FEA

The most important advantage of using finite element analysis to determine natural frequency is that the analyzed system is represented by many small building blocks of arbitrary geometry and physical properties, which can be described using numerical approximation.[39,40] Thus, the behavior of non-homogeneous objects with complex geometries can be approximated by creating a model of the object using these small building blocks.[39,40] In other words, it is possible to use FEA to approximately determine the natural frequencies of a wide range of objects with different geometries and physical properties. In contrast, the Lagrangian method has solutions for only a few geometries, and requires homogeneity of material.[20]

This advantage comes at a price. The computing requirements for finite element analysis are many orders of magnitude greater than those of the Lagrangian method.[39] However, modern computers are capable of handling this level of computation and producing results within 0.1% of RUS measured frequencies.

A second limitation of FEA is related to the first: elastic constants cannot be calculated using known resonant frequencies. The Levenberg-Marquardt algorithm, explained in the previous section, worked only because the Lagrangian method is computationally non-demanding. Modern computers can complete multiple iterations of the Lagrangian quickly. However, FEA computational requirements are much higher. It is not practical, at this time, to use iterative processes to determine elastic constants. Other solutions, while possible, are not implemented in any commercially available FEA code.

Lastly, the FEA frequency solution assumes free-body vibration.[39] While this is generally a good assumption, it means that FEA analysis does not include any real displacement results. Calculated mode shapes show displacement off the object relative to itself. Actual displacement will depend on initial conditions and excitation forces.[39,40] As will become evident later, this limitation sets limits on the ability of FEA to predict measured resonant frequencies. It is important to note that the other computational methods outlined above also share this limitation.[20]

3. STEEL BAR WITH NOTCH

This Section contains experimental results and FEA for the steel bar samples with the cut notch. The effect of the defect position and size on the RUS spectrum was analyzed and discussed in more detail.

3.1 SAMPLES

Examined specimens were standard 4140 steel 12.6 x 12.6 x 26.2 bars with cut notches, Figure 3.1. A cut was made partway through each specimen, at some random location and random depth. Locations and depth of the cuts are summarized in Table 3.1 and on Figure 3.1. A 0.75 mm thick diamond blade width produced a cut approximately 1.0 mm in width. The dimensions of the notch were measured using an optical microscope. Resonant spectra of the specimens were collected before and after cutting the notches.

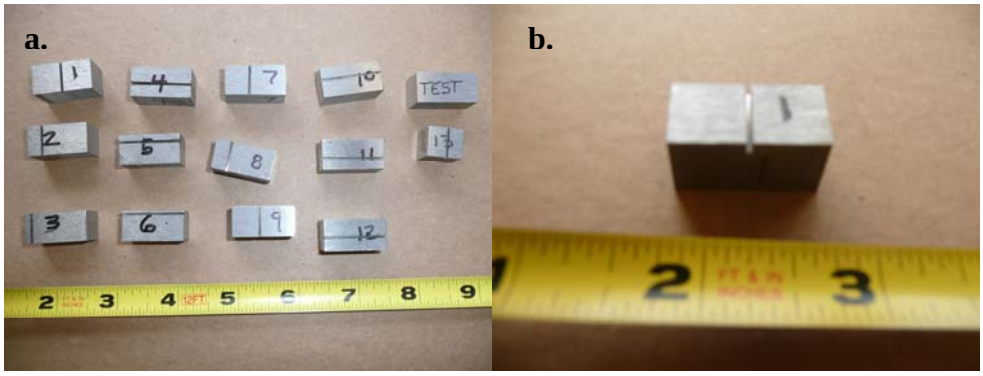

Figure 3.1 (a) Prepared specimens after introduction of 1 mm cut. (b) Close-up of Specimen #1

In Table 3.1, the X, Y, and Z dimensions correspond to the length, width, and height of the specimens, and to the X, Y, and Z axes in SolidWorks/CosmosWorks FEA

software. X and Y axes shown in Figure 3.2. The initial weight is the mass of the sample prior to cutting. The Cut Location Plane is the plane of the cut, and the Axis is the axis parallel to the cut. The Distance from Axis is the distance between the edge of the specimen and the centerline of the notch. The Depth and Width of the cut are specified, and all cuts extend the full length of the specimen.

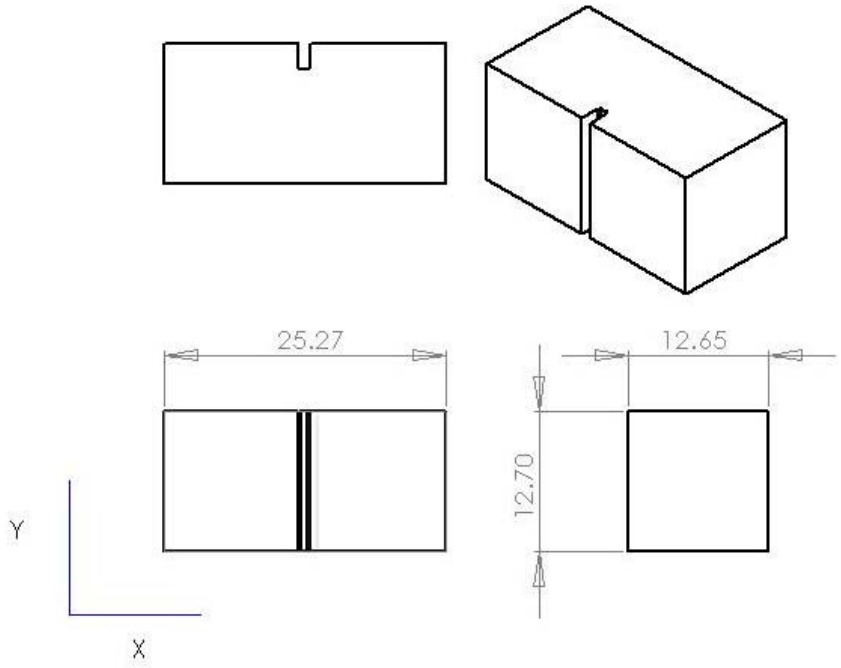

Figure 3.2 Schematic of samples. Dimensions in mm. X and Y axes shown (Z is out-of-plane).

Table 3.1 Dimensions of cut steel specimens.

	Dimensions				Elastic Constants				Cut Location				
Sample	X (mm)	Y (mm)	Z (mm)	Initial Weight (g)	C11 (GPa)	C44 (GPa)	Young's Modulus (GPa)	Poisson's Ratio	Plane	Axis	Distance from Axis (mm)	Depth (mm)	Width (mm)
1	25.27	12.68	12.65	31.96	273.6	83.0	212.8	0.282	Y-Z	Y	12.60	2.35	1.05
2	25.25	12.68	12.66	31.92	273.7	82.9	212.6	0.283	Y-Z	Y	6.25	2.35	1.05
3	25.26	12.68	12.65	31.95	274.2	83.0	213.0	0.283	Y-Z	Y	2.68	2.35	1.05
4	25.36	12.65	12.67	32.04	272.6	83.0	212.6	0.281	X-Y	X	5.55	2.35	1.05
5	25.25	12.65	12.67	31.94	273.2	83.0	212.8	0.282	X-Y	X	3.08	2.35	1.05
6	25.21	12.65	12.68	31.90	274.2	82.9	212.8	0.283	X-Y	X	1.51	2.35	1.05
7	25.30	12.68	12.65						Y-Z	Y	10.30	0.71	1.00
8	24.88	12.68	12.65						Y-Z	Y	6.58	1.20	1.00
9	25.34	12.64	12.68						Y-Z	Y	11.15	2.00	1.00
10	25.22	12.65	12.68						X-Y	X	5.30	0.67	0.90
11	25.30	12.65	12.68						X-Y	X	4.72	0.87	0.90
12	25.48	12.65	12.67						X-Y	X	5.53	1.35	0.90

3.2 RESONANT SPECTRA OF THE SAMPLES

The resonant frequency spectrum of each specimen was measured using resonant ultrasound spectroscopy equipment (Galaxy Quasar Model QRI-2600) in the tripod set up as shown in Figure 3.3.

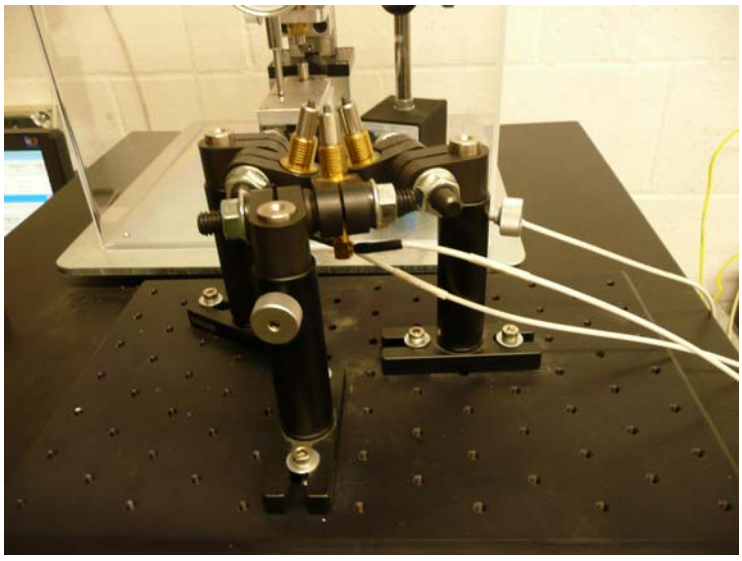

Figure 3.3 Photograph of the tripod transducer RUS setup.

The resonant frequency spectra of all the specimens were collected using RUS before cutting the notches. Test results were fitted to obtain elastic constants, namely Young's modulus, (E), and Poisson's ratio, (υ) of the material using Galaxy RPModel v2.68b software based on the Levenberg-Marquardt algorithm and Lagrangian minimization, as it is explained in Section 2.2. The Young's modulus of the 4140 steel was found to be 212.8 ± 0.16 GPa, while Poisson's ratio was calculated to be 0.2824 ± 0.0008, Table 3.1. These values are in good agreement with the published information. The first 40 eigenvalues (resonant frequencies) for all six samples prior to cutting the notches are given in Tables A.2-A.7 in Appendix A.

Resonant frequencies of the samples with the cuts that were described in Table 3.1 are also collected. Tables A.2-A.7 in Appendix A list the first forty modes for Samples 1-6 as determined by RUS. The first seven modes for samples 7-12 as measured by RUS are shown in Tables A.8-A.13 in Appendix A.

3.3 FEA MODEL

A finite element model of each specimen was constructed using the measured dimensions of the specimens and the calculated elastic constants. A frequency analysis was performed on the finite element model using commercially available FEM software (Dassault Systems SolidWorks Education Edition SP4.0 2007 and CosmosWorks SP3.1 2004) to determine the predicted resonant frequency spectra. Results of the finite element frequency analysis for the specimens prior to the cut were compared to both the frequency spectrum as determined by RUS and the frequency spectrum as determined by Lagrangian minimization, Appendix A, Tables A.2-A.7. The average magnitude of the error between any two methods was about 0.3%, with a standard deviation of ±0.2%.

The finite element model was then modified to determine how modal frequency varied based on the depth and location of the cut. A total of six cut locations were modeled, three on each face of the specimen, Table 3.1. At each location, the cut depth was varied from 0.1 mm to 2.3 mm (corresponding to about 20% of specimen thickness). This resulted in a total of about 140 different finite element models. Figure 3.4 shows a sample of the results for Specimen 1.

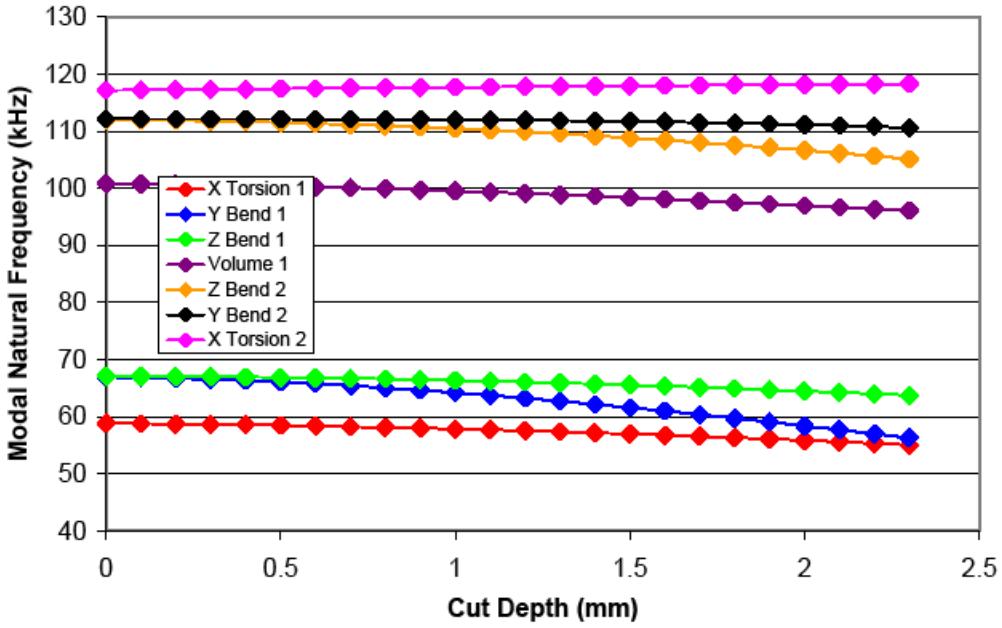

Figure 3.4 Specimen 1 resonant frequencies from FEA.

The resonant frequencies from the finite element modes were compared to six specimens with cuts in identical locations to the finite element models (Specimens 1-6). The average error between measured and predicted resonant frequency (average of first forty modes on six specimens) was 0.63%, with a standard deviation of 0.7%. (Appendix A). In no case was the difference between measured and predicted resonant frequency greater than 10%. These results validate the use of FEA to predict resonant frequency, and show substantial increase in accuracy compared to previous studies.[14,15,19]

For each of the seventy cases, the resonant frequency spectrum was determined using finite element analysis. Frequency spectra of models that included a cut were compared to the original modal frequencies of the model with no cut to determine the change in modal resonant frequency cause by the cut. Change in modal resonant frequency vs. cut depth can be found in Appendix A, Tables A.14-A.19. The frequency change is calculated as:

$$Change = \frac{f_{Cut} - f_{Original}}{f_{Original}} \qquad \text{Eqn. 3.1}$$

where f is the resonant frequency.

The change in frequency associated with each vibration mode was analyzed as a function of cut depth and location to determine eventual existence of a certain pattern. Modes were identified via visual analysis of the mode shape predicted by the nodal eigenvectors. For example, for Specimen 1 (defect parallel to Y axis, located approximately in the center of the sample), first seven modes, and modes shapes are shown in Figures 3.5-3.11. It has to be emphasized that particular vibration modes are referred to by name wherever practical in Figures 3.5 – 3.11, and for the rest of this thesis. For example, the first bending mode about the Y axis will be referred to as Y Bend 1, or sometimes Y1. Where it is not practical to refer to a mode by name, they are referred to by number, with the numbering system matching the sequential order of frequencies in the original specimen (prior to addition of any defect).

Note: All figures from SolidWorks are ¾ view, with (roughly) Y axis vertical, X axis horizontal, and Z axis out-of-plane

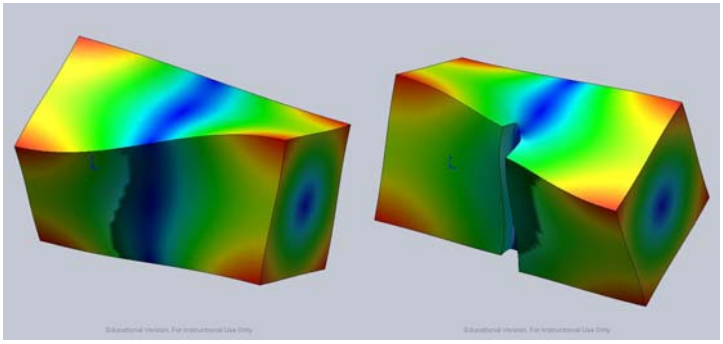

Figure 3.5 First torsional mode about X axis (X Torsion 1) for samples without (left) and with (right) the notch.

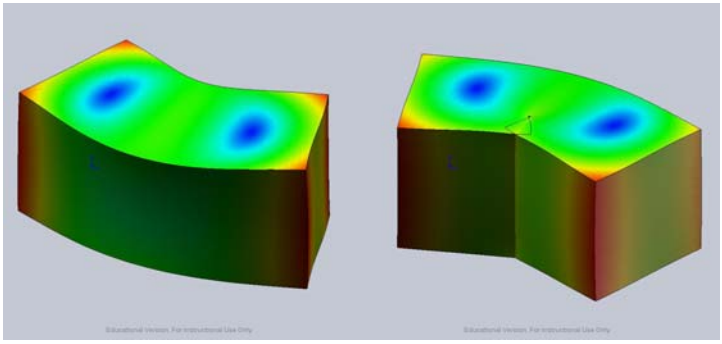

Figure 3.6 First bending mode about Y axis (Y Bend 1) for samples without (left) and with (right) the notch.

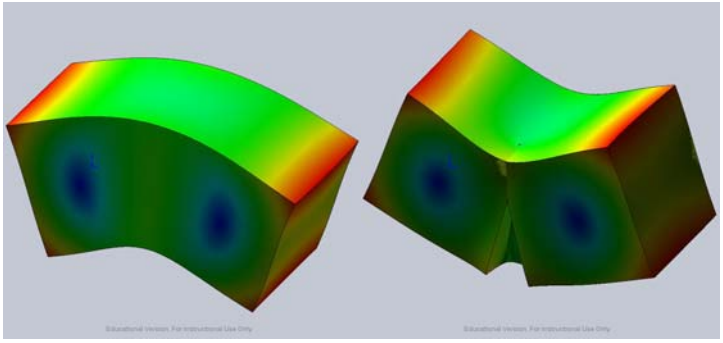

Figure 3.7 First bending mode about Z axis (Z Bend 1) for samples without (left) and with (right) the notch.

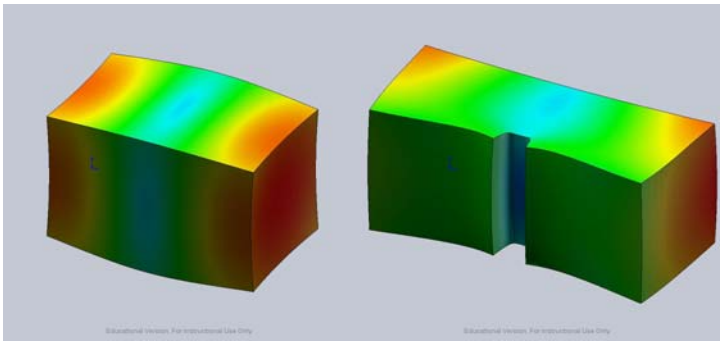

Figure 3.8 First volumetric mode (Volume 1) for samples without (left) and with (right) the notch.

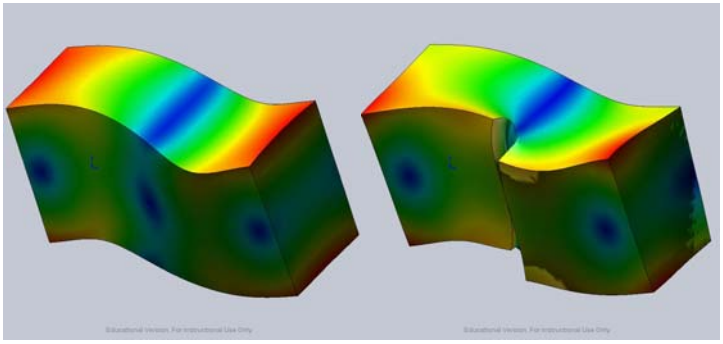

Figure 3.9 Second bending mode about Z axis (Z Bend 2) for samples without (left) and with (right) the notch.

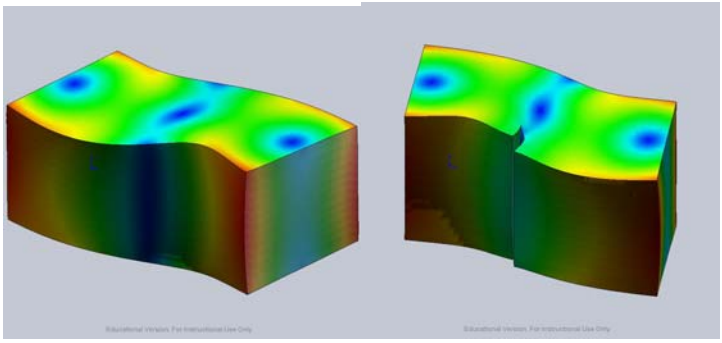

Figure 3.10 Second bending mode about Y axis (Y Bend 2) for samples without (left) and with (right) the notch.

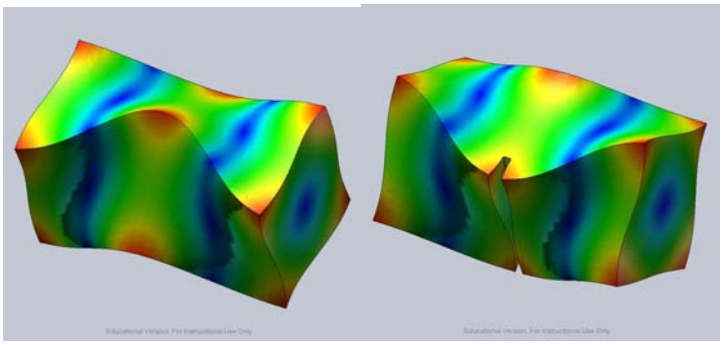

Figure 3.11 Second torsional mode about X axis (X Torsion 2) for samples without (left) and with (right) the notch.

Initially, the frequency shift analysis included over forty modes. For several reasons, it was determined that the seven lowest-order modes provided the best frequency data. Firstly, for most cut locations and cut depths, the first seven modes had relatively large changes in frequency; greater than one percent change in frequency, and thus greater than the average error between frequencies determined by RUS and FEA. While some higher-order modes also showed large changes in frequency for particular cut locations, few of them showed large changes in frequency for all cut locations. However, those modes were not taken into account, since higher-order modes were difficult to identify in finite element frequency spectra. Many higher-order modes had similar mode shapes, and tended to alter greatly in appearance as depth of the cut increased. Once the depth of the cut was greater than one percent of specimen thickness, visual inspection of mode shapes was inadequate for determining the identity of modes; unlike in the case of lower-order modes.

Lastly, higher-order modes tended to group into clusters within tight frequency ranges. As cut depth increased, certain modes shifted more than others. Frequency shifts of higher-order modes approximated third or fourth order equations. Plots of frequency vs. cut dept often showed modes crossing and re-crossing each other as cut depth increased. As a result, it was not possible to match a particular resonant frequency with a particular mode using relative position in the frequency spectra.

Figures 3.12 – 3.17 show the frequency shift of the first seven modes as a function of cut depth, where depth is expressed as a percentage of specimen thickness, while Figures 3.18-3.23 show the frequency shift of the first seven modes as a function of cut location, where cut location is expresses as a percentage of the length of the specimen, measured from the end. Change in resonant frequency of each mode is expressed as a percentage of the resonant frequency of the mode prior to any cut being made in the specimen, Eqn. 3.1.

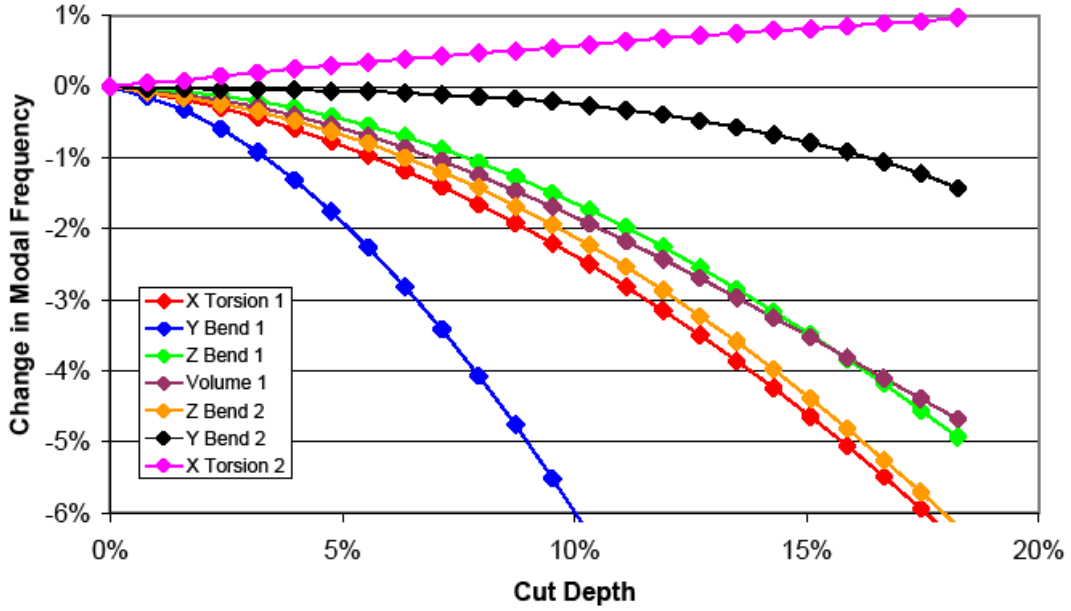

Figure 3.12 Modal frequency vs. cut depth for specimen with defect located at 50% and parallel to Y axis.

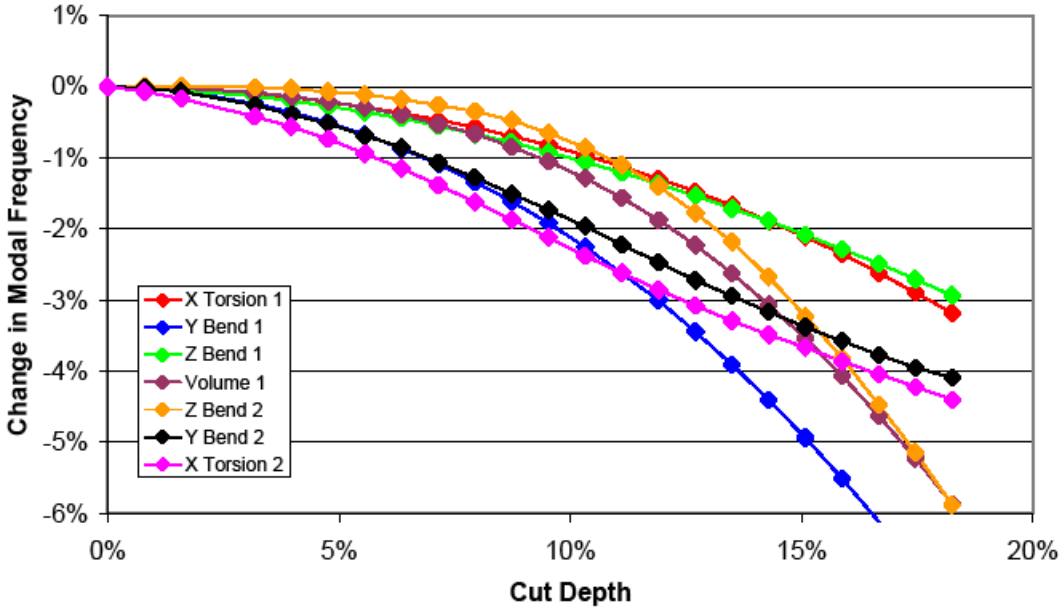

Figure 3.13 Modal frequency vs. cut depth for specimen with defect located at 25% and parallel to Y axis.

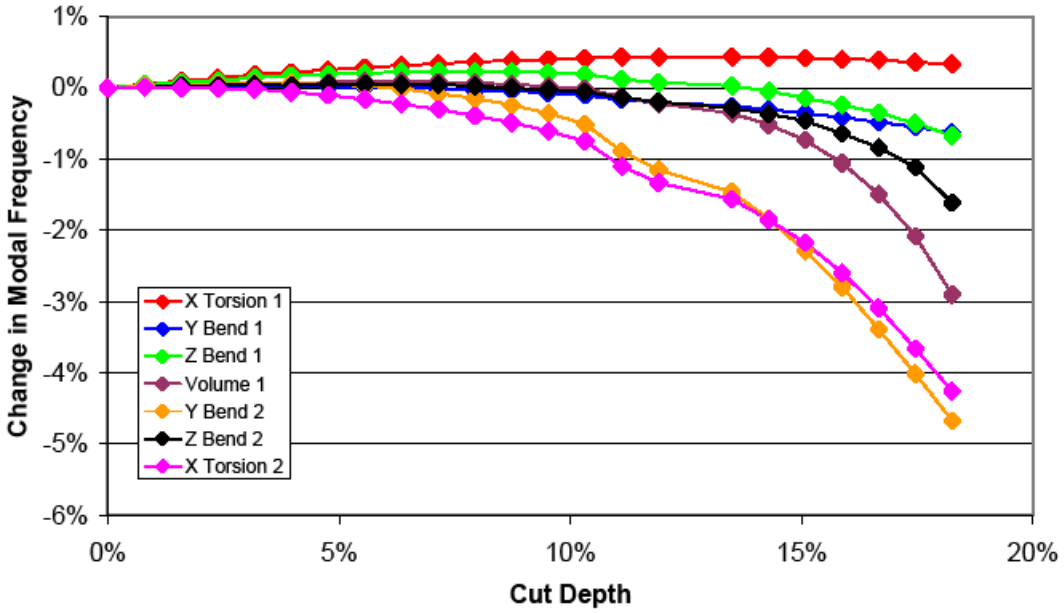

Figure 3.14 Modal frequency vs. cut depth for specimen with defect located at 11% and parallel to Y axis.

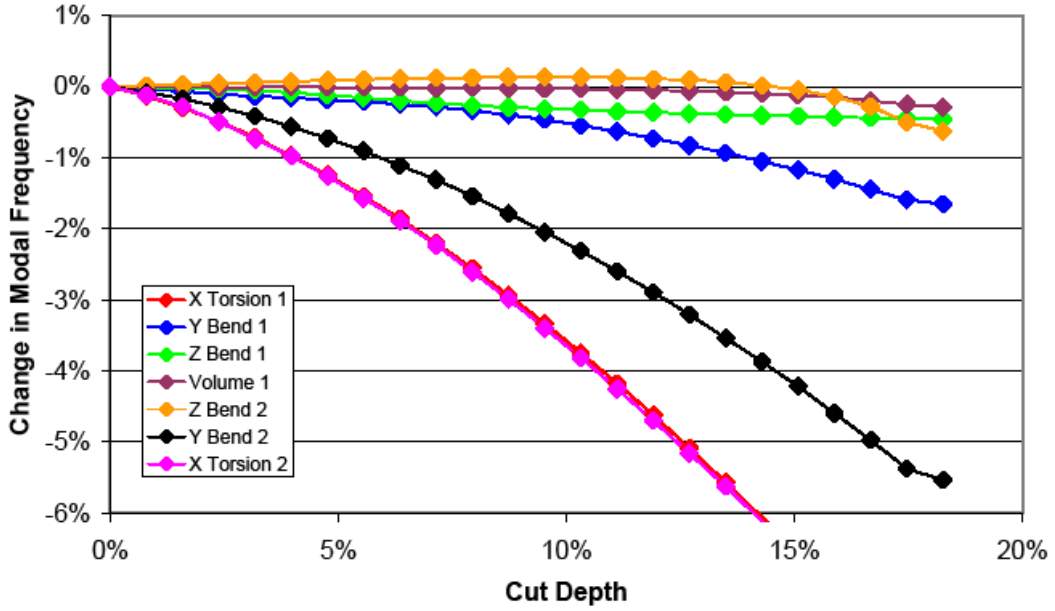

Figure 3.15 Modal frequency vs. cut depth for specimen with defect located at 44% and parallel to X axis.

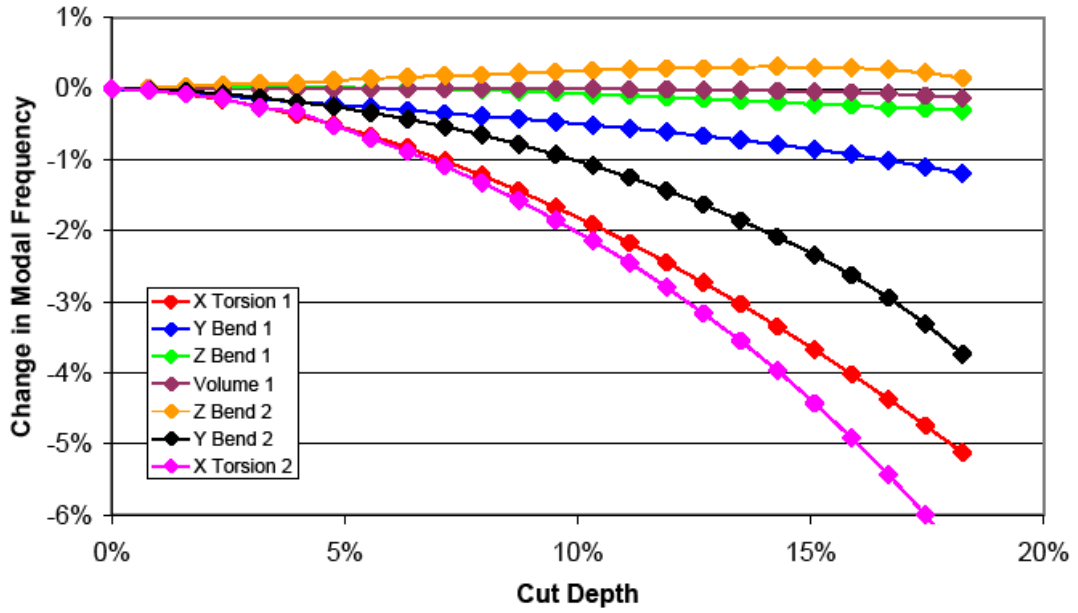

Figure 3.16 Modal frequency vs. cut depth for specimen with defect located at 24% and parallel to X axis.

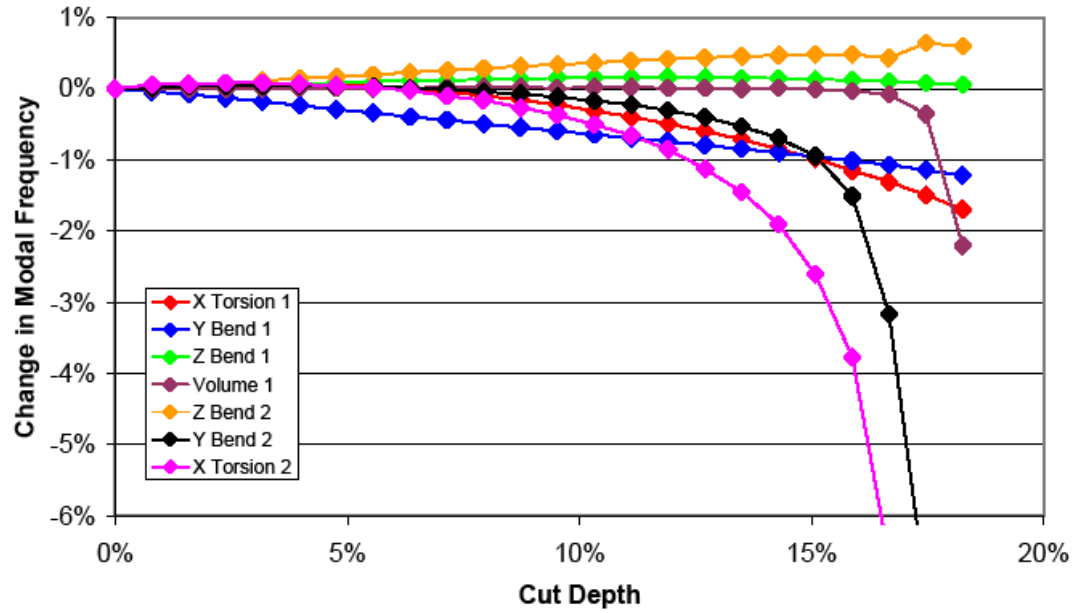

Figure 3.17 Modal frequency vs. cut depth for specimen with defect located at 12% and parallel to X axis.

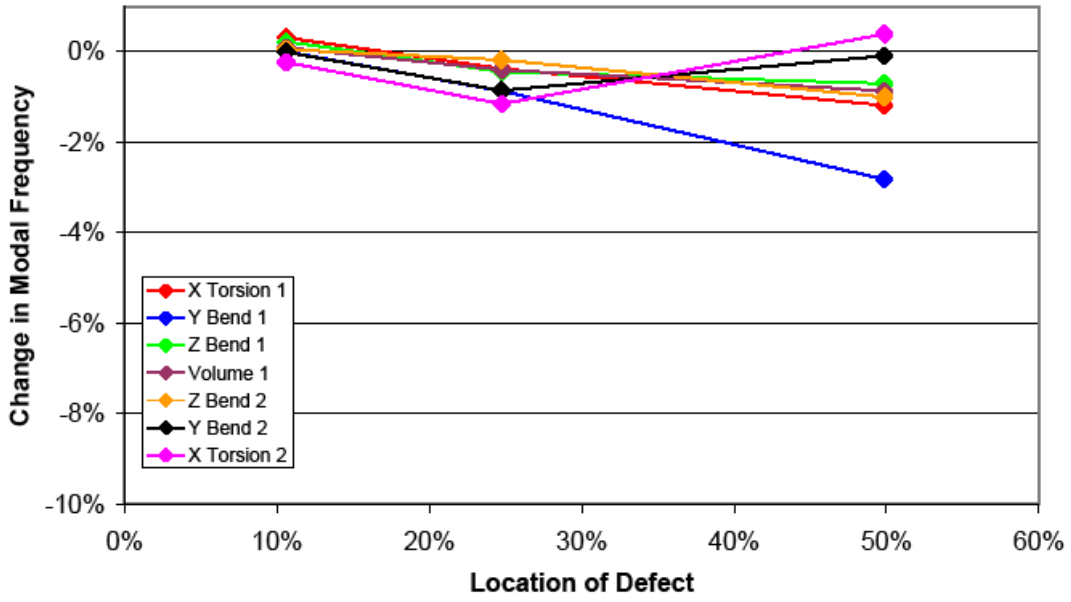

Figure 3.18 Modal frequency vs. cut location for specimen with defect of 6% depth and parallel to Y axis.

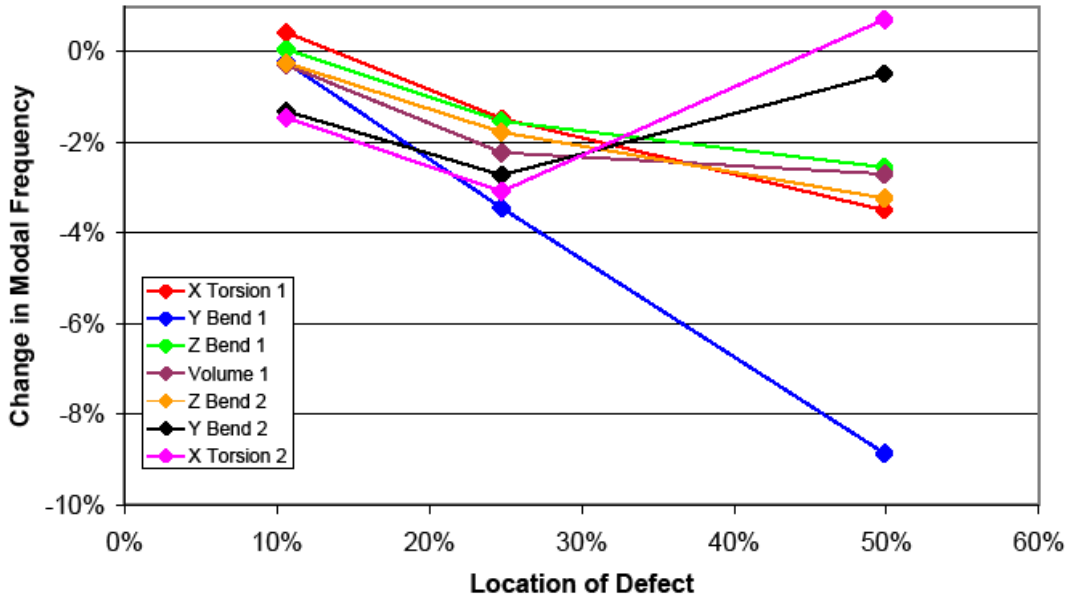

Figure 3.19 Modal frequency vs. cut location for specimen with defect of 12% depth and parallel to Y axis.

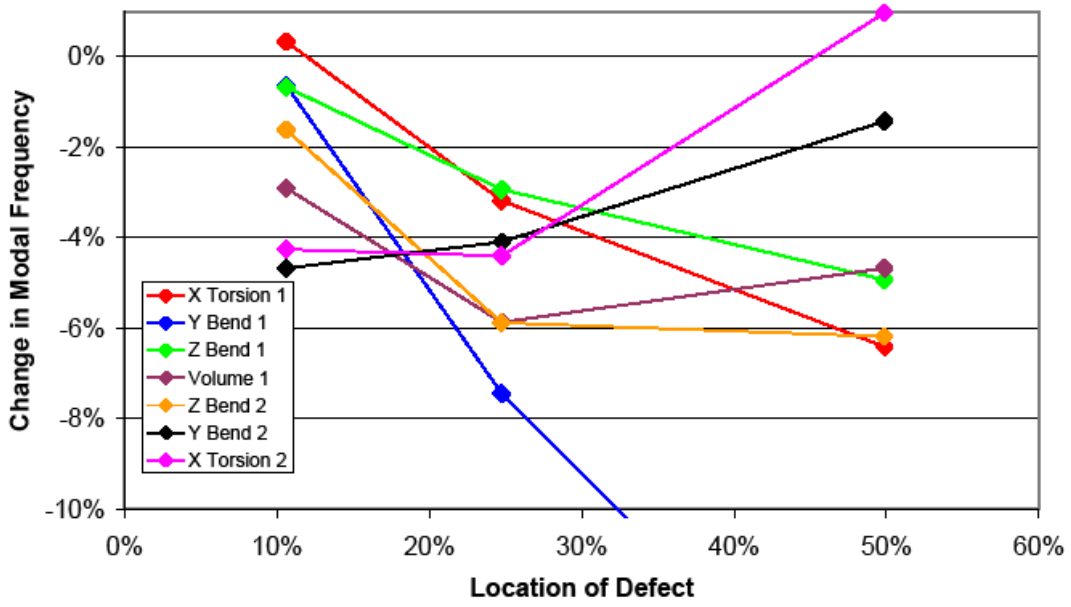

Figure 3.20 Modal frequency vs. cut location for specimen with defect of 18% depth and parallel to Y axis.

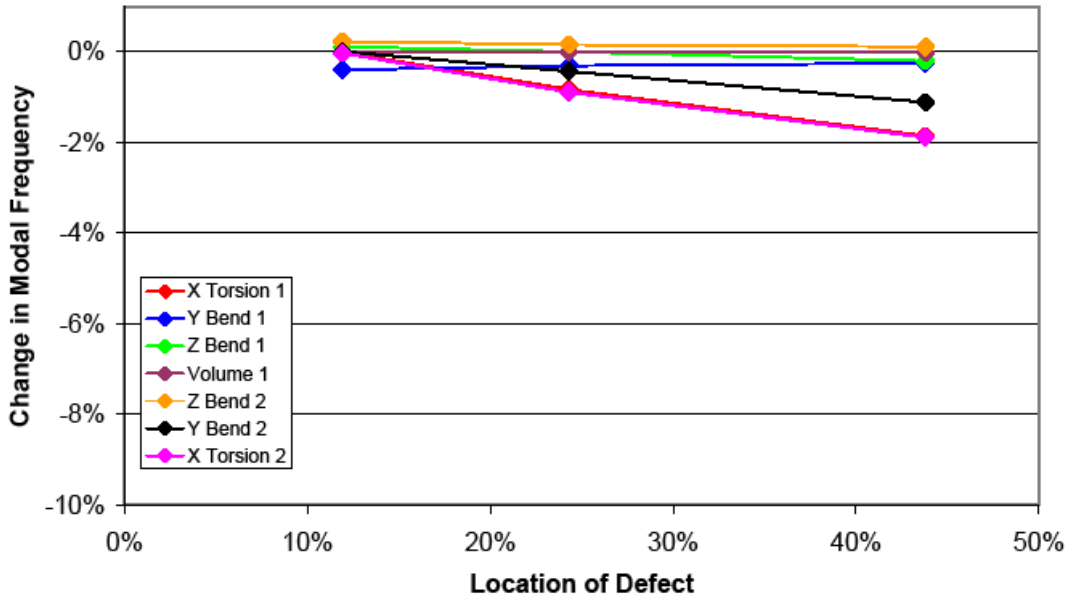

Figure 3.21 Modal frequency vs. cut location for specimen with defect of 6% depth and parallel to X axis.

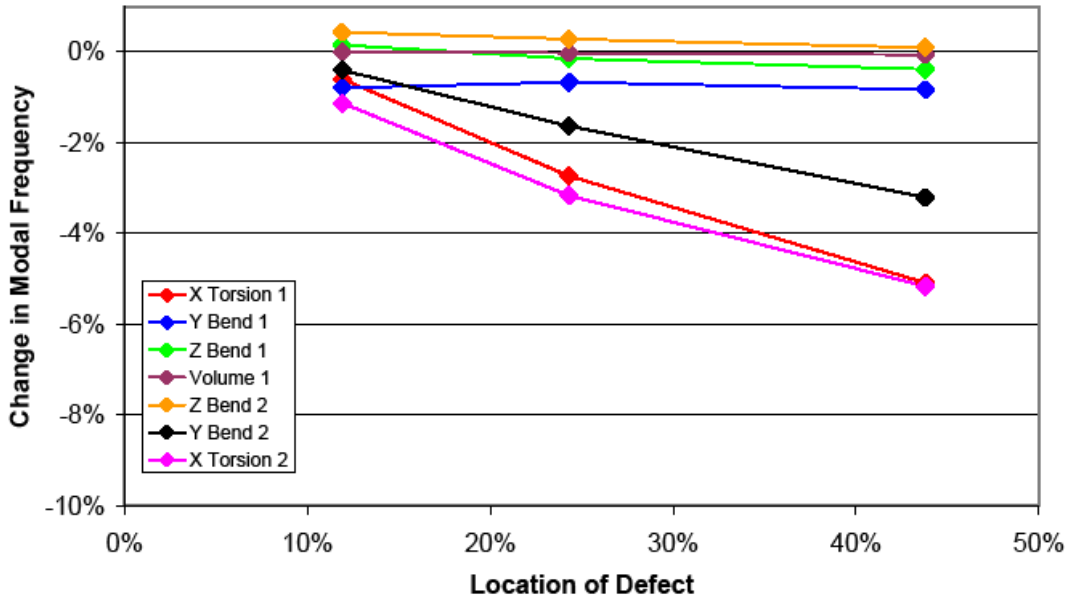

Figure 3.22 Modal frequency vs. cut location for specimen with defect of 12% depth and parallel to X axis.

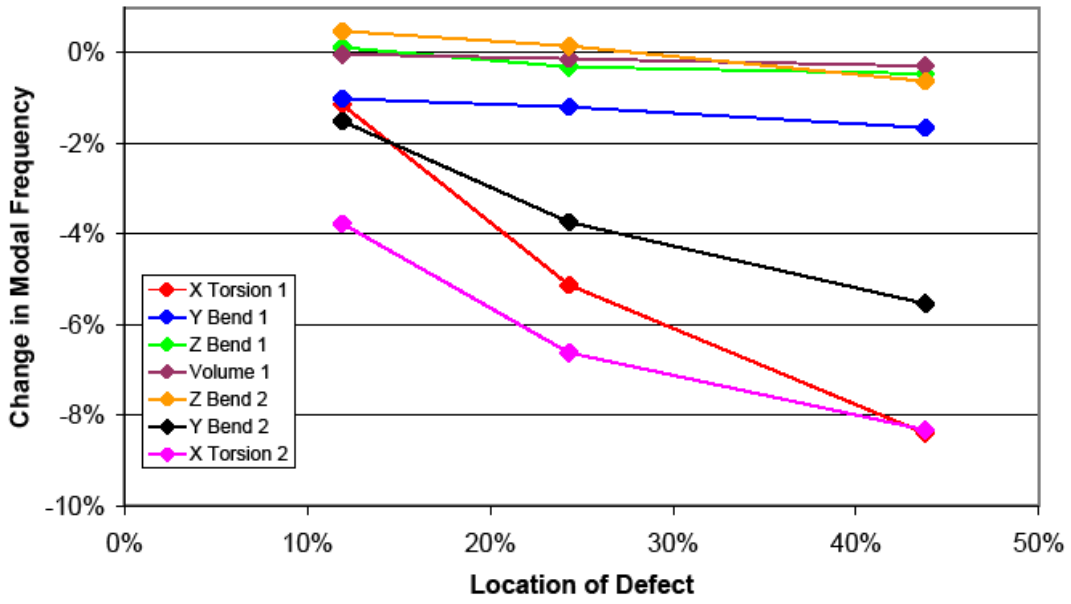

Figure 3.23 Modal frequency vs. cut location for specimen with defect of 18% depth and parallel to X axis.

3.4 DEFECT ASSESSMENT

As expected, the results of both the RUS measurements and the FEA models demonstrate that resonant frequency is affected by the presence of a defect. Since certain modes are more sensitive to certain types of defects (see Section 1 and 2), it should be possible to get information about a defect in a specimen by analyzing the change in the resonant frequencies of the specimen. To that end, the frequency shift data from the finite element models (Tables A.14-A.19 in Appendix A) were analyzed to determine if a relationship exists between shift in modal resonant frequency and the position and depth of the cut. After testing several different fitting functions, it was found that the following function for frequency shift of n-th mode provides the best results:

$$\Delta F_n = C_{0n} + C_{1n}D + C_{2n}DL + C_{3n}DL^2 + C_{4n}D^2 + C_{5n}D^2L + C_{6n}D^2L^2 \quad \text{Eqn. 3.2}$$

where D is depth of the defect expresses as a percent of specimen thickness, and L is location of the defect expresses as a percent of the specimen length. Change in modal resonant frequency (ΔF) is expressed as a percent of the modal resonant frequency of the specimen with no defect, as given by Equation 3.1. Higher-order functions of L and D were tested, but it was found that a second-order function produced results with the lowest average error between measured and predicted values.

Regression analysis was performed on the modal frequencies determined from by FEA to determine the constants C_{in} from Equation 3.2 for each of the first seven modes, and the results are shown in Table 3.2.

Table 3.2 Regression analysis results.

Defect Parallel to Y Axis

i	n	X Torsion 1 1	Y Bend 1 2	Z Bend 1 3	Volume 1 4	Z Bend 2 5	Y Bend 2 6	X Torsion 2 7
0		-0.0001	0.0004	0.0000	-0.0014	-0.0016	-0.0005	0.0001
1	**D**	0.1156	-0.0525	0.2010	0.1585	-0.0809	0.5304	0.4647
2	**DL**	-0.4427	0.8397	-1.3433	0.1450	2.1488	-4.0803	-4.3511
3	**DL2**	0.0291	-2.4471	1.7720	-1.1321	-4.0829	6.1974	7.1071
4	**D2**	0.4995	1.8767	-0.5560	-0.0993	1.6625	-3.9127	-2.9982
5	**D2L**	-8.2134	-22.4447	-0.1125	-16.1471	-28.6781	18.6853	14.7971
6	**D2L2**	8.8257	23.1135	-2.9632	28.1882	43.9760	-24.1047	-17.8407

Defect Parallel to X Axis

i	n	X Torsion 1 1	Y Bend 1 2	Z Bend 1 3	Volume 1 4	Z Bend 2 5	Y Bend 2 6	X Torsion 2 7
0		0.0006	-0.0002	0.0002	-0.0002	-0.0005	-0.0004	-0.0004
1	**D**	0.1322	-0.0814	0.0281	0.0117	0.0698	0.1212	0.3647
2	**DL**	-0.8313	0.2530	-0.0305	-0.0260	-0.1874	-0.3202	-1.7777
3	**DL2**	0.0624	-0.1729	-0.2771	0.0671	0.4170	-0.4080	1.0408
4	**D2**	0.0958	0.0028	0.0917	-0.0595	-0.1569	-0.4979	-2.4870
5	**D2L**	-7.6890	-0.2735	-1.9504	0.0867	0.7157	-4.3141	2.1964
6	**D2L2**	9.5363	-1.9055	4.3070	-0.6275	-3.3941	6.2430	0.4288

A program was created that determined L and D using a known ΔF's for the first seven modes. The program code can be found in Appendix D. Essentially, the program assumes a value of L and D, and then calculates ΔF for one or more modes based on the constants C_{in} input by the user. The program repeats this process iteratively for a large number of L and D values, then chooses the best fit L and D based on a least squares error between ΔF calculated and ΔF actual. If at least two resonant modes are considered in the analysis, the program should converge on a solution of L and D that approximates the value of ΔF for both modes.

While the constants (C_{in}) are determined using the FEA frequency data, L and D can be determined from any set of modal frequencies. Therefore, the frequency measured by RUS for samples 112 (Table 3.1) were input into the program to estimate L and D for each specimen. Estimates of L and D were compared to actual location and depth of the cuts in the specimens, and the results of this analysis using the first three modes, and using the first seven resonant modes, are presented in Table 3.3. Results for each of the twelve specimens are presented individually, and the average results are given as Average Error (Actual).

The modal frequencies calculated using FEA were also input into the program to estimate L and D for each finite element model. Estimates of L and D were compared to the values of L and D used in the FEM model. The results of this analysis are presented in Table 3.3. Results for the approximately 140 finite element models are not shown, but the average results are given as Average Error (FEM).

Table 3.3 Errors in predicted position (L) and depth (D) for 3 modes and 7 modes.

Cut Parallel to Y Axis

Actual		**Predicted Using First Seven Modes**				**Predicted Using First 3 Modes**			
				Error				**Error**	
Depth	**Location**	**Depth**	**Location**	**Depth**	**Location**	**Depth**	**Location**	**Depth**	**Location**
18.6%	**50%**	18.1%	50.0%	0.5%	0.1%	18.3%	49.0%	0.2%	0.9%
18.6%	**25%**	18.5%	25.0%	0.0%	0.2%	18.8%	24.5%	0.2%	0.3%
18.6%	**11%**	19.6%	10.5%	1.0%	0.1%	19.6%	10.5%	1.0%	0.1%
5.6%	**41%**	5.4%	45.0%	0.2%	4.3%	5.8%	43.0%	0.2%	2.3%
9.5%	**26%**	9.2%	28.5%	0.3%	2.1%	10.0%	26.0%	0.5%	0.4%
15.8%	**44%**	15.4%	48.5%	0.4%	4.5%	15.4%	47.5%	0.4%	3.5%
		Average Error (FEM)		0.4%	1.5%			0.4%	1.3%
		Average Error (Actual)		0.4%	1.9%			0.4%	1.2%

Cut Parallel to X Axis

Actual		**Predicted Using First Seven Modes**				**Predicted Using First 3 Modes**			
				Error				**Error**	
Depth	**Location**	**Depth**	**Location**	**Depth**	**Location**	**Depth**	**Location**	**Depth**	**Location**
18.6%	**44%**	17.1%	51.0%	1.5%	7.2%	22.5%	25.5%	3.9%	18.3%
18.6%	**24%**	18.1%	23.5%	0.4%	0.8%	17.5%	25.0%	1.1%	0.7%
18.6%	**12%**	25.0%	13.0%	6.4%	1.1%	25.0%	10.0%	6.4%	1.9%
5.3%	**42%**	4.8%	34.0%	0.5%	7.8%	5.6%	29.0%	0.3%	12.8%
6.9%	**37%**	6.3%	35.5%	0.6%	1.7%	6.7%	32.5%	0.2%	4.7%
10.7%	**44%**	11.5%	33.5%	0.8%	10.1%	12.5%	29.5%	1.8%	14.1%
		Average Error (FEM)		0.3%	1.8%			0.3%	1.5%
		Average Error (Actual)		1.7%	4.8%			2.3%	8.8%

3.5 DISCUSSION

A high degree of agreement can be realized between actual location (L) and depth (D) and estimated location and depth, as shown in Table 3.1. Note from Table 3.3 that the fit between actual location and depth vs. predicted location and predicted depth is much better for the FEA data than for the actual RUS results. This is expected, since the actual RUS measurements are subject to a host of minor sources of error that cause the resonant frequencies to be slightly off predicted values. Where direct comparison was possible (Specimens 1-6, cut depth 18%), discrepancy between measured and calculated resonant frequencies averaged 0.63%. Sources of error include error in specimen dimensions, particularly in cut depth and location. Cuts are modeled as perfectly straight and parallel to the axis. However, in reality, cuts were slightly angled relative to the axis, and wider at the top than the bottom. Other sources of error include internal damping of the specimen. This is not a significant source of error in this case, evidenced by the fact that FEA predicted frequencies are within one percent of actual measurements; but later we will see that it has a large effect on thin cracks.

Lower-order modes are typically the most sensitive to the depth of the cut. Particularly the first Y bending mode (Y Bend 1), when the cut is parallel to the Y axis, and the first X torsional mode (X Torsion 1) when the cut is parallel to the X axis. This is to be expected, since those modes are most affected by changes in stiffness along those axes. Reduction in specimen thickness can be expressed as a reduction in specimen stiffness. In fact, previous studies have attempted to use stiffness as a predictor of crack depth with some success.[19] Higher-order modes are sensitive to cut depth, but typically have some "threshold depth value." At cut depths less than the threshold value, there is very little change in modal frequency. This is particularly noticeable when the cut is near the edge of the specimen.

It should be noted that, as the cut length increases, the frequency shift will approach 100% in all cases regardless of location. The approximation used in this

analysis [$\Delta F = f(D,D^2,L,L^2)$] should only be used for certain values of depth. Therefore, part of any prediction of depth and location must include an analysis of the FEA output to determine the order of the best-fit function.

4. FATIGUE CRACKED STEEL BAR

4.1 METHOD

Specimens were machined from standard 4140 steel, according to the drawing that is shown in Figure 4.1. Specimens were machined with the V-shaped notch at once side, which served as a stress concentrator for crack initiation and propagation by fatigue. Resonant frequencies for each specimen were determined by a wide-spectrum frequency scan using RUS equipment and procedure that is described in more detail in Section 2. Each experimental peak represents a particular resonant vibration mode. Five specimens were prepared.

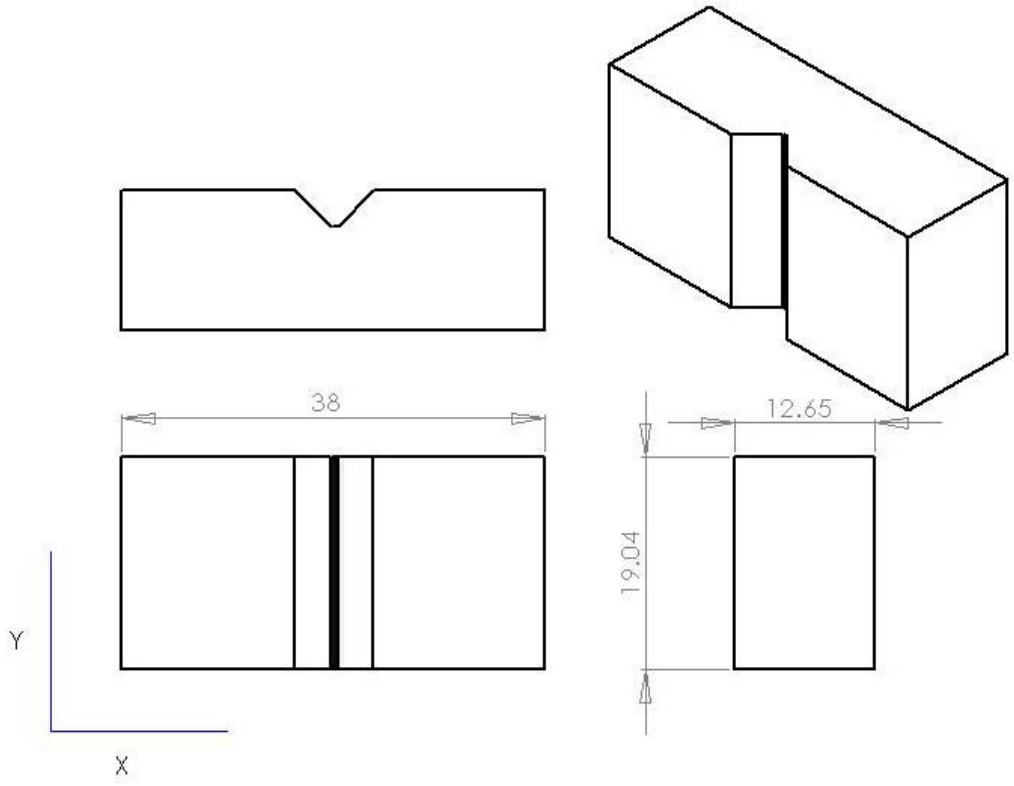

Figure 4.1 Schematic of specimen. Dimensions in mm. X and Y axis shown for front view (Z axis out of plane).

Specimens were then subjected to cyclic fatigue loading using a four-point setup on the servo-hydraulic testing machine MTS Model LVDT 380.50, as shown in Figures 4.2 and 4.3. Subjected to cyclic loads of 1,000 lb min/5,000 lb max, fatigue cracks developed at the notch tip after approximately 70,000 cycles. Once a fatigue crack initiated, the load was progressively reduced in order to grow the crack slowly. Approximately every 50,000 cycles (depending on load and crack depth), the resonant frequency spectrum of the specimen was again measured suing RUS equipment. The average depth of the fatigue crack was also measured examining the surface of the sample with an optical microscope Keyence Model VHX-600, Figure 4.4. Resonant frequency as measured by RUS for different specimens and different crack depths are given in Tables B.1-B.5 in Appendix B.

Figure 4.2 (a) MTS 100 kip cyclic loading machine and (b) four-point bending setup.

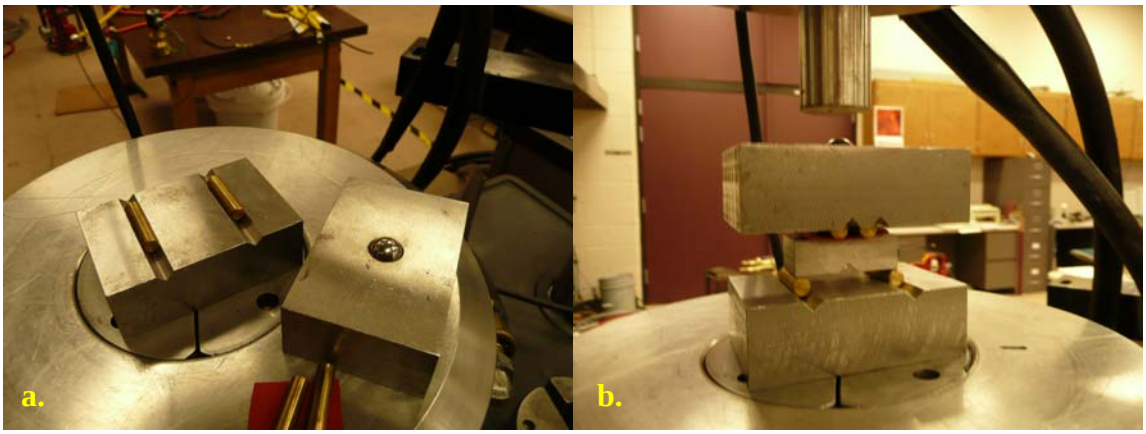

Figure 4.3 (a) Four-point bending assembly and (b) test specimen.

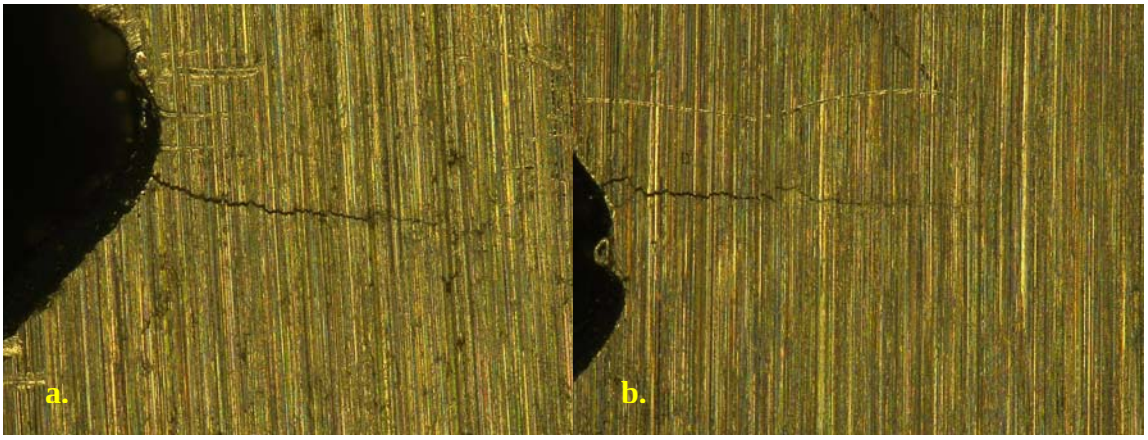

Figure 4.4 Crack in Specimen #1 (a) front and (b) back faces (magnified x100).

Elastic constants of the material that are needed for FEA were determined by preparing a separate specimen without the notch from the same 4140 steel stock and fitting a RUS resonant frequency spectrum to the Lagrangian model as outlined in Section 2. Elastic constants, and other physical data, are included in Table 4.1. Dimensions X, Y, and Z are the length, width, and height of the specimens, and correspond to the X, Y, and Z axes in Solidworks/Cosmosworks. The defect is in the Defect Location Plane, and runs parallel to the Defect Location Axis. Distance from Axis is the distance between the Axis (and the edge of the specimen) and the defect.

Table 4.1 Elastic constants and density of fatigue cracked steel specimens.

Sample	X (mm)	Y (mm)	Z (mm)	Initial Weight (g)	C11 (GPa)	C44 (GPa)	Young's Modulus (GPa)	Poisson's Ratio	Plane	Axis	Distance from Axis (mm)
1	38.07	19.04	12.65						Y-Z	Y	19.56
2	37.94	19.04	12.65	70.00					Y-Z	Y	18.77
3	38.01	19.04	12.65	70.23					Y-Z	Y	18.87
4		19.04	12.65	70.27					Y-Z	Y	19.43
5		19.04	12.65	70.66					Y-Z	Y	19.06
Control	3.19	12.65	19.02	6.12	276.1	83.5	214.2	0.283			

A FEA model was constructed using commercially available finite element software (Dassault Systems SolidWorks Education Edition SP4.0 2007 and CosmosWorks SP3.1 2004) as described in Section 2 and average specimen dimensions. Resonant frequency spectra were determined for varying crack depths, from 0.0 to 3.0 mm, and for the crack width of 0.2 mm using finite element analysis. FEA frequency spectra may be seen in Tables B.6 in Appendix B. Where possible, mode shapes were identified visually from FEA eigenvectors, Figure 4.5.

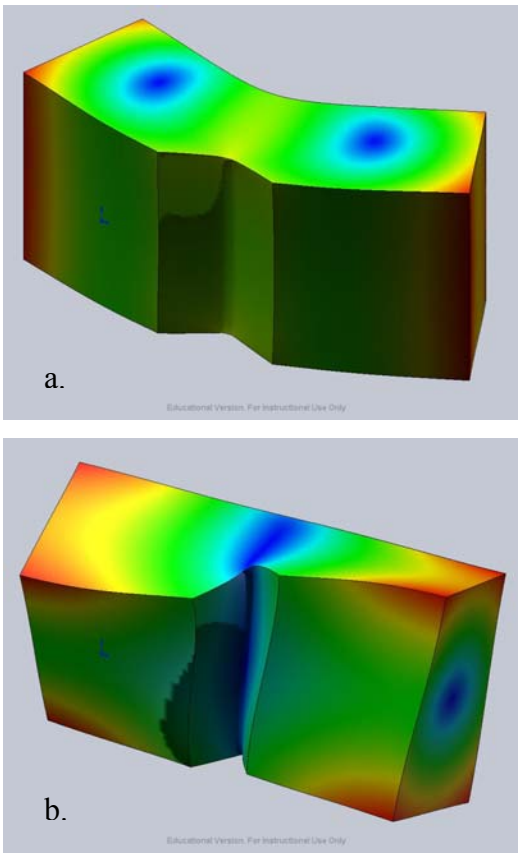

Figure 4.5 FEA models of (a) Y Bend 1, (b) X Torsion 1, and (c) Z Bend 1

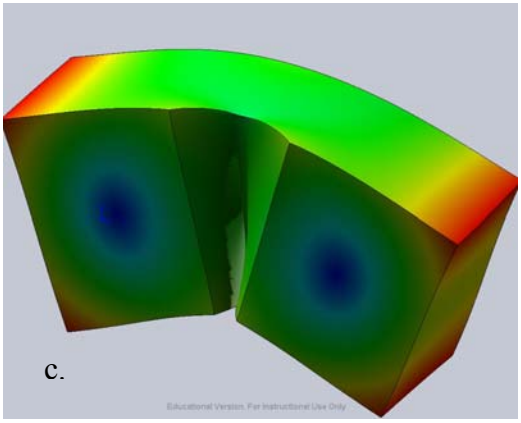

Figure 4.5 (continued) FEA models of (a) Y Bend 1, (b) X Torsion 1, and (c) Z Bend 1

4.2 RESULTS

Resulting resonant frequencies measured by RUS for each specimen are given in Tables B.1-B.5 of Appendix B. Table B.6 in the same appendix list resonant frequencies as a function of length that were calculated using FEA. It is worth noting that FEA model results agreed closely with RUS measurements for the specimens without to fatigue cracking. Average magnitude of error between predicted and measured resonant frequencies was in all cases less than 0.4% for all samples, as shown in Appendix B.

Figures 4.6 – 4.12 show shift in measured resonant frequency (expressed as a percentage of initial resonant frequency, Equation 3.1) vs. crack depth (expressed as a percentage of specimen thickness) for the first seven vibrational modes. FEA predicted frequency shift data for each mode is also displayed on these plots as a solid black line. At some point during the fatigue process, excessive loading caused Specimens 1 and 5 to plastically deform, resulting in a 0.025 mm bow along the X-axis of the specimen (equivalent to a roughly 2.5 m radius of curvature). This deformation of Specimens 1 and 5 was first noted after the crack had exceeded 1 mm in depth (approximately 8% of specimen thickness), but may have occurred earlier. Although this deformation appears small, it is significant for reasons explained later.

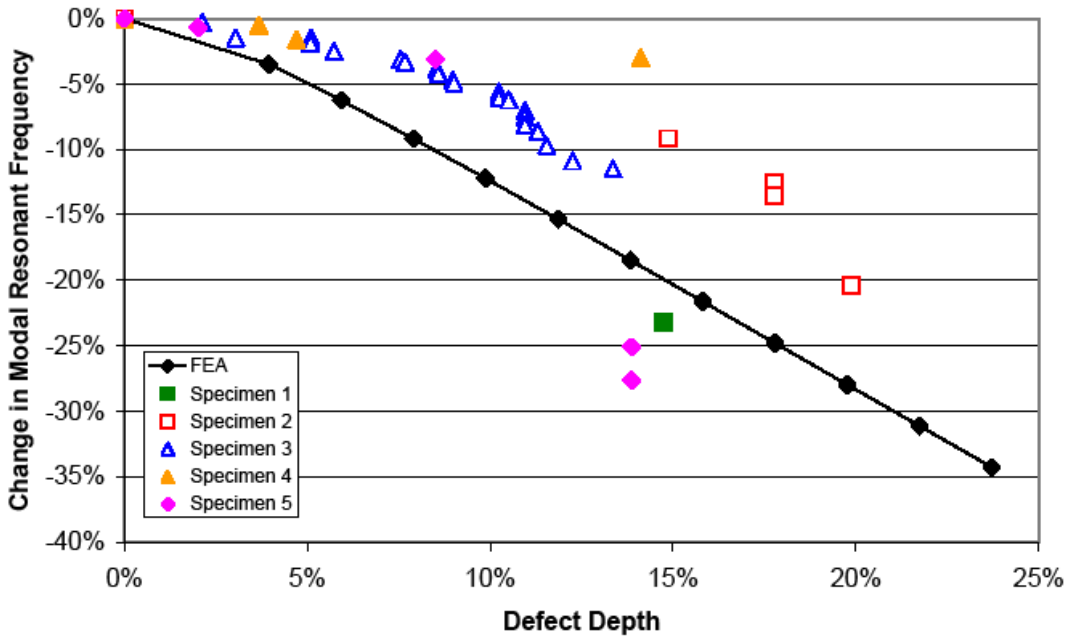

Figure 4.6 Change in frequency vs. defect depth for mode Y Bend 1.

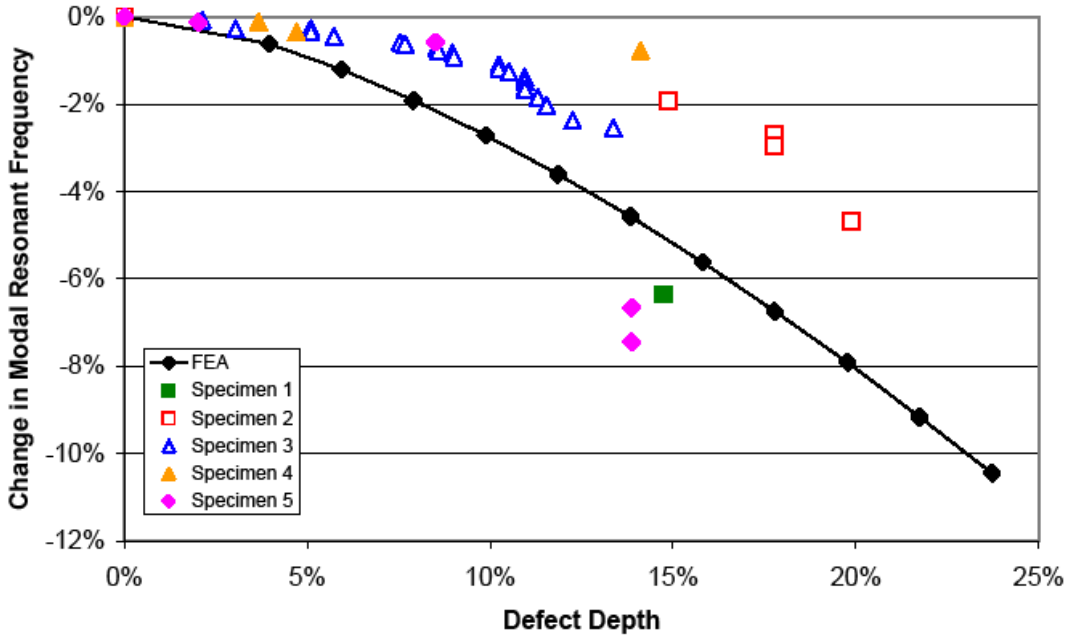

Figure 4.7 Change in frequency vs. defect depth for mode X Torsion 1.

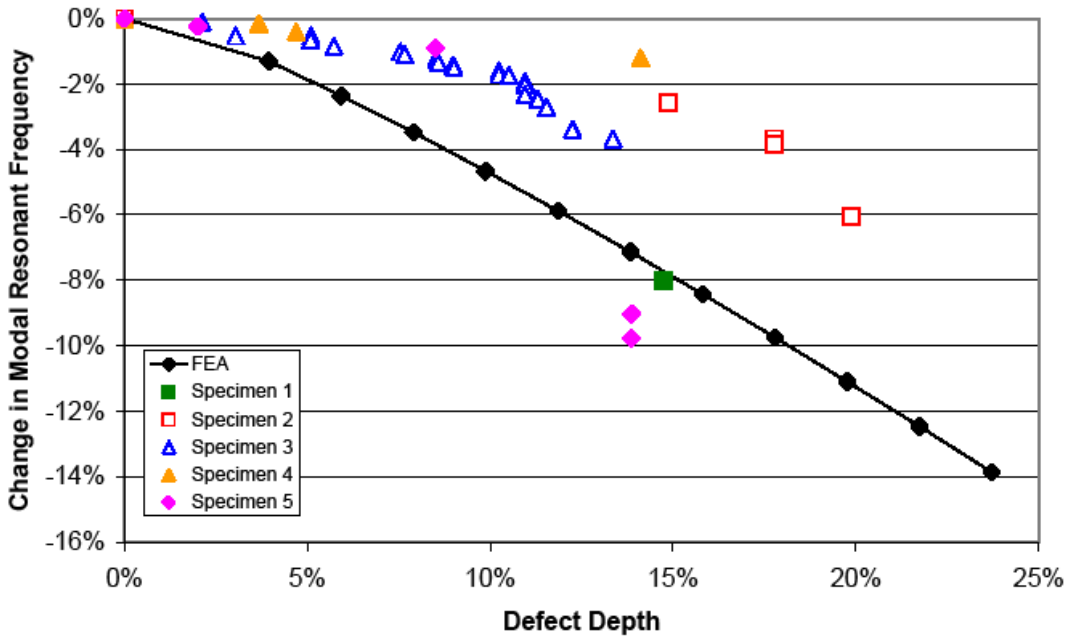

Figure 4.8 Change in frequency vs. defect depth for mode Z Bend 1.

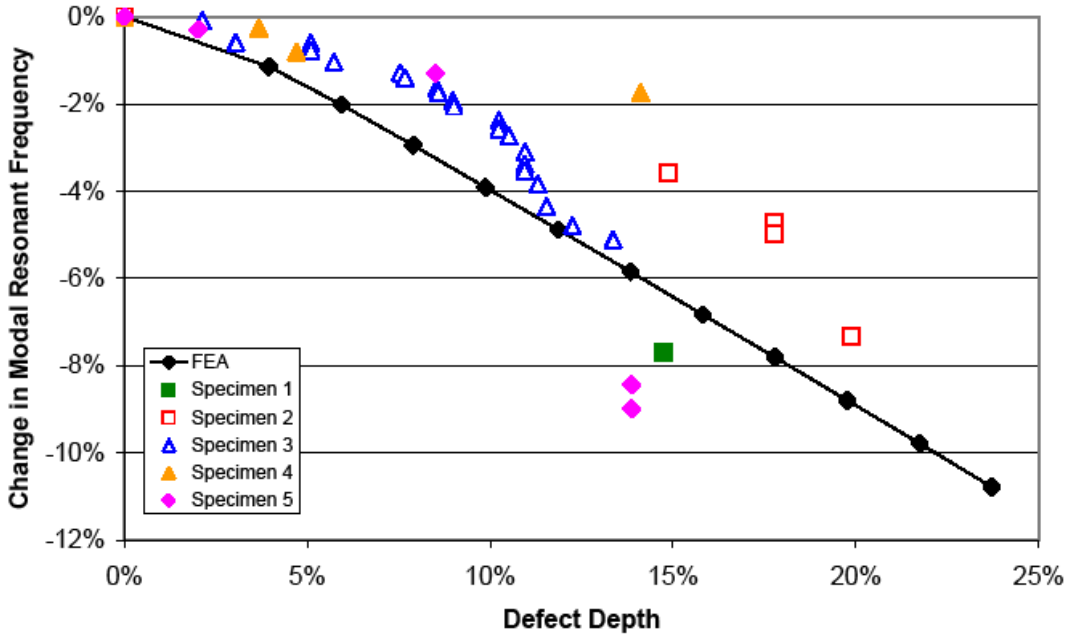

Figure 4.9 Change in frequency vs. defect depth for mode Volume 1.

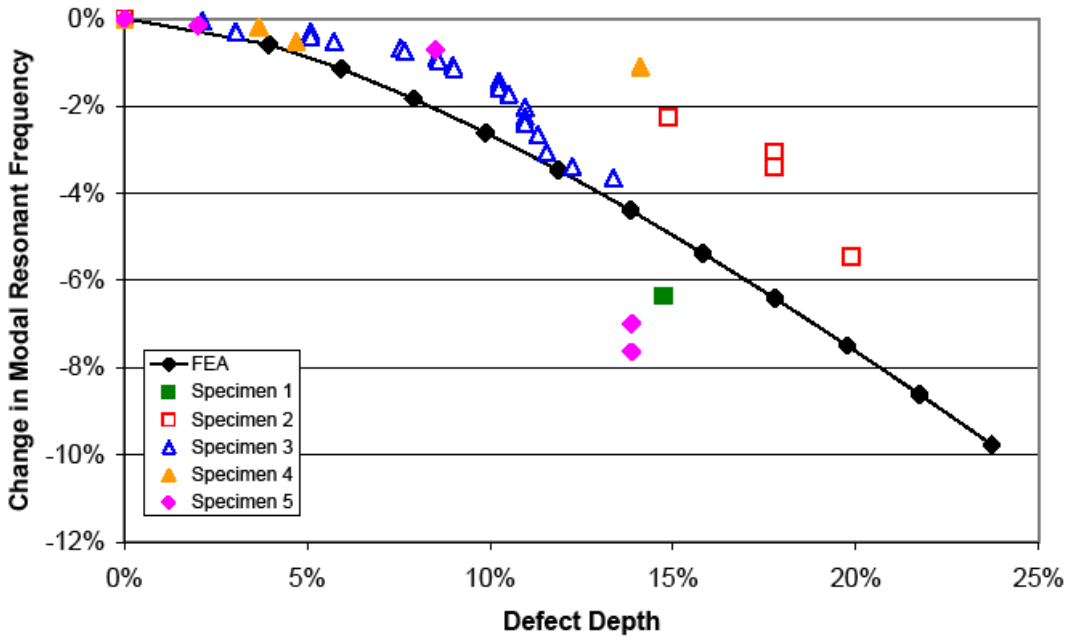

Figure 4.10 Change in frequency vs. defect depth for mode Z Bend 2.

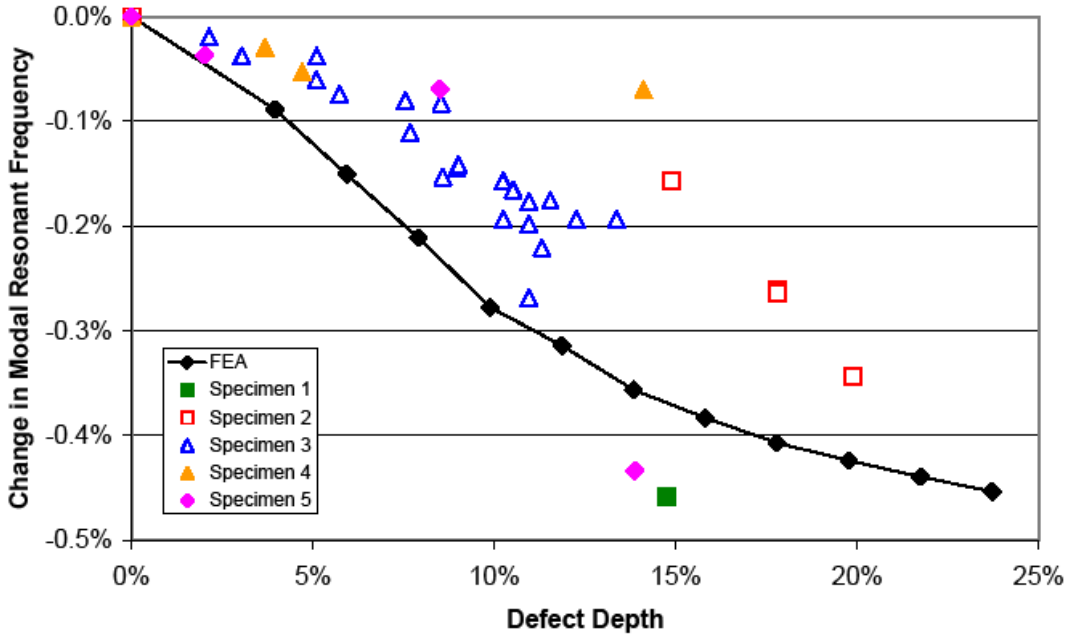

Figure 4.11 Change in frequency vs. defect depth for mode X Torsion 2.

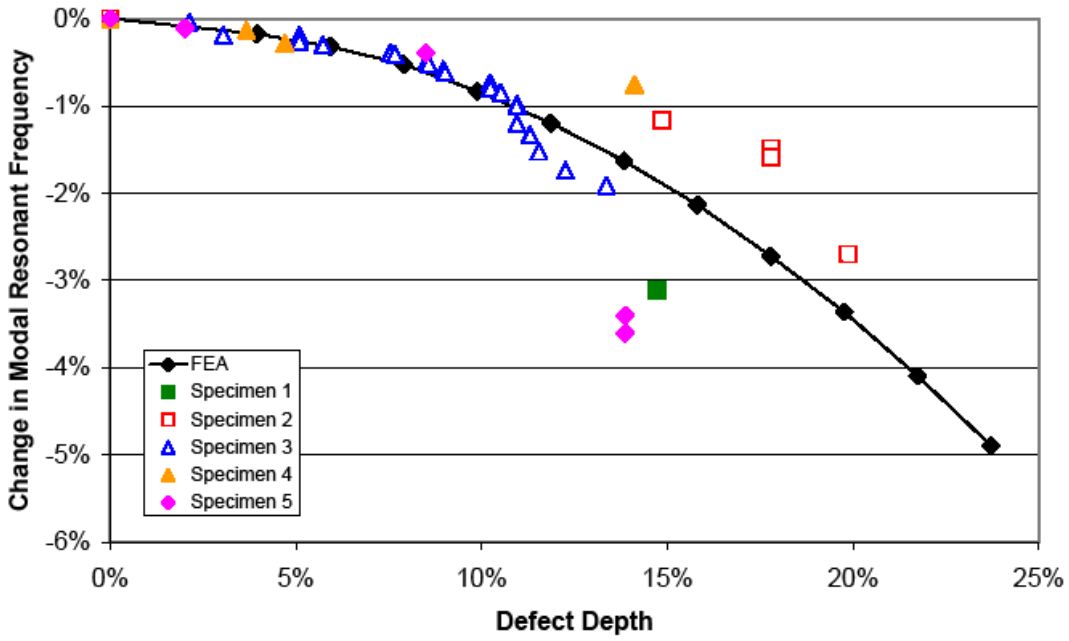

Figure 4.12 Change in frequency vs. defect depth for mode Y Bend 2.

4.3 DISCUSSION

Figures 4.6-4.12 show RUS measured data and FEA predicted data. Unlike in the case of the cut notch that was described in previous section (Section 3), calculated frequency shift is, in most cases, substantially large than measured frequency shift. Adjusting variables in the FEA model (crack width from 0.1 to 0.01 mm, crack location from ±0.5 mm of center, elastic constants, specimen dimensions, etc.) failed to eliminate that discrepancy.

These results are in agreement with the results published by Belayev et al on the effect of defects in silicon wafers on resonant peaks.[14] They suggested that contact forces that generate during RUS might be the source of the error. FEA models do not include the effects of contact forces between the two surfaces of the crack, i.e. the friction at the crack tip. However, if the RUS excitation is sufficiently large, such contact forces may be expected to affect the measured frequency spectrum.

To examine that possibility, the ultrasound attenuation (Q^{-1}) was calculated from the resonant peaks using Equation 4.1.[8,31,37]

$$Q_k^{-1} = \frac{\Delta f_k}{f_{ko}} \qquad \text{Eqn. 4.1}$$

where f_{kn} is the frequency associated with the k^{th} eigenmode, and Δf_k is the full width at half maximum, FWHM, of that mode. Ultrasound attenuation is the fraction of the energy that is attenuated by some dissipative process such as friction at the crack tip. The Q^{-1} vs. crack depth for several modes shapes are shown in Figures 4.13-4.15. For comparison, the Q^{-1} for the samples with the cut, wide notch (Section 3) is also plotted in the same Figures.

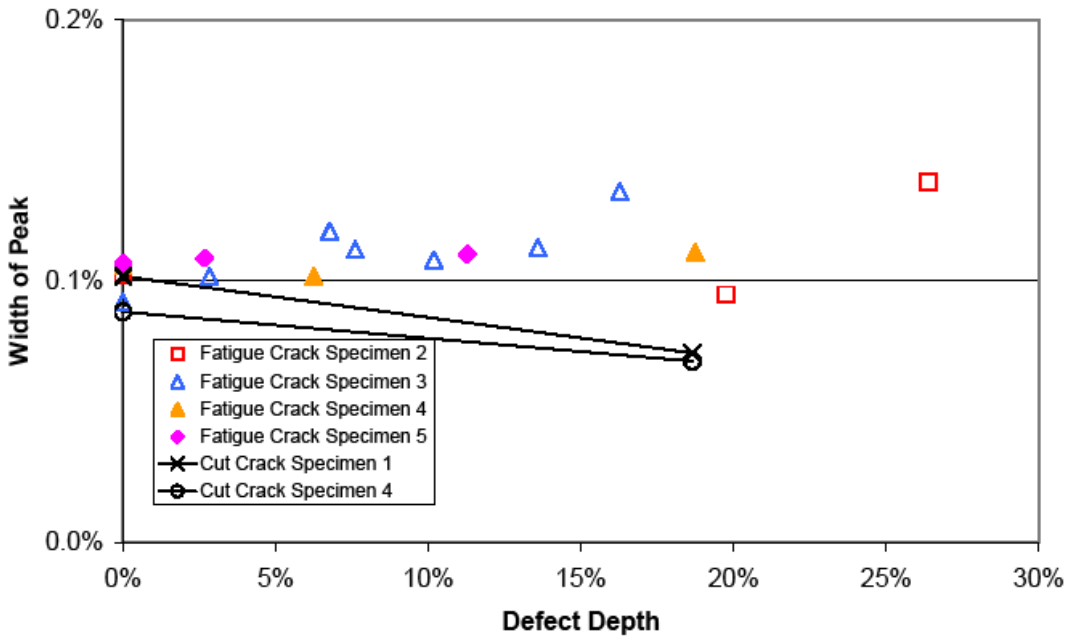

Figure 4.13 Half-peak damping vs. defect depth for mode Z Bend 1.

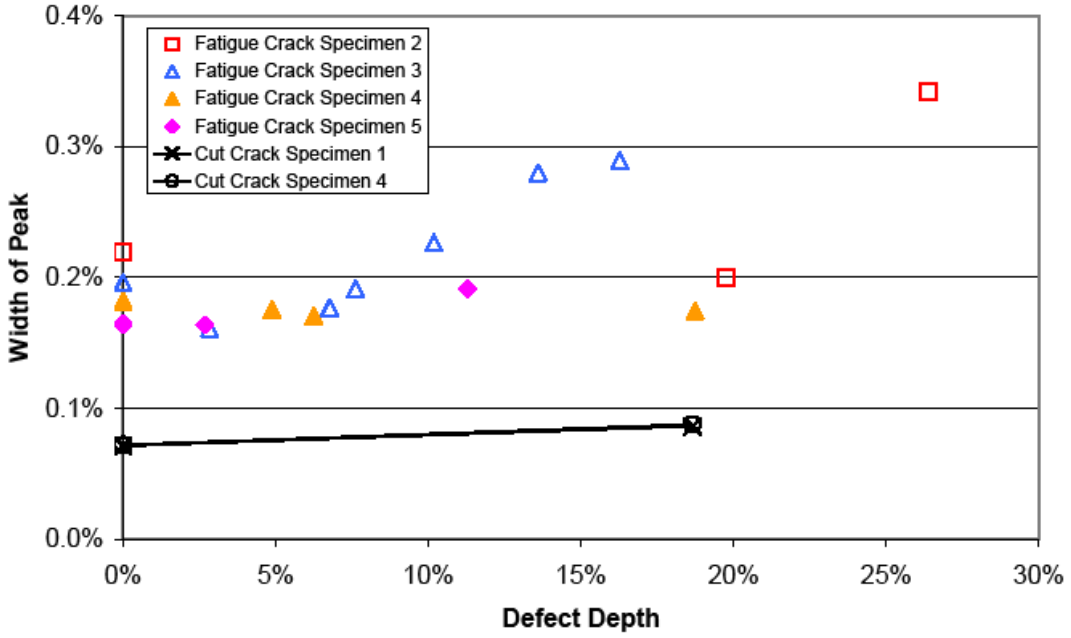

Figure 4.14 Half-peak damping vs. defect depth for mode Y Bend 1.

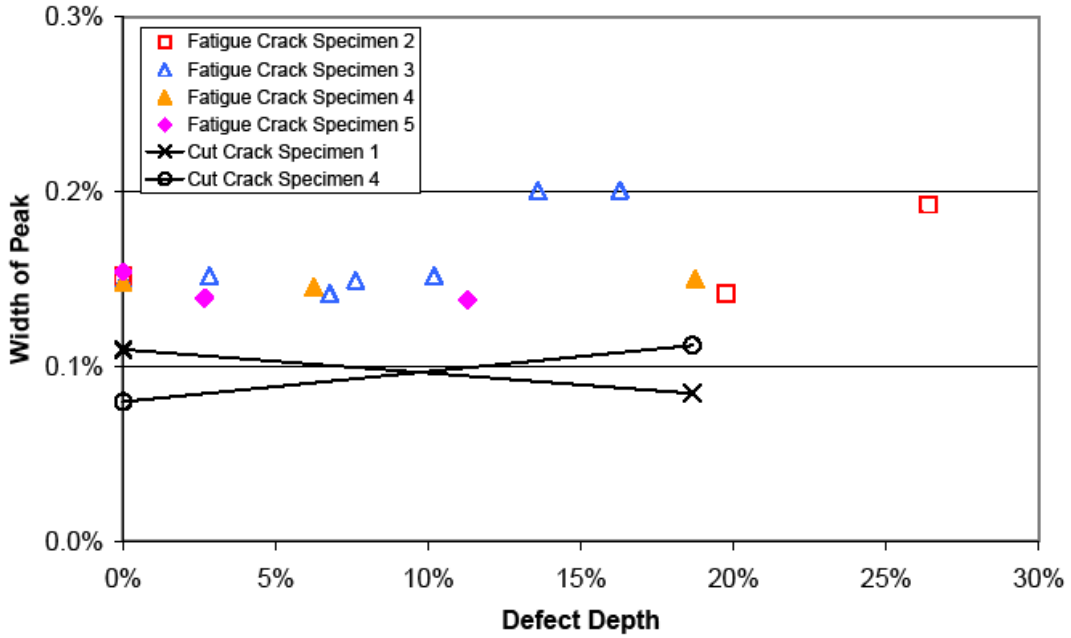

Figure 4.15 Half-peak damping vs. defect depth for mode X Torsion 1.

There are two types of contact forces present: constraint forces and friction forces. Constraint forces are forces normal to the crack face, caused by strain in the normal direction. Constraint forces probably do not cause much energy loss (Q^{-1}). Friction forces are forces parallel to the crack face caused by the faces sliding relative to each other. Friction forces are responsible for the majority of the energy loss measured by Q^{-1}. It seems probable that certain modes will be more influenced by one or the other type of contact force. This may account for the difference in measured Q^{-1} between the various modes. However, further research is needed to confirm this.

Cut specimens experience very little change in Q^{-1} as cut depth increases. Two modes show small increases, and the third mode actually decreases with cut depth. In contrast, the fatigue samples show increasing Q^{-1} width in two modes, and no change in the third. The increase in half-peak width of the two modes of the fatigue cracked specimens (first bending mode about the Y axis, and the first torsional mode about the Z axis) indicates energy most likely associated with friction forces within the crack.

Additional evidence that interaction between the crack faces reduced the frequency change can be found by comparing the results from Specimen 1 and Specimen 5 to the FEA model. Both Specimen 1 and 5 deformed plastically as a result of excessive loading. Since resonant frequency is dependant on the dimensions of an object, some frequency change is to be expected from plastic deformation. In other words, bending the specimen should change the resonant frequencies. FEM analysis indicates that the difference in modal natural frequency between an undeformed specimen and one plastically deformed (i.e. bent) as Specimen 1 and 5 should be on the order of 1-2% for any mode.

Note from Figure 4.6-4.12 that Specimen 1 and Specimen 5 showed change in modal natural frequency that is much greater than 1-2% on several modes. Given the nature of the applied load, it is reasonable to assume that the fatigue cracks in these two specimens are wider than those of the other specimens (Specimens 2-4) which did not deform. This indicates that the crack width has a significant impact on the modal natural

frequency. In fact, Specimens 1 and 5 show frequency shift that is quite close to predicted values for all modes.

Also note from Figures 4.6-4.12 that some modes (notable, Volume 1 and Y Bending 2) have very small difference between FEA predicted and RUS measured change in resonant frequency. This may be because these modes generate less friction between the crack surfaces. The volumetric mode has mostly compressive and tensile forces on the crack, with little to no shear. The second bending mode about the Y axis has causes almost no deflection at the crack location (as opposed to the first Y bending mode, which has great deflection at the crack location). These results also tend to indicate that interaction between the crack surfaces is responsible for the discrepancy between calculated and measured frequency values. Furthermore, it shows that by carefully selecting certain modes for analysis, prediction of crack depth may be possible based on FEA data.

It should be noted that, for some modes, measured resonant frequencies tracked calculated frequencies, offset by some constant. This behavior is evident in the data from Figure 4.6-4.12. In the lowest-order mode (Y Bend 1), actual results begin to track actual results at about 7 or 8% depth (approximately 1 mm). Note that this offset depth varies from mode to mode. Therefore, FEA may be a useful method of predicting the response of certain modes to certain types of defects, but further study is necessary to confirm this hypothesis.

5. DETECTION OF CRACK IN CERAMIC PLATE

5.1 METHOD

Specimens were machined from high-alumina ceramic (McMaster-Carr High-Alumina Ceramic #8462K25) according to drawings shown in Figure 5.1. Specimens were machined with the notch at one side, which served as a stress concentrator for crack initiation. Cracks were initiated and propagated down the centerline of each specimen using a double-torsion setup, as shown in Figure 5.2.[42] A gradually increasing load was applied to the specimen. By observing a real-time graph of load vs. time, it was possible to determine when a crack initiated. In general, the load required to initiate a crack was about 30 lb (130 N). Initial crack length varied from 4 to 20 millimeters. The notched end was removed from each specimen, leaving a rectangular parallelepiped with (ideally) a thin crack running partway down the centerline.

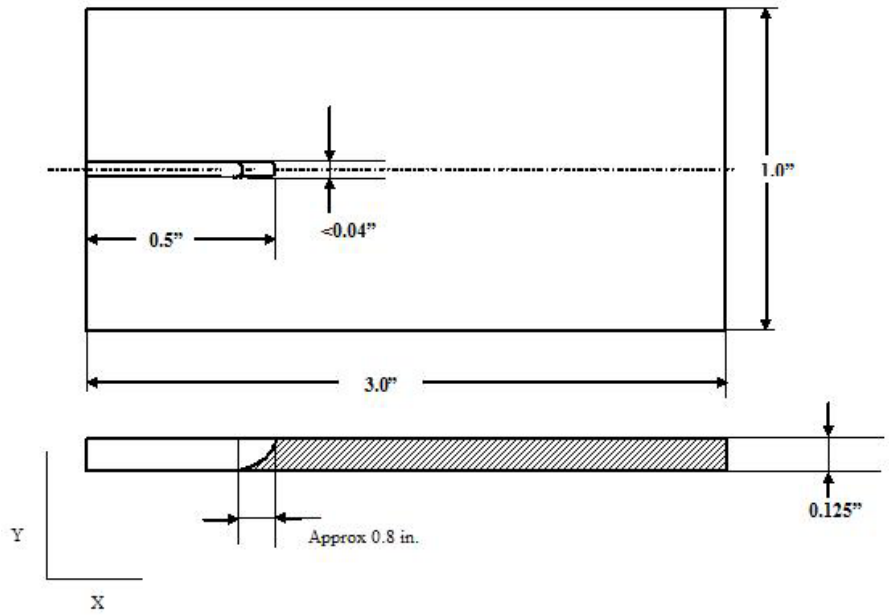

Figure 5.1 Schematic of specimen prior to crack initiation. Dimensions in inches. X and Y axes shown (Z is out-of-plane).

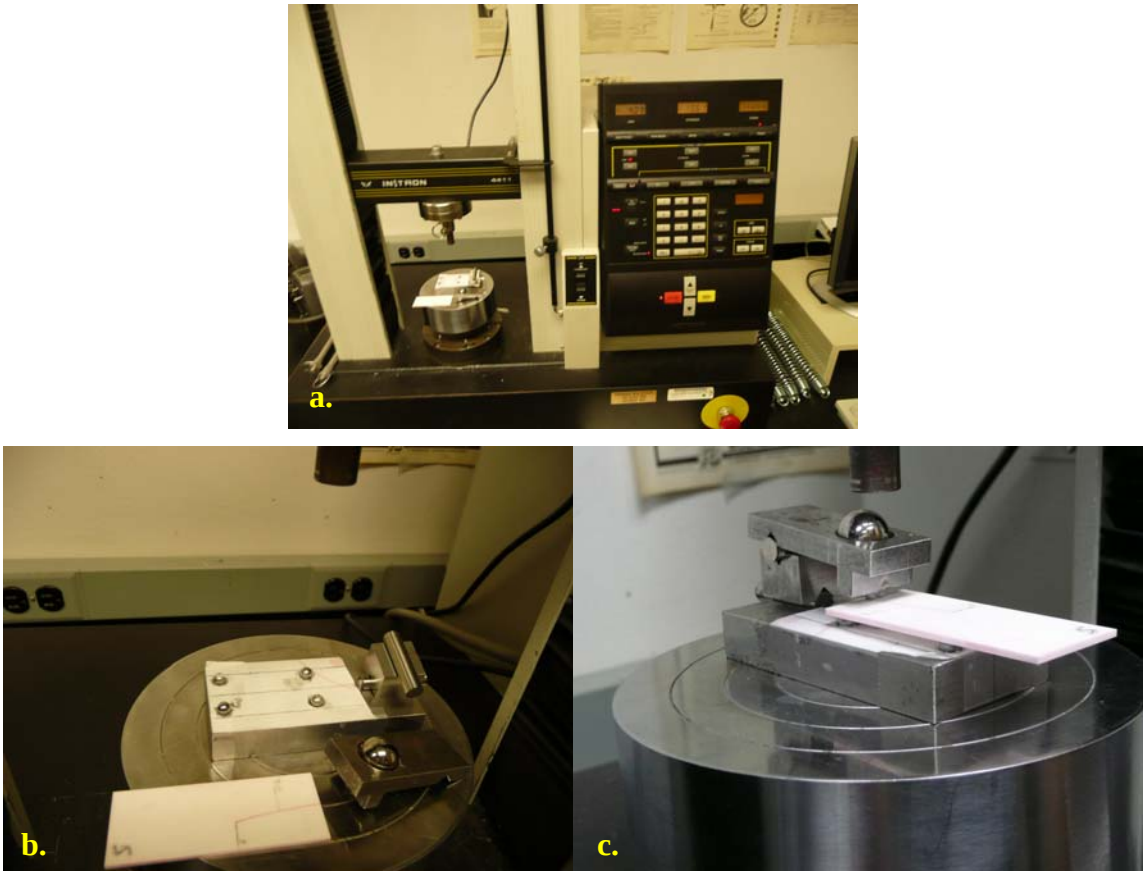

Figure 5.2 (a) Instron load machine with (b) double-torsion loading fixture and (c) specimen setup.

Resonant frequencies for each specimen were determined by a wide-spectrum frequency scan using RUS equipment (setup identical to that shown in Sections 3 and 4). Specimens were then returned to the double-torsion apparatus. A gradually increasing load was applied (using Instron 4411 5 kN Tension Tester with LabVIEW 8.20) in an attempt to extend the crack in small increments. It was possible to identify when the

crack began to propagate by closely observing a real-time graph of load vs. time. Generally speaking, the load required to incrementally propagate the crack was between 2 and 20 lbs (9 to 90 N). Incremental crack growth varied from less than a millimeter to up to 15 millimeters. Crack length was measured using calipers. Each time the crack propagated, the specimen was removed and the resonant frequencies re-measured using RUS equipment. Table 5.1 lists dimensions, weights, and position of the crack for all examined samples with the crack, namely Specimens 2, 5, 7, and 9; while Figure 5.3 shows examined samples with the cracks.

Elastic constants for the ceramic material (alumina) were determined using two additional specimens (namely, Specimens 4 and 10) that were machined without a notch but from the same ceramic stock, Figure 5.4. Resonant frequencies for these specimens were determined using the RUS equipment described in Section 2. The resulting resonant frequency spectra were used to determine the elastic moduli of the ceramic material using the Lagrangian least-squares fit method as outlined in Section 2.

Table 5.1 Elastic constants, dimensions, and weight of ceramic material. X, Y, Z, and Planes are defined in Figure 4.1.

Sample	X (mm)	Y (mm)	Z (mm)	Initial Weight (g)	C11 (GPa)	C44 (GPa)	Young's Modulus (GPa)	Poisson's Ratio	Plane	Axis
4	48.23	1.49	25.36	7.07	463.4	145.7	370.3	0.271		
10	48.09	1.43	25.36	6.76	463.4	145.7	370.3	0.271		
2	62.55	1.50	25.36	9.24					X-Y	X
5	62.51	1.50	25.40	9.18					X-Y	X
7	62.49	1.43	25.38	8.82					X-Y	X
9	62.43	1.43	25.36	8.87					X-Y	X
FEM Model	62.50	1.46	25.38	8.87	463.4	145.7	370.3	0.271	X-Y	X

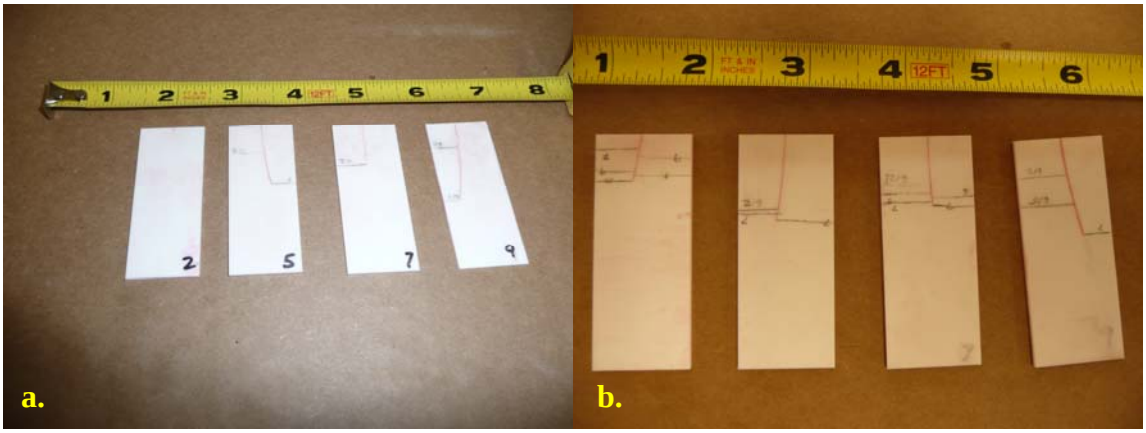

Figure 5.3 Ceramic alumina specimens (cracked) (a) front and (b) back. Cracks highlighted on specimens with red dye penetrant.

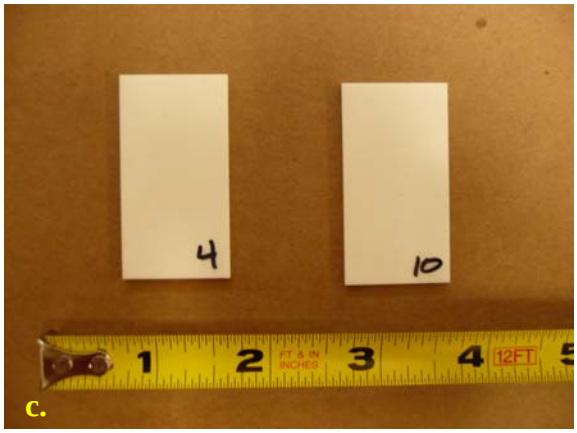

Figure 5.4 Ceramic alumina specimens (control)

An FEA model was made using commercially available finite element software (Dassault Systems SolidWorks Education Edition SP4.0 2007 and CosmosWorks SP3.1 2004) using the methodology that was previously described in more detail in Sections 3 and 4. Resonant frequency spectra were determined for varying crack depths from 0 to

20 mm, and for crack width of 0.2 mm, using finite element analysis. Where possible, mode shapes were identified visually from FEA eigenvectors, Figure 5.5. In addition, resonant frequencies for the samples without the crack, Figure 5.4, were calculated using FEA.

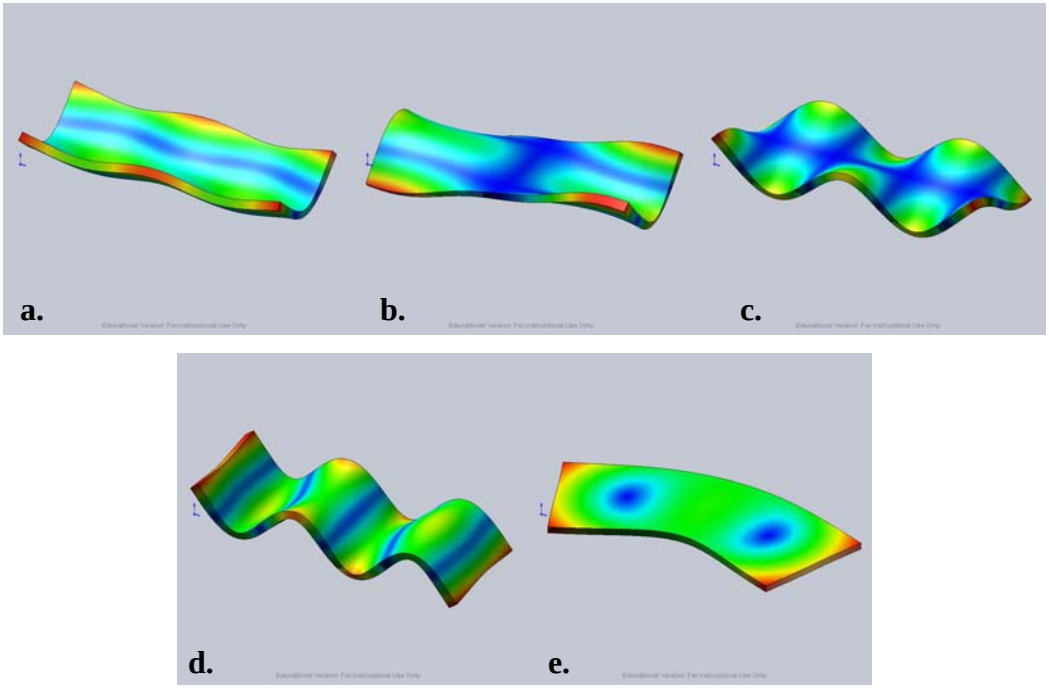

Figure 5.5 FEA models of (a) X Bend 1, (b) Mode 8, (c) X Torsion 4, (d) Z Bend 4, and (e) Y Bend 1.

5.2 RESULTS

Resulting resonant frequencies measured by RUS for each specimen are given in Tables C.1-C.6 in Appendix C as a function of measured crack size. Table C-7 in the same Appendix list the resonant frequencies as a function of length that were calculated using FEA. Because the specimens were re-machined after the crack was initiated, no RUS frequency spectra were available for the samples without a crack. However, it is

worth noting that the initial RUS frequency spectra of the specimen with the shortest initial crack (Specimen #2, approximately 2 mm average crack length) was very close to the predicted frequency spectra of the uncracked specimen FEA model. Also, FEA model results for the plates without crack shown in Figure 5.4 agreed closely with RUS measurements, with average magnitude of error between predicted and measured resonant frequencies of about 1% for modes with resonant frequencies greater than 20 kHz. This indicates that the FEA model is a reasonable predictor for resonant frequency behavior of the actual specimens without the crack.

Figures 5.6 – 5.13 show shift in measured resonant frequency (expressed as a percentage of initial resonant frequency, Equation 5.1) vs. crack depth (expressed as a percentage of specimen thickness) for vibrational modes 7 – 14. FEA predicted frequency shift data is also displayed for each mode on those plots as a solid black line.

$$Change = \frac{f_{Cut} - f_{Original}}{f_{Original}} \qquad \text{Eqn. 5.1}$$

where f is the resonant frequency. Since it was not possible to measure resonant frequencies of the specimens with crack length equal to 0, $f_{Original}$ in Eqn. 5.1 1is defined as the initial resonant frequencies of the specimen with the shortest initial crack (Specimen #2, approximately 2 mm average crack length).

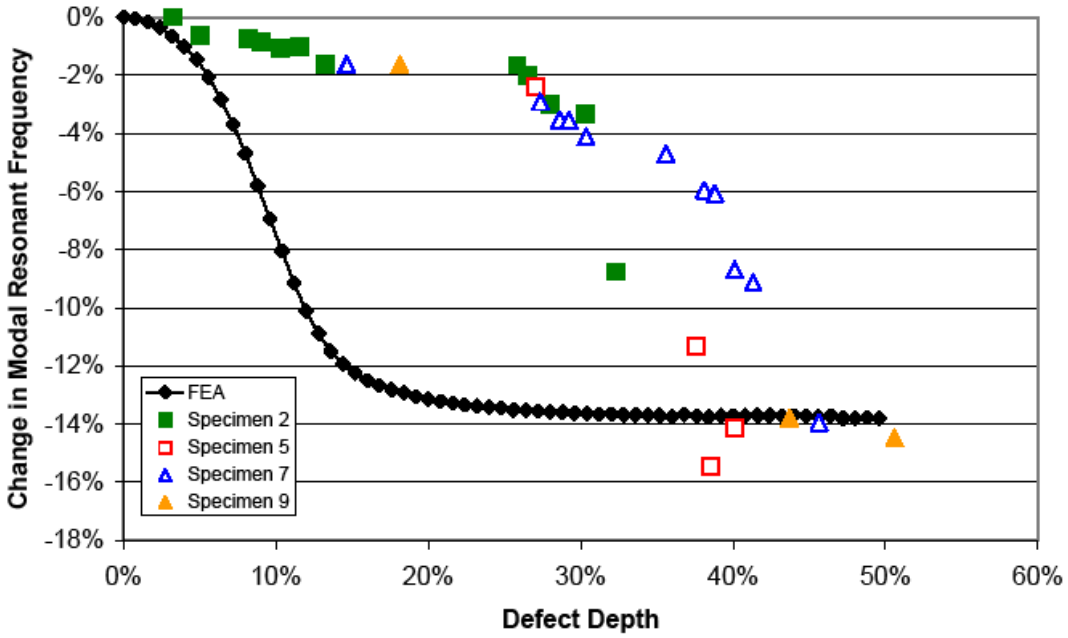

Figure 5.6 Change in frequency vs. defect depth for mode X Bend 1.

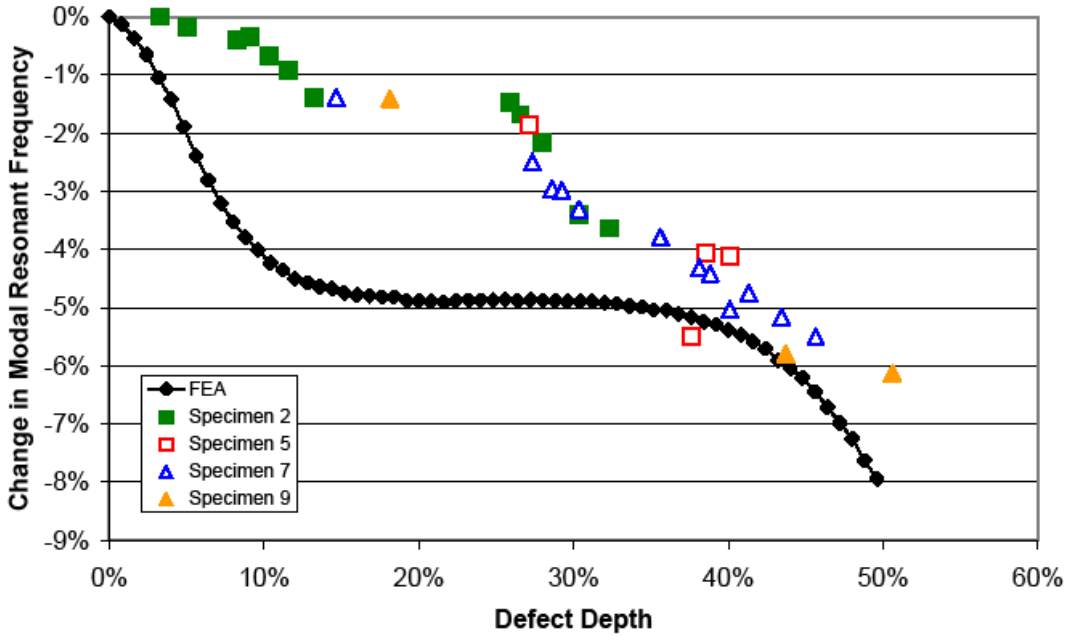

Figure 5.7 Change in frequency vs. defect depth for Mode 8.

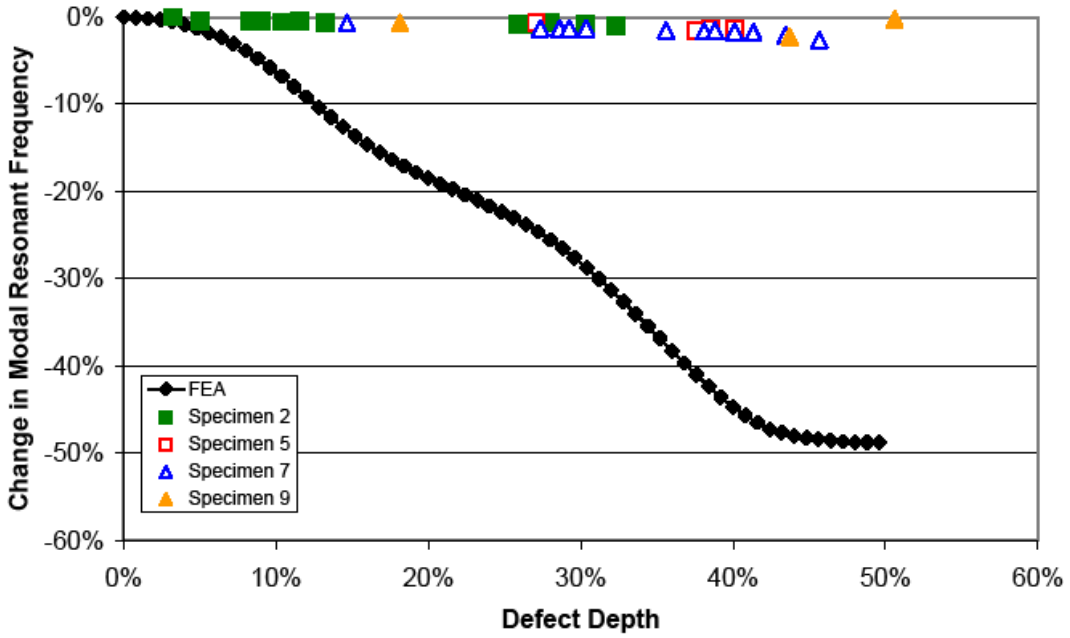

Figure 5.8 Change in frequency vs. defect depth for mode X Torsion 4.

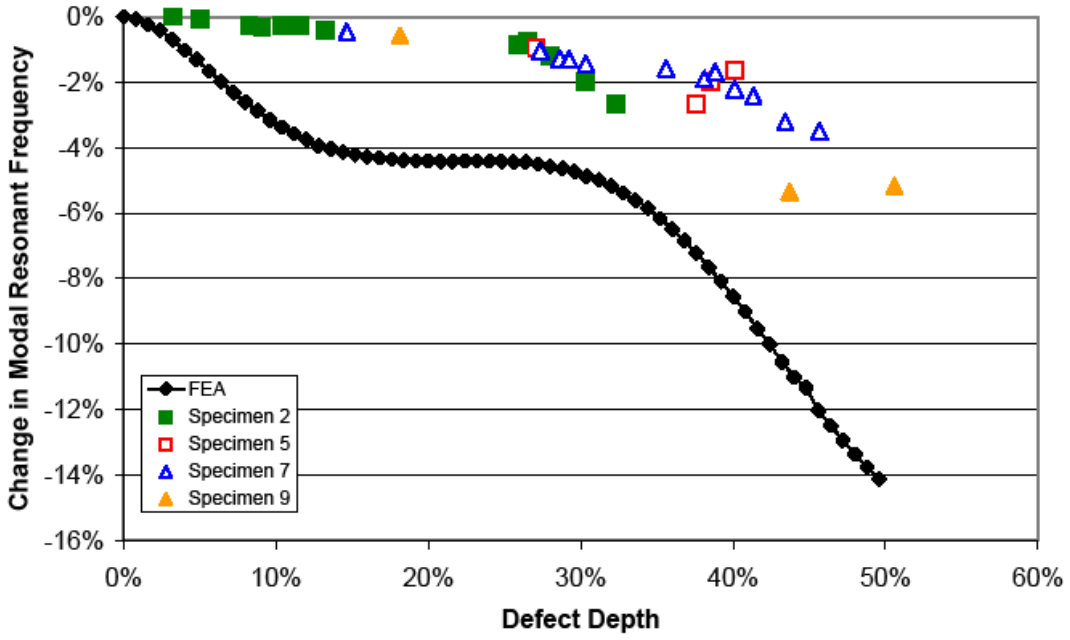

Figure 5.9 Change in frequency vs. defect depth for Mode 10.

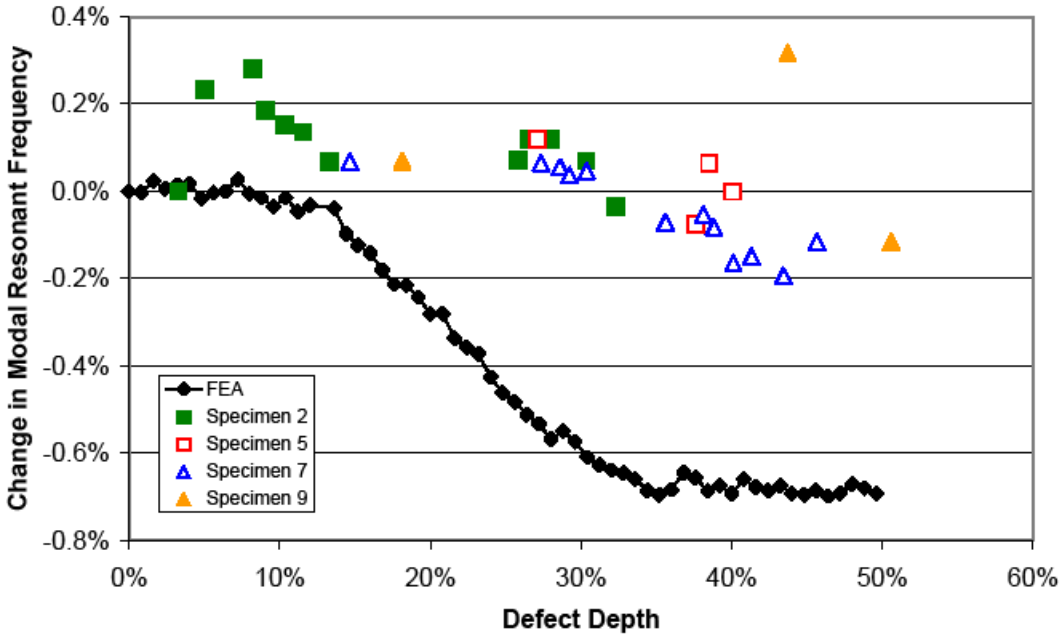

Figure 5.10 Change in frequency vs. defect depth for mode Z Bend 4.

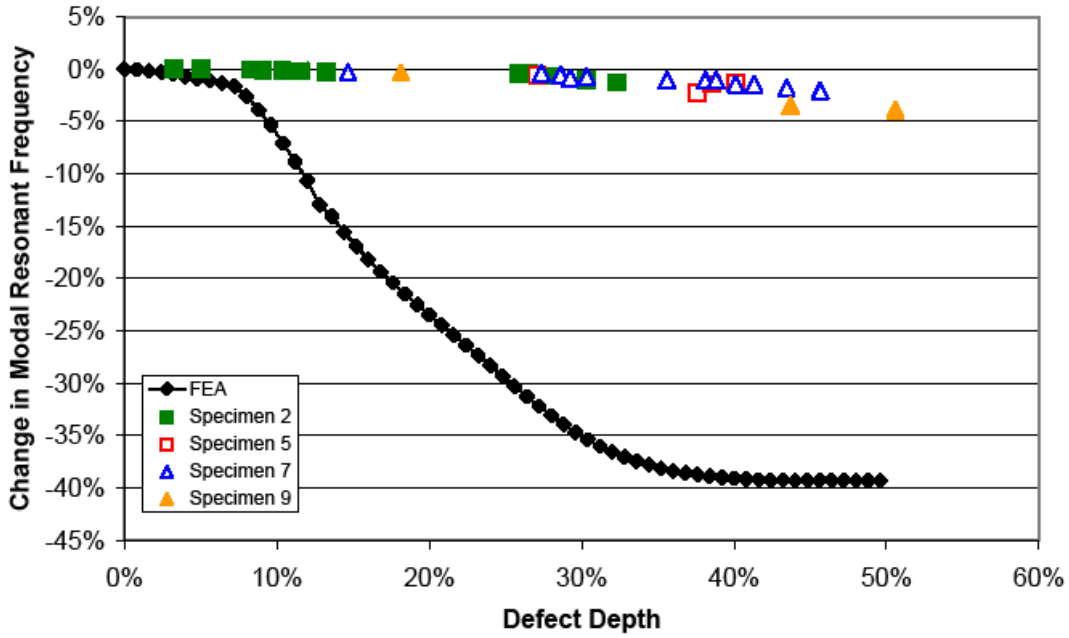

Figure 5.11 Change in frequency vs. defect depth for Mode 12.

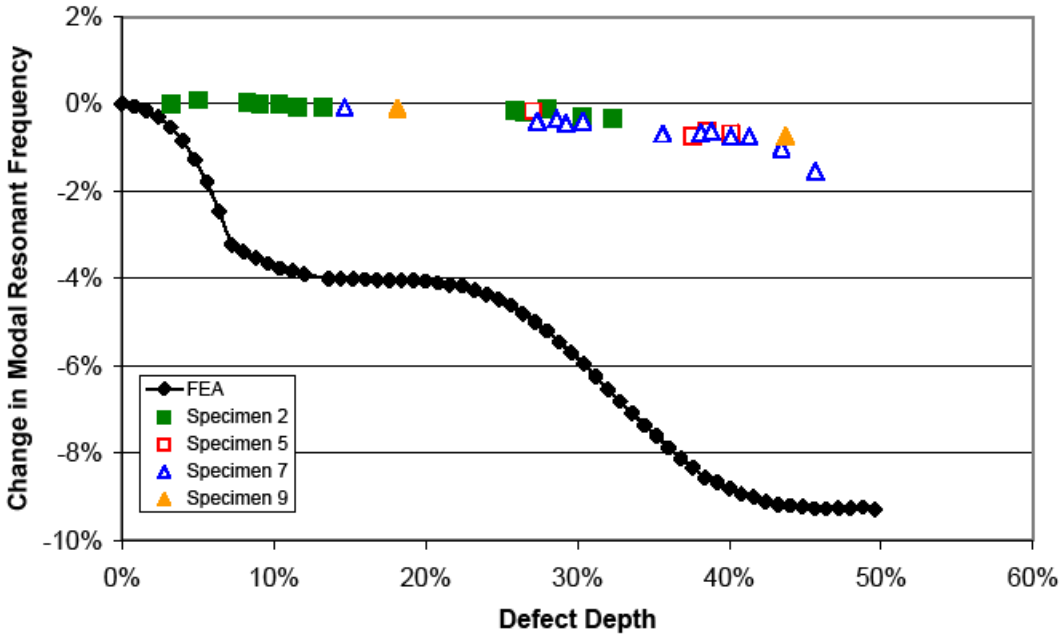

Figure 5.12 Change in frequency vs. defect depth for mode X Torsion 5.

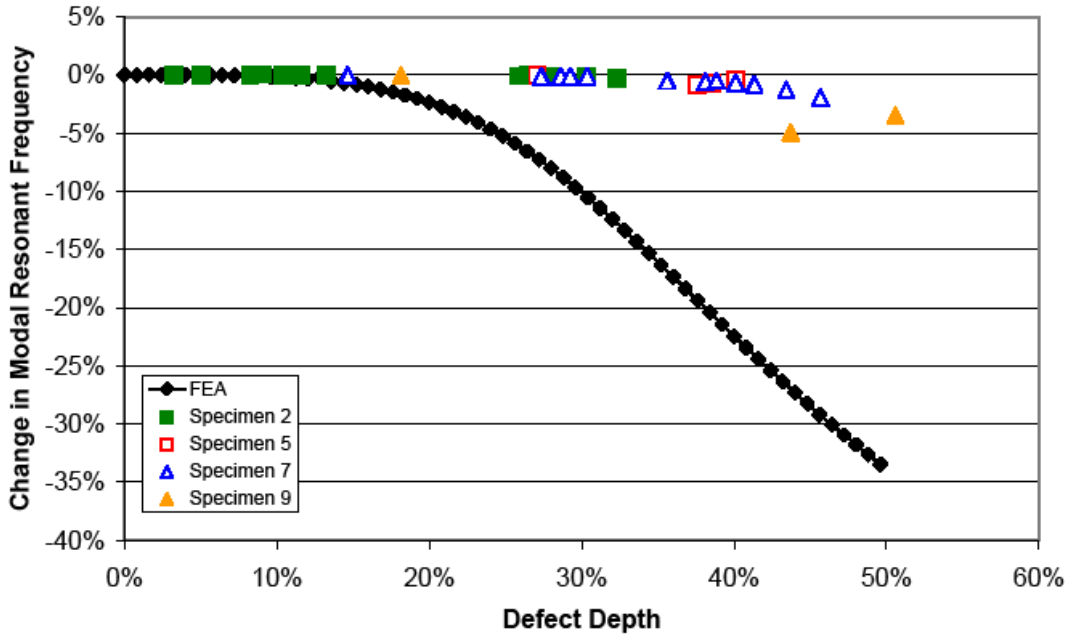

Figure 5.13 Change in frequency vs. defect depth for mode Y Bend 1.

Modes 1 - 6 had resonant frequencies below 20 kHz, and were not used in this analysis. RUS equipment does not reliably identify resonant modes below a certain threshold frequency due to the resonant response of the test equipment obscuring the results of the measurement.[31] Schwarz et al state that their lab equipment identifies resonant frequencies larger than 10 kHz.[12] The equipment used in these analyses produced inconsistent and unclear results below 20 kHz (Figure 5.14). Therefore, it was not possible to consistently identify resonant modes in that frequency range for ceramic specimens, i.e. the first six modes were disregarded. Only Modes 7 though 14 were considered in this analysis. These modes were chosen because their resonant frequencies are significantly affected by the crack geometry, and because they were readily identifiable in both the RUS spectra and the FEA eigenvector mode shape analysis.

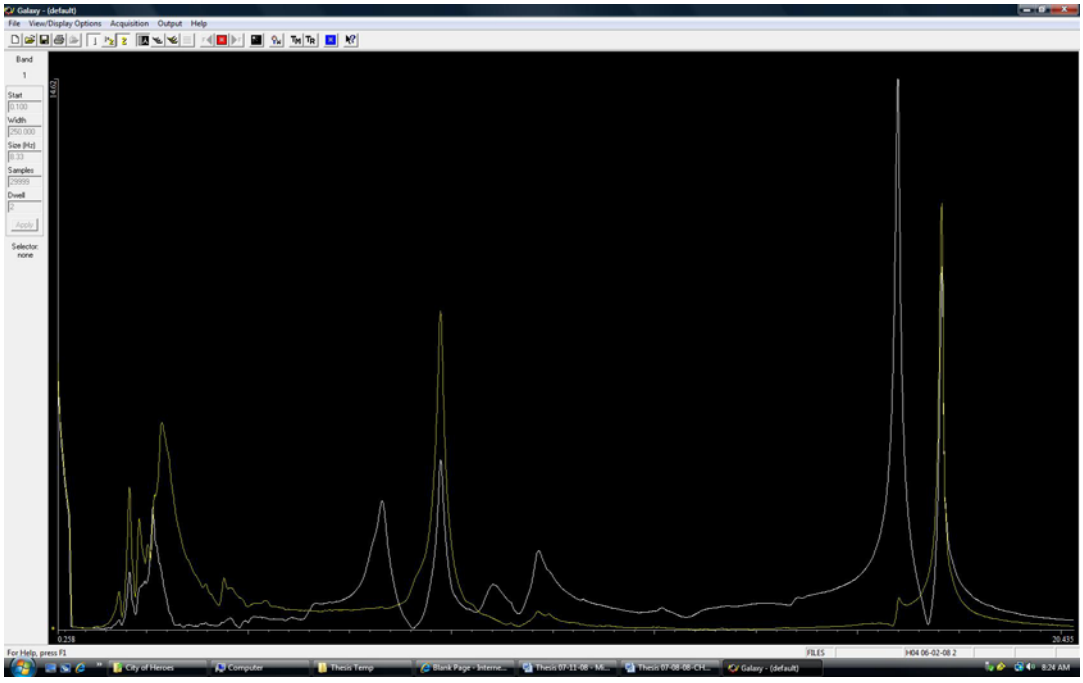

Figure 5.14 Resonant frequency spectra 0.1 – 20 kHz measured using RUS.

As crack length increases, some resonant frequencies change more than others, as it can be seen in Figures 5.6 – 5.13. Therefore, the order of the modes often changes as crack depth increases. This makes it difficult to identify which peak response frequency in the RUS data is associated with which particular mode. Modes 7 through 14 are easier to identify in this respect, since there is clear separation between them in the RUS results, and they do not appear to switch order.

5.3 DISCUSSION

Figures 5.6 – 5.13 show RUS measured data and FEA predicted data. As in the case of the steel specimens with fatigue cracks (Section 4), but unlike the case of the steel specimens with the cut notch (Section 3), calculated frequency shift is, in most cases, substantially larger than measured frequency shift. Adjusting variables in the FEA model (crack width from 0.5 – 0.1 mm, elastic constants, crack angle 0º - 30º offset from centerline of sample, etc) failed to eliminate the discrepancy.

However, it should be noted that, for some modes, the measured data followed the same trend as the predicted data, offset by some constant. This behavior is evident in the data from Figure 5.6 – 5.13. In some modes (X Bend 1, Z Bend 4), measured data begins to track actual results when the crack reaches about 30% of the length of the specimen. Note that this offset length varies from mode to mode, and is not evident in all modes. Therefore, FEA may be a useful method of predicting the response of certain modes to certain types of defects, but further study is necessary to confirm this hypothesis. However, this trend is not quite as clear in the ceramic specimens as it is in the data for the fatigue cracked steel specimens in Section 4.

Part of the scatter in the RUS data is probably because the actual cracks were not perfectly straight, while the cracks for FEA were modeled to be perfectly straight down the centerline of the sample. In all four specimens, the divergence from the sample centerline increased with crack length. FEA models were analyzed to determine how much this divergence affected the results. This data is presented in Tables C.7-C.9 of

Appendix C. After examining the FEA data, it was decided to consider cracks that had a deviation from centerline of the sample less than 4 mm, since it introduced error smaller than 10% when compared to the perfectly straight crack. This criteria would eliminate all data from Specimen #9, and the last data point from Specimen #4).

The discrepancy between measured and calculated shifts in resonant frequencies are in agreement with the results published by Belyaev et al on the effect of defects in silicon wafers on resonant peaks (see Section 4.3 for further discussion).[14] These results extend Belyaev et al.'s results by demonstrating that this "offset" effect appears across multiple modes. Further, these results demonstrate that, for some modes, the difference between predicted and actual frequency shift may become constant over certain frequency ranges. It may be possible, by taking advantage of this near-constant offset, to use FEA analysis supplemented by some experimental results to predict actual frequency shift of a wide range of defect sizes and locations. Further research is needed to confirm this, however.

The results for the ceramic specimens eliminate plastic deformation of the sample as a possible cause of the observed discrepancy. Unlike the steel samples with fatigue cracks (Section 4), the ceramic samples do not plastically deform when loaded. None of the ceramic samples had any measureable deformation due to loading. While deformation may have contributed to the discrepancy between measured and calculated resonant frequencies in the steel samples, notably steel fatigue cracked Specimens 1 and 5; plastic deformation was clearly not present in the ceramic specimens. Therefore, the discrepancy between FEA calculated and RUS measured resonant frequencies cannot have been caused by plastic deformation of the ceramic specimens.

As with the steel fatigue crack specimens with fatigue cracks discussed in Section 4, frequency divergence is most likely the result of interaction forces generated between the crack faces at the crack tip. To examine that possibility, the ultrasound attenuation (Q^{-1}) was calculated from the resonant peaks using Equation 5.3.[8,31,37] The Q^{-1} vs. crack depth for several mode shapes are shown in Figure 5.15. As it is described in Section 3 and Section 4, cut specimens experience very little (approximately $\approx 0.1\%$)

change in Q^{-1} as cut depth increases (Section 3, shown in Figures 4.13 – 4.15). In contrast, the ceramic specimens show increasing Q^{-1} width in most modes. The increase in half-peak width of the modes of the ceramic specimens indicates energy most likely associated with friction forces at the crack tip.

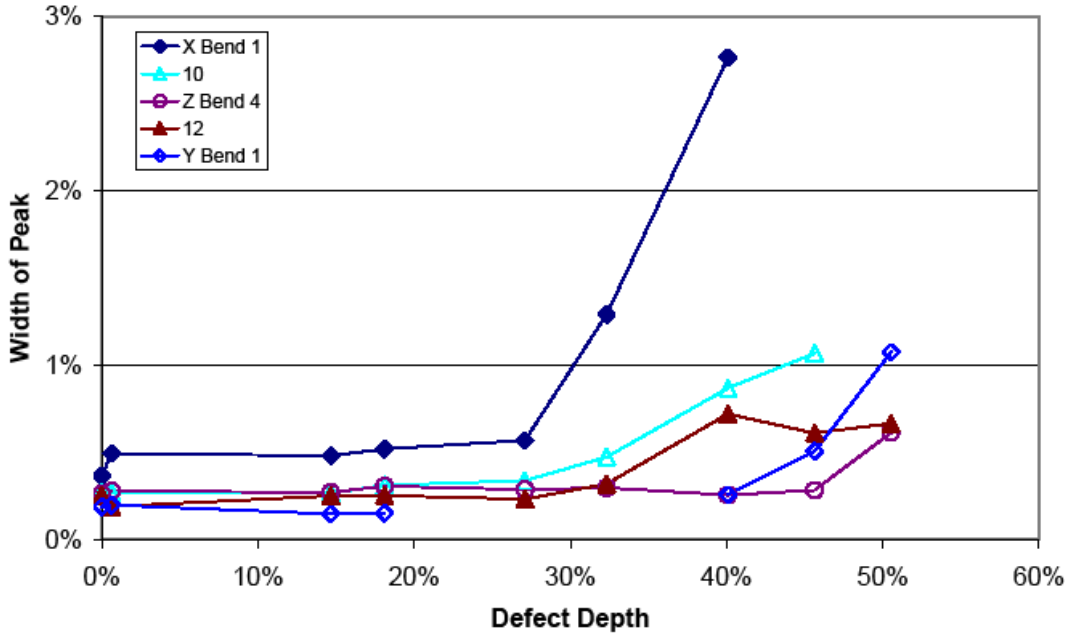

Figure 5.15 Ceramic specimen half-peak damping vs. defect depth for selected modes.

As with the steel samples with fatigue cracks, there are two types of contact forces present: constraint forces and friction forces. Constraint forces are forces normal to the crack face, caused by strain in the normal direction. Constraint forces probably do not cause much energy loss (Q^{-1}). Friction forces are forces parallel to the crack face caused by the faces sliding relative to each other. Friction forces are responsible for the majority of the energy loss measured by Q^{-1}. It seems probable that certain modes should be more influenced by one or the other type of contact force. This may account for the difference in measured Q^{-1} between the various modes. However, further research is needed to confirm this.

The results for damping vs. crack length tend to support Belyaev et al's hypothesis that contact forces within the crack cause the measured frequency shift to be smaller than the actual frequency shift.[14] As crack length increases, so does the width per unit amplitude of the modal peaks, demonstrating increasing energy loss in the specimen with increasing crack depth. This supports the conclusion that contact forces between crack faces cause the energy loss.

6. CONCLUSIONS

In this work, Resonant Ultrasound Spectroscopy (RUS) in combination with Finite Element Analysis (FEA) was used to determine the size and location of a defect in a material of known geometry and physical constants. Analysis of FEA resonant frequency spectra can be used to determine acceptable criteria for the frequency spectrum of an object without the requirement of testing a large number of undamaged and damaged objects. In addition, it is possible to determine not only if on object has a defect, but to determine location and size of the defect by analyzing the frequency spectrum. However, experimental results also indicate that there are limits to the applicability of such a method, the primary one being a lower limit to the size of crack – especially thickness of the crack - for which this method can be applied.

Analysis of the steel specimens with 1 mm wide cuts (Section 3) demonstrates that FEA estimates of resonant frequencies are quite close to measured resonant frequencies, with an average error of 0.63% between measured and calculated resonant frequencies. Therefore, FEA results can be used to predict behavior of actual objects. By analyzing the predicted resonant frequencies of many different FEA models, trends in the behavior of particular resonant modes became evident. When the measured resonant frequencies of specimens with defects of arbitrary location and depth was analyzed using the method outlined in Section 3, these trends in the FEA data could be used to determine location of the defect with an average error less than 5%, and depth with an average error of less than 2%. These results demonstrate the practicability of using FEA to determine acceptance/rejection criteria for NDT in some cases.

Lower-order modes are typically the most sensitive to the depth of the cut. Particularly the first Y bending mode (Y Bend 1), when the cut is parallel to the Y axis, and the first X torsional mode (X Torsion 1) when the cut is parallel to the X axis. This is to be expected, since those modes are most affected by changes in stiffness along those axes. Higher-order modes are sensitive to cut depth, but typically have some "threshold depth value." At cut depths less than the threshold value, there is very little

change in modal frequency. This is particularly noticeable when the cut is near the edge of the specimen.

Analysis of the steel specimens with sharp cracks introduced by fatigue (Section 4) demonstrates that FEA estimates of resonant frequency may not be accurate for some types of defects. Unlike the case of the cut notch, calculated frequency shift due to a particular defect varied greatly from measured frequency shift. This discrepancy did not appear to be caused by any discrepancy between actual and modeled dimensions or physical constants. Most probably, it is caused by contact forces that generate between the two surfaces of the crack during vibration. The strain caused by the RUS technique, while small, was significant enough to cause interaction between the faces if the crack was very thin. This hypothesis is supported by the fact that ultrasound attenuation increases as the crack depth increases, which indicates the presence of some energy dissipating process, such as friction. Another indicator that the thinness of the crack caused the discrepancy is that, when two of the test specimens were accidentally bent in such a way that the crack became much wider, their measured resonant frequency spectrum came much closer to the FEA predicted resonant frequency spectrum.

Analysis of the ceramic specimens with thin cracks (Section 5) also demonstrates that FEA estimates of resonant frequency may not be accurate for some types of defects. Again, calculated frequency shift due to a particular defect varied greatly from measured frequency shift. This variance did not appear to be caused by any discrepancy between actual and modeled dimensions or physical constants. As with the fatigue cracked steel specimens (Section 4), the ceramic specimens showed significant increase in ultrasound attenuation with increasing crack depth in some modes. This tends to support the hypothesis that interaction between crack faces causes the discrepancy in measured vs. calculated frequency.

Analysis of both the steel specimens with fatigue cracks (Section 4) and the ceramic specimens (Section 5) indicates that mode shapes with more relative motion between the crack surfaces and constrained displacement at the crack tip tend to have a greater discrepancy between measured and calculated frequency. In the steel specimens,

this is evident in the marked difference between Y Bend 1 and its first harmonic, Y Bend 2. Y Bend 1 had significant relative motion between the crack faces due to the nature of the mode shape, and calculated frequency shifts are substantially different than measured frequency shifts. In contrast, Y Bend 2 has much less relative motion between crack faces, and measured results for resonant frequency shift are quite close to calculated results. Likewise, in the ceramic specimens, Z Bend 4 has little relative motion between crack faces, and good agreement between measured and calculated frequency shift (although both measured and calculated shifts are very small). In contrast, Y Bend 1 has much more motion between crack faces, and a great difference between measured and calculated resonant frequency shift. This tends to support the hypothesis that interaction between the crack faces is the cause of the discrepancy between measured and calculated resonant frequency shifts.

Based on these results, it is clear that resonant ultrasound spectroscopy can be used in conjunction with FEA to identify the presence of a defect, and to categorize the defect, if the defect is sufficiently large. Very small defects (Section 3) may be within the margin of error of FEA and RUS measurements, and thus cannot be analyzed. Very thin defects (Section 4 and 5) may have contact forces that cannot currently be modeled using commercial finite element analysis programs, and thus cannot be analyzed using FEA. However, defects of sufficient width, depth, and breadth may be analyzed using a FEA, and thus FEA can be used to determine an acceptance/rejection criteria for non-destructive testing using RUS.

Further study is required to determine the minimum width at which FEA models adequately predict resonant frequencies, which may vary with material and/or with the type of RUS equipment used and the strength of the ultrasonic signal. Additional research is also needed to determine a method of finite element analysis that will adequately model contact forces between two surfaces in a frequency analysis.

REFERENCES

[1] Munson, R. & Malloy, J. H. How to conduct an objective investigation of a gas-turbine event. *Combined Cycle Journal* (3rd Quarter), 90-94 (2007).

[2] Witek, L. Stress and fatigue analysis of modified wing-fuselage connector for agricultural aircraft. *Journal of Aircraft* **43** (3), 773-778 (2006).

[3] Witek, L. Failure analysis of the wing-fuselage connector of an agricultural aircraft. *Engineering Failure Analysis* **13** (4), 572-581 (2006).

[4] Transportation Safety Board of Canada, Accident investigation report A00W0105. (2000).

[5] Shull, P. J. *Nondestructive evaluation: theory, techniques, and applications*. (Marcel Dekker, New York, 2002).

[6] Hellier, C. & NetLibrary Inc. *Handbook of non-destructive evaluation.* (McGraw-Hill, New York, 2003).

[7] Bray, D. E. & Stanley, R. K. *Nondestructive evaluation: a tool in design, manufacturing, and service*, Rev. ed. (CRC Press, Boca Raton, FL, 1997).

[8] Migliori, A. & Sarrao, J. L. *Resonant ultrasound spectroscopy: applications to physics, materials measurements, and nondestructive evaluation*. (Wiley, New York, 1997).

[9] Kaewunruen, S. & Remennikov, A. M. Field trials for dynamic characteristics of railway track and its components using impact excitation technique. *Ndt & E International* **40** (7), 510-519 (2007).

[10] Erauw, J. P., Vander Gucht, A., & Cambier, F. Assessment of impact acoustic resonance as a non-destructive testing method for advanced ceramic parts. *Euro Ceramics VIII **8**, Pts 1-3* 264-268, 921-924 (2004).

[11] Gheorghiu, C., Rhazi, J. E., & Labossiere, P. Impact resonance method for fatigue damage detection in reinforced concrete beams with carbon fibre reinforced polymer. *Canadian Journal of Civil Engineering* **32** (6), 1093-1102 (2005).

[12] Schwarz, R. B. & Vuorinen, J. F. Resonant ultrasound spectroscopy: applications, current status and limitations. *Journal of Alloys and Compounds* **310** (1-2), 243-250 (2000).

[13] Cawley, P. & Adams, R. D. Location of defects in structures from measurements of natural frequencies. *Journal of Strain Analysis for Engineering Design* **14** (2), 49-57 (1979).

[14] Belyaev, A., Polupan, O., Dallas, W., Ostapenko, S., Hess, D. Crack detection and analyses using resonance ultrasonic vibrations in full-size crystalline silicon wafers. *Applied Physics Letters* **88** (11), 1-3 (2006).

[15] Belyaev, A., Polupan, O., Ostapenko, S. Hess, D., Kalejs, J. P. Resonance ultrasonic vibration diagnostics of elastic stress in full-size silicon wafers. *Semiconductor Science and Technology* **21** (3), 254 (2006).

[16] Dallas, W., Polupan, O., & Ostapenko, S. Resonance ultrasonic vibrations for crack detection in photovoltaic silicon wafers. *Measurement Science & Technology* **18** (3), 852-858 (2007).

[17] Kam, T. Y. & Lee, T. Y. Detection of cracks in structures using modal test data. *Engineering Fracture Mechanics* **42** (2), 381-387 (1992).

[18] Lee, Y. S. & Chung, M. J. A study on crack detection using eigenfrequency test data. *Computers & Structures* **77** (3), 327-342 (2000).

[19] Rizos, P. F., Aspragathos, N., & Dimarogonas, A. D. Identification of crack location and magnitude in a cantilever beam from the vibration modes. *Journal of Sound and Vibration* **138** (3), 381-388 (1990).

[20] De Silva, C. W. *Vibration : fundamentals and practice*. (CRC Press, Boca Raton, Fla., 2000).

[21] McGovern, S. Spring-Mass System, Available at http://www.2pi.us/, (2008).

[22] Fertis, Demeter G. *Mechanical and structural vibrations*. (Wiley, New York, 1995).

[23] Lzyvzl Forced Vibration Response, Available at http://en.wikipedia.org/wiki/Vibration, (2007).

[24] Thomson, W.T. *Theory of vibration with applications*. (Prentice-Hall, Englewood Cliffs, NJ, 1972).

[25] Fletcher, N. H. & Rossing, T. D. *The physics of musical instruments*, 2nd ed. (Springer, New York, 1998).

[26] Morse, P. M & Ingard, K. U. *Theoretical acoustics*. (McGraw-Hill, New York, 1968).

[27] Gough, C. E. The mass-loaded and nonlinear vibrating string problem revisited. *European Journal of Physics* **5** (2), L11 (2000).

[28] Ulrich, T. J. University of Nevada Reno. Dept. of Physics Thesis (MS), 2000.

[29] Vuorinen, R.B. Schwarz; F.F. Resonant ultrasound spectroscopy: applications, current status and limitations. *Journal of Alloys and Compounds* **310** (1), 7 (2000).

[30] Zadler, B. J., Le Rousseau, J. H. L., Scales, J. A., & Smith, M. L. Resonant Ultrasound Spectroscopy: theory and application. *Geophysical Journal International* **156** (1), 154-169 (2004).

[31] Leisure, R. G. & Willis, F. A. Resonant ultrasound spectroscopy. *Journal of Physics-Condensed Matter* **9** (28), 6001-6029 (1997).

[32] Migliori, A. & Maynard, J. D. Implementation of a modern resonant ultrasound spectroscopy system for the measurement of the elastic moduli of small solid specimens. *Rev Sci Instrum* **76** (12), 11-19 (2005).

[33] Chawla, K. K. *Composite materials : science and engineering*, 2nd ed. (Springer, New York, 1998).

[34] Radovic, M., Lara-Curzio, E., & Riester, L. Comparison of different experimental techniques for determination of elastic properties of solids. *Materials Science and Engineering a-Structural Materials Properties Microstructure and Processing* **368** (1-2), 56-70 (2004).

[35] Visscher, W. M., Migliori, A., Bell, T. M., & Reinert, R. A. On the normal-modes of free-vibration of inhomogeneous and anisotropic elastic objects. *Journal of the Acoustical Society of America* **90** (4), 2154-2162 (1991).

[36] Stekel, A. Sarrao, J., Bell, T., Lei, M. Leisure, R.., *et al.* Method for identification of the vibrational-modes of a rectangular parallelepiped. *Journal of the Acoustical Society of America* **92** (2), 663-668 (1992).

[37] Migliori, A., Sarrao, J.L., Visscher, W., Bell, T., Lei, M. Resonant ultrasound spectroscopic techniques for measurement of the elastic-moduli of solids. *Physica B* **183** (1-2), 1-24 (1993).

[38] Gupta, K. K. & Meek, J. L. *Finite element multidisciplinary analysis*. (American Institute of Aeronautics and Astronautics, Reston, VA, 2000).

[39] Reddy, J. N. *An introduction to the finite element method*, 3rd ed. (McGraw-Hill Higher Education, New York, NY, 2006).

[40] Ross, C. T. F. *Advanced finite element methods*. (Horwood, Chichester, 1998).

[41] Abaqus Help File (Abaqus).

[42] Evans, A. G. *Fracture in ceramic materials : toughening mechanisms, machining damage, shock*. (Noyes Publications, Park Ridge, NJ, 1984).

APPENDIX A

Table A-1 List of abbreviations used in appendices

Mode	Name of the mode shape corresponding to each particular resonant frequency
FEM	Resonant frequency of specimen (kHz) calculated using finite element analysis
RUS	Resonant frequency of specimen (kHz) measured using resonant ultrasound spectroscopy
Lagrange	Resonant frequency of specimen (kHz) calculated using Lagrangian minimization (RPModel software - refer to Section 2)
RUS vs. FEM	Difference between FEM calculated frequency and RUS measured frequency (Equation A.1)

$$RUSvs.FEM = \frac{|RUS - FEM|}{RUS} * 100 \qquad \text{Eqn. A.1}$$

RUS vs. Lagrange	Difference between Lagrange calculated frequency and RUS measured frequency (Equation A.2)

$$RUSvs.Lagrange = \frac{|RUS - Lagrange|}{RUS} * 100 \qquad \text{Eqn. A.2}$$

FEM vs. Lagrange	Difference between FEM calculated frequency and Lagrange calculated frequency (Equation A.3)

$$FEMvs.Lagrange = \frac{|FEM - Lagrange|}{FEM} * 100 \qquad \text{Eqn. A.3}$$

Defect Depth	Measured depth (aka length) of cut or crack in specimen (mm), averaged between front and back of specimen (Equation A.4). Sometimes expressed as a fraction of specimen thickness or length.

$$DefectDepth = \frac{DefectDepthFront + DefectDepthBack}{2} \qquad \text{Eqn. A.3}$$

Attenuation	Ultrasound attenuation (Q^{-1}) given in Equation 4.1.
Defect Width	Measured width of cut or crack (i.e. offset from centerline) in specimen (mm).

Table A-2 Steel Specimen #1 resonant frequencies before and after 1 mm cut

Before Defect							After Defect			
Mode	**FEM (kHz)**	**Lagrange (kHz)**	**RUS (kHz)**	**RUS vs. FEM**	**RUS vs. Lagrange**	**FEM vs. Lagrange**	**Mode**	**FEM (kHz)**	**RUS (kHz)**	**RUS vs. FEM**
X Torsion 1	58.832	58.848	59.109	0.47%	0.44%	0.03%	**X Torsion 1**	54.690	55.325	1.15%
Y Bend 1	66.942	66.953	67.052	0.16%	0.15%	0.02%	**Y Bend 1**	55.352	56.177	1.47%
Z Bend 1	67.068	67.021	67.314	0.37%	0.44%	0.07%	**Z Bend 1**	63.445	63.868	0.66%
Volume 1	100.790	100.777	100.772	0.02%	0.00%	0.01%	**Volume 1**	95.742	95.984	0.25%
Z Bend 2	112.040	112.110	112.124	0.07%	0.01%	0.06%	**Z Bend 2**	104.460	105.572	1.05%
Y Bend 2	112.160	112.172	112.582	0.37%	0.36%	0.01%	**Y Bend 2**	110.220	110.696	0.43%
X Torsion 2	117.130	117.196	117.611	0.41%	0.35%	0.06%	**X Torsion 2**	118.290	118.690	0.34%
	134.090	134.271	133.932	0.12%	0.25%	0.13%		132.990	132.962	0.02%
	139.660	139.827	139.462	0.14%	0.26%	0.12%		134.940	135.103	0.12%
	159.460	159.620	159.304	0.10%	0.20%	0.10%		159.080	159.421	0.21%
	159.610	159.704	159.777	0.10%	0.05%	0.06%		159.590	160.761	0.73%
	160.350	160.500	160.129	0.14%	0.23%	0.09%		159.790		
	160.930	161.060	160.899	0.02%	0.10%	0.08%		161.270	161.013	0.16%
	161.040	161.120	161.669	0.39%	0.34%	0.05%		161.960	161.792	0.10%
	163.060	163.357	163.253	0.12%	0.06%	0.18%		162.510	162.807	0.18%
	168.840	169.142	169.146	0.18%	0.00%	0.18%		164.320	165.390	0.65%
	174.260	174.428	174.945	0.39%	0.30%	0.10%		167.910	168.349	0.26%
	178.000	178.211	177.834	0.09%	0.21%	0.12%		176.470	177.001	0.30%
	178.050	178.405	178.452	0.23%	0.03%	0.20%		177.030	177.081	0.03%
	178.410	178.783	178.524	0.06%	0.15%	0.21%		177.500	177.894	0.22%
	178.700	178.815	178.969	0.15%	0.09%	0.06%		179.160	179.545	0.21%

Refer to Appendix A, Table A-1 for explanation of abbreviations.

Continued on next page.

Table A-2 Continued

Before Defect							After Defect			
Mode	**FEM (kHz)**	**Lagrange (kHz)**	**RUS (kHz)**	**RUS vs. FEM**	**RUS vs. Lagrange**	**FEM vs. Lagrange**	**Mode**	**FEM (kHz)**	**RUS (kHz)**	**RUS vs. FEM**
	179.170	179.241	179.501	0.18%	0.14%	0.04%		179.740	180.035	0.16%
	180.790	181.072	180.214	0.32%	0.48%	0.16%		181.150	180.846	0.17%
	180.820	181.090	181.019	0.11%	0.04%	0.15%		181.290	181.540	0.14%
	181.350	181.388	181.594	0.13%	0.11%	0.02%		181.730	181.734	0.00%
	194.320	194.641	194.634	0.16%	0.00%	0.17%		191.300	191.915	0.32%
	195.890	196.313	195.809	0.04%	0.26%	0.22%		195.330	195.434	0.05%
	196.420	196.612	197.028	0.31%	0.21%	0.10%		196.640	197.266	0.32%
	197.860	198.195	198.222	0.18%	0.01%	0.17%		197.430	198.089	0.33%
	203.610	203.968	203.815	0.10%	0.08%	0.18%		198.080	198.336	0.13%
	212.840	213.266	213.352	0.24%	0.04%	0.20%		208.280	208.876	0.29%
	214.430	214.954	214.529	0.05%	0.20%	0.24%		210.820	211.455	0.30%
	214.700	215.099	215.252	0.26%	0.07%	0.19%		210.930	211.847	0.43%
	215.370	215.595	215.611	0.11%	0.01%	0.10%		211.940	212.731	0.37%
	217.300	217.518	217.409	0.05%	0.05%	0.10%		212.810	213.602	0.37%
	218.300	218.631	218.558	0.12%	0.03%	0.15%		215.770	216.020	0.12%
	218.340	218.647	219.135	0.36%	0.22%	0.14%		218.590	218.962	0.17%
	220.870	221.311	221.507	0.29%	0.09%	0.20%		221.880	222.422	0.24%
	226.790	227.020	226.684	0.05%	0.15%	0.10%		224.580	225.733	0.51%
	229.230	230.193	230.111	0.38%	0.04%	0.42%		226.400	226.590	0.08%
			Average:	0.19%	0.16%	0.12%			**Average:**	0.33%

Refer to Appendix A, Table A-1 for explanation of abbreviations.

Table A-3 Steel Specimen #2 resonant frequencies before and after 1 mm cut

Before Defect							After Defect			
Mode	**FEM (kHz)**	**Lagrange (kHz)**	**RUS (kHz)**	**RUS vs FEM**	**RUS vs Lagrange**	**FEM vs Lagrange**	**Mode**	**FEM (kHz)**	**RUS (kHz)**	**RUS vs FEM**
X Torsion 1	58.879	58.921	59.160	0.47%	0.40%	0.07%	**X Torsion 1**	56.776	57.254	0.83%
Y Bend 1	67.042	67.096	67.204	0.24%	0.16%	0.08%	**Y Bend 1**	61.509	62.007	0.80%
Z Bend 1	67.110	67.155	67.375	0.39%	0.33%	0.07%	**Z Bend 1**	64.897	65.337	0.67%
Volume 1	100.850	100.909	100.881	0.03%	0.03%	0.06%	**Volume 1**	94.130	94.698	0.60%
Z Bend 2	112.110	112.214	112.233	0.11%	0.02%	0.09%	**Z Bend 2**	104.570	105.762	1.13%
Y Bend 2	112.190	112.268	112.676	0.43%	0.36%	0.07%	**Y Bend 2**	107.280	107.533	0.24%
X Torsion 2	117.230	117.339	117.738	0.43%	0.34%	0.09%	**X Torsion 2**	111.790	112.450	0.59%
	134.060	134.215	133.875	0.14%	0.25%	0.12%		128.890	129.327	0.34%
	139.650	139.832	139.456	0.14%	0.27%	0.13%		136.170	136.085	0.06%
	159.550	159.719	159.359	0.12%	0.23%	0.11%		143.760	144.680	0.64%
	159.650	159.793	159.767	0.07%	0.02%	0.09%		150.630	151.643	0.67%
	160.330	160.465	160.236	0.06%	0.14%	0.08%		156.020	156.659	0.41%
	161.020	161.188	160.994	0.02%	0.12%	0.10%		157.540	158.211	0.42%
	161.090	161.238	161.769	0.42%	0.33%	0.09%		160.820	160.261	0.35%
	163.040	163.310	163.200	0.10%	0.07%	0.17%		161.430	161.583	0.09%
	168.830	169.111	169.086	0.15%	0.01%	0.17%		166.790	167.015	0.13%
	174.400	174.635	175.129	0.42%	0.28%	0.13%		169.980	170.447	0.27%
	178.090	178.273	177.909	0.10%	0.20%	0.10%		172.060	171.808	0.15%
	178.160	178.486	178.494	0.19%	0.00%	0.18%		172.100	172.919	0.47%
	178.550	178.808	178.555	0.00%	0.14%	0.14%		177.130	177.840	0.40%
	178.570	178.881	179.041	0.26%	0.09%	0.17%		178.210	178.789	0.32%

Refer to Appendix A, Table A-1 for explanation of abbreviations.

Continued on next page.

Table A-3 Continued

Before Defect							After Defect			
Mode	**FEM (kHz)**	**Lagrange (kHz)**	**RUS (kHz)**	**RUS vs FEM**	**RUS vs Lagrange**	**FEM vs Lagrange**	**Mode**	**FEM (kHz)**	**RUS (kHz)**	**RUS vs FEM**
	179.030	179.245	179.533	0.28%	0.16%	0.12%		178.990		
	180.820	181.025	180.293	0.29%	0.41%	0.11%		179.300	179.827	0.29%
	180.880	181.112	181.083	0.11%	0.02%	0.13%		180.800	181.193	0.22%
	181.350	181.492	181.709	0.20%	0.12%	0.08%		182.390	182.781	0.21%
	194.290	194.644	194.593	0.16%	0.03%	0.18%		186.350	187.271	0.49%
	196.010	196.371	195.828	0.09%	0.28%	0.18%		194.340	194.558	0.11%
	196.330	196.626	197.091	0.39%	0.24%	0.15%		194.880	195.367	0.25%
	197.840	198.205	198.156	0.16%	0.02%	0.18%		196.100	196.410	0.16%
	203.640	204.004	203.843	0.10%	0.08%	0.18%		200.320	201.057	0.37%
	212.850	213.279	213.329	0.22%	0.02%	0.20%		200.550		
	214.500	214.985	214.509	0.00%	0.22%	0.23%		207.380	207.824	0.21%
	214.630	215.110	215.226	0.28%	0.05%	0.22%		208.680	209.737	0.50%
	215.410	215.670	215.713	0.14%	0.02%	0.12%		211.640	211.962	0.15%
	217.380	217.644	217.514	0.06%	0.06%	0.12%		212.690	213.035	0.16%
	218.400	218.800	218.718	0.15%	0.04%	0.18%		215.510	216.118	0.28%
	218.420	218.813	219.252	0.38%	0.20%	0.18%		218.390	219.026	0.29%
	220.900	221.420	221.624	0.33%	0.09%	0.24%		219.390	219.924	0.24%
	226.870	227.158	226.840	0.01%	0.14%	0.13%		221.770	222.051	0.13%
	229.400	230.451	230.357	0.42%	0.04%	0.46%		225.640	226.560	0.41%
			Average:	0.20%	0.15%	0.14%			**Average:**	0.37%

Refer to Appendix A, Table A-1 for explanation of abbreviations.

Table A-4 Steel Specimen #3 resonant frequencies before and after 1 mm cut

Before Defect							After Defect			
Mode	**FEM (kHz)**	**Lagrange (kHz)**	**RUS (kHz)**	**RUS vs FEM**	**RUS vs Lagrange**	**FEM vs Lagrange**	**Mode**	**FEM (kHz)**	**RUS (kHz)**	**RUS vs FEM**
X Torsion 1	58.847	58.903	59.118	0.46%	0.36%	0.10%	**X Torsion 1**	59.012	59.267	0.43%
Y Bend 1	66.966	67.033	67.039	0.11%	0.01%	0.10%	**Y Bend 1**	66.482	66.593	0.17%
Z Bend 1	67.090	67.115	67.310	0.33%	0.29%	0.04%	**Z Bend 1**	66.485	66.813	0.49%
Volume 1	100.810	100.882	100.764	0.05%	0.12%	0.07%	**Volume 1**	96.461	97.683	1.25%
Z Bend 2	112.060	112.200	112.135	0.07%	0.06%	0.12%	**Y Bend 2**	105.960	106.809	0.79%
Y Bend 2	112.170	112.277	112.587	0.37%	0.28%	0.10%	**Z Bend 2**	109.180	110.475	1.17%
X Torsion 2	117.160	117.305	117.577	0.35%	0.23%	0.12%	**X Torsion 2**	111.520	112.368	0.75%
	134.080	134.327	133.944	0.10%	0.29%	0.18%		121.720	123.737	1.63%
	139.650	139.911	139.480	0.12%	0.31%	0.19%		127.260	130.354	2.37%
	159.480	159.730	159.280	0.13%	0.28%	0.16%		136.190	136.237	0.03%
	159.640	159.833	159.803	0.10%	0.02%	0.12%		149.710	150.630	0.61%
	160.340	160.579	160.121	0.14%	0.29%	0.15%		150.980	152.683	1.12%
	160.960	161.184	160.888	0.04%	0.18%	0.14%		157.790	159.343	0.97%
	161.060	161.256	161.639	0.36%	0.24%	0.12%		160.150	160.269	0.07%
	163.050	163.433	163.247	0.12%	0.11%	0.23%		160.790	160.634	0.10%
	168.830	169.226	169.127	0.18%	0.06%	0.23%		163.560	164.232	0.41%
	174.330	174.588	174.922	0.34%	0.19%	0.15%		163.820	164.560	0.45%
	178.010	178.340	177.848	0.09%	0.28%	0.19%		165.740	166.335	0.36%
	178.070	178.509	178.450	0.21%	0.03%	0.25%		167.450	168.738	0.76%
	178.400	178.897	178.524	0.07%	0.21%	0.28%		175.270	175.805	0.30%
	178.700	178.968	178.985	0.16%	0.01%	0.15%		177.830	178.309	0.27%

Refer to Appendix A, Table A-1 for explanation of abbreviations.

Continued on next page.

Table A-4 Continued

Before Defect							After Defect			
Mode	**FEM (kHz)**	**Lagrange (kHz)**	**RUS (kHz)**	**RUS vs FEM**	**RUS vs Lagrange**	**FEM vs Lagrange**	**Mode**	**FEM (kHz)**	**RUS (kHz)**	**RUS vs FEM**
	179.190	179.414	179.516	0.18%	0.06%	0.13%		178.680	178.562	0.07%
	180.810	181.156	180.245	0.31%	0.51%	0.19%		179.310	179.859	0.31%
	180.830	181.178	181.103	0.15%	0.04%	0.19%		179.910	180.529	0.34%
	181.370	181.538	181.603	0.13%	0.04%	0.09%		180.950	181.453	0.28%
	194.310	194.789	194.629	0.16%	0.08%	0.25%		181.940	182.437	0.27%
	195.880	196.415	195.817	0.03%	0.31%	0.27%		184.410	185.090	0.37%
	196.440	196.778	197.031	0.30%	0.13%	0.17%		186.810	187.206	0.21%
	197.860	198.343	198.212	0.18%	0.07%	0.24%		195.620	195.383	0.12%
	203.620	204.104	203.826	0.10%	0.14%	0.24%		195.660	196.305	0.33%
	212.840	213.414	213.354	0.24%	0.03%	0.27%		196.130	197.097	0.49%
	214.430	215.076	214.521	0.04%	0.26%	0.30%		201.740	202.792	0.52%
	214.700	215.252	215.229	0.25%	0.01%	0.26%		204.960	205.485	0.26%
	215.380	215.743	215.601	0.10%	0.07%	0.17%		207.550	208.257	0.34%
	217.330	217.688	217.402	0.03%	0.13%	0.16%		213.860	214.692	0.39%
	218.340	218.807	218.557	0.10%	0.11%	0.21%		214.740	215.707	0.45%
	218.360	218.826	219.091	0.33%	0.12%	0.21%		216.130	216.935	0.37%
	220.880	221.497	221.500	0.28%	0.00%	0.28%		216.830	217.509	0.31%
	226.820	227.205	226.704	0.05%	0.22%	0.17%		216.920	217.815	0.41%
	229.300	230.402	230.086	0.34%	0.14%	0.48%		219.160	220.135	0.44%
			Average:	0.18%	0.16%	0.19%			**Average:**	0.52%

Refer to Appendix A, Table A-1 for explanation of abbreviations.

Table A-5 Steel Specimen #4 resonant frequencies before and after 1 mm cut

Before Defect

Mode	FEM (kHz)	Lagrange (kHz)	RUS (kHz)	RUS vs FEM	RUS vs Lagrange	FEM vs Lagrange
X Torsion 1	58.568	58.674	58.955	0.66%	0.48%	0.18%
Z Bend 1	66.759	66.628	66.806	0.07%	0.27%	0.20%
Y Bend 1	66.782	66.682	66.971	0.28%	0.43%	0.15%
Volume 1	100.410	100.464	100.472	0.06%	0.01%	0.05%
Y Bend 2	111.610	111.877	111.861	0.22%	0.01%	0.24%
Z Bend 2	111.680	111.925	112.357	0.60%	0.38%	0.22%
X Torsion 2	116.610	116.853	117.258	0.55%	0.35%	0.21%
	133.430	134.411	133.962	0.40%	0.34%	0.74%
	139.040	139.821	139.385	0.25%	0.31%	0.56%
	158.790	159.405	159.025	0.15%	0.24%	0.39%
	158.880	159.468	159.758	0.55%	0.18%	0.37%
	159.650	160.590	159.844	0.12%	0.47%	0.59%
	160.290	160.775	160.594	0.19%	0.11%	0.30%
	160.360	160.824	161.273	0.57%	0.28%	0.29%
	162.410	163.476	163.334	0.57%	0.09%	0.66%
	168.230	169.221	169.131	0.53%	0.05%	0.59%
	173.510	173.933	174.376	0.50%	0.25%	0.24%
	177.190	178.064	177.642	0.25%	0.24%	0.49%
	177.310	178.325	178.406	0.61%	0.05%	0.57%
	177.550	178.627	178.477	0.52%	0.08%	0.61%
	177.620	178.784	178.855	0.69%	0.04%	0.66%

After Defect

Mode	FEM (kHz)	RUS (kHz)	RUS vs FEM
X Torsion 1	53.811	54.287	0.88%
Y Bend 1	65.826	65.921	0.14%
Z Bend 1	66.650	66.604	0.07%
Volume 1	100.480	100.120	0.36%
Y Bend 2	105.830	105.380	0.43%
X Torsion 2	107.340	106.810	0.50%
Z Bend 2	111.330	110.890	0.40%
	111.480	111.250	0.21%
	119.900	119.450	0.38%
	126.840	126.250	0.47%
	136.550	135.160	1.03%
	136.640	136.730	0.07%
	148.350	147.440	0.62%
	153.880	153.040	0.55%
	156.890	155.990	0.58%
	158.570	157.620	0.60%
	163.260	162.620	0.39%
	164.880	164.260	0.38%
	166.860	166.110	0.45%
	170.150	169.210	0.56%
	171.950	170.780	0.69%

Refer to Appendix A, Table A-1 for explanation of abbreviations.

Continued on next page.

Table A-5 Continued

Before Defect							After Defect			
Mode	FEM (kHz)	Lagrange (kHz)	RUS (kHz)	RUS vs FEM	RUS vs Lagrange	FEM vs Lagrange	Mode	FEM (kHz)	RUS (kHz)	RUS vs FEM
	178.060	179.121	179.381	0.74%	0.14%	0.60%		173.510	172.380	0.66%
	180.100	180.988	179.994	0.06%	0.55%	0.49%		176.830	175.940	0.51%
	180.150	181.190	181.127	0.54%	0.03%	0.58%		177.870	177.100	0.43%
	180.550	181.197	181.451	0.50%	0.14%	0.36%		182.230	181.510	0.40%
	193.400	194.643	194.614	0.62%	0.01%	0.64%		182.740	182.080	0.36%
	194.970	196.263	195.686	0.37%	0.29%	0.66%		187.010	186.000	0.54%
	195.310	196.499	196.899	0.81%	0.20%	0.61%		191.130	189.340	0.95%
	196.960	198.181	198.191	0.62%	0.01%	0.62%		191.480	190.580	0.47%
	202.460	203.887	203.664	0.59%	0.11%	0.70%		195.840	194.580	0.65%
	211.570	213.242	213.265	0.79%	0.01%	0.79%		198.240	196.830	0.72%
	213.520	214.925	214.248	0.34%	0.32%	0.66%		201.540	200.020	0.76%
	213.560	215.039	215.138	0.73%	0.05%	0.69%		204.160	202.830	0.66%
	214.450	215.423	215.466	0.47%	0.02%	0.45%		204.850	203.520	0.65%
	216.430	217.223	217.070	0.29%	0.07%	0.37%		207.290	206.190	0.53%
	217.280	218.228	218.147	0.40%	0.04%	0.44%		209.550	208.450	0.53%
	217.500	218.245	218.674	0.54%	0.20%	0.34%		211.780	210.650	0.54%
	219.670	221.061	221.321	0.75%	0.12%	0.63%		216.720	215.560	0.54%
	225.870	226.693	226.344	0.21%	0.15%	0.36%		222.700	221.590	0.50%
	228.190	229.578	229.519	0.58%	0.03%	0.61%		223.040	221.920	0.50%
			Average:	0.46%	0.18%	0.47%			**Average:**	0.52%

Refer to Appendix A, Table A-1 for explanation of abbreviations.

Table A-6 Steel Specimen #5 resonant frequencies before and after 1 mm cut

Before Defect							After Defect			
Mode	**FEM (kHz)**	**Lagrange (kHz)**	**RUS (kHz)**	**RUS vs FEM**	**RUS vs Lagrange**	**FEM vs Lagrange**	**Mode**	**FEM (kHz)**	**RUS (kHz)**	**RUS vs FEM**
X Torsion 1	58.882	58.910	59.164	0.48%	0.43%	0.05%	**X Torsion 1**	55.982	56.229	0.44%
Z Bend 1	67.012	67.043	67.133	0.18%	0.13%	0.05%	**Y Bend 1**	66.243	66.512	0.40%
Y Bend 1	67.060	67.091	67.308	0.37%	0.32%	0.05%	**Z Bend 1**	66.858	67.031	0.26%
Volume 1	100.850	100.865	100.795	0.05%	0.07%	0.01%	**Volume 1**	100.740	100.710	0.03%
Y Bend 2	112.160	112.208	112.182	0.02%	0.02%	0.04%	**Y Bend 2**	108.220	108.458	0.22%
Z Bend 2	112.210	112.253	112.653	0.39%	0.36%	0.04%	**X Torsion 2**	109.860	110.082	0.20%
X Torsion 2	117.230	117.319	117.702	0.40%	0.33%	0.08%	**Z Bend 2**	112.430	112.414	0.01%
	134.220	134.306	133.938	0.21%	0.27%	0.06%		117.960	116.564	1.20%
	139.770	139.881	139.482	0.21%	0.29%	0.08%		123.290	122.215	0.88%
	159.650	159.743	159.322	0.21%	0.26%	0.06%		132.610	132.226	0.29%
	159.710	159.804	159.747	0.02%	0.04%	0.06%		136.200	135.553	0.48%
	160.500	160.550	160.204	0.18%	0.22%	0.03%		141.570	141.144	0.30%
	161.100	161.195	160.946	0.10%	0.15%	0.06%		146.900	146.826	0.05%
	161.140	161.237	161.754	0.38%	0.32%	0.06%		156.190	156.373	0.12%
	163.220	163.407	163.280	0.04%	0.08%	0.11%		158.720	158.639	0.05%
	169.000	169.201	169.209	0.12%	0.00%	0.12%		159.520	159.031	0.31%
	174.430	174.608	175.105	0.39%	0.28%	0.10%		162.950	162.839	0.07%
	178.200	178.295	177.860	0.19%	0.24%	0.05%		165.400	165.136	0.16%
	178.320	178.492	178.530	0.12%	0.02%	0.10%		167.040	167.241	0.12%
	178.590	178.761	178.574	0.01%	0.10%	0.10%		167.130	167.589	0.27%
	178.760	178.930	179.004	0.14%	0.04%	0.10%		175.070	175.277	0.12%

Refer to Appendix A, Table A-1 for explanation of abbreviations.

Continued on next page.

Table A-6 Continued

Before Defect							After Defect			
Mode	FEM (kHz)	Lagrange (kHz)	RUS (kHz)	RUS vs FEM	RUS vs Lagrange	FEM vs Lagrange	Mode	FEM (kHz)	RUS (kHz)	RUS vs FEM
	179.060	179.234	179.546	0.27%	0.17%	0.10%		175.410	175.849	0.25%
	181.030	181.135	180.204	0.46%	0.52%	0.06%		176.480	176.356	0.07%
	181.050	181.201	181.124	0.04%	0.04%	0.08%		179.250		
	181.420	181.507	181.648	0.13%	0.08%	0.05%		181.710	178.955	1.54%
	194.420	194.633	194.646	0.12%	0.01%	0.11%		182.850	181.716	0.62%
	196.200	196.425	195.844	0.18%	0.30%	0.11%		183.480	182.943	0.29%
	196.420	196.638	197.087	0.34%	0.23%	0.11%		185.540	183.635	1.04%
	197.980	198.200	198.251	0.14%	0.03%	0.11%		189.130	185.586	1.91%
	203.790	204.048	203.837	0.02%	0.10%	0.13%		192.840	189.454	1.79%
	212.990	213.303	213.371	0.18%	0.03%	0.15%		195.480	193.155	1.20%
	214.680	215.051	214.582	0.05%	0.22%	0.17%		195.490	195.817	0.17%
	214.770	215.154	215.319	0.25%	0.08%	0.18%		199.350	195.970	1.72%
	215.540	215.716	215.682	0.07%	0.02%	0.08%		204.220	199.721	2.25%
	217.480	217.651	217.475	0.00%	0.08%	0.08%		206.840	204.266	1.26%
	218.490	218.803	218.717	0.10%	0.04%	0.14%		212.540	206.983	2.68%
	218.500	218.814	219.256	0.34%	0.20%	0.14%		214.190	212.925	0.59%
	221.010	221.387	221.588	0.26%	0.09%	0.17%		216.070	214.433	0.76%
	226.950	227.148	226.712	0.10%	0.19%	0.09%		219.640	216.215	1.58%
	229.410	230.421	230.323	0.40%	0.04%	0.44%		221.470	219.958	0.69%
			Average:	0.19%	0.16%	0.10%			**Average:**	0.68%

Refer to Appendix A, Table A-1 for explanation of abbreviations.

Table A-7 Steel Specimen #6 resonant frequencies before and after 1 mm cut

Before Defect							After Defect			
Mode	**FEM (kHz)**	**Lagrange (kHz)**	**RUS (kHz)**	**RUS vs FEM**	**RUS vs Lagrange**	**FEM vs Lagrange**	**Mode**	**FEM (kHz)**	**RUS (kHz)**	**RUS vs FEM**
X Torsion 1	58.918	58.948	59.220	0.51%	0.46%	0.05%	**X Torsion 1**	57.850	58.302	0.78%
Z Bend 1	67.119	67.149	67.242	0.18%	0.14%	0.04%	**Z Bend 1**	66.310	66.696	0.58%
Y Bend 1	67.192	67.222	67.457	0.39%	0.35%	0.04%	**Y Bend 1**	67.235	67.411	0.26%
Volume 1	100.950	100.965	100.941	0.01%	0.02%	0.01%	**X Torsion 2**	92.492	100.760	8.21%
Y Bend 2	112.200	112.245	112.283	0.07%	0.03%	0.04%	**Volume 1**	94.642	103.670	8.71%
Z Bend 2	112.260	112.314	112.733	0.42%	0.37%	0.05%	**Y Bend 2**	99.395	107.019	7.12%
X Torsion 2	117.300	117.391	117.807	0.43%	0.35%	0.08%		101.310		
	134.090	134.182	133.907	0.14%	0.21%	0.07%		109.290	108.883	0.37%
	139.730	139.829	139.531	0.14%	0.21%	0.07%	**Z Bend 2**	112.860	112.609	0.22%
	159.640	159.740	159.432	0.13%	0.19%	0.06%		115.460	113.174	2.02%
	159.740	159.834	159.776	0.02%	0.04%	0.06%		118.640	122.828	3.41%
	160.390	160.441	160.268	0.08%	0.11%	0.03%		130.030	125.654	3.48%
	161.130	161.226	161.077	0.03%	0.09%	0.06%		136.040	136.232	0.14%
	161.180	161.287	161.832	0.40%	0.34%	0.07%		141.360	141.173	0.13%
	163.100	163.280	163.227	0.08%	0.03%	0.11%		152.840		
	168.890	169.088	169.156	0.16%	0.04%	0.12%		159.190	159.829	0.40%
	174.530	174.711	175.260	0.42%	0.31%	0.10%		160.260	161.068	0.50%
	178.210	178.298	177.973	0.13%	0.18%	0.05%		160.480	161.381	0.56%
	178.320	178.483	178.527	0.12%	0.02%	0.09%		162.220	162.186	0.02%
	178.680	178.855	178.594	0.05%	0.15%	0.10%		163.350	163.454	0.06%
	178.730	178.884	179.059	0.18%	0.10%	0.09%		163.760	164.039	0.17%

Refer to Appendix A, Table A-1 for explanation of abbreviations.

Continued on next page.

Table A-7 Continued

Before Defect							After Defect			
Mode	FEM (kHz)	Lagrange (kHz)	RUS (kHz)	RUS vs FEM	RUS vs Lagrange	FEM vs Lagrange	Mode	FEM (kHz)	RUS (kHz)	RUS vs FEM
	179.140	179.309	179.602	0.26%	0.16%	0.09%		166.170	165.701	0.28%
	180.860	180.992	180.356	0.28%	0.35%	0.07%		175.010	167.851	4.27%
	180.940	181.090	181.079	0.08%	0.01%	0.08%		176.520	176.212	0.17%
	181.440	181.542	181.725	0.16%	0.10%	0.06%		176.570	177.782	0.68%
	194.470	194.667	194.641	0.09%	0.01%	0.10%		179.120	177.925	0.67%
	196.140	196.354	195.883	0.13%	0.24%	0.11%		180.190	179.053	0.64%
	196.470	196.674	197.125	0.33%	0.23%	0.10%		180.790	181.090	0.17%
	198.010	198.227	198.247	0.12%	0.01%	0.11%		181.780	182.646	0.47%
	203.740	204.016	203.917	0.09%	0.05%	0.14%		183.240	183.122	0.06%
	212.970	213.294	213.399	0.20%	0.05%	0.15%		185.700	186.806	0.59%
	214.610	214.975	214.570	0.02%	0.19%	0.17%		188.330	189.576	0.66%
	214.770	215.131	215.358	0.27%	0.11%	0.17%		193.380	194.025	0.33%
	215.520	215.692	215.741	0.10%	0.02%	0.08%		195.760	195.233	0.27%
	217.520	217.691	217.607	0.04%	0.04%	0.08%		196.230	196.985	0.38%
	218.530	218.858	218.859	0.15%	0.00%	0.15%		202.110	197.787	2.19%
	218.580	218.873	219.393	0.37%	0.24%	0.13%		207.080	203.091	1.96%
	221.120	221.477	221.665	0.25%	0.08%	0.16%		208.960	208.813	0.07%
	227.020	227.216	226.901	0.05%	0.14%	0.09%		212.430	211.595	0.39%
	229.540	230.545	230.770	0.53%	0.10%	0.44%		213.110	214.692	0.74%
			Average:	0.19%	0.15%	0.10%			**Average:**	1.37%

Refer to Appendix A, Table A-1 for explanation of abbreviations.

Table A-8 Steel Specimen #7 resonant frequencies before and after 1 mm cut

Before Defect Mode	RUS (kHz)	After Defect Mode	RUS (kHz)
X Torsion 1	59.257	**X Torsion 1**	58.706
Y Bend 1	67.103	**Y Bend 1**	65.794
Z Bend 1	67.430	**Z Bend 1**	66.970
Volume 1	100.872	**Volume 1**	100.204
Z Bend 2	112.203	**Z Bend 2**	111.910
Y Bend 2	112.776	**Y Bend 2**	111.993
X Torsion 2	117.784	**X Torsion 2**	117.756

Refer to Appendix A, Table A-1 for explanation of abbreviations.

Table A-9 Steel Specimen #8 resonant frequencies before and after 1 mm cut

Before Defect Mode	RUS (kHz)	After Defect Mode	RUS (kHz)
X Torsion 1	60.166	**X Torsion 1**	59.562
Y Bend 1	68.565	**Y Bend 1**	66.972
Z Bend 1	68.849	**Z Bend 1**	68.055
Volume 1	102.260	**Volume 1**	101.116
Z Bend 2	113.446	**Y Bend 2**	111.440
Y Bend 2	113.930	**Z Bend 2**	112.924
X Torsion 2	119.545	**X Torsion 2**	117.293

Refer to Appendix A, Table A-1 for explanation of abbreviations.

Table A-10 Steel Specimen #9 resonant frequencies before and after 1 mm cut

Before Defect Mode	RUS (kHz)	After Defect Mode	RUS (kHz)
X Torsion 1	58.997	**X Torsion 1**	56.290
Z Bend 1	66.762	**Y Bend 1**	59.094
Y Bend 1	66.896	**Z Bend 1**	64.303
Volume 1	100.422	**Volume 1**	96.602
Y Bend 2	111.918	**Z Bend 2**	106.817
Z Bend 2	112.356	**Y Bend 2**	111.235
X Torsion 2	117.307	**X Torsion 2**	117.534

Refer to Appendix A, Table A-1 for explanation of abbreviations.

Table A-11 Steel Specimen #10 resonant frequencies before and after 1 mm cut

Before Defect Mode	RUS (kHz)	After Defect Mode	RUS (kHz)
X Torsion 1	59.356	**X Torsion 1**	58.715
Z Bend 1	67.411	**Z Bend 1**	67.312
Y Bend 1	67.611	**Y Bend 1**	67.505
Volume 1	101.074	**Volume 1**	101.082
Y Bend 2	112.47	**Y Bend 2**	112.202
Z Bend 2	112.867	**Z Bend 2**	112.540
X Torsion 2	118.044	**X Torsion 2**	116.818

Refer to Appendix A, Table A-1 for explanation of abbreviations.

Table A-12 Steel Specimen #11 resonant frequencies before and after 1 mm cut

Before Defect Mode	RUS (kHz)	After Defect Mode	RUS (kHz)
X Torsion 1	58.985	**X Torsion 1**	58.038
Z Bend 1	66.766	**Z Bend 1**	66.617
Y Bend 1	66.938	**Y Bend 1**	66.820
Volume 1	100.456	**Volume 1**	100.457
Y Bend 2	111.912	**Y Bend 2**	111.360
Z Bend 2	112.341	**Z Bend 2**	112.045
X Torsion 2	117.284	**X Torsion 2**	115.393

Refer to Appendix A, Table A-1 for explanation of abbreviations.

Table A-13 Steel Specimen #12 resonant frequencies before and after 1 mm cut

Before Defect Mode	RUS (kHz)	After Defect Mode	RUS (kHz)
X Torsion 1	58.719	**X Torsion 1**	56.626
Z Bend 1	66.294	**Y Bend 1**	66.141
Y Bend 1	66.647	**Z Bend 1**	66.044
Volume 1	99.971	**Volume 1**	99.940
Y Bend 2	111.519	**Y Bend 2**	109.597
Z Bend 2	111.950	**Z Bend 2**	111.615
X Torsion 2	116.745	**X Torsion 2**	112.611

Refer to Appendix A, Table A-1 for explanation of abbreviations.

Table A-14 Steel Specimen #1 FEM calculated frequencies for cuts of various depths

	Defect Depth (mm)										
Mode	**0.0**	**0.1**	**0.2**	**0.3**	**0.4**	**0.5**	**0.6**	**0.7**	**0.8**	**0.9**	**1.0**
X Torsion 1	58.83	58.78	58.72	58.66	58.57	58.48	58.38	58.26	58.14	58.00	57.86
Y Bend 1	66.94	66.84	66.72	66.55	66.33	66.06	65.77	65.43	65.06	64.66	64.22
Z Bend 1	67.07	67.04	67.02	66.98	66.93	66.87	66.79	66.70	66.60	66.48	66.35
Volume 1	100.79	100.72	100.67	100.60	100.50	100.38	100.24	100.09	99.92	99.73	99.53
Z Bend 2	112.04	111.95	111.87	111.77	111.65	111.50	111.33	111.15	110.92	110.69	110.45
Y Bend 2	112.16	112.13	112.13	112.12	112.12	112.11	112.09	112.09	112.06	112.03	112.00
X Torsion 2	117.13	117.20	117.23	117.31	117.36	117.43	117.48	117.53	117.59	117.63	117.69
8	134.09	134.06	134.05	134.04	134.04	134.03	133.99	133.96	133.97	133.89	133.85
9	139.66	139.59	139.55	139.51	139.40	139.29	139.21	139.05	138.90	138.74	138.55
10	159.46	159.44	159.43	159.43	159.44	159.44	159.44	159.44	159.43	159.44	159.44
11	159.61	159.58	159.59	159.59	159.57	159.57	159.58	159.56	159.55	159.52	159.51
12	160.35	160.32	160.35	160.38	160.43	160.46	160.49	160.53	160.57	160.61	160.66
Z Bend 3	160.93	160.92	160.92	160.93	160.94	160.95	160.96	160.95	160.96	160.96	160.95
Y Bend 3	161.04	161.09	161.16	161.22	161.30	161.36	161.41	161.49	161.55	161.60	161.64
15	163.06	163.03	163.04	163.04	163.04	163.04	163.03	163.00	163.00	162.99	162.96
16	168.84	168.79	168.80	168.78	168.76	168.78	168.76	168.69	168.68	168.64	168.61
X Torsion 3	174.26	174.17	174.02	173.82	173.62	173.35	173.05	172.77	172.41	172.02	171.61
18	178.00	177.98	178.00	178.02	178.00	178.00	177.99	177.99	177.95	177.93	177.93
19	178.05	178.02	178.02	178.03	178.03	178.03	178.02	178.03	177.99	178.00	177.97
20	178.41	178.35	178.35	178.34	178.34	178.33	178.34	178.32	178.33	178.29	178.29
21	178.70	178.75	178.83	178.94	179.01	179.10	179.19	179.26	179.33	179.40	179.45
22	179.17	179.14	179.17	179.12	179.13	179.15	179.14	179.14	179.17	179.16	179.15
23	180.79	180.79	180.82	180.84	180.88	180.92	180.95	180.96	180.99	181.00	181.02
24	180.82	180.83	180.86	180.88	180.90	180.94	180.98	180.98	181.02	181.04	181.07
Volume 2	181.35	181.30	181.29	181.30	181.31	181.27	181.30	181.32	181.34	181.35	181.35

Refer to Appendix A, Table A-1 for explanation of abbreviations.

Continued on next page.

Table A-14 Continued

	Defect Depth (mm)										
Mode	**0.0**	**0.1**	**0.2**	**0.3**	**0.4**	**0.5**	**0.6**	**0.7**	**0.8**	**0.9**	**1.0**
26	194.32	194.25	194.27	194.24	194.21	194.18	194.14	194.09	194.07	193.98	193.91
33	195.89	195.85	195.84	195.86	195.86	195.86	195.85	195.86	195.86	195.86	195.86
34	196.42	196.47	196.59	196.65	196.72	196.82	196.90	196.95	197.03	197.09	197.14
29	197.86	197.79	197.82	197.79	197.78	197.76	197.75	197.74	197.73	197.71	197.67
30	203.61	203.56	203.50	203.42	203.33	203.23	203.11	202.95	202.81	202.58	202.34
31	212.84	212.80	212.80	212.77	212.75	212.77	212.76	212.72	212.74	212.69	212.67
32	214.43	214.38	214.34	214.29	214.21	214.17	214.09	213.99	213.96	213.81	213.73
33	214.70	214.64	214.64	214.61	214.62	214.58	214.56	214.55	214.49	214.43	214.38
34	215.37	215.41	215.51	215.61	215.68	215.76	215.84	215.89	215.95	216.01	216.05
35	217.30	217.29	217.32	217.35	217.35	217.37	217.38	217.36	217.31	217.24	217.15
36	218.30	218.22	218.07	217.83	217.54	217.20	216.83	216.41	215.91	215.41	214.84
37	218.34	218.32	218.37	218.40	218.46	218.50	218.47	218.48	218.44	218.43	218.40
38	220.87	220.95	221.05	221.17	221.24	221.34	221.45	221.52	221.59	221.69	221.74
Volume 3	226.79	226.76	226.76	226.78	226.78	226.79	226.79	226.81	226.82	226.81	226.82
X Torsion 4	229.23	229.30	229.40	229.45	229.56	229.59	229.67	229.73	229.74	229.85	229.90

Refer to Appendix A, Table A-1 for explanation of abbreviations.

Continued on next page.

Table A-14 Continued

	Defect Depth (mm)												
Mode	**1.1**	**1.2**	**1.3**	**1.4**	**1.5**	**1.6**	**1.7**	**1.8**	**1.9**	**2.0**	**2.1**	**2.2**	**2.3**
X Torsion 1	57.70	57.54	57.36	57.17	56.98	56.78	56.56	56.34	56.10	55.86	55.60	55.34	55.06
Y Bend 1	63.76	63.25	62.73	62.18	61.60	61.01	60.39	59.75	59.09	58.41	57.72	57.01	56.29
Z Bend 1	66.22	66.06	65.91	65.74	65.56	65.36	65.16	64.95	64.73	64.50	64.26	64.01	63.76
Volume 1	99.31	99.09	98.85	98.60	98.34	98.07	97.80	97.51	97.24	96.95	96.65	96.36	96.08
Z Bend 2	110.15	109.86	109.54	109.20	108.83	108.42	108.02	107.58	107.12	106.65	106.15	105.65	105.11
Y Bend 2	111.97	111.93	111.86	111.79	111.72	111.62	111.52	111.40	111.28	111.13	110.97	110.79	110.56
X Torsion 2	117.72	117.77	117.82	117.88	117.93	117.97	118.01	118.06	118.08	118.13	118.18	118.20	118.27
8	133.84	133.77	133.72	133.65	133.61	133.57	133.51	133.42	133.38	133.30	133.21	133.17	133.11
9	138.37	138.20	137.96	137.72	137.48	137.24	136.98	136.71	136.45	136.17	135.88	135.61	135.32
10	159.46	159.45	159.46	159.45	159.46	159.47	159.48	159.47	159.50	159.50	159.51	159.53	159.52
11	159.49	159.47	159.44	159.40	159.38	159.34	159.31	159.28	159.24	159.21	159.17	159.16	159.11
12	160.71	160.74	160.77	160.84	160.88	160.94	160.95	161.03	161.06	161.09	161.14	161.17	161.22
Z Bend 3	160.94	160.94	160.92	160.89	160.85	160.81	160.78	160.70	160.63	160.52	160.43	160.26	160.07
Y Bend 3	161.68	161.74	161.78	161.81	161.82	161.87	161.88	161.89	161.90	161.94	161.92	161.93	161.96
15	162.97	162.92	162.92	162.87	162.87	162.82	162.78	162.76	162.74	162.70	162.65	162.61	162.60
16	168.60	168.53	168.52	168.47	168.42	168.37	168.31	168.27	168.22	168.17	168.10	168.07	168.00
X Torsion 3	171.15	170.69	170.20	169.68	169.14	168.59	168.05	167.48	166.93	166.37	165.83	165.33	164.87
18	177.90	177.88	177.85	177.79	177.76	177.71	177.65	177.59	177.52	177.44	177.37	177.28	177.17
19	177.93	177.88	177.84	177.78	177.71	177.61	177.54	177.42	177.30	177.16	177.00	176.86	176.68
20	178.26	178.24	178.20	178.17	178.14	178.11	178.07	178.03	177.96	177.93	177.81	177.76	177.66
21	179.52	179.57	179.60	179.65	179.69	179.70	179.72	179.76	179.75	179.77	179.76	179.78	179.74
22	179.18	179.16	179.17	179.17	179.17	179.17	179.15	179.18	179.17	179.17	179.15	179.16	179.12
23	181.03	181.07	181.05	181.07	181.10	181.11	181.10	181.10	181.12	181.11	181.14	181.14	181.12
24	181.11	181.11	181.12	181.16	181.18	181.16	181.16	181.21	181.22	181.23	181.26	181.22	181.25
Volume 2	181.36	181.35	181.39	181.40	181.41	181.45	181.49	181.49	181.52	181.54	181.58	181.60	181.63

Refer to Appendix A, Table A-1 for explanation of abbreviations.

Continued on next page.

Table A-14 Continued

	Defect Depth (mm)												
Mode	**1.1**	**1.2**	**1.3**	**1.4**	**1.5**	**1.6**	**1.7**	**1.8**	**1.9**	**2.0**	**2.1**	**2.2**	**2.3**
26	193.83	193.71	193.60	193.49	193.34	193.17	193.04	192.83	192.63	192.42	192.18	191.94	191.68
33	195.84	195.85	195.83	195.82	195.81	195.80	195.78	195.74	195.67	195.62	195.56	195.49	195.40
34	197.20	197.26	197.30	197.35	197.38	197.39	197.39	197.43	197.44	197.44	197.45	197.45	197.42
29	197.64	197.59	197.54	197.51	197.47	197.41	197.35	197.27	197.19	197.10	197.00	196.90	196.79
30	202.11	201.83	201.55	201.26	200.92	200.58	200.21	199.87	199.53	199.21	198.90	198.60	198.37
31	212.66	212.62	212.56	212.48	212.46	212.35	212.26	212.11	212.00	211.82	211.63	211.41	211.20
32	213.60	213.48	213.15	212.66	212.05	211.51	211.01	210.56	210.12	209.71	209.32	208.99	208.65
33	214.30	213.76	213.35	213.21	213.08	212.98	212.83	212.76	212.60	212.49	212.41	212.28	211.70
34	216.10	216.14	216.16	216.11	216.32	216.30	216.27	216.24	216.22	216.18	216.12	216.04	215.95
35	217.02	216.84	216.66	216.46	215.92	215.57	215.16	214.75	214.27	213.80	213.46	213.25	213.05
36	214.31	214.26	214.17	214.10	213.98	213.89	213.79	213.64	213.47	213.25	212.86	212.29	212.13
37	218.39	218.35	218.34	218.36	218.38	218.36	218.40	218.42	218.44	218.45	218.47	218.51	218.52
38	221.80	221.84	221.86	221.92	221.96	221.96	222.00	221.99	221.99	221.96	221.96	221.93	221.92
Volume 3	226.79	226.80	226.78	226.75	226.74	226.73	226.68	226.65	226.62	226.57	226.52	226.47	226.41
X Torsion 4	229.94	229.99	230.01	230.04	230.05	230.03	229.91	229.52	228.80	227.93	227.08	226.28	225.46

Refer to Appendix A, Table A-1 for explanation of abbreviations.

Table A-15 Steel Specimen #2 FEM calculated frequencies for cuts of various depths

	Defect Depth (mm)										
Mode	**0.0**	**0.1**	**0.2**	**0.3**	**0.4**	**0.5**	**0.6**	**0.7**	**0.8**	**0.9**	**1.0**
X Torsion 1	58.88	58.87	58.87		58.83	58.80	58.75	58.71	58.66	58.61	58.54
Z Bend 1	67.04	67.03	67.01		66.95	66.91	66.86	66.80	66.75	66.67	66.59
Y Bend 1	67.11	67.10	67.07		66.95	66.87	66.77	66.66	66.53	66.38	66.21
Volume 1	100.85	100.85	100.83		100.77	100.71	100.64	100.56	100.45	100.32	100.18
Y Bend 2	112.11	112.09	112.03		111.82	111.67	111.53	111.34	111.15	110.91	110.68
Z Bend 2	112.19	112.20	112.20		112.18	112.16	112.11	112.07	111.99	111.90	111.80
X Torsion 2	117.23	117.15	117.03		116.74	116.57	116.37	116.13	115.88	115.61	115.33
8	134.06	134.07	134.06		134.02	133.97	133.93	133.85	133.76	133.70	133.54
9	139.65	139.64	139.61		139.48	139.41	139.30	139.15	139.01	138.88	138.67
10	159.55	159.54	159.51		159.36	159.22	159.06	158.85	158.60	158.31	158.00
11	159.65	159.62	159.53		159.26	159.03	158.74	158.35	157.88	157.32	156.68
12	160.33	160.34	160.37		160.41	160.46	160.48	160.52	160.51	160.57	160.58
Z Bend 3	161.02	160.98	160.92		160.74	160.65	160.57	160.49	160.41	160.36	160.31
Y Bend 3	161.09	161.07	161.05		160.96	160.90	160.82	160.72	160.63	160.49	160.35
15	163.04	163.04	163.05		163.02	162.99	162.99	162.94	162.90	162.86	162.82
16	168.83	168.82	168.81		168.71	168.64	168.60	168.49	168.40	168.31	168.20
X Torsion 3	174.40	174.41	174.35		174.22	174.13	173.94	173.81	173.60	173.38	173.13
18	178.09	178.06	178.01		177.81	177.64	177.47	177.27	177.05	176.82	176.57
19	178.16	178.17	178.17		178.12	177.98	177.76	177.52	177.23	176.92	176.59
20	178.55	178.52	178.45		178.17	178.11	178.06	178.01	177.93	177.90	177.81
21	178.57	178.57	178.60		178.67	178.70	178.75	178.81	178.86	178.90	178.94
22	179.03	179.04	178.98		178.94	178.95	178.95	178.89	178.88	178.85	178.84
23	180.82	180.81	180.80		180.78	180.74	180.73	180.64	180.55	180.48	180.41
24	180.88	180.91	180.96		180.99	180.98	180.97	180.94	180.94	180.91	180.92
Volume 2	181.35	181.33	181.34		181.37	181.42	181.49	181.57	181.64	181.71	181.81

Refer to Appendix A, Table A-1 for explanation of abbreviations.

Continued on next page.

Table A-15 Continued

	Defect Depth (mm)										
Mode	**0.0**	**0.1**	**0.2**	**0.3**	**0.4**	**0.5**	**0.6**	**0.7**	**0.8**	**0.9**	**1.0**
26	194.29	194.29	194.25		194.10	193.99	193.84	193.66	193.48	193.21	192.91
27	196.01	195.96	195.93		195.80	195.73	195.64	195.56	195.48	195.38	195.27
28	196.33	196.33	196.32		196.30	196.29	196.27	196.23	196.22	196.18	196.15
29	197.84	197.82	197.78		197.60	197.50	197.38	197.25	197.16	197.01	196.90
30	203.64	203.69	203.66		203.71	203.71	203.72	203.71	203.68	203.64	203.61
31	212.85	212.86	212.86		212.85	212.84	212.85	212.79	212.76	212.69	212.64
32	214.50	214.47	214.38		213.96	213.58	213.11	212.51	211.85	211.13	210.35
33	214.63	214.66	214.66		214.54	214.49	214.45	214.32	214.16	213.99	213.75
34	215.41	215.34	215.28		215.06	214.96	214.86	214.75	214.63	214.50	214.33
35	217.38	217.31	217.23		217.00	216.88	216.75	216.63	216.54	216.42	216.32
36	218.40	218.37	218.31		217.90	217.64	217.30	216.90	216.46	216.04	215.63
37	218.42	218.48	218.49		218.57	218.59	218.62	218.65	218.64	218.70	218.70
38	220.90	220.85	220.76		220.52	220.40	220.28	220.23	220.18	220.13	220.09
Volume 3	226.87	226.86	226.85		226.78	226.72	226.64	226.53	226.40	226.21	225.99
X Torsion 4	229.40	229.55	229.59		229.67	229.62	229.58	229.52	229.41	229.30	229.18

Refer to Appendix A, Table A-1 for explanation of abbreviations.

Continued on next page.

Table A-15 Continued

	Defect Depth (mm)												
Mode	**1.1**	**1.2**	**1.3**	**1.4**	**1.5**	**1.6**	**1.7**	**1.8**	**1.9**	**2.0**	**2.1**	**2.2**	**2.3**
X Torsion 1	58.47	58.40	58.31	58.22	58.12	58.01	57.90	57.77	57.64	57.50	57.34	57.17	57.01
Z Bend 1	66.52	66.42	66.33	66.23	66.13	66.02	65.89	65.78	65.65	65.51	65.38	65.23	65.08
Y Bend 1	66.03	65.82	65.60	65.35	65.09	64.80	64.49	64.15	63.80	63.41	63.01	62.58	62.11
Volume 1	100.00	99.79	99.55	99.28	98.96	98.61	98.20	97.75	97.28	96.75	96.18	95.58	94.93
Y Bend 2	110.42	110.17	109.91	109.62	109.34	109.06	108.81	108.56	108.32	108.10	107.88	107.68	107.52
Z Bend 2	111.66	111.46	111.23	110.96	110.62	110.20	109.74	109.19	108.57	107.91	107.17	106.42	105.59
X Torsion 2	115.04	114.75	114.44	114.16	113.88	113.62	113.37	113.14	112.93	112.70	112.49	112.28	112.07
8	133.41	133.26	133.08	132.84	132.60	132.32	132.01	131.65	131.26	130.84	130.43	129.96	129.49
9	138.47	138.29	138.09	137.90	137.68	137.49	137.29	137.09	136.92	136.73	136.58	136.47	136.31
10	157.64	157.24	156.79	156.33	155.85	155.30	154.77	154.21	153.65	153.07	152.49	151.89	151.31
11	155.97	155.19	154.35	153.45	152.50	151.52	150.54	149.56	148.57	147.61	146.65	145.74	144.88
12	160.61	160.61	160.66	160.67	160.70	160.74	160.76	160.76	160.78	160.78	160.80	160.80	160.81
Z Bend 3	160.24	160.18	160.12	160.05	159.93	159.83	159.70	159.55	159.37	159.14	158.88	158.60	158.24
Y Bend 3	160.21	160.01	159.79	159.56	159.30	159.02	158.70	158.38	158.04	157.65	157.28	156.90	156.51
15	162.75	162.72	162.65	162.58	162.50	162.42	162.31	162.24	162.11	162.00	161.87	161.74	161.59
16	168.08	168.01	167.89	167.79	167.68	167.59	167.48	167.39	167.26	167.20	167.07	167.00	166.92
X Torsion 3	172.88	172.63	172.36	172.09	171.82	171.57	171.30	171.10	170.87	170.67	170.50	170.32	170.19
18	176.31	176.00	175.71	175.39	175.09	174.75	174.42	174.11	173.77	173.45	173.15	172.83	172.54
19	176.24	175.90	175.56	175.20	174.85	174.53	174.20	173.88	173.58	173.30	172.97	172.69	172.41
20	177.77	177.70	177.66	177.61	177.58	177.53	177.47	177.42	177.37	177.35	177.31	177.23	177.22
21	178.98	179.02	179.03	179.06	179.07	179.09	179.10	179.13	179.11	179.10	179.12	179.09	179.06
22	178.83	178.80	178.78	178.76	178.71	178.67	178.64	178.59	178.56	178.51	178.42	178.38	178.33
23	180.33	180.27	180.21	180.13	180.07	180.01	179.94	179.85	179.80	179.70	179.62	179.53	179.44
24	180.89	180.89	180.92	180.91	180.91	180.92	180.91	180.88	180.89	180.86	180.84	180.81	180.81
Volume 2	181.88	181.92	182.00	182.06	182.12	182.17	182.22	182.29	182.30	182.35	182.38	182.38	182.39

Refer to Appendix A, Table A-1 for explanation of abbreviations.

Continued on next page.

Table A-15 Continued

	Defect Depth (mm)												
Mode	**1.1**	**1.2**	**1.3**	**1.4**	**1.5**	**1.6**	**1.7**	**1.8**	**1.9**	**2.0**	**2.1**	**2.2**	**2.3**
26	192.61	192.25	191.87	191.41	190.97	190.52	190.06	189.57	189.06	188.58	188.05	187.57	187.06
27	195.19	195.09	195.00	194.94	194.84	194.78	194.72	194.63	194.59	194.53	194.51	194.43	194.39
28	196.09	196.08	196.01	195.94	195.90	195.80	195.73	195.65	195.58	195.47	195.34	195.22	195.08
29	196.80	196.70	196.61	196.53	196.46	196.41	196.35	196.33	196.25	196.25	196.19	196.18	196.15
30	203.59	203.48	203.41	203.33	203.17	203.01	202.86	202.63	202.37	202.11	201.78	201.38	201.07
31	212.56	212.43	212.20	211.77	211.25	210.73	210.22	209.70	209.23	208.83	208.40	208.07	207.76
32	209.52	208.67	207.79	206.94	206.11	205.28	204.52	203.80	203.11	202.48	201.93	201.45	200.92
33	213.48	213.14	212.78	212.59	212.48	212.36	212.30	212.07	211.62	211.17	210.68	210.15	209.58
34	214.17	213.95	213.71	213.43	213.14	212.81	212.44	212.20	212.10	212.11	211.94	211.85	211.77
35	216.23	216.14	216.07	216.02	215.95	215.89	215.84	215.80	215.74	215.71	215.67	215.61	215.60
36	215.24	214.92	214.66	214.46	214.26	214.10	213.90	213.74	213.61	213.43	213.26	213.11	212.95
37	218.71	218.71	218.72	218.75	218.73	218.75	218.73	218.71	218.69	218.68	218.60	218.58	218.51
38	220.06	220.07	220.01	219.97	219.96	219.93	219.90	219.85	219.82	219.74	219.67	219.63	219.51
Volume 3	225.69	225.37	225.02	224.64	224.27	223.91	223.57	223.25	222.95	222.66	222.44	222.23	222.01
X Torsion 4	229.01	228.82	228.62	228.42	228.23	228.01	227.79	227.61	227.34	227.08	226.81	226.55	226.27

Refer to Appendix A, Table A-1 for explanation of abbreviations.

Table A-16 Steel Specimen #3 FEM calculated frequencies for cuts of various depths

	Defect Depth (mm)										
Mode	**0.0**	**0.1**	**0.2**	**0.3**	**0.4**	**0.5**	**0.6**	**0.7**	**0.8**	**0.9**	**1.0**
X Torsion 1	58.85	58.88	58.90	58.93	58.96	58.98	59.00	59.02	59.03	59.05	59.06
Y Bend 1	66.97	66.97	66.98	66.98	66.98	66.98	66.98	66.97	66.97	66.96	66.95
Z Bend 1	67.09	67.12	67.14	67.16	67.19	67.21	67.22	67.23	67.24	67.25	67.25
Volume 1	100.81	100.82	100.84	100.86	100.87	100.88	100.89	100.90	100.90	100.89	100.88
Y Bend 2	112.06	112.09	112.10	112.13	112.14	112.14	112.12	112.09	112.05	111.97	111.90
Z Bend 2	112.17	112.18	112.20	112.21	112.22	112.21	112.23	112.23	112.23	112.22	112.20
X Torsion 2	117.16	117.17	117.16	117.15	117.14	117.09	117.04	116.97	116.89	116.81	116.70
8	134.08	134.12	134.16	134.18	134.19	134.20	134.19	134.20	134.16	134.11	134.04
8	139.65	139.70	139.75	139.79	139.78	139.78	139.75	139.74	139.67	139.59	139.47
10	159.48	159.54	159.61	159.65	159.70	159.73	159.75	159.77	159.76	159.73	159.66
11	159.64	159.64	159.64	159.62	159.58	159.50	159.40	159.26	159.07	158.79	158.42
12	160.34	160.37	160.36	160.40	160.41	160.44	160.41	160.38	160.24	160.05	159.83
Y Bend 3	160.96	160.98	160.99	160.99	161.02	161.01	161.02	161.02	161.05	161.07	161.08
Z Bend 3	161.06	161.04	161.00	160.92	160.83	160.75	160.63	160.56	160.57	160.57	160.59
15	163.05	163.12	163.13	163.18	163.19	163.21	163.19	163.17	163.14	163.10	163.07
16	168.83	168.91	168.93	169.01	169.03	169.04	169.05	169.01	168.94	168.85	168.76
X Torsion 3	174.33	174.28	174.19	174.02	173.85	173.66	173.42	173.16	172.83	172.48	172.10
18	178.01	178.04	178.04	178.06	178.05	178.06	178.00	177.90	177.76	177.59	177.34
19	178.07	178.11	178.11	178.12	178.14	178.08	178.07	178.05	178.06	178.05	178.03
20	178.40	178.54	178.67	178.82	178.95	179.10	179.22	179.35	179.43	179.51	179.58
21	178.70	178.71	178.71	178.68	178.62	178.59	178.49	178.39	178.26	178.07	177.81
22	179.19	179.18	179.20	179.18	179.17	179.14	179.15	179.15	179.13	179.14	179.12
23	180.81	180.82	180.80	180.82	180.84	180.85	180.80	180.77	180.77	180.73	180.69
24	180.83	180.86	180.92	180.99	181.02	181.07	181.10	181.11	181.09	181.05	180.99
Volume 2	181.37	181.36	181.37	181.35	181.34	181.31	181.28	181.28	181.31	181.33	181.42

Refer to Appendix A, Table A-1 for explanation of abbreviations.

Continued on next page.

Table A-16 Continued

	Defect Depth (mm)										
Mode	**0.0**	**0.1**	**0.2**	**0.3**	**0.4**	**0.5**	**0.6**	**0.7**	**0.8**	**0.9**	**1.0**
26	194.31	194.36	194.41	194.42	194.40	194.34	194.26	194.10	193.82	193.41	192.80
27	195.88	195.96	196.00	196.08	196.08	196.11	196.12	196.11	196.07	195.96	195.83
28	196.44	196.46	196.47	196.45	196.45	196.46	196.47	196.48	196.45	196.45	196.41
29	197.86	197.91	197.96	197.97	197.92	197.83	197.74	197.57	197.33	197.09	196.86
30	203.62	203.67	203.75	203.74	203.75	203.76	203.75	203.74	203.72	203.66	203.58
31	212.84	212.90	212.98	213.04	213.13	213.17	213.25	213.33	213.38	213.40	213.43
32	214.43	214.45	214.40	214.31	214.10	213.72	213.16	212.33	211.17	209.71	208.00
33	214.70	214.77	214.79	214.79	214.82	214.75	214.75	214.71	214.54	214.38	214.16
34	215.38	215.39	215.39	215.40	215.38	215.33	215.20	215.08	214.90	214.63	214.21
35	217.33	217.33	217.33	217.28	217.18	217.00	216.78	216.57	216.44	216.31	216.19
36	218.34	218.29	218.15	217.94	217.72	217.53	217.41	217.31	217.24	217.17	217.11
37	218.36	218.39	218.39	218.36	218.32	218.22	218.05	217.84	217.44	216.92	216.17
38	220.88	220.90	220.83	220.80	220.67	220.61	220.44	220.24	220.09	219.87	219.72
Volume 3	226.82	226.84	226.85	226.85	226.86	226.82	226.76	226.68	226.55	226.28	225.86
X Torsion 4	229.30	229.17	229.01	228.70	228.48	228.20	227.91	227.58	227.31	226.94	226.68

Refer to Appendix A, Table A-1 for explanation of abbreviations.

Continued on next page.

Table A-16 Continued

	Defect Depth (mm)												
Mode	**1.1**	**1.2**	**1.3**	**1.4**	**1.5**	**1.6**	**1.7**	**1.8**	**1.9**	**2.0**	**2.1**	**2.2**	**2.3**
X Torsion 1	59.07	59.08	59.09	59.10	59.10		59.10	59.10	59.10	59.09	59.08	59.06	59.05
Y Bend 1	66.94	66.92	66.90	66.85	66.83		66.80	66.76	66.73	66.69	66.64	66.60	66.55
Z Bend 1	67.24	67.23	67.22	67.17	67.14		67.11	67.06	66.99	66.93	66.86	66.76	66.64
Volume 1	100.86	100.83	100.80	100.68	100.59		100.45	100.29	100.07	99.75	99.31	98.71	97.89
Y Bend 2	111.79	111.66	111.49	111.06	110.77		110.42	110.00	109.49	108.93	108.26	107.56	106.82
Z Bend 2	112.17	112.14	112.11	112.02	111.95		111.85	111.76	111.65	111.45	111.23	110.92	110.36
X Torsion 2	116.59	116.45	116.28	115.87	115.60		115.33	114.99	114.61	114.12	113.54	112.87	112.17
8	133.96	133.84	133.66	133.08	132.62		131.98	131.09	129.97	128.62	127.03	125.36	123.65
8	139.36	139.17	138.95	138.42	138.10		137.75	137.44	137.13	136.88	136.67	136.51	136.37
10	159.73	159.62	159.49	159.06	158.71		158.23	157.61	156.85	155.89	154.84	153.65	152.44
11	157.89	157.21	156.25	153.17	150.93		148.27	145.26	142.02	138.82	135.67	132.75	130.17
12	159.43	159.09	158.68	157.60	156.91		156.12	155.25	154.30	153.28	152.32	151.42	150.59
Y Bend 3	161.07	161.08	161.10	161.07	161.04		160.99	160.91	160.81	160.67	160.42	160.06	159.35
Z Bend 3	160.58	160.63	160.63	160.72	160.71		160.73	160.72	160.70	160.73	160.75	160.76	160.76
15	163.00	162.89	162.77	162.53	162.36		162.20	162.04	161.87	161.69	161.47	161.15	160.79
16	168.61	168.36	168.13	167.51	167.16		166.82	166.51	166.20	166.00	165.72	165.41	164.77
X Torsion 3	171.61	171.12	170.58	169.21	168.42		167.56	166.67	165.88	165.19	164.62	164.20	163.90
18	177.00	176.58	176.02	174.49	173.52		172.53	171.53	170.66	169.66	168.41	167.11	166.14
19	178.02	178.04	178.01	178.00	178.00		177.97	177.97	177.96	177.94	177.91	177.90	177.90
20	179.66	179.72	179.76	179.78	179.78		179.81	179.74	179.72	179.67	179.60	179.53	179.44
21	177.46	177.01	176.38	174.69	173.71		172.74	171.76	170.74	169.86	169.18	168.60	168.09
22	179.11	179.08	179.07	178.98	178.95		178.85	178.77	178.59	178.33	177.78	176.97	176.13
23	180.61	180.49	180.37	180.15	180.05		179.92	179.80	179.71	179.51	179.28	179.06	178.91
24	180.95	180.94	180.91	180.88	180.87		180.86	180.83	180.78	180.62	180.33	180.11	180.04
Volume 2	181.46	181.50	181.56	181.59	181.66		181.72	181.75	181.76	181.80	181.83	181.86	181.89

Refer to Appendix A, Table A-1 for explanation of abbreviations.

Continued on next page.

Table A-16 Continued

	Defect Depth (mm)												
Mode	**1.1**	**1.2**	**1.3**	**1.4**	**1.5**	**1.6**	**1.7**	**1.8**	**1.9**	**2.0**	**2.1**	**2.2**	**2.3**
26	191.93	190.83	189.54	186.81	185.61		184.45	183.38	182.33	181.49	181.12	181.04	180.99
27	195.60	195.20	194.56	192.17	190.63		189.18	187.93	186.93	186.16	185.59	185.11	184.78
28	196.38	196.27	196.19	195.99	195.99		195.92	195.88	195.87	195.86	195.81	195.78	195.76
29	196.69	196.58	196.53	196.50	196.45		196.38	196.46	196.41	196.35	196.30	196.25	196.24
30	203.42	203.19	201.97	199.13	198.40		197.89	197.51	197.22	196.93	196.62	196.34	196.04
31	213.36	213.66	213.83	213.82	213.87		213.90	213.91	213.93	213.97	213.96	213.97	213.94
32	206.03	203.98	202.84	201.17	199.52		197.39	194.98	192.75	190.88	189.42	188.34	187.57
33	213.85	213.10	212.30	210.34	209.21		208.09	206.95	205.84	204.84	203.92	203.10	202.35
34	213.72	212.75	211.49	208.40	207.22		206.45	205.99	205.68	205.50	205.33	205.24	205.16
35	216.14	216.00	215.92	215.83	215.78		215.69	215.63	215.58	215.47	215.40	215.25	215.11
36	217.10	217.08	217.11	217.11	217.13		217.15	217.18	217.16	217.17	217.16	217.11	217.07
37	215.24	214.29	213.36	211.94	211.24		210.55	209.94	209.43	209.02	208.65	208.31	207.99
38	219.54	219.36	219.16	218.68	218.39		218.10	217.86	217.67	217.44	217.28	217.12	216.97
Volume 3	225.18	224.26	223.22	221.40	220.82		220.37	220.00	219.65	219.30	218.85	218.29	217.60
X Torsion 4	226.25	225.83	225.18	223.81	223.12		222.53	221.99	221.48	221.00	220.59	220.13	219.76

Refer to Appendix A, Table A-1 for explanation of abbreviations.

Table A-17 Steel Specimen #4 FEM calculated frequencies for cuts of various depths

	Defect Depth (mm)										
Mode	**0.0**	**0.1**	**0.2**	**0.3**	**0.4**	**0.5**	**0.6**	**0.7**	**0.8**	**0.9**	**1.0**
X Torsion 1	58.57	58.49	58.39	58.28	58.15	58.00	57.84	57.67	57.48	57.28	57.07
Y Bend 1	66.76	66.74	66.72	66.69	66.67	66.66	66.64	66.62	66.59	66.57	66.53
Z Bend 1	66.78	66.78	66.77	66.76	66.74	66.73	66.70	66.68	66.65	66.62	66.61
Volume 1	100.41	100.40	100.41	100.40	100.40	100.41	100.40	100.40	100.40	100.39	100.40
Y Bend 2	111.61	111.52	111.42	111.29	111.15	110.98	110.80	110.60	110.37	110.15	109.89
Z Bend 2	111.68	111.70	111.71	111.73	111.75	111.76	111.78	111.79	111.81	111.82	111.82
X Torsion 2	116.61	116.47	116.28	116.03	115.75	115.47	115.14	114.78	114.41	114.01	113.57
8	133.43	133.36	133.26	133.16	133.03	132.86	132.69	132.50	132.29	132.05	131.82
9	139.04	138.99	138.95	138.93	138.87	138.78	138.72	138.63	138.54	138.44	138.35
10	158.79	158.58	158.29	157.89	157.32	156.58	155.57	154.26	152.60	150.56	148.29
11	158.88	158.83	158.74	158.64	158.53	158.39	158.22	158.04	157.86	157.74	157.42
12	159.65	159.67	159.68	159.69	159.68	159.71	159.69	159.68	159.66	159.58	159.48
Y Bend 3	160.29	160.18	160.02	159.84	159.62	159.33	159.01	158.64	158.21	157.67	157.21
Z Bend 3	160.36	160.34	160.31	160.24	160.13	159.97	159.70	159.23	158.39	156.99	155.04
15	162.41	162.42	162.38	162.31	162.20	162.01	161.75	161.40	160.97	160.37	159.74
16	168.23	168.31	168.34	168.40	168.41	168.36	168.19	167.20	165.56	164.18	163.30
X Torsion 3	173.51	173.29	173.02	172.68	172.32	171.92	171.51	171.07	170.66	170.25	169.80
18	177.19	176.54	175.77	174.69	173.56	172.38	171.18	170.04	169.01	168.12	167.43
19	177.31	176.78	175.69	174.49	173.00	171.31	169.56	168.60	168.37	168.20	168.02
20	177.55	177.33	177.36	177.35	177.32	177.31	177.26	177.19	177.08	176.95	176.76
21	177.62	177.62	177.61	177.57	177.55	177.47	177.39	177.29	177.17	177.00	176.82
22	178.06	178.05	178.00	177.97	177.96	177.89	177.83	177.80	177.75	177.72	177.68
23	180.10	180.06	180.00	179.92	179.82	179.74	179.65	179.53	179.41	179.28	179.10
24	180.15	180.30	180.42	180.50	180.62	180.79	180.87	180.94	181.01	181.07	181.13
Volume 2	180.55	180.58	180.62	180.71	180.75	180.81	180.91	181.01	181.13	181.23	181.39

Refer to Appendix A, Table A-1 for explanation of abbreviations.

Continued on next page.

Table A-17 Continued

	Defect Depth (mm)										
Mode	**0.0**	**0.1**	**0.2**	**0.3**	**0.4**	**0.5**	**0.6**	**0.7**	**0.8**	**0.9**	**1.0**
26	193.40	193.25	192.81	191.90	190.63	189.17	187.48	185.68	183.76	181.82	179.93
27	194.97	194.43	193.99	193.77	193.66	193.56	193.48	193.39	193.29	193.20	193.06
28	195.31	195.24	195.17	195.10	194.99	194.87	194.77	194.64	194.53	194.39	194.25
29	196.96	196.89	196.81	196.69	196.53	196.31	196.04	195.72	195.34	194.88	194.33
30	202.46	202.06	201.54	201.01	200.41	199.82	199.27	198.75	198.29	197.87	197.46
31	211.57	211.04	210.37	209.68	208.88	208.11	207.33	206.59	205.93	205.25	204.68
32	213.52	213.30	212.93	212.53	211.99	211.37	210.69	210.00	209.23	208.50	207.77
33	213.56	213.45	213.27	213.11	212.82	212.61	212.33	212.04	211.74	211.43	211.10
34	214.45	214.36	214.25	214.14	214.03	213.88	213.72	213.55	213.36	213.15	212.94
35	216.43	216.38	216.25	215.91	215.41	214.73	213.97	213.17	212.24	211.23	210.20
36	217.28	217.04	216.75	216.58	216.47	216.36	216.42	216.28	216.18	216.03	215.90
37	217.50	217.53	217.48	217.35	217.13	216.68	215.93	215.32	214.63	213.89	213.22
38	219.67	219.25	218.75	218.22	217.81	217.62	217.53	217.42	217.33	217.24	217.17
39	225.87	225.80	225.72	225.63	225.48	225.30	225.12	224.89	224.66	224.40	224.20
40	228.19	227.98	227.66	227.26	226.91	226.58	226.26	225.92	225.63	225.38	225.14

Refer to Appendix A, Table A-1 for explanation of abbreviations.

Continued on next page.

Table A-17 Continued

	Defect Depth (mm)												
Mode	**1.1**	**1.2**	**1.3**	**1.4**	**1.5**	**1.6**	**1.7**	**1.8**	**1.9**	**2.0**	**2.1**	**2.2**	**2.3**
X Torsion 1	56.85	56.62	56.37	56.12	55.86	55.59	55.31	55.02	54.72	54.41	54.10	53.78	53.65
Y Bend 1	66.49	66.45	66.40	66.34	66.27	66.21	66.14	66.06	65.98	65.89	65.79	65.70	65.66
Z Bend 1	66.59	66.57	66.56	66.55	66.54	66.53	66.52	66.51	66.51	66.50	66.49	66.48	66.48
Volume 1	100.39	100.38	100.38	100.37	100.36	100.35	100.33	100.31	100.29	100.26	100.21	100.16	100.12
Y Bend 2	109.62	109.33	109.03	108.71	108.38	108.03	107.66	107.29	106.90	106.48	106.06	105.61	105.43
Z Bend 2	111.83	111.83	111.83	111.82	111.80	111.79	111.75	111.70	111.63	111.52	111.37	111.12	110.98
X Torsion 2	113.12	112.65	112.16	111.65	111.13	110.59	110.05	109.48	108.90	108.32	107.74	107.14	106.90
8	131.52	131.22	130.87	130.51	130.11	129.68	129.21	128.65	127.79	125.69	123.07	120.54	119.58
9	138.23	138.10	137.94	137.87	137.66	137.48	137.28	137.08	136.85	136.59	136.27	135.74	135.33
10	145.72	142.92	140.00	136.89	133.81	130.68	127.54	124.44	121.36	118.34	115.38	112.51	111.38
11	157.18	156.90	156.76	156.43	156.13	155.81	155.48	155.12	154.76	154.35	153.90	153.40	153.17
12	159.50	159.38	159.26	159.09	158.91	158.68	158.39	158.08	157.69	157.26	156.78	156.24	156.00
Y Bend 3	156.62	156.00	155.30	154.56	152.81	150.81	148.69	146.45	144.16	141.87	139.60	137.55	136.93
Z Bend 3	152.57	149.83	146.91	143.90	140.84	137.81	134.79	131.85	129.25	127.97	127.27	126.64	126.38
15	158.74	157.67	156.17	154.63	153.80	153.01	152.18	151.35	150.50	149.63	148.80	147.92	147.58
16	162.76	162.40	162.17	161.99	161.84	161.67	161.49	161.21	160.78	160.17	159.34	158.34	157.92
X Torsion 3	169.41	169.02	168.66	168.33	168.03	167.74	167.49	167.24	167.02	166.80	166.62	166.42	166.35
18	166.84	166.37	166.00	165.67	165.41	165.18	164.99	164.84	164.70	164.59	164.49	164.40	164.37
19	167.78	167.49	167.12	166.70	166.18	165.61	165.00	164.37	163.80	163.35	163.03	162.83	162.76
20	176.57	176.32	176.03	175.70	175.35	174.93	174.46	173.95	173.38	172.75	172.07	171.31	170.98
21	176.58	176.08	174.91	173.74	172.78	171.98	171.36	170.85	170.46	170.14	169.88	169.67	169.59
22	177.66	177.62	177.57	177.52	177.45	177.34	177.19	177.02	176.82	176.62	176.42	176.22	176.16
23	178.94	178.74	178.54	178.36	178.15	177.98	177.82	177.71	177.62	177.54	177.47	177.39	177.35
24	181.19	181.25	181.30	181.34	181.38	181.43	181.47	181.49	181.52	181.54	181.56	181.57	181.57
Volume 2	181.48	181.57	181.67	181.76	181.84	181.93	181.98	182.05	182.09	182.14	182.17	182.19	182.19

Refer to Appendix A, Table A-1 for explanation of abbreviations.

Continued on next page.

Table A-17 Continued

	Defect Depth (mm)												
Mode	**1.1**	**1.2**	**1.3**	**1.4**	**1.5**	**1.6**	**1.7**	**1.8**	**1.9**	**2.0**	**2.1**	**2.2**	**2.3**
26	178.20	176.81	176.28	175.96	175.63	175.27	174.90	174.53	174.11	173.69	173.27	172.85	172.69
27	192.92	192.78	192.60	192.41	192.21	191.97	191.72	191.42	191.10	190.78	190.38	189.95	189.77
28	194.10	194.00	193.79	193.62	193.44	193.23	192.99	192.74	192.41	192.08	191.67	191.22	191.04
29	193.74	193.07	192.30	191.53	190.77	190.03	189.31	188.64	188.04	187.48	187.00	186.58	186.44
30	197.13	196.82	196.59	196.34	196.14	195.99	195.80	195.64	195.54	195.40	195.27	195.15	195.11
31	204.14	203.76	203.21	202.83	202.49	202.16	201.86	201.08	200.09	199.11	198.26	197.48	197.22
32	207.10	206.48	205.92	205.42	204.44	203.29	202.16	201.58	201.31	201.10	200.86	200.66	200.58
33	210.74	210.40	210.04	209.67	209.30	208.79	208.53	208.16	207.77	207.39	207.02	206.65	206.49
34	212.72	212.49	212.24	211.96	211.68	211.38	211.06	210.70	210.33	209.96	209.53	209.09	208.94
35	209.10	208.32	206.81	205.63	205.02	204.70	204.41	204.15	203.97	203.77	203.62	203.49	203.45
36	215.72	215.59	215.29	215.03	214.73	214.39	214.01	213.56	213.06	212.50	211.88	211.16	210.85
37	212.50	211.70	211.03	210.30	209.53	208.91	208.01	207.25	206.48	205.75	205.01	204.30	204.03
38	217.07	217.07	216.88	216.78	216.69	216.60	216.53	216.47	216.40	216.31	216.24	216.17	216.16
39	223.96	223.77	223.55	223.33	223.16	222.97	222.82	222.65	222.50	222.35	222.21	222.07	222.00
40	224.88	224.70	224.51	224.34	224.19	224.02	223.85	223.68	223.46	223.25	223.01	222.62	222.50

Refer to Appendix A, Table A-1 for explanation of abbreviations.

Table A-18 Steel Specimen #5 FEM calculated frequencies for cuts of various depths

	Defect Depth (mm)										
Mode	**0.0**	**0.1**	**0.2**	**0.3**	**0.4**	**0.5**	**0.6**	**0.7**	**0.8**	**0.9**	**1.0**
X Torsion 1	58.88	58.87	58.84	58.79	58.74	58.66	58.58	58.49	58.39	58.28	58.16
Y Bend 1	67.01	66.99	66.97	66.94	66.92	66.89	66.86	66.84	66.81	66.78	66.75
Z Bend 1	67.06	67.07	67.07	67.07	67.08	67.08	67.07	67.07	67.06	67.05	67.05
Volume 1	100.85	100.84	100.85	100.84	100.84	100.85	100.85	100.85	100.85	100.85	100.85
Y Bend 2	112.16	112.15	112.12	112.08	112.02	111.95	111.88	111.78	111.68	111.56	111.43
Z Bend 2	112.21	112.23	112.25	112.27	112.30	112.29	112.34	112.37	112.39	112.42	112.43
X Torsion 2	117.23	117.20	117.14	117.07	116.92	116.85	116.62	116.41	116.19	115.95	115.68
8	134.22	134.26	134.28	134.31	134.31	134.34	134.29	134.26	134.22	134.17	134.10
9	139.77	139.81	139.83	139.85	139.88	139.88	139.90	139.90	139.90	139.89	139.87
10	159.65	159.63	159.61	159.55	159.43	159.21	159.02	158.69	158.22	157.59	156.71
11	159.71	159.72	159.74	159.71	159.68	159.81	159.57	159.50	159.41	159.29	159.15
12	160.50	160.55	160.55	160.60	160.63	160.66	160.66	160.65	160.69	160.68	160.70
Y Bend 3	161.10	161.10	161.09	161.04	160.98	161.04	160.78	160.69	160.47	160.26	159.99
Z Bend 3	161.14	161.15	161.18	161.19	161.20	161.14	161.18	161.14	161.07	160.94	160.73
15	163.22	163.26	163.28	163.30	163.28	163.28	163.18	163.11	162.98	162.84	162.63
16	169.00	169.04	169.05	169.07	169.04	169.00	168.96	168.89	168.79	168.69	168.55
X Torsion 3	174.43	174.38	174.31	174.14	173.97	173.72	173.46	173.15	172.78	172.25	172.01
18	178.20	178.23	178.25	178.35	178.33	178.35	178.37	178.37	178.36	178.34	178.32
19	178.32	178.29	178.17	177.95	177.63	177.17	176.59	175.89	175.02	174.03	172.91
20	178.59	178.71	178.71	178.75	178.77	178.75	178.77	178.75	178.71	178.63	178.54
21	178.76	178.66	178.54	178.20	177.78	177.36	176.38	175.36	174.08	172.66	170.67
22	179.06	179.14	179.19	179.22	179.23	179.29	179.22	179.20	179.18	179.12	179.06
23	181.03	181.06	181.07	181.05	180.98	180.92	180.84	180.76	180.67	180.59	180.49
24	181.05	181.08	181.10	181.19	181.24	181.37	181.37	181.41	181.46	181.53	181.58
25	181.42	181.45	181.50	181.56	181.63	181.56	181.76	181.83	181.92	181.99	182.06

Refer to Appendix A, Table A-1 for explanation of abbreviations.

Continued on next page.

Table A-18 Continued

	Defect Depth (mm)										
Mode	**0.0**	**0.1**	**0.2**	**0.3**	**0.4**	**0.5**	**0.6**	**0.7**	**0.8**	**0.9**	**1.0**
26	194.42	194.46	194.47	194.45	194.39	194.14	193.62	192.68	191.43	189.88	188.02
27	196.20	196.15	196.01	195.74	195.38	194.96	194.70	194.55	194.44	194.32	194.14
28	196.42	196.48	196.51	196.52	196.52	196.48	196.48	196.45	196.40	196.33	196.27
29	197.98	198.02	198.01	197.99	197.95	197.88	197.77	197.63	197.43	197.17	196.83
30	203.79	203.76	203.66	203.45	203.15	202.75	202.26	201.71	201.06	200.32	199.56
31	212.99	212.95	212.78	212.50	212.06	211.52	210.81	210.01	209.08	208.07	206.99
32	214.68	214.64	214.52	214.31	214.00	213.66	213.22	212.70	212.09	211.36	210.53
33	214.77	214.87	214.91	214.97	214.99	214.92	214.87	214.75	214.54	214.27	213.91
34	215.54	215.58	215.61	215.64	215.64	215.67	215.64	215.61	215.61	215.58	215.57
35	217.48	217.50	217.52	217.52	217.47	217.40	217.16	216.68	215.94	215.01	213.96
36	218.49	218.46	218.39	218.28	218.12	217.86	217.67	217.43	216.98	216.30	215.35
37	218.50	218.55	218.56	218.51	218.45	218.31	218.12	217.87	217.71	217.58	217.47
38	221.01	220.99	220.87	220.63	220.33	219.88	219.54	219.14	218.81	218.56	218.34
39	226.95	226.98	227.00	226.99	226.97	226.85	226.76	226.59	226.33	225.97	225.48
40	229.41	229.37	229.21	229.03	228.77	228.50	228.04	227.52	226.98	226.37	225.87

Refer to Appendix A, Table A-1 for explanation of abbreviations.

Continued on next page.

Table A-18 Continued

	Defect Depth (mm)												
Mode	**1.1**	**1.2**	**1.3**	**1.4**	**1.5**	**1.6**	**1.7**	**1.8**	**1.9**	**2.0**	**2.1**	**2.2**	**2.3**
X Torsion 1	58.04	57.90	57.76	57.60	57.44	57.27	57.10	56.91	56.72	56.52	56.31	56.09	55.87
Y Bend 1	66.73	66.70	66.67	66.64	66.60	66.57	66.53	66.49	66.44	66.39	66.34	66.28	66.21
Z Bend 1	67.03	67.02	67.01	66.99	66.98	66.96	66.95	66.93	66.91	66.90	66.88	66.87	66.85
Volume 1	100.84	100.85	100.85	100.84	100.84	100.83	100.83	100.82	100.81	100.80	100.78	100.75	100.72
Y Bend 2	111.28	111.12	110.95	110.76	110.55	110.33	110.08	109.82	109.54	109.22	108.86	108.45	107.97
Z Bend 2	112.46	112.48	112.50	112.52	112.53	112.53	112.55	112.56	112.54	112.54	112.51	112.46	112.38
X Torsion 2	115.39	115.06	114.72	114.36	113.95	113.52	113.07	112.58	112.04	111.47	110.86	110.20	109.47
8	134.00	133.89	133.77	133.60	133.42	133.17	132.85	132.41	131.69	130.42	128.04	124.93	121.67
9	139.84	139.80	139.75	139.66	139.57	139.37	138.54	135.49	131.73	127.75	123.80	119.89	116.05
10	155.53	153.97	151.96	149.48	146.58	143.38	140.49	139.60	139.26	138.88	138.26	137.09	135.13
11	158.98	158.78	158.53	158.18	157.65	156.73	155.75	154.59	153.21	151.63	149.86	147.91	145.83
12	160.68	160.63	160.52	160.23	159.63	158.91	158.36	157.93	157.54	157.16	156.79	156.38	155.97
Y Bend 3	159.67	159.26	158.83	158.25	157.55	156.65	154.95	152.67	149.99	147.17	144.50	142.34	141.02
Z Bend 3	160.33	159.62	158.15	155.88	152.91	149.50	145.87	142.21	138.69	135.79	133.99	132.99	132.27
15	162.36	162.01	161.60	161.19	160.93	160.80	160.67	160.55	160.40	160.22	159.97	159.71	159.34
16	168.39	168.18	167.95	167.63	167.22	166.63	165.86	164.97	164.13	163.53	163.20	163.01	162.90
X Torsion 3	171.51	170.98	170.42	169.81	169.23	168.71	168.33	168.01	167.77	167.54	167.36	167.21	167.05
18	178.27	178.18	178.07	177.92	177.74	177.51	177.25	176.96	176.63	176.24	175.81	175.33	174.80
19	171.73	170.59	169.50	168.58	167.82	167.18	166.71	166.33	166.03	165.80	165.61	165.47	165.34
20	178.40	178.17	177.79	176.81	174.93	172.91	171.16	169.82	168.85	168.13	167.61	167.19	166.89
21	168.71	166.73	165.06	163.97	163.35	162.98	162.71	162.44	162.04	161.35	160.39	159.29	158.16
22	179.01	178.92	178.84	178.71	178.55	178.41	178.18	177.93	177.62	177.33	176.98	176.65	176.32
23	180.37	180.24	180.13	180.00	179.86	179.75	179.64	179.55	179.46	179.40	179.34	179.29	179.22
24	181.63	181.66	181.72	181.73	181.74	181.79	181.80	181.80	181.80	181.80	181.77	181.74	181.53
25	182.14	182.23	182.28	182.35	182.43	182.50	182.55	182.63	182.68	182.74	182.78	182.82	182.88

Refer to Appendix A, Table A-1 for explanation of abbreviations.

Continued on next page.

Table A-18 Continued

	Defect Depth (mm)												
Mode	**1.1**	**1.2**	**1.3**	**1.4**	**1.5**	**1.6**	**1.7**	**1.8**	**1.9**	**2.0**	**2.1**	**2.2**	**2.3**
26	185.90	183.57	181.22	179.39	178.58	178.11	177.74	177.38	177.01	176.59	176.14	175.66	175.16
27	193.97	193.74	193.49	193.19	192.85	192.46	192.03	191.56	191.05	190.54	190.00	189.42	188.84
28	196.22	196.13	196.01	195.79	195.33	194.67	193.95	193.14	191.94	189.98	187.52	184.80	182.26
29	196.40	195.86	195.19	194.34	193.35	192.21	191.00	189.79	188.64	187.61	186.68	185.89	185.20
30	198.76	197.95	197.18	196.54	196.20	196.04	195.92	195.77	195.42	194.41	193.59	193.06	192.64
31	205.90	204.81	203.80	202.84	201.99	201.17	200.35	199.46	198.55	197.65	196.75	195.90	195.07
32	209.56	208.44	207.20	205.87	204.54	203.30	202.24	201.38	200.75	200.28	199.85	199.51	199.20
33	213.45	212.90	212.29	211.63	210.94	210.29	209.63	209.04	208.46	207.96	207.48	207.04	206.67
34	215.55	215.51	215.47	215.45	215.37	215.27	215.18	215.06	214.93	214.75	214.58	214.33	214.06
35	212.80	211.62	210.28	208.40	206.07	203.58	200.92	198.40	196.42	195.85	195.69	195.56	195.42
36	214.14	212.64	211.02	209.76	208.76	207.92	207.18	206.49	205.90	205.37	204.88	204.43	204.02
37	217.32	217.16	216.97	216.74	216.46	216.14	215.76	215.32	214.81	214.26	213.63	212.91	212.13
38	218.16	217.97	217.79	217.62	217.44	217.29	217.12	216.97	216.79	216.61	216.40	216.18	215.95
39	224.89	224.35	223.86	223.44	223.09	222.79	222.52	222.29	222.09	221.92	221.74	221.57	221.39
40	225.46	225.07	224.73	224.42	224.15	223.87	223.67	223.47	223.27	223.11	222.91	222.75	222.57

Refer to Appendix A, Table A-1 for explanation of abbreviations.

Table A-19 Steel Specimen #6 FEM calculated frequencies for cuts of various depths

	Defect Depth (mm)										
Mode	**0.0**	**0.1**	**0.2**	**0.3**	**0.4**	**0.5**	**0.6**	**0.7**	**0.8**	**0.9**	**1.0**
X Torsion 1	58.92	58.94	58.95	58.96	58.96	58.96	58.95	58.94	58.92	58.89	58.86
Y Bend 1	67.12	67.09	67.07	67.03	67.00	66.96	66.93	66.89	66.85	66.83	66.79
Z Bend 1	67.19	67.20	67.21	67.22	67.23	67.24	67.25	67.26	67.27	67.27	67.28
Volume 1	100.95	100.94	100.94	100.95	100.95	100.96	100.96	100.95	100.96	100.97	100.97
Y Bend 2	112.20	112.21	112.24	112.25	112.25	112.25	112.24	112.24	112.21	112.19	112.15
Z Bend 2	112.26	112.29	112.32	112.34	112.39	112.42	112.45	112.48	112.52	112.55	112.58
X Torsion 2	117.30	117.37	117.38	117.40	117.40	117.38	117.35	117.32	117.27	117.18	117.11
8	134.09	134.20	134.30	134.43	134.52	134.64	134.74	134.84	134.93	135.01	135.10
9	139.73	139.79	139.86	139.94	140.02	140.10	140.17	140.25	140.30	140.38	140.44
10	159.64	159.70	159.74	159.75	159.78	159.79	159.81	159.81	159.80	159.80	159.74
11	159.74	159.82	159.89	159.98	160.04	160.09	160.11	160.12	160.08	160.03	159.93
12	160.39	160.43	160.49	160.60	160.69	160.75	160.84	160.89	160.95	160.98	161.03
Y Bend 3	161.13	161.18	161.20	161.25	161.27	161.30	161.30	161.30	161.29	161.26	161.20
Z Bend 3	161.18	161.23	161.27	161.31	161.34	161.40	161.43	161.46	161.51	161.53	161.54
15	163.10	163.14	163.18	163.20	163.22	163.22	163.23	163.24	163.21	163.20	163.13
16	168.89	168.91	168.92	168.92	168.90	168.86	168.82	168.79	168.72	168.66	168.56
X Torsion 3	174.53	174.62	174.66	174.68	174.66	174.64	174.56	174.49	174.39	174.20	173.96
18	178.21	178.24	178.28	178.36	178.40	178.45	178.48	178.51	178.50	178.37	177.96
19	178.32	178.44	178.50	178.53	178.56	178.58	178.58	178.55	178.53	178.40	178.20
20	178.68	178.80	178.88	178.86	178.86	178.87	178.84	178.77	178.67	178.63	178.63
21	178.73	178.92	179.11	179.30	179.50	179.62	179.72	179.77	179.75	179.66	179.48
22	179.14	179.36	179.56	179.74	179.90	180.01	180.07	180.09	180.06	179.99	179.87
23	180.86	180.86	180.90	180.91	180.96	180.99	181.02	181.03	181.10	181.09	181.07
24	180.94	181.01	181.09	181.21	181.29	181.35	181.38	181.37	181.32	181.22	181.11
Volume 2	181.44	181.48	181.54	181.59	181.67	181.78	181.87	181.98	182.09	182.17	182.24

Refer to Appendix A, Table A-1 for explanation of abbreviations.

Continued on next page.

Table A-19 Continued

	Defect Depth (mm)										
Mode	**0.0**	**0.1**	**0.2**	**0.3**	**0.4**	**0.5**	**0.6**	**0.7**	**0.8**	**0.9**	**1.0**
26	194.47	194.59	194.73	194.81	194.91	194.99	195.06	195.11	195.17	195.21	194.90
27	196.14	196.26	196.35	196.41	196.45	196.47	196.45	196.35	196.15	195.71	195.23
28	196.47	196.67	196.85	197.05	197.21	197.35	197.45	197.53	197.53	197.55	197.53
29	198.01	198.14	198.28	198.38	198.49	198.59	198.67	198.74	198.79	198.82	198.81
30	203.74	203.98	204.18	204.33	204.47	204.54	204.56	204.48	204.24	203.79	203.03
31	212.97	213.23	213.46	213.59	213.71	213.74	213.66	213.44	213.00	212.22	210.95
32	214.61	214.73	214.80	214.83	214.88	214.85	214.76	214.61	214.41	214.06	213.45
33	214.77	214.98	215.14	215.34	215.52	215.70	215.86	216.02	216.14	216.21	216.22
34	215.52	215.61	215.70	215.82	215.93	216.02	216.10	216.19	216.29	216.42	216.56
35	217.52	217.55	217.61	217.66	217.69	217.71	217.72	217.71	217.63	217.42	216.78
36	218.53	218.61	218.64	218.64	218.67	218.68	218.61	218.53	218.39	218.20	218.01
37	218.58	218.68	218.77	218.87	218.94	218.99	219.03	219.05	219.03	218.90	218.53
38	221.12	221.32	221.49	221.63	221.74	221.77	221.74	221.57	221.27	220.73	220.09
39	227.02	227.06	227.13	227.22	227.27	227.31	227.35	227.34	227.32	227.16	226.77
40	229.54	229.71	229.68	229.74	229.73	229.60	229.48	229.27	228.95	228.36	227.25

Refer to Appendix A, Table A-1 for explanation of abbreviations.

Continued on next page.

Table A-19 Continued

	Defect Depth (mm)												
Mode	**1.1**	**1.2**	**1.3**	**1.4**	**1.5**	**1.6**	**1.7**	**1.8**	**1.9**	**2.0**	**2.1**	**2.2**	**2.3**
X Torsion 1	58.83	58.79	58.74	58.69	58.63	58.57	58.50	58.42	58.34	58.24	58.15	58.04	57.92
Y Bend 1	66.75	66.72	66.69	66.65	66.62	66.59	66.55	66.52	66.48	66.44	66.40	66.35	66.30
Z Bend 1	67.29	67.29	67.30	67.30	67.30	67.30	67.30	67.29	67.28	67.27	67.26	67.25	67.23
Volume 1	100.97	100.96	100.97	100.97	100.96	100.96	100.95	100.96	100.94	100.92	100.87	100.59	98.72
Y Bend 2	112.12	112.07	112.01	111.95	111.86	111.75	111.61	111.42	111.14	110.51	108.65	104.27	101.11
Z Bend 2	112.62	112.64	112.67	112.70	112.73	112.75	112.77	112.79	112.80	112.80	112.75	112.98	112.93
X Torsion 2	116.99	116.87	116.71	116.53	116.30	115.98	115.60	115.07	114.24	112.88	109.55	103.21	96.65
8	135.16	135.22	135.25	135.27	135.26	135.10	134.61	132.26	126.13	119.45	114.32	111.86	110.63
9	140.47	140.51	140.54	140.56	140.49	140.29	138.70	131.68	124.01	116.65	110.79	107.18	102.99
10	159.54	159.10	158.27	156.58	153.14	147.42	141.47	138.42	136.68	136.74	136.39	136.34	136.28
11	159.85	159.77	159.69	159.51	158.28	151.87	144.12	139.26	134.47	128.74	124.16	121.21	117.95
12	161.03	161.02	160.97	160.85	160.57	160.16	159.82	159.31	156.95	151.23	145.04	138.82	133.45
Y Bend 3	161.11	160.98	160.78	160.40	158.96	156.38	150.47	144.45	142.17	141.69	141.47	141.74	141.61
Z Bend 3	161.55	161.51	161.39	160.97	159.86	158.10	154.01	148.06	141.49	134.58	128.45	122.78	119.50
15	163.08	162.97	162.80	162.56	162.12	161.54	161.15	160.76	160.30	159.94	159.88	159.65	159.48
16	168.44	168.30	168.12	167.44	163.78	162.68	162.40	162.28	162.01	161.54	161.13	160.71	155.93
X Torsion 3	173.66	173.16	172.26	168.55	167.56	165.65	163.64	162.66	162.37	161.64	161.40	161.00	160.60
18	177.11	175.47	172.68	171.24	168.62	166.22	164.90	164.23	162.63	162.32	162.69	161.55	160.80
19	177.74	176.76	174.89	171.93	169.45	167.17	165.16	164.39	164.08	163.94	163.84	162.38	162.30
20	178.64	178.64	178.62	178.13	172.47	168.19	167.86	167.59	164.42	164.01	163.91	163.72	163.68
21	179.26	179.05	178.83	178.62	178.55	178.18	175.51	168.17	167.34	167.01	166.92	163.88	163.86
22	179.70	179.52	179.37	179.14	178.78	178.46	177.50	176.92	176.43	174.06	168.12	166.97	166.60
23	180.89	180.67	180.44	180.17	178.83	178.55	178.41	178.26	178.07	176.11	175.97	175.56	175.37
24	181.07	181.06	181.03	180.21	179.89	179.67	178.91	178.49	178.30	177.92	177.66	177.41	177.09
Volume 2	182.32	182.37	182.45	181.02	180.98	180.97	179.54	179.48	179.39	178.11	177.88	177.66	177.38

Refer to Appendix A, Table A-1 for explanation of abbreviations.

Continued on next page.

Table A-19 Continued

	Defect Depth (mm)												
Mode	**1.1**	**1.2**	**1.3**	**1.4**	**1.5**	**1.6**	**1.7**	**1.8**	**1.9**	**2.0**	**2.1**	**2.2**	**2.3**
26	193.37	190.63	186.08	182.49	182.55	182.62	180.95	180.94	180.89	179.38	179.41	179.32	179.30
27	195.23	195.23	195.18	193.37	190.34	184.26	182.63	182.63	180.99	180.94	180.99	180.90	180.88
28	197.49	197.44	196.75	195.13	190.96	187.25	185.04	183.92	182.60	182.48	182.44	182.26	182.12
29	198.74	198.53	197.56	195.20	192.86	189.08	187.93	187.26	183.73	183.42	183.62	183.34	183.28
30	201.77	199.79	197.77	197.31	195.59	193.11	191.54	188.54	186.89	186.65	186.89	186.42	183.39
31	208.87	205.87	202.28	199.80	195.62	195.31	195.21	191.28	190.33	189.90	189.59	188.55	186.33
32	212.38	210.22	206.19	200.71	197.73	197.52	196.89	195.12	195.00	194.85	193.90	189.29	189.02
33	215.13	212.09	207.86	201.93	199.64	199.26	197.35	197.24	197.08	196.90	195.14	194.52	194.15
34	216.17	215.45	211.27	207.43	205.44	204.34	199.80	199.16	198.85	198.55	197.12	196.62	196.37
35	216.70	216.03	215.76	215.26	213.76	206.36	203.75	203.32	202.96	200.52	197.91	197.65	197.09
36	217.48	216.84	216.93	215.92	214.87	214.12	213.49	213.03	207.97	203.43	203.14	202.85	202.79
37	217.94	217.60	217.02	217.12	216.29	214.68	213.86	213.10	212.19	211.24	210.26	209.18	208.12
38	219.53	219.10	218.56	218.22	217.25	217.37	217.37	214.94	212.76	212.43	211.76	211.32	210.33
39	224.97	222.26	220.59	219.27	217.99	217.73	217.48	217.39	216.61	215.89	215.07	214.42	213.86
40	226.10	224.95	221.83	220.01	219.73	219.04	218.60	217.58	217.66	217.71	217.70	217.65	215.18

Refer to Appendix A, Table A-1 for explanation of abbreviations.

APPENDIX B

Table B-1 Steel Specimen #1 RUS measured frequencies for fatigue cracks of various depths

Defect Depth (mm)	
0.00	**1.87**
RUS (kHz)	**RUS (kHz)**
29.141	22.385
32.683	30.604
41.850	38.489
62.637	57.809
69.612	65.185
71.078	69.475
71.711	70.752
98.981	97.037
99.056	98.403
107.682	106.740
108.837	108.564
109.370	108.991
115.358	114.746
116.359	116.011
119.006	118.668
119.370	118.739
121.125	121.045
122.701	121.358
127.963	127.098
134.235	132.629
134.358	134.036
134.477	134.140
140.127	134.629
140.956	136.894

Refer to Appendix A, Table A-1 for explanation of abbreviations.

Table B-2 Steel Specimen #2 RUS measured frequencies for fatigue cracks of various depths

Defect Depth (mm)				
0.00	**1.88**	**2.25**	**2.25**	**2.52**
RUS	**RUS**	**RUS**	**RUS**	**RUS**
(kHz)	**(kHz)**	**(kHz)**	**(kHz)**	**(kHz)**
29.166	26.485	25.490	25.229	23.200
32.696	32.066	31.814	31.727	31.163
42.016	40.937	40.471	40.404	39.475
62.777	60.519	59.818	59.654	58.168
69.675	68.108	67.533	67.304	65.872
71.326	71.144	70.909	70.839	70.036
71.980	71.214	71.140	71.138	71.081
99.027	98.711	98.493	98.437	97.862
99.285	98.778	98.672	98.654	98.537
107.704	107.320	107.206	107.173	106.808
109.159	109.152	109.114	109.116	109.088
109.647	109.455	109.354	109.341	109.202
115.449	115.364	115.255	115.248	115.101
116.618	116.489	116.420	116.412	116.334
119.119	119.077	119.041	119.041	118.824
119.330	119.077	119.126	119.112	118.964
121.354	121.352	121.329	121.328	121.311
122.803	122.427	122.240	122.174	121.821
128.155	127.830	127.667	127.633	127.336
134.279	133.566	133.320	133.244	132.720
134.531	134.496	134.445	134.444	134.373
134.622	134.567	134.549	134.552	134.447
140.234	139.112	138.240	138.103	136.504
141.351	139.531	139.028	138.887	137.896

Refer to Appendix A, Table A-1 for explanation of abbreviations.

Table B-3 Steel Specimen #3 RUS measured frequencies for fatigue cracks of various depths

Defect Depth (mm)												
0.00 RUS (kHz)	**0.27 RUS (kHz)**	**0.39 RUS (kHz)**	**0.65 RUS (kHz)**	**0.65 RUS (kHz)**	**0.73 RUS (kHz)**	**0.96 RUS (kHz)**	**0.97 RUS (kHz)**	**1.08 RUS (kHz)**	**1.09 RUS (kHz)**	**1.14 RUS (kHz)**	**1.14 RUS (kHz)**	**1.30 RUS (kHz)**
29.138	29.041	28.704	28.704	28.583	28.398	28.232	28.164	28.000	27.902	27.756	27.710	27.506
32.664	32.638	32.570	32.570	32.546	32.514	32.473	32.460	32.431	32.410	32.389	32.363	32.304
41.888	41.843	41.664	41.664	41.607	41.535	41.460	41.425	41.374	41.329	41.287	41.263	41.218
62.664	62.610	62.287	62.287	62.179	62.017	61.856	61.784	61.632	61.572	61.451	61.376	61.169
69.614	69.583	69.398	69.398	69.321	69.235	69.135	69.093	68.998	68.946	68.856	68.821	68.604
71.168	71.154	71.141	71.141	71.125	71.115	71.111	71.089	71.109	71.059	71.065	71.067	71.056
71.790	71.761	71.651	71.651	71.605	71.570	71.508	71.492	71.441	71.414	71.369	71.345	71.262
98.985	98.964	98.914	98.914	98.889	98.880	98.870	98.841	98.816	98.804	98.798	98.816	98.766
99.125	99.103	99.019	99.019	98.973	98.957	98.926	98.890	98.877	98.863	98.831	98.816	98.778
107.689	107.684	107.626	107.626	107.586	107.557	107.549	107.515	107.517	107.482	107.447	107.441	107.374
108.934	108.940	108.937	108.937	108.905	108.914	108.916	108.886	108.921	108.879	108.883	108.880	108.875
109.443	109.441	109.419	109.419	109.383	109.384	109.369	109.331	109.358	109.309	109.305	109.300	109.274
115.434	115.429	115.410	115.410	115.352	115.356	115.354	115.318	115.338	115.295	115.294	115.284	115.271
116.462	116.454	116.430	116.430	116.407	116.403	116.394	116.363	116.375	116.342	116.334	116.328	116.301
119.121	119.124	119.118	119.118	119.077	119.087	119.084	119.050	119.083	119.049	119.043	119.041	119.030
119.407	119.406	119.381	119.381	119.347	119.347	119.342	119.298	119.333	119.294	119.296	119.291	119.278
121.194	121.190	121.193	121.193	121.154	121.168	121.169	121.129	121.169	121.127	121.128	121.130	121.114
122.827	122.817	122.778	122.778	122.728	122.726	122.700	122.660	122.673	122.628	122.616	122.609	122.561
128.045	128.030	128.001	128.001	127.954	127.942	127.924	127.876	127.891	127.843	127.820	127.821	127.772
134.279	134.267	134.171	134.171	134.114	134.072	134.015	133.963	133.940	133.887	133.827	133.811	133.708
134.509	134.505	134.414	134.414	134.381	134.411	134.405	134.353	134.400	134.332	134.364	134.369	134.348
134.581	134.505	134.506	134.506	134.458	134.473	134.474	134.438	134.473	134.431	134.428	134.433	134.415
140.196	140.178	140.071	140.071	140.003	139.962	139.903	139.848	139.828	139.762	139.708	139.679	139.556
141.172	141.102	140.767	140.767	140.646	140.511	140.368	140.283	140.225	140.146	140.063	140.033	139.965

Refer to Appendix A, Table A-1 for explanation of abbreviations.

Continued on next page.

Table B-3 Continued

Defect Depth (mm)								
1.30 RUS (kHz)	**1.33 RUS (kHz)**	**1.39 RUS (kHz)**	**1.39 RUS (kHz)**	**1.39 RUS (kHz)**	**1.43 RUS (kHz)**	**1.46 RUS (kHz)**	**1.55 RUS (kHz)**	**1.69 RUS (kHz)**
27.367	27.323	27.082	26.931	26.766	26.618	26.316	25.966	25.788
32.275	32.254	32.209	32.176	32.123	32.061	31.994	31.887	31.829
41.172	41.166	41.077	41.035	40.910	40.862	40.748	40.465	40.347
61.043	60.948	60.712	60.544	60.452	60.251	59.931	59.657	59.459
68.500	68.409	68.190	68.045	67.946	67.764	67.484	67.247	67.066
71.030	71.050	71.027	70.977	70.925	70.833	70.696	70.539	70.418
71.215	71.179	71.084	71.068	71.042	71.011	71.043	71.030	71.030
98.750	98.754	98.683	98.670	98.611	98.547	98.503	98.361	98.283
98.750	98.754	98.745	98.740	98.715	98.683	98.699	98.682	98.678
107.340	107.295	107.250	107.213	107.198	107.126	107.067	107.009	106.962
108.870	108.869	108.872	108.889	108.864	108.848	108.882	108.887	108.882
109.271	109.263	109.249	109.253	109.227	109.201	109.216	109.199	109.187
115.263	115.247	115.256	115.256	115.230	115.198	115.229	115.193	115.179
116.291	116.279	116.278	116.277	116.261	116.222	116.252	116.245	116.232
119.033	119.031	119.051	119.045	119.036	119.008	119.024	119.032	119.030
119.258	119.261	119.253	119.255	119.224	119.193	119.224	119.195	119.174
121.115	121.111	121.102	121.124	121.110	121.101	121.132	121.133	121.132
122.543	122.534	122.508	122.496	122.447	122.406	122.408	122.358	122.331
127.749	127.739	127.706	127.694	127.670	127.617	127.617	127.579	127.551
133.650	133.602	133.512	133.457	133.433	133.332	133.234	133.175	133.097
134.328	134.323	134.321	134.346	134.334	134.311	134.342	134.334	134.328
134.414	134.416	134.402	134.409	134.403	134.381	134.422	134.417	134.406
139.497	139.470	139.328	139.262	139.146	139.015	138.885	138.470	138.274
139.903	139.895	139.775	139.712	139.539	139.455	139.304	139.053	138.923

Refer to Appendix A, Table A-1 for explanation of abbreviations.

Table B-4 Steel Specimen #4 RUS measured frequencies for fatigue cracks of various depths

Defect Depth (mm)			
0.00	**0.47**	**0.60**	**1.79**
RUS (kHz)	**RUS (kHz)**	**RUS (kHz)**	**RUS (kHz)**
29.403	29.245	28.930	28.514
32.808	32.764	32.689	32.551
42.034	41.965	41.862	41.523
62.880	62.709	62.367	61.784
69.829	69.699	69.459	69.056
71.193	71.172	71.155	71.143
71.979	71.880	71.771	71.434
99.023	99.003	98.973	98.945
99.288	99.230	99.169	99.020
107.733	107.699	107.634	107.509
108.934	108.936	108.940	108.933
109.516	109.510	109.473	109.424
115.493	115.480	115.459	115.414
116.467	116.454	116.427	116.405
119.124	119.118	119.112	119.095
119.437	119.428	119.408	119.352
121.208	121.201	121.209	121.199
122.875	122.850	122.805	122.727
128.078	128.068	128.024	127.974
134.233	134.208	134.108	133.945
134.422	134.420	134.417	134.393
134.422	134.420	134.417	134.463
140.275	140.200	140.070	139.844
141.408	141.277	141.065	140.595

Refer to Appendix A, Table A-1 for explanation of abbreviations.

Table B-5 Steel Specimen #5 RUS measured frequencies for fatigue cracks of various depths

Defect Depth (mm)				
0.00 RUS (kHz)	**0.26 RUS (kHz)**	**1.08 RUS (kHz)**	**1.76 RUS (kHz)**	**1.76 RUS (kHz)**
28.780	28.578	27.877	21.558	20.826
32.428	32.383	32.238	30.267	30.013
41.484	41.383	41.108	37.742	37.429
62.253	62.070	61.447	56.999	56.652
69.246	69.141	68.751	64.406	63.958
70.803	70.777	70.754	68.807	68.662
71.232	71.152	70.950	70.496	70.496
98.651	98.584	98.453	96.472	96.284
98.876	98.838	98.777	98.277	98.253
107.600	107.558	107.467	106.583	106.508
108.481	108.466	108.471	108.304	108.484
108.986	108.959	108.916	108.506	108.484
115.038	115.005	114.958	114.397	114.358
116.235	116.201	116.177	115.806	115.806
118.981	118.970	118.970	118.653	118.554
119.371	119.337	119.305	118.653	118.661
120.879	120.861	120.878	120.764	120.783
122.667	122.612	122.552	121.256	121.135
127.740	127.698	127.633	126.776	126.708
134.064	134.031	133.917	132.337	132.144
134.234	134.171	134.097	133.122	132.563
134.497	134.472	134.479	133.873	133.837
139.936	139.852	139.546	134.233	134.180
140.424	140.199	139.739	136.494	136.185

Refer to Appendix A, Table A-1 for explanation of abbreviations.

Table B-6 FEM calculated frequencies for fatigue cracks of various depths using steel specimen with average dimensions

Defect Depth (mm)	0.00	0.50	0.75	1.00	1.25	1.50	1.75	2.00	2.25	2.50	2.75	3.00
Mode	FEM (kHz)	FEM (kHz)	FEM (kHz)	FEM (kHz)	FEM (kHz)	FEM (kHz)	FEM (kHz)	FEM (kHz)	FEM (kHz)	FEM (kHz)	FEM (kHz)	FEM (kHz)
Y Bend 1	29.006	27.99	27.19	26.34	25.46	24.56	23.65	22.732	21.812	20.891	19.975	19.062
X Torsion 1	32.522	32.32	32.13	31.90	31.64	31.35	31.034	30.694	30.328	29.949	29.542	29.124
Z Bend 1	41.823	41.28	40.84	40.37	39.87	39.36	38.839	38.299	37.747	37.18	36.609	36.024
Volume 1	62.639	61.92	61.38	60.79	60.18	59.58	58.975	58.361	57.748	57.128	56.508	55.886
Z Bend 2	69.563	69.15	68.76	68.28	67.75	67.15	66.506	65.819	65.103	64.348	63.571	62.767
X Torsion 2	70.974	70.91	70.87	70.82	70.78	70.75	70.721	70.702	70.685	70.673	70.662	70.652
Y Bend 2	71.617	71.49	71.39	71.24	71.02	70.76	70.449	70.088	69.666	69.208	68.683	68.111
X Bend 1	98.652	98.55	98.46	98.39	98.33	98.27	98.22	98.171	98.12	98.084	98.054	98.039
9	98.916	98.75	98.59	98.40	98.15	97.88	97.541	97.182	96.794	96.375	95.92	95.431
10	107.27	107.20	107.16	107.09	107.02	106.92	106.82	106.68	106.55	106.4	106.22	106.06
11	108.93	108.92	108.91	108.90	108.89	108.87	108.86	108.83	108.81	108.79	108.77	108.73
12	109.43	109.34	109.30	109.24	109.18	109.13	109.07	109.02	108.97	108.92	108.88	108.82
13	115.14	115.03	114.93	114.86	114.76	114.67	114.59	114.51	114.43	114.34	114.26	114.18
14	116.15	116.11	116.08	116.04	115.99	115.96	115.91	115.87	115.83	115.8	115.75	115.71
15	119.08	119.04	118.95	118.88	118.80	118.70	118.59	118.48	118.36	118.23	118.09	117.96
16	119.1	119.09	119.02	119.00	118.94	118.91	118.85	118.82	118.76	118.7	118.65	118.61
17	121.25	121.24	121.24	121.24	121.23	121.23	121.23	121.22	121.21	121.19	120.97	120.76
18	122.83	122.72	122.59	122.42	122.25	122.05	121.85	121.63	121.42	121.21	121.2	121.17
19	127.62	127.50	127.41	127.31	127.22	127.12	127.03	126.92	126.8	126.7	126.59	126.48
20	134.23	134.04	133.88	133.71	133.51	133.34	133.14	132.94	132.74	132.55	132.33	132.14
21	134.48	134.47	134.46	134.43	134.40	134.35	134.32	134.29	134.23	134.18	134.13	134.06
22	134.7	134.71	134.69	134.69	134.67	134.66	134.64	134.67	134.67	134.63	134.6	134.48
23	140.28	140.03	139.73	139.40	138.98	138.53	138.03	137.5	136.95	136.37	135.78	135.25
24	141.01	139.84	138.99	138.02	137.07	136.11	135.18	134.21	133.29	132.39	131.53	130.68

Refer to Appendix A, Table A-1 for explanation of abbreviations.

Table B-6 Error between RUS measured and FEM calculated frequencies for steel specimens prior to fatigue cracking

Sample Number	1	2	3	4	5
Mode	RUS vs. FEM	RUS vs. FEM	RUS vs. FEM	RUS vs. FEM	RUS vs. FEM
Y Bend 1	0.46%	0.55%	0.45%	1.35%	0.79%
X Torsion 1	0.49%	0.53%	0.43%	0.87%	0.29%
Z Bend 1	0.06%	0.46%	0.16%	0.50%	0.82%
Volume 1	0.00%	0.22%	0.04%	0.38%	0.62%
Z Bend 2	0.07%	0.16%	0.07%	0.38%	0.46%
X Torsion 2	0.15%	0.49%	0.27%	0.31%	0.24%
Y Bend 2	0.13%	0.50%	0.24%	0.50%	0.54%
X Bend 1	0.33%	0.38%	0.34%	0.37%	0.00%
9	0.14%	0.37%	0.21%	0.37%	0.04%
10	0.38%	0.40%	0.39%	0.43%	0.31%
11	0.09%	0.21%	0.00%	0.00%	0.41%
12	0.05%	0.20%	0.01%	0.08%	0.41%
13	0.19%	0.27%	0.25%	0.31%	0.09%
14	0.18%	0.40%	0.27%	0.27%	0.07%
15	0.06%	0.03%	0.03%	0.04%	0.08%
16	0.23%	0.19%	0.26%	0.28%	0.23%
17	0.10%	0.09%	0.05%	0.03%	0.31%
18	0.11%	0.02%	0.00%	0.04%	0.13%
19	0.27%	0.42%	0.33%	0.36%	0.09%
20	0.00%	0.04%	0.04%	0.00%	0.12%
21	0.09%	0.04%	0.02%	0.04%	0.18%
22	0.17%	0.06%	0.09%	0.21%	0.15%
23	0.11%	0.03%	0.06%	0.00%	0.25%
24	0.04%	0.24%	0.11%	0.28%	0.42%
Average	**0.2%**	**0.3%**	**0.2%**	**0.3%**	**0.3%**

Refer to Appendix A, Table A-1 for explanation of abbreviations.

Table B-7 Half-peak width for selected cut steel and fatigue cracked specimens.

Note: Defect Depth here expressed as a percentage for specimen thickness.

Fatigue Crack Specimen 2	**Defect Depth**	0.0%	19.7%	26.4%	
	Mode	**Attenuation**	**Attenuation**	**Attenuation**	
	Y Bend 1	0.22%	0.20%	0.34%	
	X Torsion 1	0.15%	0.14%	0.19%	
	Z Bend 1	0.10%	0.09%	0.14%	
Fatigue Crack Specimen 3	**Defect Depth**	0.0%	2.8%	6.8%	7.6%
	Mode	**Attenuation**	**Attenuation**	**Attenuation**	**Attenuation**
	Y Bend 1	0.20%	0.16%	0.18%	0.19%
	X Torsion 1	0.15%	0.15%	0.14%	0.15%
	Z Bend 1	0.09%	0.10%	0.12%	0.11%
Fatigue Crack Specimen 4	**Defect Depth**	0.0%	4.9%	6.2%	18.7%
	Mode	**Attenuation**	**Attenuation**	**Attenuation**	**Attenuation**
	Y Bend 1	0.18%	0.18%	0.17%	0.17%
	X Torsion 1	0.15%		0.15%	0.15%
	Z Bend 1	0.11%		0.10%	0.11%
Fatigue Crack Specimen 5	**Defect Depth**	0.0%	2.7%	11.3%	
	Mode	**Attenuation**	**Attenuation**	**Attenuation**	
	Y Bend 1	0.16%	0.16%	0.19%	
	X Torsion 1	0.15%	0.14%	0.14%	
	Z Bend 1	0.11%	0.11%	0.11%	
Cut Crack Specimen 1	**Defect Depth**	0.0%	18.7%		
	Mode	**Attenuation**	**Attenuation**		
	X Torsion 1	0.07%	0.09%		
	Y Bend 1	0.11%	0.08%		
	Z Bend 1	0.10%	0.07%		
Cut Crack Specimen 4	**Defect Depth**	0.0%	18.7%		
	Mode	**Attenuation**	**Attenuation**		
	X Torsion 1	0.07%	0.09%		
	Y Bend 1	0.08%	0.11%		
	Z Bend 1	0.09%	0.07%		

Refer to Appendix A, Table A-1 for explanation of abbreviations.

APPENDIX C

Table C-1 Ceramic Specimen #4 resonant frequencies

Mode	FEM (kHz)	Lagrange (kHz)	RUS (kHz)	RUS vs FEM	RUS vs Lagrange	FEM vs Lagrange
1	6.392	6.389	6.700			
2	7.496	7.588	7.783			
3	16.496	16.670	16.939			
4	17.586	17.570	17.830			
5	23.390	23.289	23.539	0.63%	1.06%	0.43%
6	27.849	27.816	28.037	0.67%	0.79%	0.12%
7	28.672	28.863	28.978	1.06%	0.40%	0.67%
8	34.446	34.379	34.794	1.00%	1.19%	0.19%
9	39.010	39.053	39.225	0.55%	0.44%	0.11%
10	45.205	45.484	45.621	0.91%	0.30%	0.62%
11	53.431	53.888	53.785	0.66%	0.19%	0.86%
12	57.139	56.889	57.320	0.32%	0.75%	0.44%
13	63.420	63.164	63.647	0.36%	0.76%	0.40%
14	64.680	65.047	65.166	0.75%	0.18%	0.57%
15	67.408	67.605	66.323	1.64%	1.93%	0.29%
16	68.908	68.658	69.090	0.26%	0.63%	0.36%
17	72.371	72.893	72.704	0.46%	0.26%	0.72%
18	76.929	77.090	77.254	0.42%	0.21%	0.21%
19	83.723	83.530	83.930	0.25%	0.48%	0.23%
20	92.690	93.036	92.984	0.32%	0.06%	0.37%
21	93.443	95.313	93.732	0.31%	1.69%	2.00%
22	94.780	97.007	95.071	0.31%	2.04%	2.35%
23	99.793	100.077	98.096	1.73%	2.02%	0.28%
24	109.170	110.257	107.797	1.27%	2.28%	1.00%
25	112.530	115.211	112.806	0.24%	2.13%	2.38%
26	114.660	117.960	114.908	0.22%	2.66%	2.88%
27	119.440	120.012	119.813	0.31%	0.17%	0.48%
28	122.070	123.755	122.249	0.15%	1.23%	1.38%
29	123.600	125.034	123.905	0.25%	0.91%	1.16%
30	123.960	128.153	124.291	0.27%	3.11%	3.38%
			Average:	0.59%	1.07%	0.92%

Refer to Appendix A, Table A-1 for explanation of abbreviations.

Table C-2 Ceramic Specimen #10 resonant frequencies

Mode	FEM (kHz)	Lagrange (kHz)	RUS (kHz)	RUS vs FEM	RUS vs Lagrange	FEM vs Lagrange
1	6.171	6.139	6.410			
2	7.223	7.251	7.499			
3	15.904	15.954	16.209			
4	16.986	16.894	17.290			
5	22.470	22.294	22.630	0.71%	1.48%	0.78%
6	26.796	26.639	26.951	0.58%	1.16%	0.59%
7	27.663	27.679	27.958	1.06%	1.00%	0.06%
8	33.289	33.085	33.569	0.83%	1.44%	0.61%
9	37.604	37.449	37.778	0.46%	0.87%	0.41%
10	43.672	43.695	43.993	0.73%	0.68%	0.05%
11	51.571	51.697	51.861	0.56%	0.32%	0.24%
12	55.287	54.836	55.357	0.13%	0.94%	0.82%
13	61.037	60.579	61.204	0.27%	1.02%	0.75%
14	62.405	62.403	62.800	0.63%	0.63%	0.00%
15	66.516	66.051	66.522	0.01%	0.71%	0.70%
16	67.698	67.511	66.639	1.59%	1.31%	0.28%
17	69.891	70.020	70.151	0.37%	0.19%	0.18%
18	74.176	73.979	74.385	0.28%	0.55%	0.27%
19	81.082	80.597	81.103	0.03%	0.62%	0.60%
20	89.485	89.373	89.665	0.20%	0.33%	0.13%
21	90.502	91.888	90.587	0.09%	1.44%	1.53%
22	91.657	93.307	91.827	0.19%	1.61%	1.80%
23	100.060	99.795	98.300	1.79%	1.52%	0.26%
24	108.790	109.648	107.922	0.80%	1.60%	0.79%
25	109.380	110.794	108.899	0.44%	1.74%	1.29%
26	111.160	113.865	111.168	0.01%	2.43%	2.43%
27	115.350	115.315	115.552	0.17%	0.21%	0.03%
28	118.050	119.026	118.004	0.04%	0.87%	0.83%
29	119.270	120.431	119.375	0.09%	0.88%	0.97%
30	120.210	123.698	120.285	0.06%	2.84%	2.90%
			Average:	0.47%	1.09%	0.74%

Refer to Appendix A, Table A-1 for explanation of abbreviations.

Table C-3 Ceramic Specimen #2 resonant frequencies

Defect Depth (mm)	**2.05**	**3.16**	**5.16**	**5.69**	**6.48**	**7.23**	**8.30**
Defect Width (mm)	**0.40**	**0.45**	**0.86**	**0.94**	**1.15**	**1.33**	**1.52**
	RUS (kHz)	**RUS (kHz)**	**RUS (kHz)**	**RUS (kHz)**	**RUS (kHz)**	**RUS (kHz)**	**RUS (kHz)**
Z Bend 1	4.386	4.703	4.838	4.741	4.717	4.715	4.778
X Torsion 1	6.062	5.914	5.919	5.903	5.897	5.896	5.882
Z Bend 2	11.181	11.032	11.079	10.971	10.993	11.014	10.908
X Torsion 2	12.998	12.826	12.790	12.728	12.698	12.675	12.639
Z Bend 3	21.022	20.844	20.778	20.714	20.761	20.760	20.760
X Torsion 3	21.022	20.915	20.891	20.828	20.864	20.829	20.854
X Bend 1	24.240	24.083	24.058	24.031	23.976	23.991	23.845
8	26.377	26.329	26.275	26.284	26.201	26.133	26.013
X Torsion 4	31.593	31.459	31.435	31.445	31.421	31.430	31.389
10	33.731	33.702	33.647	33.625	33.648	33.636	33.591
Z Bend 4	34.649	34.730	34.746	34.713	34.702	34.696	34.672
12	43.999	44.005	43.977	43.946	43.920	43.914	43.869
X Torsion 5	44.743	44.784	44.766	44.746	44.746	44.712	44.712
Y Bend 1	45.056	45.061	45.062	45.078	45.059	45.064	45.049
Z Bend 5	51.246	51.227	51.200	51.196	51.240	51.211	51.195
16	56.616	56.568	56.543	56.562	56.577	56.522	56.510
X Torsion 6	60.668	60.629	60.615	60.606	60.628	60.615	60.596
18	64.404	64.482	64.490	64.505	64.490	64.460	64.370
19	66.030	66.329	66.009	66.021	65.993	65.978	65.897
Z Bend 6	70.391	70.372	70.341	70.368	70.329	70.320	70.283
21	71.666	71.710	71.703	71.707	71.670	71.713	71.653
22	72.687	72.754	72.787	72.785	72.776	72.745	72.696
Volume 1	76.044	76.060	76.051	76.060	76.045	76.067	76.057
X Torsion 7	79.792	79.814	79.849	79.834	79.799	79.962	79.761
25	83.282	83.227	83.301	83.295	83.298	83.302	83.249
26	85.937	85.961	85.971	85.964	85.962	85.957	85.954
Y Bend 2	88.221	88.226	88.198	88.201	88.186	88.141	88.126
Z Bend 7	93.105	93.152	93.130	93.114	93.137	93.097	93.102
29	95.285	95.361	95.326	95.344	95.343	95.310	95.251
X Torsion 8	102.562	102.592	102.573	102.570	102.568	102.547	102.536

Refer to Appendix A, Table A-1 for explanation of abbreviations.

Continued on next page.

Table C-3 Continued

Defect Depth (mm)	**16.17**	**16.62**	**17.51**	**18.98**	**20.21**
Defect Width (mm)	**3.09**	**3.24**	**3.51**	**4.08**	**4.47**
	RUS (kHz)	**RUS (kHz)**	**RUS (kHz)**	**RUS (kHz)**	**RUS (kHz)**
Z Bend 1	4.615	4.872	5.051	4.275	4.442
X Torsion 1	5.911	5.910	5.910	5.917	5.893
Z Bend 2	11.008	11.002	10.943	11.017	11.046
X Torsion 2	12.659	12.695	12.716	12.588	12.635
Z Bend 3	20.756	20.769	20.658	20.599	20.613
X Torsion 3	20.873	20.857	20.822	20.745	20.729
X Bend 1	23.839	23.753	23.505	23.432	22.115
8	25.987	25.934	25.806	25.477	25.418
X Torsion 4	31.352	31.349	31.416	31.330	31.268
10	33.443	33.470	33.322	33.067	32.834
Z Bend 4	34.674	34.690	34.690	34.673	34.637
12	43.816	43.800	43.708	43.549	43.442
X Torsion 5	44.670	44.657	44.690	44.613	44.593
Y Bend 1	45.020	45.034	45.016	44.987	44.948
Z Bend 5	51.193	51.229	51.219	51.171	51.132
16	56.419	56.429	56.336	56.309	56.072
X Torsion 6	60.532	60.543	60.537	60.470	60.441
18	64.394	64.406	64.298	64.248	63.717
19	65.881	65.873	65.755	65.738	65.471
Z Bend 6	70.306	70.297	70.304	70.265	70.109
21	71.602	71.562	71.526	71.487	71.270
22	72.697	72.710	72.620	72.565	72.441
Volume 1	76.047	76.036	76.041	76.043	76.046
X Torsion 7	79.713	79.696	79.712	79.632	79.591
25	83.259	83.241	83.163	83.122	83.018
26	85.941	85.934	85.925	85.896	85.890
Y Bend 2	88.096	88.087	88.020	87.999	87.720
Z Bend 7	93.090	93.104	93.043	93.028	92.911
29	95.164	95.167	95.108	95.028	94.845
X Torsion 8	102.487	102.484	102.465	102.416	102.353

Refer to Appendix A, Table A-1 for explanation of abbreviations.

Table C-4 Ceramic Specimen #5 resonant frequencies

Defect Depth (mm)	**16.94**	**23.52**	**24.08**	**25.06**
Defect Width (mm)	**1.48**	**2.73**	**2.81**	**2.98**
	RUS (kHz)	**RUS (kHz)**	**RUS (kHz)**	**RUS (kHz)**
Z Bend 1	4.302	4.538	4.256	4.842
X Torsion 1	5.994	5.865	5.897	5.848
Z Bend 2	11.043	10.939	11.069	10.014
X Torsion 2	12.752	12.542	12.493	12.617
Z Bend 3	20.720	20.420	20.536	20.840
X Torsion 3	20.884	20.557	20.716	20.930
X Bend 1	23.896	21.758	20.776	21.088
8	26.089	25.140	25.516	25.502
X Torsion 4	31.309	31.038	31.074	31.125
10	33.410	32.834	33.055	33.172
Z Bend 4	34.513	34.446	34.494	34.472
12	43.681	42.927	43.289	43.299
X Torsion 5	44.491	44.240	44.294	44.263
Y Bend 1	45.072	44.729	44.759	44.910
Z Bend 5	50.991	50.793	50.878	50.907
16	56.293	55.565	55.831	55.918
X Torsion 6	60.331	59.965	60.047	60.061
18	64.068	63.565	63.894	63.844
19	65.624	65.267	65.386	65.379
Z Bend 6	69.959	69.646	69.785	69.792
21	71.252	70.821	71.037	71.088
22	72.279	71.933	72.186	72.100
Volume 1	76.090	76.062	76.081	76.104
X Torsion 7	79.311	79.034	79.157	79.102
25	82.796	82.343	82.447	82.465
26	85.970	85.689	85.811	85.812
Y Bend 2	87.706	87.147	87.391	87.448
Z Bend 7	92.581	92.327	92.581	92.535
29	94.734	94.147	94.303	94.316
X Torsion 8	101.981	101.677	101.790	101.796

Refer to Appendix A, Table A-1 for explanation of abbreviations.

Table C-5 Ceramic Specimen #7 resonant frequencies

Defect Depth (mm)	**9.16**	**17.09**	**17.88**	**18.28**	**18.97**	**22.25**	**23.82**
Defect Width (mm)	**0.36**	**0.63**	**0.67**	**0.65**	**0.72**	**0.93**	**1.07**
	RUS (kHz)	**RUS (kHz)**	**RUS (kHz)**	**RUS (kHz)**	**RUS (kHz)**	**RUS (kHz)**	**RUS (kHz)**
Z Bend 1	4.301	4.150	4.267	4.290	4.703	4.627	4.360
X Torsion 1	5.748	5.692	5.658	5.671	5.668	5.636	5.647
Z Bend 2	10.573		10.715	10.420	10.666	10.383	10.537
X Torsion 2	12.461	12.022	12.095	12.076	12.173	12.060	12.039
Z Bend 3	19.990	19.852	19.861	19.918	19.885	19.834	19.842
X Torsion 3	20.092	19.946	19.952	20.000	19.951	20.024	19.896
X Bend 1	23.159	22.862	22.720	22.713	22.583	22.442	22.158
8	25.200	24.921	24.804	24.796	24.717	24.594	24.462
X Torsion 4	30.221	30.027	30.016	30.025	30.032	29.956	29.928
10	32.301	32.115	32.037	32.030	31.985	31.943	31.836
Z Bend 4	33.245	33.244	33.241	33.235	33.238	33.199	33.205
12	42.155	42.131	42.055	41.939	41.982	41.834	41.836
X Torsion 5	42.937	42.800	42.826	42.781	42.803	42.679	42.688
Y Bend 1	45.082	45.027	45.038	45.048	45.036	44.866	44.845
Z Bend 5	49.118	49.064	49.061	49.081	49.072	49.059	49.030
16	54.287	54.111	54.117	54.108	54.036	54.021	53.912
X Torsion 6	58.224	58.076	58.046	58.070	58.050	57.894	57.901
18	61.743	61.751	61.759	61.771	61.774	61.697	61.649
19	63.290	63.243	63.223	63.241	63.178	63.049	63.043
Z Bend 6	67.515	67.437	67.455	67.436	67.409	67.416	67.354
21	68.779	68.713	68.725	68.738	68.671	68.659	68.581
22	69.729	69.719	69.715	69.687	69.730	69.586	69.563
Volume 1	76.049	76.054	76.074	76.061	76.077	76.003	76.002
X Torsion 7	76.608	76.522	76.535	76.448	76.537	76.313	76.304
25	79.941	79.920	79.891	79.910	79.872	79.674	79.702
26	84.712	84.612	84.605	84.560	84.549	84.516	84.435
Y Bend 2	85.948	85.950	85.952	85.941	85.942	85.814	85.826
Z Bend 7	89.396	89.384	89.386	89.379	89.382	89.358	89.339
29	91.538	91.411	91.412	91.414	91.382	91.120	91.093
X Torsion 8	98.540	98.469	98.484	98.465	98.472	98.340	98.349

Refer to Appendix A, Table A-1 for explanation of abbreviations.

Continued on next page.

Table C-5 Continued

Defect Depth (mm)	**24.26**	**25.07**	**25.82**	**27.14**	**28.53**
Defect Width (mm)	**1.08**	**1.12**	**1.24**	**1.37**	**1.51**
	RUS (kHz)	**RUS (kHz)**	**RUS (kHz)**	**RUS (kHz)**	**RUS (kHz)**
Z Bend 1	4.645	4.696	4.538	4.311	4.764
X Torsion 1	5.640	5.651	5.640	5.645	5.628
Z Bend 2	10.239	10.462	10.662	10.763	10.453
X Torsion 2	12.114	12.049	12.051	12.004	12.016
Z Bend 3	19.842	19.833	19.762	19.720	19.071
X Torsion 3	19.936	19.991	19.904		19.732
X Bend 1	22.132	21.522	21.423		20.306
8	24.438	24.282	24.352	24.249	24.164
X Torsion 4	29.950	29.914	29.889	29.779	29.631
10	31.900	31.736	31.668	31.408	31.319
Z Bend 4	33.195	33.168	33.173	33.158	33.184
12	41.835	41.683	41.668	41.526	41.422
X Torsion 5	42.704	42.654	42.651	42.532	42.305
Y Bend 1	44.868	44.794	44.717	44.500	44.198
Z Bend 5	49.067	49.053	49.063	49.018	48.983
16	53.927	53.832	53.909	53.661	53.503
X Torsion 6	57.923	57.867	57.843	57.573	57.175
18	61.631	61.565	61.580	61.269	60.471
19	63.024	62.917	62.939	62.703	62.400
Z Bend 6	67.354	67.292	67.390	67.306	67.128
21	68.555	68.503	68.599	68.460	68.280
22	69.546	69.508	69.446	69.216	68.811
Volume 1	76.072	75.991	76.053	75.996	75.599
X Torsion 7	76.359	76.257	76.275	76.082	76.055
25	79.668	79.600	79.601	79.405	79.038
26	84.436	84.311	84.409	84.325	84.126
Y Bend 2	85.824	85.754	85.729	85.556	85.275
Z Bend 7	89.363	89.323	89.366	89.298	89.137
29	91.120	90.956	90.922	90.555	89.629
X Torsion 8	98.355	98.290	98.271	98.149	97.946

Refer to Appendix A, Table A-1 for explanation of abbreviations.

Table C-6 Ceramic Specimen #9 resonant frequencies

Defect Depth (mm)	**11.33**	**27.29**	**31.59**
Defect Width (mm)	**1.52**	**4.59**	**5.43**
	RUS (kHz)	**RUS (kHz)**	**RUS (kHz)**
Z Bend 1	4.349	4.322	4.312
X Torsion 1	5.853	5.691	5.277
Z Bend 2	10.927	10.299	10.815
X Torsion 2	12.500	12.033	11.500
Z Bend 3	20.182	20.034	15.337
X Torsion 3	20.279	20.217	18.025
X Bend 1	23.157	20.341	20.184
8	25.263	24.155	24.070
X Torsion 4	30.463	29.996	30.595
10	32.394	30.849	30.904
Z Bend 4	33.515	33.598	33.453
12	42.395	41.055	40.882
X Torsion 5	43.225	42.954	
Y Bend 1	45.167	42.954	43.605
Z Bend 5	49.621	49.393	49.374
16	54.619	53.449	53.329
X Torsion 6	58.669	57.874	57.385
18	62.105	59.293	
19	63.640	62.805	61.715
Z Bend 6	68.090	67.401	65.396
21	69.308	68.160	67.276
22	70.105	68.606	68.581
Volume 1	76.164	76.055	72.884
X Torsion 7	77.187	76.348	76.071
25	80.475	79.143	76.573
26	85.340	84.373	83.827
Y Bend 2	86.063	85.279	84.262
Z Bend 7	90.218	90.060	84.543
29	92.100	90.383	89.502
X Torsion 8	99.402	98.711	97.203

Refer to Appendix A, Table A-1 for explanation of abbreviations.

Table C-7 FEM calculated frequencies for cracks of various depths using ceramic specimen with average dimensions.

Note: Defect width in FEM models includes the width of the modeled crack as well as the offset from the centerline.

Defect Depth (mm)	**0.0**	**0.5**	**1.0**	**1.5**	**2.0**	**2.5**	**3.0**	**3.5**
Defect Width (mm)	**0.0**	**0.2**	**0.2**	**0.2**	**0.2**	**0.2**	**0.2**	**0.2**
	FEA (kHz)	**FEA (kHz)**	**FEA (kHz)**	**FEA (kHz)**	**FEA (kHz)**	**FEA (kHz)**	**FEA (kHz)**	**FEA (kHz)**
Z Bend 1	3.758	3.758	3.758	3.759	3.758	3.759	3.759	3.759
X Torsion 1	5.663	5.664	5.662	5.661	5.661	5.654	5.652	5.645
Z Bend 2	10.386	10.383	10.385	10.386	10.386	10.384	10.384	10.385
X Torsion 2	12.118	12.120	12.117	12.101	12.084	12.061	12.026	11.995
Z Bend 3	20.126	20.123	20.124	20.117	20.097	20.095	20.084	20.067
X Torsion 3	20.172	20.164	20.145	20.113	20.073	20.019	19.940	19.846
X Bend 1	23.430	23.418	23.391	23.350	23.275	23.193	23.091	22.947
8	25.576	25.543	25.482	25.409	25.308	25.213	25.091	24.965
X Torsion 4	30.514	30.498	30.462	30.420	30.341	30.254	30.118	29.965
10	32.752	32.727	32.674	32.615	32.524	32.416	32.323	32.205
Z Bend 4	33.796	33.795	33.804	33.798	33.801	33.802	33.790	33.795
12	42.781	42.766	42.713	42.649	42.595	42.478	42.389	42.305
X Torsion 5	43.539	43.516	43.475	43.412	43.309	43.172	42.986	42.759
Y Bend 1	45.828	45.830	45.836	45.836	45.835	45.833	45.834	45.825
Z Bend 5	49.960	49.961	49.960	49.966	49.979	49.971	49.975	49.958
16	55.127	55.123	55.063	55.006	54.926	54.863	54.775	54.706
X Torsion 6	59.029	58.999	58.927	58.817	58.629	58.317	57.884	57.232
18	62.937	62.948	62.951	62.931	62.904	62.847	62.727	62.491
19	64.387	64.380	64.333	64.256	64.104	63.916	63.662	63.440
Z Bend 6	68.686	68.704	68.690	68.679	68.679	68.674	68.647	68.642
21	70.041	70.013	69.995	69.940	69.901	69.834	69.793	69.725
22	70.983	70.989	70.933	70.859	70.737	70.535	70.243	69.897
Volume 1	77.428	77.439	77.441	77.443	77.442	77.451	77.455	77.453
X Torsion 7	77.884	77.864	77.786	77.662	77.476	77.228	76.934	76.587
25	81.446	81.466	81.421	81.395	81.334	81.222	81.097	80.942
26	86.201	86.180	86.129	86.095	86.052	85.986	85.946	85.901
Y Bend 2	87.209	87.222	87.214	87.209	87.210	87.226	87.201	87.195
Z Bend 7	91.154	91.159	91.149	91.149	91.143	91.108	91.104	91.078
29	93.152	93.132	93.032	92.816	92.547	92.082	91.489	90.798
X Torsion 8	100.410	100.400	100.380	100.380	100.330	100.280	100.270	100.230

Refer to Appendix A, Table A-1 for explanation of abbreviations.

Continued on next page.

Table C-7 Continued

Defect Depth (mm)	4.0	4.5	5.0	5.5	6.0	6.5	7.0	7.5
Defect Width (mm)	0.2	0.2	0.2	0.2	0.2	0.2	0.2	0.2
	FEA (kHz)	FEA (kHz)	FEA (kHz)	FEA (kHz)	FEA (kHz)	FEA (kHz)	FEA (kHz)	FEA (kHz)
Z Bend 1	3.759	3.758	3.759	3.759	3.759	3.758	3.759	3.758
X Torsion 1	5.638	5.633	5.621	5.610	5.596	5.582	5.562	5.542
Z Bend 2	10.384	10.383	10.383	10.383	10.381	10.382	10.379	10.381
X Torsion 2	11.952	11.891	11.829	11.751	11.668	11.567	11.454	11.323
Z Bend 3	20.044	20.016	19.981	19.935	19.865	19.786	19.659	19.500
X Torsion 3	19.741	19.602	19.462	19.286	19.090	18.876	18.643	18.404
X Bend 1	22.766	22.566	22.331	22.072	21.805	21.546	21.287	21.059
8	24.858	24.756	24.674	24.606	24.550	24.493	24.463	24.423
X Torsion 4	29.796	29.587	29.343	29.067	28.760	28.435	28.078	27.724
10	32.104	31.996	31.895	31.812	31.719	31.645	31.583	31.525
Z Bend 4	33.796	33.805	33.794	33.791	33.784	33.791	33.780	33.785
12	42.213	42.094	41.668	41.119	40.494	39.758	38.995	38.221
X Torsion 5	42.467	42.136	42.064	42.006	41.947	41.897	41.871	41.841
Y Bend 1	45.830	45.818	45.804	45.790	45.765	45.749	45.703	45.682
Z Bend 5	49.968	49.986	49.961	49.953	49.941	49.925	49.927	49.920
16	54.642	54.576	54.529	54.491	54.458	54.447	54.419	54.410
X Torsion 6	56.266	55.002	53.478	51.902	50.411	49.087	48.020	47.154
18	62.058	61.602	61.194	60.835	60.542	60.299	60.072	59.880
19	63.326	63.238	63.242	63.215	63.213	63.183	63.199	63.194
Z Bend 6	68.629	68.627	68.612	68.569	68.611	68.611	68.603	68.593
21	69.700	69.644	69.609	69.553	69.528	69.534	69.504	69.494
22	69.506	69.130	68.846	68.597	68.375	68.219	68.126	68.049
Volume 1	77.449	77.454	77.465	77.445	77.441	77.445	77.440	77.474
X Torsion 7	76.241	75.952	75.713	75.559	75.453	75.369	75.316	75.317
25	80.730	80.509	80.302	80.088	79.886	79.698	79.496	79.317
26	85.896	85.833	85.823	85.816	85.824	85.813	85.820	85.805
Y Bend 2	87.177	87.156	87.157	87.096	87.094	87.037	86.985	86.939
Z Bend 7	91.054	91.060	90.960	90.927	90.857	90.810	90.737	90.683
29	90.030	89.281	88.671	88.195	87.852	87.634	87.499	87.412
X Torsion 8	100.220	100.200	100.160	95.684	89.721	84.268	79.241	74.597

Refer to Appendix A, Table A-1 for explanation of abbreviations.

Continued on next page.

Table C-7 Continued

Defect Depth (mm)	8.0	8.5	9.0	9.5	10.0	10.5	11.0	11.5
Defect Width (mm)	0.2	0.2	0.2	0.2	0.2	0.2	0.2	0.2
	FEA (kHz)	FEA (kHz)	FEA (kHz)	FEA (kHz)	FEA (kHz)	FEA (kHz)	FEA (kHz)	FEA (kHz)
Z Bend 1	3.758	3.758	3.758	3.758	3.757	3.757	3.757	3.757
X Torsion 1	5.519	5.493	5.460	5.425	5.387	5.343	5.293	5.238
Z Bend 2	10.376	10.376	10.377	10.376	10.375	10.373	10.372	10.370
X Torsion 2	11.180	11.019	10.847	10.660	10.471	10.268	10.066	9.864
Z Bend 3	19.292	19.029	18.745	18.428	18.098	17.753	17.411	17.067
X Torsion 3	18.145	17.890	17.630	17.389	17.163	16.949	16.754	16.581
X Bend 1	20.879	20.735	20.633	20.559	20.500	20.458	20.425	20.398
8	24.407	24.390	24.380	24.363	24.352	24.349	24.344	24.344
X Torsion 4	27.354	27.011	26.668	26.353	26.060	25.782	25.535	25.304
10	31.459	31.431	31.397	31.371	31.349	31.341	31.326	31.312
Z Bend 4	33.672	33.783	33.763	33.754	33.748	33.735	33.724	33.723
12	37.248	36.771	36.130	35.540	34.996	34.505	34.046	33.587
X Torsion 5	41.559	41.796	41.794	41.792	41.790	41.782	41.781	41.781
Y Bend 1	45.720	45.577	45.526	45.449	45.368	45.266	45.160	45.035
Z Bend 5	49.851	49.891	49.875	49.860	49.839	49.826	49.811	49.784
16	54.230	54.409	54.407	54.397	54.405	54.381	54.357	54.352
X Torsion 6	46.534	45.919	45.417	44.992	44.614	44.237	43.916	43.571
18	59.592	59.440	59.257	59.050	58.807	58.561	58.302	58.013
19	63.347	63.187	63.189	63.194	63.172	63.179	63.145	63.135
Z Bend 6	68.700	68.520	68.502	68.447	68.391	68.328	68.270	68.208
21	69.629	69.482	69.483	69.474	69.480	69.464	69.478	69.451
22	68.002	67.945	67.926	67.950	67.904	67.891	67.901	67.867
Volume 1	77.239	77.462	77.474	77.470	77.479	77.478	77.469	77.483
X Torsion 7	75.250	75.242	75.240	75.152	75.028	74.868	74.600	74.289
25	79.011	78.963	78.775	78.606	78.450	78.299	78.188	78.096
26	85.789	85.747	85.711	85.650	85.585	85.496	85.408	85.318
Y Bend 2	86.887	86.767	86.678	86.587	86.457	86.310	86.135	85.939
Z Bend 7	90.716	90.540	90.464	90.406	90.383	90.320	90.291	90.249
29	87.456	87.311	87.338	87.328	87.283	87.190	87.052	86.875
X Torsion 8	70.368	66.458	62.842	59.520	56.448	53.602	50.955	48.499

Refer to Appendix A, Table A-1 for explanation of abbreviations.

Continued on next page.

Table C-7 Continued

Defect Depth (mm)	12.0	12.5	13.0	13.5	14.0	14.5	15.0	15.5
Defect Width (mm)	0.2	0.2	0.2	0.2	0.2	0.2	0.2	0.2
	FEA (kHz)	FEA (kHz)	FEA (kHz)	FEA (kHz)	FEA (kHz)	FEA (kHz)	FEA (kHz)	FEA (kHz)
Z Bend 1	3.757	3.757	3.756	3.756	3.755	3.756	3.755	3.754
X Torsion 1	5.177	5.109	5.036	4.959	4.875	4.784	4.690	4.595
Z Bend 2	10.371	10.370	10.370	10.370	10.368	10.368	10.367	10.367
X Torsion 2	9.665	9.477	9.291	9.118	8.956	8.809	8.677	8.553
Z Bend 3	16.731	16.392	16.069	15.744	15.443	15.134	14.839	14.553
X Torsion 3	16.424	16.286	16.169	16.063	15.972	15.893	15.822	15.754
X Bend 1	20.370	20.349	20.333	20.318	20.304	20.296	20.289	20.278
8	24.327	24.328	24.323	24.321	24.327	24.330	24.330	24.331
X Torsion 4	25.083	24.877	24.682	24.493	24.303	24.113	23.907	23.701
10	31.309	31.309	31.306	31.304	31.308	31.307	31.307	31.302
Z Bend 4	33.714	33.701	33.701	33.682	33.675	33.670	33.652	33.640
12	33.155	32.743	32.329	31.919	31.500	31.091	30.661	30.243
X Torsion 5	41.780	41.772	41.754	41.737	41.722	41.679	41.640	41.591
Y Bend 1	44.899	44.747	44.577	44.383	44.176	43.948	43.698	43.429
Z Bend 5	49.775	49.757	49.747	49.738	49.725	49.711	49.699	49.695
16	54.303	54.266	54.206	54.146	54.070	53.988	53.900	53.805
X Torsion 6	43.249	42.923	42.596	42.262	41.935	41.620	41.303	41.015
18	57.706	57.393	57.072	56.738	56.385	56.050	55.699	55.375
19	63.106	63.087	63.073	63.036	62.998	62.964	62.912	62.824
Z Bend 6	68.115	68.063	67.969	67.897	67.841	67.771	67.715	67.690
21	69.440	69.432	69.436	69.393	69.364	69.355	69.318	69.309
22	67.878	67.822	67.780	67.680	67.577	67.412	67.165	66.841
Volume 1	77.480	77.483	77.481	77.480	77.481	77.490	77.491	77.484
X Torsion 7	73.862	73.400	72.885	72.350	71.830	71.320	70.912	70.565
25	78.008	77.972	77.948	77.927	77.913	77.888	77.845	77.775
26	85.227	85.141	85.120	85.028	84.963	84.954	84.947	84.911
Y Bend 2	85.714	85.441	85.084	84.721	84.272	83.720	83.081	82.332
Z Bend 7	90.243	90.210	90.198	90.203	90.196	90.214	90.179	90.192
29	86.567	86.166	85.725	85.240	84.745	84.263	83.826	83.445
X Torsion 8	46.219	44.092	42.103	40.242	38.510	36.883	35.357	33.927

Refer to Appendix A, Table A-1 for explanation of abbreviations.

Continued on next page.

Table C-7 Continued

Defect Depth (mm)	16.0	16.5	17.0	17.5	18.0	18.5	19.0	19.5
Defect Width (mm)	0.2	0.2	0.2	0.2	0.2	0.2	0.2	0.2
	FEA (kHz)	FEA (kHz)	FEA (kHz)	FEA (kHz)	FEA (kHz)	FEA (kHz)	FEA (kHz)	FEA (kHz)
Z Bend 1	3.755	3.754	3.755	3.754	3.754	3.754	3.754	3.754
X Torsion 1	4.490	4.387	4.281	4.176	4.069	3.963	3.857	3.753
Z Bend 2	10.367	10.366	10.366	10.366	10.365	10.365	10.368	10.365
X Torsion 2	8.447	8.352	8.266	8.191	8.127	8.072	8.022	7.981
Z Bend 3	14.267	14.001	13.737	13.480	13.233	12.994	12.762	12.537
X Torsion 3	15.712	15.664	15.626	15.584	15.550	15.522	15.495	15.471
X Bend 1	20.264	20.258	20.252	20.245	20.244	20.237	20.236	20.229
8	24.332	24.328	24.331	24.328	24.327	24.324	24.324	24.324
X Torsion 4	23.485	23.253	23.001	22.721	22.425	22.091	21.737	21.359
10	31.299	31.297	31.275	31.254	31.236	31.199	31.152	31.119
Z Bend 4	33.633	33.623	33.616	33.604	33.610	33.602	33.590	33.584
12	29.818	29.406	29.007	28.627	28.264	27.941	27.644	27.374
X Torsion 5	41.530	41.448	41.364	41.275	41.163	41.057	40.947	40.820
Y Bend 1	43.137	42.825	42.493	42.148	41.782	41.395	40.995	40.580
Z Bend 5	49.686	49.671	49.677	49.681	49.677	49.675	49.678	49.672
16	53.691	53.598	53.502	53.418	53.327	53.246	53.167	53.115
X Torsion 6	40.714	40.450	40.213	39.999	39.788	39.612	39.462	39.316
18	55.043	54.744	54.441	54.151	53.867	53.585	53.310	53.002
19	62.734	62.633	62.455	62.239	61.927	61.527	61.032	60.452
Z Bend 6	67.678	67.621	67.620	67.624	67.605	67.592	67.597	67.590
21	69.272	69.247	69.223	69.232	69.197	69.191	69.185	69.185
22	66.463	66.043	65.601	65.176	64.808	64.504	64.247	64.082
Volume 1	77.494	77.481	77.483	77.489	77.482	77.481	77.482	77.472
X Torsion 7	70.326	70.163	70.032	69.949	69.909	69.891	69.857	69.873
25	77.703	77.544	77.391	77.203	76.938	76.679	76.418	76.121
26	84.894	84.890	84.905	84.884	84.886	84.858	84.825	84.792
Y Bend 2	81.504	80.573	79.608	78.636	77.640	76.692	75.740	74.854
Z Bend 7	90.181	90.156	90.178	90.002	89.430	88.971	88.572	88.187
29	83.119	82.847	82.632	82.474	82.357	82.296	82.218	82.205
X Torsion 8	32.567	31.294	30.103	28.967	27.903	26.890	25.936	25.027

Refer to Appendix A, Table A-1 for explanation of abbreviations.

Continued on next page.

Table C-7 Continued

Defect Depth (mm)	20.0	20.5	21.0	21.5	22.0	22.5	23.0	23.5
Defect Width (mm)	0.2	0.2	0.2	0.2	0.2	0.2	0.2	0.2
	FEA (kHz)	FEA (kHz)	FEA (kHz)	FEA (kHz)	FEA (kHz)	FEA (kHz)	FEA (kHz)	FEA (kHz)
Z Bend 1	3.753	3.754	3.754	3.753	3.753	3.752	3.753	3.753
X Torsion 1	3.652	3.552	3.454	3.360	3.267	3.178	3.092	3.007
Z Bend 2	10.365	10.365	10.365	10.365	10.366	10.360	10.363	10.363
X Torsion 2	7.940	7.913	7.888	7.867	7.845	7.838	7.815	7.816
Z Bend 3	12.319	12.106	11.904	11.698	11.506	11.316	11.136	10.950
X Torsion 3	15.444	15.413	15.391	15.360	15.343	15.315	15.272	15.229
X Bend 1	20.229	20.221	20.224	20.218	20.218	20.211	20.224	20.216
8	24.317	24.315	24.304	24.300	24.287	24.285	24.269	24.257
X Torsion 4	20.963	20.558	20.130	19.696	19.271	18.826	18.410	17.997
10	31.055	30.988	30.915	30.837	30.733	30.622	30.511	30.386
Z Bend 4	33.580	33.578	33.573	33.564	33.561	33.565	33.578	33.574
12	27.146	26.931	26.756	26.624	26.473	26.364	26.277	26.211
X Torsion 5	40.688	40.574	40.453	40.332	40.226	40.109	39.999	39.910
Y Bend 1	40.154	39.713	39.262	38.806	38.347	37.879	37.411	36.946
Z Bend 5	49.678	49.692	49.670	49.675	49.668	49.658	49.657	49.653
16	53.080	53.022	52.991	52.974	52.967	52.983	52.946	52.945
X Torsion 6	39.191	39.087	39.023	38.959	38.891	38.821	38.797	38.761
18	52.691	52.356	51.940	51.481	50.984	50.366	49.687	48.910
19	59.828	59.168	58.496	57.853	57.256	56.711	56.261	55.853
Z Bend 6	67.588	67.596	67.579	67.569	67.518	67.497	67.450	67.387
21	69.182	69.184	69.172	69.159	69.174	69.152	69.152	69.141
22	63.944	63.845	63.782	63.754	63.687	63.650	63.629	63.644
Volume 1	77.459	77.453	77.428	77.425	77.417	77.391	77.366	77.339
X Torsion 7	69.867	69.834	69.806	69.820	69.782	69.769	69.672	69.611
25	75.851	75.559	75.322	75.068	74.864	74.698	74.537	74.431
26	84.759	84.705	84.621	84.555	84.478	84.390	84.326	84.271
Y Bend 2	73.999	73.199	72.441	71.735	71.078	70.460	69.860	69.328
Z Bend 7	87.823	87.503	87.186	86.890	86.574	86.265	85.938	85.622
29	82.201	82.167	82.141	82.145	82.047	82.074	81.848	81.707
X Torsion 8	24.169	23.351	22.575	21.836	21.132	20.462	19.827	19.220

Refer to Appendix A, Table A-1 for explanation of abbreviations.

Continued on next page.

Table C-7 Continued

Defect Depth (mm)	24.0	24.5	25.0	25.5	26.0	26.5	27.0	27.5
Defect Width (mm)	0.2	0.2	0.2	0.2	0.2	0.2	0.2	0.2
	FEA (kHz)	FEA (kHz)	FEA (kHz)	FEA (kHz)	FEA (kHz)	FEA (kHz)	FEA (kHz)	FEA (kHz)
Z Bend 1	3.752	3.752	3.752	3.752	3.753	3.752	3.752	3.752
X Torsion 1	2.926	2.847	2.771	2.698	2.627	2.559	2.493	2.429
Z Bend 2	10.363	10.362	10.363	10.362	10.364	10.363	10.364	10.363
X Torsion 2	7.804	7.802	7.797	7.794	7.787	7.783	7.790	7.788
Z Bend 3	10.787	10.619	10.454	10.299	10.144	9.998	9.852	9.712
X Torsion 3	15.170	15.109	15.027	14.903	14.751	14.555	14.312	14.049
X Bend 1	20.206	20.218	20.216	20.218	20.218	20.218	20.217	20.215
8	24.236	24.223	24.197	24.177	24.148	24.117	24.065	24.031
X Torsion 4	17.601	17.218	16.877	16.585	16.332	16.090	15.986	15.875
10	30.245	30.102	29.949	29.799	29.629	29.476	29.297	29.142
Z Bend 4	33.564	33.568	33.562	33.573	33.567	33.564	33.568	33.562
12	26.147	26.102	26.059	26.030	26.004	25.990	25.987	25.977
X Torsion 5	39.808	39.764	39.705	39.647	39.615	39.567	39.539	39.532
Y Bend 1	36.477	36.007	35.543	35.084	34.632	34.182	33.743	33.313
Z Bend 5	49.658	49.650	49.648	49.652	49.636	49.638	49.635	49.630
16	52.945	52.972	52.956	52.928	52.917	52.885	52.853	52.789
X Torsion 6	38.742	38.705	38.684	38.673	38.638	38.639	38.629	38.594
18	48.083	47.213	46.317	45.386	44.459	43.528	42.603	41.691
19	55.534	55.240	55.032	54.824	54.680	54.556	54.456	54.389
Z Bend 6	67.351	67.290	67.214	67.159	67.085	66.986	66.953	66.868
21	69.113	69.102	69.078	69.039	69.023	68.980	68.953	68.929
22	63.636	63.599	63.612	63.598	63.604	63.573	63.586	63.584
Volume 1	77.280	77.240	77.136	76.980	76.687	76.113	75.124	73.840
X Torsion 7	69.512	69.401	69.265	69.093	68.887	68.676	68.396	68.075
25	74.341	74.295	74.258	74.199	74.217	74.208	74.184	74.158
26	84.200	84.155	84.123	84.087	83.752	83.314	82.879	82.430
Y Bend 2	68.811	68.323	67.859	67.420	66.996	66.588	66.184	65.819
Z Bend 7	85.272	84.916	83.980	82.243	80.680	79.457	78.576	77.990
29	81.461	81.156	80.791	80.340	79.797	79.218	78.699	78.308
X Torsion 8	18.634	18.081	17.550	17.041	16.554	16.131	15.641	15.216

Refer to Appendix A, Table A-1 for explanation of abbreviations.

Continued on next page.

Table C-7 Continued

Defect Depth (mm)	28.0	28.5	29.0	29.5	30.0	30.5	31.0
Defect Width (mm)	0.2	0.2	0.2	0.2	0.2	0.2	0.2
	FEA (kHz)	FEA (kHz)	FEA (kHz)	FEA (kHz)	FEA (kHz)	FEA (kHz)	FEA (kHz)
Z Bend 1	3.753	3.751	3.753	3.752	3.752	3.752	3.750
X Torsion 1	2.368	2.310	2.253	2.198	2.145	2.094	2.045
Z Bend 2	10.363	10.363	10.363	10.359	10.362	10.360	10.360
X Torsion 2	7.781	7.781	7.778	7.781	7.779	7.783	7.777
Z Bend 3	9.579	9.448	9.317	9.192	9.066	8.943	8.827
X Torsion 3	13.766	13.476	13.180	12.883	12.602	12.314	12.042
X Bend 1	20.214	20.211	20.217	20.196	20.199	20.203	20.194
8	23.988	23.928	23.859	23.791	23.721	23.625	23.545
X Torsion 4	15.798	15.747	15.701	15.670	15.648	15.634	15.629
10	29.039	28.810	28.661	28.514	28.373	28.241	28.126
Z Bend 4	33.561	33.564	33.560	33.562	33.569	33.566	33.562
12	25.975	25.977	25.973	25.976	25.966	25.970	25.956
X Torsion 5	39.522	39.502	39.500	39.507	39.504	39.517	39.490
Y Bend 1	32.882	32.456	32.055	31.652	31.258	30.875	30.496
Z Bend 5	49.633	49.640	49.630	49.635	49.624	49.632	49.629
16	52.723	52.661	52.559	52.512	52.396	52.296	52.176
X Torsion 6	38.568	38.499	38.324	37.810	37.134	36.357	35.640
18	40.820	39.999	39.304	38.940	38.818	38.752	38.722
19	54.294	54.278	54.237	54.214	54.198	54.189	54.186
Z Bend 6	66.878	66.785	66.736	66.720	66.679	66.681	66.662
21	68.911	68.878	68.861	68.855	68.841	68.823	68.828
22	63.533	63.503	63.461	63.354	63.187	62.828	62.304
Volume 1	72.409	70.948	69.481	68.044	66.632	65.248	63.922
X Torsion 7	67.686	67.232	66.664	66.080	65.525	64.988	64.652
25	74.137	74.072	73.969	73.820	73.627	73.444	73.294
26	81.951	81.484	80.994	80.487	79.975	79.483	78.976
Y Bend 2	65.427	65.060	64.693	64.328	63.968	63.583	63.229
Z Bend 7	77.346	76.803	76.385	76.046	75.840	75.717	75.595
29	78.105	77.990	77.914	77.862	77.828	77.787	77.781
X Torsion 8	14.805	14.411	14.032	13.668	13.317	12.979	12.655

Refer to Appendix A, Table A-1 for explanation of abbreviations.

Table C-8 FEM calculated frequencies for 10 mm crack depth and various offsets from centerline using ceramic specimen with average dimensions.

Note: Defect width in FEM models includes the width of the modeled crack as well as the offset from the centerline.

Defect Depth (mm)	**10.0**	**10.0**	**10.0**	**10.0**	**10.0**	**10.0**	**10.0**	**10.0**
Defect Width (mm)	**0.00**	**0.25**	**0.50**	**0.75**	**1.00**	**1.25**	**1.50**	**1.75**
	FEA (kHz)	**FEA (kHz)**	**FEA (kHz)**	**FEA (kHz)**	**FEA (kHz)**	**FEA (kHz)**	**FEA (kHz)**	**FEA (kHz)**
Z Bend 1	3.757	3.754	3.757	3.757	3.758	3.756	3.757	3.757
X Torsion 1	5.387	5.395	5.399	5.396	5.393	5.396	5.395	5.395
Z Bend 2	10.375	10.372	10.368	10.366	10.354	10.342	10.327	10.310
X Torsion 2	10.471	10.518	10.515	10.521	10.522	10.531	10.536	10.540
Z Bend 3	18.098	18.142	18.125	18.131	18.146	18.136	18.141	18.153
X Torsion 3	17.163	17.214	17.207	17.195	17.186	17.168	17.145	17.127
X Bend 1	20.500	20.500	20.505	20.504	20.507	20.506	20.496	20.502
8	24.352	24.349	24.346	24.335	24.355	24.356	24.351	24.350
X Torsion 4	26.060	26.134	26.109	26.093	26.076	26.036	26.008	25.967
10	31.349	31.360	31.363	31.351	31.341	31.344	31.339	31.319
Z Bend 4	33.748	33.741	33.739	33.725	33.726	33.692	33.662	33.638
12	34.996	35.139	35.101	35.068	35.043	35.001	34.976	34.942
X Torsion 5	41.790	41.792	41.780	41.789	41.767	41.759	41.731	41.718
Y Bend 1	45.368	45.391	45.378	45.339	45.296	45.245	45.155	45.083
Z Bend 5	49.839	49.836	49.849	49.852	49.853	49.836	49.839	49.840
16	54.405	54.419	54.388	54.393	54.370	54.394	54.359	54.345
X Torsion 6	44.614	44.700	44.689	44.664	44.626	44.608	44.566	44.541
18	58.807	58.850	58.853	58.861	58.836	58.811	58.789	58.779
19	63.172	63.146	63.182	63.168	63.162	63.174	63.189	63.154
Z Bend 6	68.391	68.417	68.455	68.434	68.441	68.478	68.502	68.533
21	69.480	69.490	69.459	69.473	69.442	69.420	69.413	69.398
22	67.904	67.894	67.913	67.842	67.827	67.788	67.723	67.630
Volume 1	77.479	77.474	77.476	77.486	77.473	77.455	77.448	77.428
X Torsion 7	75.028	75.061	75.027	75.003	74.989	74.917	74.874	74.829
25	78.450	78.485	78.475	78.489	78.448	78.426	78.400	78.382
26	85.585	85.598	85.585	85.587	85.540	85.520	85.470	85.402
Y Bend 2	86.457	86.512	86.514	86.522	86.542	86.572	86.600	86.651
Z Bend 7	90.383	90.368	90.406	90.401	90.469	90.491	90.538	90.580
29	87.283	87.245	87.206	87.138	87.022	86.954	86.785	86.678
X Torsion 8	56.448	56.624	56.540	56.434	56.269	56.046	55.799	55.502

Refer to Appendix A, Table A-1 for explanation of abbreviations.

Continued on next page.

Table C-8 Continued

Defect Depth (mm)	**10.0**	**10.0**	**10.0**	**10.0**	**10.0**	**10.0**	**10.0**	**10.0**
Defect Width (mm)	**2.00**	**2.25**	**2.50**	**2.75**	**3.00**	**3.25**	**3.50**	**3.75**
	FEA (kHz)	**FEA (kHz)**	**FEA (kHz)**	**FEA (kHz)**	**FEA (kHz)**	**FEA (kHz)**	**FEA (kHz)**	**FEA (kHz)**
Z Bend 1	3.756	3.756	3.755	3.756	3.756	3.754	3.755	3.755
X Torsion 1	5.396	5.394	5.387	5.386	5.384	5.386	5.383	5.383
Z Bend 2	10.297	10.282	10.259	10.238	10.217	10.195	10.173	10.147
X Torsion 2	10.548	10.555	10.554	10.561	10.570	10.576	10.582	10.588
Z Bend 3	18.149	18.146	18.166	18.173	18.182	18.192	18.201	18.216
X Torsion 3	17.100	17.077	17.030	16.992	16.955	16.914	16.870	16.818
X Bend 1	20.507	20.510	20.513	20.514	20.514	20.516	20.514	20.517
8	24.348	24.345	24.347	24.339	24.335	24.329	24.328	24.310
X Torsion 4	25.924	25.869	25.791	25.731	25.669	25.598	25.518	25.442
10	31.312	31.299	31.266	31.250	31.240	31.214	31.201	31.174
Z Bend 4	33.596	33.553	33.494	33.442	33.377	33.307	33.227	33.150
12	34.899	34.856	34.796	34.749	34.713	34.680	34.645	34.611
X Torsion 5	41.692	41.687	41.587	41.569	41.538	41.501	41.464	41.417
Y Bend 1	44.969	44.856	44.707	44.530	44.323	44.077	43.789	43.449
Z Bend 5	49.841	49.833	49.839	49.830	49.836	49.826	49.818	49.804
16	54.323	54.316	54.204	54.181	54.156	54.131	54.085	54.073
X Torsion 6	44.496	44.455	44.378	44.317	44.271	44.237	44.187	44.133
18	58.762	58.739	58.698	58.652	58.617	58.601	58.587	58.543
19	63.148	63.150	63.165	63.182	63.168	63.149	63.139	63.136
Z Bend 6	68.539	68.588	68.517	68.545	68.577	68.578	68.582	68.605
21	69.375	69.335	69.332	69.271	69.237	69.193	69.163	69.115
22	67.624	67.529	67.483	67.411	67.325	67.282	67.191	67.112
Volume 1	77.421	77.400	77.383	77.362	77.348	77.327	77.308	77.278
X Torsion 7	74.752	74.697	74.600	74.542	74.464	74.382	74.306	74.252
25	78.343	78.333	78.275	78.230	78.194	78.154	78.117	78.039
26	85.367	85.293	85.116	85.007	84.879	84.764	84.594	84.466
Y Bend 2	86.682	86.717	86.789	86.836	86.885	86.939	86.984	87.037
Z Bend 7	90.605	90.637	90.708	90.741	90.762	90.789	90.814	90.811
29	86.544	86.424	86.236	86.126	86.025	85.961	85.890	85.811
X Torsion 8	55.186	54.814	54.422	54.002	53.551	53.084	52.607	52.129

Refer to Appendix A, Table A-1 for explanation of abbreviations.

Continued on next page.

Table C-8 Continued

Defect Depth (mm)	**10.0**	**10.0**	**10.0**	**10.0**	**10.0**
Defect Width (mm)	**4.00**	**4.50**	**5.00**	**5.50**	**6.00**
	FEA (kHz)	**FEA (kHz)**	**FEA (kHz)**	**FEA (kHz)**	**FEA (kHz)**
Z Bend 1	3.755	3.752	3.751	3.749	3.747
X Torsion 1	5.382	5.381	5.381	5.377	5.375
Z Bend 2	10.120	10.065	9.996	9.925	9.844
X Torsion 2	10.595	10.607	10.617	10.631	10.641
Z Bend 3	18.225	18.245	18.268	18.291	18.307
X Torsion 3	16.762	16.652	16.513	16.360	16.193
X Bend 1	20.520	20.520	20.516	20.524	20.524
8	24.306	24.277	24.246	24.191	24.086
X Torsion 4	25.364	25.184	25.011	24.835	24.696
10	31.146	31.096	31.023	30.933	30.820
Z Bend 4	33.059	32.881	32.694	32.513	32.346
12	34.583	34.532	34.480	34.439	34.410
X Torsion 5	41.382	41.271	41.149	41.007	40.856
Y Bend 1	43.058	42.067	40.784	39.189	37.309
Z Bend 5	49.798	49.764	49.733	49.695	49.640
16	54.018	53.961	53.853	53.763	53.646
X Torsion 6	44.089	44.015	43.919	43.850	43.787
18	58.512	58.458	58.393	58.340	58.273
19	63.119	63.099	63.068	63.045	63.036
Z Bend 6	68.611	68.631	68.911	68.860	68.838
21	69.072	68.994	68.614	68.559	68.452
22	67.024	66.845	66.683	66.507	66.325
Volume 1	77.266	77.211	77.160	77.100	77.036
X Torsion 7	74.172	74.049	73.927	73.798	73.663
25	77.989	77.838	77.687	77.487	77.238
26	84.286	83.936	83.571	83.209	82.841
Y Bend 2	87.088	87.183	87.284	87.372	87.444
Z Bend 7	90.841	90.846	90.855	90.837	90.750
29	85.780	85.686	85.602	85.516	85.438
X Torsion 8	51.663	50.775	49.994	49.351	48.824

Refer to Appendix A, Table A-1 for explanation of abbreviations.

Table C-9 FEM calculated frequencies for 20 mm crack depth and various offsets from centerline using ceramic specimen with average dimensions.

Note: Defect width in FEM models includes the width of the modeled crack as well as the offset from the centerline.

Defect Depth (mm)	**20.0**	**20.0**	**20.0**	**20.0**	**20.0**	**20.0**	**20.0**	**20.0**
Defect Width (mm)	**0.00**	**0.25**	**0.50**	**1.00**	**1.50**	**2.00**	**2.50**	**3.00**
	FEA (kHz)	**FEA (kHz)**	**FEA (kHz)**	**FEA (kHz)**	**FEA (kHz)**	**FEA (kHz)**	**FEA (kHz)**	**FEA (kHz)**
Z Bend 1	3.753	3.755	3.759	3.772	3.788	3.805	3.821	3.836
X Torsion 1	3.652	3.679	3.671	3.653	3.632	3.602	3.577	3.547
Z Bend 2	10.365	10.366	10.367	10.369	10.368	10.374	10.374	10.378
X Torsion 2	7.940	7.948	7.946	7.939	7.924	7.907	7.881	7.856
Z Bend 3	12.319	12.349	12.347	12.344	12.347	12.348	12.357	12.358
X Torsion 3	15.444	15.435	15.428	15.412	15.401	15.376	15.350	15.308
X Bend 1	20.229	20.228	20.228	20.224	20.219	20.216	20.203	20.200
8	24.317	24.323	24.320	24.320	24.322	24.323	24.313	24.322
X Torsion 4	20.963	21.060	21.054	21.035	21.015	20.986	20.966	20.929
10	31.055	31.040	31.032	31.030	31.046	31.059	31.046	31.066
Z Bend 4	33.580	33.581	33.586	33.587	33.580	33.575	33.580	33.580
12	27.146	27.178	27.178	27.162	27.153	27.133	27.109	27.081
X Torsion 5	40.688	40.645	40.663	40.700	40.758	40.806	40.884	40.975
Y Bend 1	40.154	40.374	40.391	40.525	40.740	41.062	41.436	41.851
Z Bend 5	49.678	49.674	49.677	49.667	49.641	49.638	49.619	49.566
16	53.080	53.026	53.100	53.251	53.400	53.547	53.690	53.851
X Torsion 6	39.191	39.196	39.192	39.150	39.081	38.992	38.892	38.779
18	52.691	52.690	52.613	52.445	52.264	52.071	51.867	51.683
19	59.828	59.976	59.990	59.963	59.951	59.930	59.931	59.926
Z Bend 6	67.588	67.502	67.475	67.432	67.318	67.136	66.891	66.596
21	69.182	69.174	69.143	69.051	68.927	68.806	68.721	68.612
22	63.944	64.011	64.017	64.014	64.033	64.061	64.054	64.089
Volume 1	77.459	77.483	77.542	77.737	78.002	78.330	78.650	78.973
X Torsion 7	69.867	69.867	69.888	69.935	70.039	70.101	70.179	70.267
25	75.851	75.897	75.890	75.880	75.865	75.850	75.800	75.719
26	84.759	84.611	84.604	84.603	84.529	84.496	84.390	84.285
Y Bend 2	73.999	74.411	74.285	73.961	73.554	73.054	72.513	71.919
Z Bend 7	87.823	87.985	87.977	87.941	87.904	87.843	87.728	87.189
29	82.201	82.105	82.050	81.805	81.369	80.795	80.097	79.367
X Torsion 8	24.169	24.235	24.169	23.931	23.544	23.017	22.385	21.645

Refer to Appendix A, Table A-1 for explanation of abbreviations.

Continued on next page.

Table C-9 Continued.

Defect Depth (mm)	**20.0**	**20.0**	**20.0**	**20.0**	**20.0**	**20.0**
Defect Width (mm)	**3.50**	**4.00**	**4.50**	**5.00**	**5.50**	**6.00**
	FEA (kHz)	**FEA (kHz)**	**FEA (kHz)**	**FEA (kHz)**	**FEA (kHz)**	**FEA (kHz)**
Z Bend 1	3.853	3.867	3.881	3.895	3.906	3.920
X Torsion 1	3.514	3.480	3.444	3.405	3.363	3.320
Z Bend 2	10.384	10.386	10.396	10.401	10.408	10.414
X Torsion 2	7.822	7.786	7.745	7.699	7.651	7.596
Z Bend 3	12.365	12.374	12.370	12.370	12.360	12.341
X Torsion 3	15.274	15.229	15.176	15.125	15.064	15.000
X Bend 1	20.179	20.166	20.148	20.130	20.109	20.085
8	24.323	24.343	24.325	24.322	24.326	24.324
X Torsion 4	20.820	20.860	20.815	20.767	20.716	20.661
10	31.083	31.080	31.093	31.101	31.094	31.095
Z Bend 4	33.581	33.561	33.572	33.558	33.567	33.549
12	27.047	26.997	26.954	26.898	26.835	26.763
X Torsion 5	41.060	41.154	41.255	41.356	41.453	41.553
Y Bend 1	42.305	42.787	43.265	43.749	44.223	44.690
Z Bend 5	49.520	49.477	49.422	49.355	49.285	49.185
16	54.017	54.151	54.318	54.490	54.645	54.824
X Torsion 6	38.655	38.492	38.343	38.193	38.024	37.831
18	51.488	51.300	51.069	50.858	50.659	50.438
19	59.926	59.895	59.924	59.928	59.904	59.877
Z Bend 6	66.218	65.801	65.320	64.860	64.053	63.699
21	68.536	68.465	68.432	68.405	68.398	68.381
22	64.110	64.179	64.167	64.180	64.545	64.492
Volume 1	79.307	79.632	79.911	80.167	80.393	80.548
X Torsion 7	70.345	70.427	70.492	70.551	70.631	70.656
25	75.625	75.504	75.222	74.892	74.507	74.083
26	84.194	84.058	83.916	83.784	83.657	83.456
Y Bend 2	71.280	70.609	69.879	69.107	68.291	67.417
Z Bend 7	86.743	86.374	86.135	85.913	85.744	85.588
29	78.620	77.905	77.344	76.993	76.754	76.636
X Torsion 8	20.896	19.928	18.972	17.958	16.901	15.805

Refer to Appendix A, Table A-1 for explanation of abbreviations.

Table C-10 FEM calculated frequencies for 30 mm crack depth and various offsets from centerline using ceramic specimen with average dimensions.

Note: Defect width in FEM models includes the width of the modeled crack as well as the offset from the centerline.

Defect Depth (mm)	**30.0**	**30.0**	**30.0**	**30.0**	**30.0**	**30.0**	**30.0**	**30.0**
Defect Width (mm)	**0.00**	**0.25**	**0.50**	**1.00**	**1.50**	**2.00**	**2.50**	**3.00**
	FEA (kHz)	**FEA (kHz)**	**FEA (kHz)**	**FEA (kHz)**	**FEA (kHz)**	**FEA (kHz)**	**FEA (kHz)**	**FEA (kHz)**
Z Bend 1	3.752	3.752	3.751	3.754	3.755	3.760	3.762	3.766
X Torsion 1	2.145	2.160	2.159	2.154	2.147	2.136	2.126	2.112
Z Bend 2	10.362	10.365	10.362	10.365	10.366	10.365	10.367	10.369
X Torsion 2	7.779	7.775	7.773	7.771	7.763	7.753	7.744	7.727
Z Bend 3	9.066	9.082	9.082	9.074	9.076	9.073	9.074	9.074
X Torsion 3	12.602	12.678	12.672	12.646	12.637	12.616	12.593	12.563
X Bend 1	20.199	20.204	20.208	20.200	20.205	20.212	20.203	20.203
8	23.721	23.729	23.720	23.734	23.748	23.763	23.773	23.812
X Torsion 4	15.648	15.635	15.635	15.635	15.624	15.617	15.608	15.591
10	28.373	28.351	28.357	28.381	28.398	28.416	28.439	28.480
Z Bend 4	33.569	33.565	33.571	33.565	33.559	33.566	33.564	33.549
12	25.966	25.943	25.941	25.936	25.915	25.886	25.834	25.789
X Torsion 5	39.504	39.458	39.482	39.532	39.620	39.735	39.887	40.062
Y Bend 1	31.258	31.480	31.491	31.579	31.761	32.012	32.342	32.704
Z Bend 5	49.624	49.628	49.632	49.627	49.627	49.628	49.618	49.608
16	52.396	52.334	52.311	52.259	52.198	52.089	51.965	51.848
X Torsion 6	37.134	37.303	37.319	37.266	37.248	37.233	37.223	37.211
18	38.818	38.818	38.816	38.811	38.787	38.769	38.767	38.745
19	54.198	54.173	54.176	54.180	54.204	54.262	54.278	54.297
Z Bend 6	66.679	66.581	66.592	66.637	66.658	66.637	66.620	66.569
21	68.841	68.855	68.863	68.842	68.811	68.766	68.705	68.626
22	63.187	63.274	63.258	63.233	63.184	63.153	63.072	62.969
Volume 1	66.632	66.760	66.719	66.528	66.255	65.883	65.429	64.884
X Torsion 7	65.525	65.612	65.595	65.534	65.479	65.388	65.295	65.177
25	73.627	73.662	73.656	73.633	73.601	73.539	73.442	73.320
26	79.975	80.211	80.276	80.460	80.756	81.140	80.834	79.469
Y Bend 2	63.968	64.134	64.060	63.831	63.493	63.040	62.478	61.790
Z Bend 7	75.840	75.852	75.835	75.832	75.778	75.787	75.666	75.554
29	77.828	77.843	77.842	77.854	77.858	77.894	77.966	78.074
X Torsion 8	13.317	13.349	13.314	13.177	12.973	12.696	12.352	11.952

Refer to Appendix A, Table A-1 for explanation of abbreviations.

Continued on next page.

Table C-10 Continued.

Defect Depth (mm)	**30.0**	**30.0**	**30.0**	**30.0**	**30.0**	**30.0**
Defect Width (mm)	**3.50**	**4.00**	**4.50**	**5.00**	**5.50**	**6.00**
	FEA (kHz)	**FEA (kHz)**	**FEA (kHz)**	**FEA (kHz)**	**FEA (kHz)**	**FEA (kHz)**
Z Bend 1	3.771	3.776	3.781	3.786	3.793	3.800
X Torsion 1	2.095	2.076	2.053	2.030	2.001	1.972
Z Bend 2	10.372	10.373	10.377	10.379	10.384	10.386
X Torsion 2	7.713	7.695	7.677	7.651	7.627	7.597
Z Bend 3	9.071	9.067	9.056	9.047	9.027	9.003
X Torsion 3	12.525	12.479	12.448	12.397	12.342	12.290
X Bend 1	20.199	20.187	20.188	20.181	20.180	20.168
8	23.849	23.884	23.921	23.956	23.983	24.021
X Torsion 4	15.570	15.556	15.529	15.508	15.478	15.444
10	28.523	28.558	28.617	28.675	28.734	28.811
Z Bend 4	33.546	33.543	33.535	33.534	33.525	33.517
12	25.755	25.678	25.601	25.524	25.435	25.349
X Torsion 5	40.270	40.523	40.846	41.213	41.633	42.146
Y Bend 1	33.131	33.586	34.074	34.579	35.095	35.613
Z Bend 5	49.607	49.576	49.552	49.520	49.489	49.448
16	51.715	51.547	51.373	51.217	51.037	50.880
X Torsion 6	37.183	37.148	37.108	37.070	37.000	36.915
18	38.753	38.745	38.749	38.739	38.742	38.733
19	54.329	54.309	54.269	54.219	54.129	53.952
Z Bend 6	66.445	66.258	65.986	65.773	65.455	65.142
21	68.539	68.434	68.338	68.255	68.190	68.142
22	62.787	62.575	62.231	61.751	61.196	60.551
Volume 1	64.277	63.614	62.900	62.115	61.253	60.353
X Torsion 7	65.096	64.997	64.854	64.773	64.689	64.656
25	73.132	72.838	72.482	72.103	71.771	71.502
26	78.423	77.830	77.731	77.797	78.032	78.439
Y Bend 2	61.006	60.110	59.139	58.060	56.888	55.646
Z Bend 7	75.285	74.934	74.617	74.411	74.280	74.201
29	78.212	78.352	78.569	78.762	78.989	79.225
X Torsion 8	11.497	11.001	10.464	9.896	9.298	8.682

Refer to Appendix A, Table A-1 for explanation of abbreviations.

Table C-11 Half-peak width for selected ceramic specimens.

Note: Defect Depth here expressed as a percentage for specimen length.

Specimen	**4**	**2**	**7**	**9**	**5**	**2**	**5**	**7**	**9**
Defect Depth	0.0%	0.6%	14.7%	18.1%	27.1%	32.3%	40.1%	45.7%	50.5%
Mode	**Attenuation**	**Attenuation**	**Attenuation**	**Attenuation**	**Attenuation**	**Attenuation**	**Attenuation**	**Attenuation**	**Attenuation**
X Bend 1	0.36%	0.49%	0.48%	0.52%	0.57%	1.29%	2.76%		
8	0.36%	0.34%	0.39%	0.51%	0.53%	0.50%	0.68%	0.56%	0.48%
X Torsion 4	0.32%	0.35%	0.45%	0.43%	0.39%	0.31%	0.53%	0.45%	
10	0.27%	0.27%	0.26%	0.31%	0.34%	0.47%	0.87%	1.07%	
Z Bend 4	0.26%	0.28%	0.27%	0.31%	0.29%	0.30%	0.25%	0.28%	0.61%
12	0.25%	0.19%	0.25%	0.25%	0.23%	0.32%	0.72%	0.61%	0.67%
X Torsion 5	0.21%	0.20%	0.24%	0.22%	0.24%	0.21%	0.37%	0.32%	
Y Bend 1	0.19%	0.20%	0.15%	0.15%			0.26%	0.51%	1.07%

Refer to Appendix A, Table A-1 for explanation of abbreviations.

APPENDIX D

This appendix contains the code text of the program used to estimate the Location/Depth of a defect based on change in resonant frequency (Section 3). Program created using MATLAB R2007a Version 7.4.0.287, created by The MathWorks, Inc.

```
%This program determines the estimated location (L)
%and depth (D) of a defect given constants Cin and
%change in modal frequencies

% Setup
clc
clear


%Get data
CurrentDirectory = cd;
cd('E:\Research\Steel Test 3\Regression Analysis');
Constants = xlsread('Input 05-29-08.xls','Mat SAS In');
InputData = xlsread('Input 05-29-08.xls','Mat Y In');
cd(CurrentDirectory);

%Calculate necessary values
NumPoints = size(InputData,1);
NumVars = 7;

%Assign data to vectors
DepthVector = InputData(:,2);
LocVector = InputData(:,1);
%Use for percentage numbers
Data = InputData(:,19:NumVars + 18);
%Use for real numbers
%Data = InputData(:,11:NumVars + 10);

%Choose which resonant frequencies to use
%from list X1 Y1 Z1 V1 Z2 Y2 X2
UseFreqs = ([1 2 3 4 5 6 7]);
NumFreqs = size(UseFreqs,2);
FreqEst = zeros(NumFreqs,1);
ErrorSq = zeros(NumFreqs,1);


N = 120;
M = 120;

%============================================================
%Begin calculation of D,L for all data points
%============================================================
Output = zeros(NumPoints,2 + NumFreqs);
%Loops through all data points
for Point = 1:NumPoints


    %============================================================
    %Begin iterative search for least squares fit of frequency
    %============================================================
    Results = zeros(M*N,3 + NumFreqs);

    %Resets error functions
    MinError = 1000;
```

```
Depth = 99;
Loc = 99;

%Loops through N possible locations
Counter = 0;
L = 0;
for i = 1:N
    %Move to next guess of location
    L = L + .6/N;

    %Loops through M possible depths
    D = 0;
    Var = zeros(1,7);
    for j = 1:M
        Counter = Counter + 1;

        %Move to next guess of depth
        D = D + .25/M;

        %Set potential variables for future use
        D2 = D*D;
        D3 = D*D*D;
        D4 = D3 * D;
        D5 = D3 * D2;
        D6 = D3 * D3;

        L2 = L*L;
        L3 = L*L*L;
        L4 = L*L*L*L;

        DL = D*L;
        DL2 = D*L2;
        DL3 = D*L3;
        DL4 = D*L4;

        D2L  = D2*L;
        D2L2 = D2*L2;
        D2L3 = D2*L3;
        D2L4 = D2*L4;

        D3L =  D3*L;
        D3L2 = D3*L2;
        D3L3 = D3*L3;
        D3L4 = D3*L4;

        D4L =  D4*L;
        D4L2 = D4*L2;
        D4L3 = D4*L3;
        D4L4 = D4*L4;

        D5L =  D5*L;
        D5L2 = D5*L2;
        D5L3 = D5*L3;
        D5L4 = D5*L4;
```

```
            D6L =  D6*L;
            D6L2 = D6*L2;
            D6L3 = D6*L3;
            D6L4 = D6*L4;

            %Sets values of L and D multiples
            %Use for 2nd Order
            Var = ([1 D DL DL2 D2 D2L D2L2]);

            %Use for 6th Order X axis
            %Var = ([1  D5  DL  D2L3  D4L3  D5L4  D6L4]);

            %Use for 6th Order Y axis
            %Var = ([1  D6  D2L2  D3L  D5L  D5L3  D5L4]);



%============================================================
            %Begin frequency calculator

%============================================================
            %Loops through each nodal frequency
            Error = 0;
            for F = 1:NumFreqs
                %Calculates value of frequencies based on current D & L
                FreqEst(F,1) = Var(1,:) * Constants(:,UseFreqs(F));

                %Determines the squared error based on the true freq
value
                TrueFreq = Data(Point,UseFreqs(F));
%                 if TrueFreq == 0
%                     ErrorSq(F,1) = (FreqEst(F,1) - TrueFreq)^2;
%                 else
%                     ErrorSq(F,1) = ((FreqEst(F,1) -
TrueFreq)/TrueFreq)^2;
%                 end
                ErrorSq(F,1) = (FreqEst(F,1) - TrueFreq)^2;
                Error = ErrorSq(F,1) + Error;
            end

%============================================================
            %End iterative frequency calculator

%============================================================

            Error = sqrt(Error);

            %Stores the calculated frequencies with D,L, and error
            %For troubleshooting purposes only
            Results(Counter,1) = D;
            Results(Counter,2) = L;
            Results(Counter,3) = Error;
            for F = 1:NumFreqs
```

```
                Results(Counter,F + 3) = FreqEst(F,1);
            end

            %Checks for least squares error point, stores value if
found
            if Error < MinError
                MinError = Error;
                Depth = D;
                Loc = L;
                FreqOut = FreqEst;
            end


        end


    end
    %=============================================================
    %End iterative search for least squares fit of frequency
    %=============================================================

    Output(Point,1) = Depth;
    Output(Point,2) = Loc;
    for F = 1:NumFreqs
        Output(Point,F+2) = FreqOut(F,1);
    end


end
%=============================================================
%End calculation of D,L for all data points
%=============================================================
```

VITA

Kevin Flynn received his Bachelor of Science degree in mechanical engineering from Pensacola Christian College in Pensacola, Florida in 2000. He entered the Mechanical Engineering program at Texas A&M University in September 2006 and received his Master of Science degree in December 2008.

Mr. Flynn may be reached at Texas A&M University's Department of Mechanical Engineering, 3123 TAMU, College Station, TX 77843. His email is flynnk@juno.com.